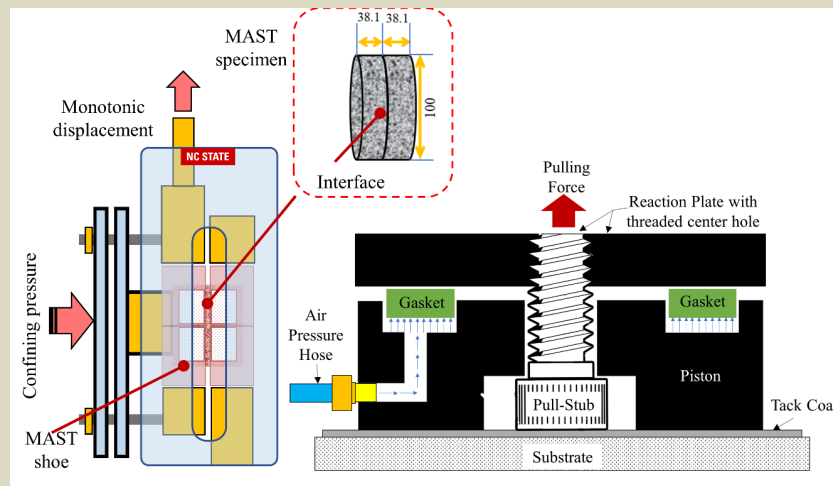




RESEARCH & DEVELOPMENT

Development of a Tack Coat Quality Control Program for Mitigating Delamination in Asphalt Pavement Layers



Schematic illustrations for (a) MAST test setup and (b) PATTI test setup

Y. Richard Kim, Ph.D., P.E., F. ASCE

Nithin Sudarsanan, Ph.D.; Jaemin Heo, Ph.D.

Ben Fonte; Lei Gabriel Xue

Dept. of Civil, Construction, & Environmental Engineering

North Carolina State University

NCDOT Project 2018-13

May 2021

Development of a Tack Coat Quality Control Program for Mitigating Delamination in Asphalt Pavement Layers

FINAL REPORT

Submitted to:
North Carolina Department of Transportation
Office of Research
(Research Projection No. RP 2018-13)

Submitted by

Y. Richard Kim, Ph.D., P.E., F.ASCE
Jimmy D. Clark Distinguished University Professor
Campus Box 7908
Department of Civil, Construction & Environmental Engineering
North Carolina State University
Raleigh, NC 27695-7908
Tel: 919-515-7758, Fax: 919-515-7908
kim@ncsu.edu

Nithin Sudarsanan, Ph. D.
Postdoctoral Researcher

Jaemin Heo, Ph.D.
Former Graduate Student

Ben Benjamin Fonte
Former Graduate Student

Lei Gabriel Xue
Graduate Research Assistant

Department of Civil, Construction & Environmental Engineering
North Carolina State University
Raleigh, NC

May 2021

Technical Report Documentation Page

1. Report No. FHWA/NC/208-13	2. Government Accession No.	3. Recipient's Catalog No.	
4. Title and Subtitle Development of a Tack Coat Quality Control Program for Mitigating Delamination in Asphalt Pavement Layers		5. Report Date May 2021	
		6. Performing Organization Code	
7. Author(s) Y. Richard Kim, Nithin Sudarsanan, Jaemin Heo, Benjamin Fonte, Lei Xue		8. Performing Organization Report No.	
9. Performing Organization Name and Address Campus Box 7908, Dept. of Civil, Construction, & Environmental Engrg. NCSU, Raleigh, NC 27695-7908		10. Work Unit No. (TRAIS)	
		11. Contract or Grant No.	
12. Sponsoring Agency Name and Address NC Department of Transportation Research and Development Unit 1020 Birch Ridge Drive Raleigh, NC 27610		13. Type of Report and Period Covered Final Report August 2017 – June 2020	
		14. Sponsoring Agency Code RP2018-13	
15. Supplementary Notes			
16. Abstract The importance of proper bonding at the asphalt concrete (AC) layer interface cannot be overemphasized when discussing the performance of AC pavements. The primary objective of this research is to develop a set of test procedure and acceptance criterion that can be used in a tack coat quality control (QC) program to mitigate debonding in asphalt pavements. This study covers the effects of tack coat application rate, AC surface conditions (milled and unmilled), confining pressure, strain rate, and temperature on interface shear strength (ISS) of double-layered AC specimens. Five types of tack coats were used in this study, including CRS-2 (Source 1), CRS-2 (Source 2), CRS-1h, NTCRS-1hM, and Ultrafuse. The experimental design was to measure the binder bond strength (BBS) of each of these five tack coats and the interface shear strength (ISS) of double-layered AC specimens that were fabricated using a warm mix designated as RS9.5C with 20% AP in a gyratory compactor. The ISS predictive model was developed as a function of confining pressure, temperature, and shear strain rate. The three-dimensional pavement analysis program, FlexPAVE™ version 1.1 was used to determine pavement responses. The shear ratio was defined as the ratio of the shear stress calculated from FlexPAVE to the shear strength along the interface. The maximum shear ratio (MSR) was used to define the debonding potential of a pavement. The normal stress to the interface and the shear strain rate determined from FlexPAVE were input to the ISS predictive model to predict the shear strength at various locations in a pavement structure. FlexPAVE simulations under numerous field conditions were also used to develop a universal relationship between the ISS and BBS that is independent of the tack coat type. The ISS-BBS relationship led to the development of a predictive model for the MSR as a function of BBS and depth of the interface. Assuming that all the tack coats considered in the study are acceptable, the MSR-BBS relationship resulted in the BBS threshold value of 75 kPa at 50°C. However, if the layer above the tack coat is an open-graded friction course (OGFC), the cut-off is maintained at 750 kPa. The experimental work verified that the time-temperature superposition is valid for the ISS and BBS. The ISS results showed that the confining pressure, temperature and strain rate have a significant effect on ISS whereas the tack coat application rate, tack coat type, and surface condition with laboratory-fabricated grooves with different angles do not have a significant effect on ISS. However, it must be noted that the monotonic loading used in measuring the ISS and the laboratory-fabricated grooves may not represent the field conditions properly. Additional research with the shear fatigue test and the milled surface in the field is recommended for future study.			
17. Key Words Bond strength, shear, layer interface,		18. Distribution Statement	
19. Security Classif. (of this report)	20. Security Classif. (of this page)	21. No. of Pages 246	22. Price

DISCLAIMER

The contents of this report reflect the views of the authors and are not necessarily the views of North Carolina State University. The authors are responsible for the facts and the accuracy of the data presented herein. The contents do not necessarily reflect the official views or policies of the North Carolina Department of Transportation at the time of publication. This report does not constitute a standard, specification, or regulation.

ACKNOWLEDGEMENTS

This research was sponsored by the North Carolina Department of Transportation. The Steering and Implementation Committee was comprised of Shihai Zhang, P.E. (Chair); Brian J. Hunter, P.E.; Clark Morrison, Ph.D., P.E.; John R.G. Olinger, P.E.; James B. Phillips, P.E.; Lamar Sylvester, P.E.; Todd Wayne Whittington, P.E.; Neil Mastin, P.E.; Christopher A. Peoples, P.E.; and Mustan Kadibhai, P.E. These advisors have given invaluable direction and support to the research team throughout the project.

EXECUTIVE SUMMARY

Background

The performance of multilayered asphalt concrete (AC) pavements and the relevance of proper bonding at the AC layer interface are inseparably linked. A sufficient bond between AC layers allows the stress and strain to be distributed adequately throughout the pavement structure. However, a weak bond can lead to pavement distress, including fatigue cracking, slippage, delamination, and eventually, the formation of potholes. The source of such failure often is not recognized as an insufficient bond between the AC layers. The bonding of AC layers typically can be improved by the use of tack coats between the layers. The additional cost incurred by the application of tack coats for a new or reconstruction pavement project is 0.1% to 0.2% of the total cost. For milling and overlay projects, the inclusion of tack coats adds 1% to 2% to the project cost. The rehabilitation of a debonded surface by replacing the top lift can be as much as 20% to 100% of the total project cost. Therefore, the type, quantity, and quality of the tack coat materials and tack coat construction practices must be considered carefully in order to prevent premature pavement failure and mitigate subsequent costs (FHWA 2016).

Objectives

The primary objective of this proposed research is to develop a set of test procedure and acceptance criterion that can be used in a tack coat quality control (QC) program to mitigate debonding in asphalt pavements. This study covers the effects of tack coat application rate, AC surface conditions (milled and unmilled), confining pressure, strain rate, and temperature on interface shear strength (ISS) of double-layered AC specimens.

Materials and Methodology

The AC loose mixture used in this study is a warm mix designated as RS9.5C with 20% reclaimed asphalt pavement (RAP). The five types of tack coats used in this study are CRS-2 (Source 1), CRS-2 (Source 2), CRS-1h, NTCRS-1hM, and Ultrafuse. The experimental design was to measure the binder bond strength (BBS) of each of these five tack coats and the ISS of double-layered AC specimens. The BBS and ISS were measured using pneumatic adhesion tension testing instrument (PATTI) and Modified Asphalt Shear Tester (MAST), respectively. Figure I-1 presents a schematic illustration of the MAST and PATTI test setups. The MAST test specimens were fabricated with different tack coat materials sandwiched between double-layered AC. The MAST tests were carried out at various confining pressures, temperatures, and (monotonic) strain rates using specimens fabricated with different tack coats, application rates, and surface conditions, as shown in Table I-1. Three application rates, 0.0452 L/m² (0.01 gal/yd²), 0.136 L/m² (0.03 gal/yd²),

and 0.226 L/m² (0.05 gal/yd²), were selected to investigate the effects of the tack coat application rate on the ISS. The PATTI tests were carried out at 13 different temperatures for each tack coat; these temperature data were used to construct BBS mastercurves.

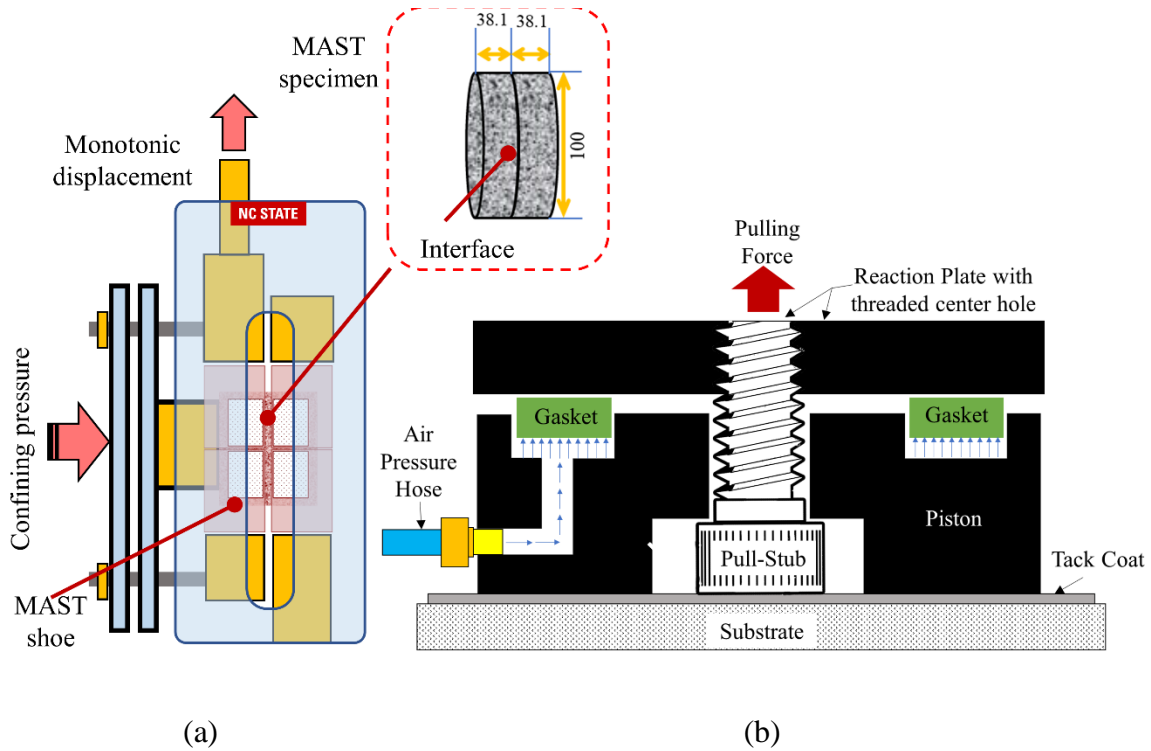


Figure I-1. Schematic illustrations for (a) MAST test setup and (b) PATTI test setup.

Table I-1. Testing Conditions for MAST Tests

Factors	Conditions				
Tack coat type	CRS-2 (Source 1)	CRS-2 (Source 2)	CRS-1h	NTCRS-1hM	Ultrafuse
Test temperature	5°C, 19°C, 35°C, 53°C				
Application rate	0.0452 L/m ² (0.01 gal/yd ²), 0.136 L/m ² (0.03 gal/yd ²), 0.226 L/m ² (0.05 gal/yd ²)				
Loading rate	50.8 mm/min (2 in./min), 5.08 mm/min (0.2 in./min), 0.508 mm/min (0.02 in./min)				
Confinement	69 kPa (10 psi), 276 kPa (40 psi), 483 kPa (70 psi)				
Surface	Ungrooved Surface (U)		Grooved Surface (G)		

The response of a pavement section also was studied by running numerical simulations using a three-dimensional finite element software package, FlexPAVE™. The section dimensions of the

simulated pavement represent those of a thick pavement structure used in North Carolina, as shown in Figure I-2. The previous NCDOT project HWY-2013-04 (Kim et al. 2015) found that a thick pavement structure is more vulnerable to debonding at the AC layer interface than a thinner structure due to the greater shear stress that is induced in a thick pavement. Also, analysis of the maximum shear ratio (MSR) indicates that a high temperature, low speed, and heavy axle load are critical conditions that are conducive for debonding at the AC layer interface (Kim et al. 2015, Cho 2016). Therefore, the thick pavement investigated in this study was loaded using a dual tire with an axle load of 80 kN running at various vehicular speeds of 1.61 km/h (1 mph), 4.82 km/h (3 mph), 8.04 km/h (5 mph), 16 km/h (10 mph), 32.2 km/h (20 mph), and 72.4 km/h (45 mph). These conditions assume a vehicle in the braking state with a frictional coefficient of 0.55 at the speed under consideration. The pavement temperature is set at 50°C.

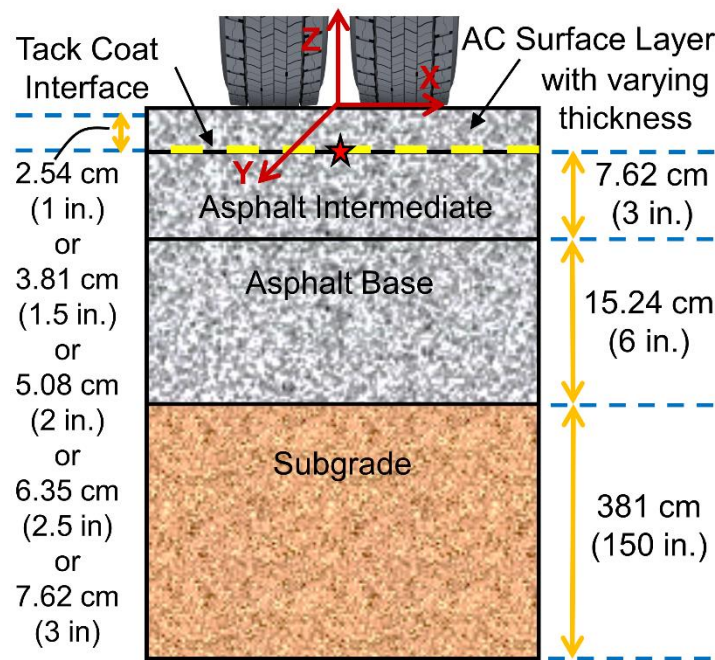


Figure I-2. Thick pavement section.

Research Approach

Figure I-3 presents a flow chart of the research approach used in this project. The end result is the minimum BBS value that is required for acceptance of a tack coat. Four phases are needed to achieve this goal, as described in the following subsections.

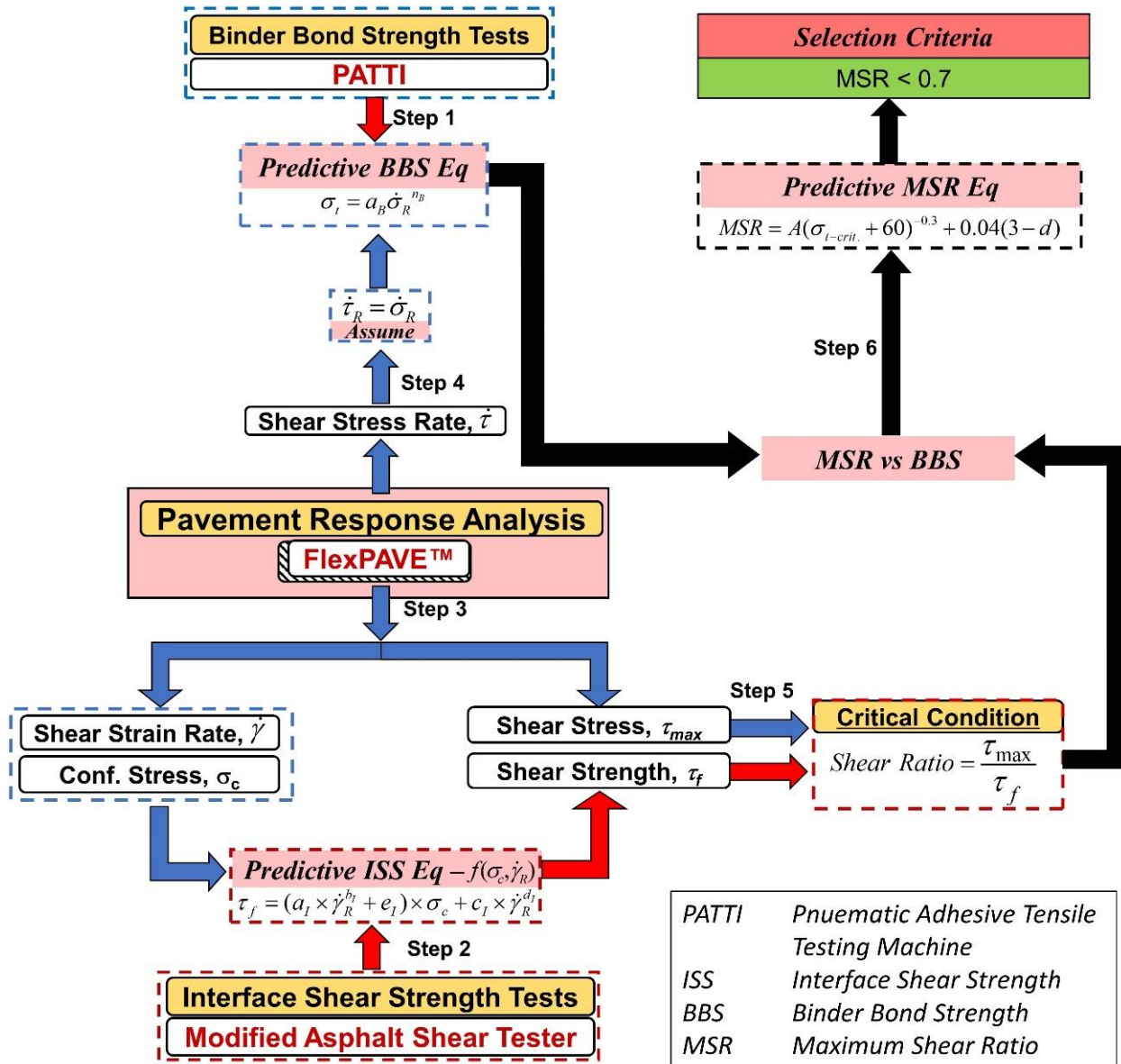


Figure I-3. Flow chart for research approach.

Phase 1: Development of Predictive Equations for the Interface Shear Strength (ISS) and Binder Bond Strength (BBS) Based on Laboratory Tests

In Phase 1, the BBS (Step 1) and ISS (Step 2) of the different tack coat interlayers were measured. The MAST tests were carried out at various confining pressures, temperatures, and (monotonic) strain rates using specimens with different tack coats sandwiched between double-layered AC. [Chapter 5](#) presents a critical evaluation of the MAST test results. Analysis of all the outcomes led to the establishment of a relationship that is based on confining pressure and reduced strain rate, which is a function of temperature and strain rate, to the ISS, as shown in Equation (1).

$$\tau_f = (a_I \times \dot{\gamma}_R^{b_I} + e_I) \times \sigma_c + c_I \times \dot{\gamma}_R^{d_I} \quad (1)$$

where

- τ_f = ISS, kPa,
 $\dot{\gamma}_R$ = reduced shear strain rate, and,
 σ_c = normal confining stress, kPa.

The parameters a_I , b_I , c_I , d_I , and e_I for the four tack coats were found and are reported in Table 6-1.

Similarly, BBS tests were conducted at 13 different temperatures. The results were used successfully to verify the validity of the time-temperature superposition (t-TS) principle for the BBS. Consequently, a relationship between the BBS and reduced stress rate was derived, as shown in Equation (2).

$$\sigma_t = a_B \dot{\sigma}_R^{n_B} \quad (2)$$

where

- $\dot{\sigma}_R$ = reduced stress rate,
 σ_t = BBS, and
 a_B, n_B = material parameters.

Phase 2: Numerical Simulations of Pavement Response

Pavement response analysis of a thick pavement structure typically used in North Carolina was carried out using the finite element program, FlexPAVE™ version 1.1. The normal stress, shear stress, and shear strain observed at the interface during the analysis were extracted and reported. [Chapter 2](#) provides details regarding the numerical simulation results.

Phase 3: Identification of Interface Debonding Potential Based on the Maximum Shear Ratio (MSR)

The debonding potential of an interface depends on its ability to resist the maximum shear stress at the interface that is induced by vehicular loads. Thus, the debonding potential is defined by a factor known as the maximum shear ratio (MSR). The shear ratio is the ratio of the shear stress to the shear strength along the interface. The maximum value of the shear ratio, i.e., the MSR, along the interface is the indicator for the potential of debonding. Higher MSR values indicate greater chance of debonding at the layer interface. If the MSR exceeds one, then the interface fails in shear, and debonding occurs.

The maximum shear stress at the interface can be derived from numerical simulations. The shear strength of a specific tack coat at the interface in the field is predicted using Equation (1). The normal pressure (confining pressure) and reduced strain rate used in Equation (1) are obtained from the FlexPAVE simulation (Step 3). Thus, the MSR for the different tack coats can be determined for the critical field condition (Step 5). All five tack coats used in this study showed the MSR value smaller than one.

The reduced shear stress rate is employed to predict the BBS using Equation (2) (Step 4) while the reduced shear strain rate is used to predict the ISS in Equation (1). Rigorous numerical simulations performed under numerous field conditions led to the establishment of a universal relationship between the ISS and BBS that is independent of the tack coat type; [Chapter 6](#) provides details. The bridging factors for establishing the universal relationship between the ISS and BBS are the shear strain rate and shear stress rate that were measured for each numerical simulation condition.

Phase 4: Evaluation of Minimum BBS Requirement for Tack Coat Acceptance

The establishment of the universal relationship between ISS and BBS led to the development of a predictive model for the MSR as a function of BBS and depth of the interface (Step 6). The predictive model is shown in Equation (3).

$$MSR = 3.051(\sigma_{t-crit.} + 60)^{-0.3} + 0.04(3 - d) \quad (3)$$

where

MSR = maximum shear ratio,

$\sigma_{t-crit.}$ = BBS at 50°C in kPa; the test stress rate must be 690 kPa/sec (100 psi/sec), and

d = depth of interface from the asphalt surface, in inches.

Typically, the PATTI test protocol recommends a tensile stress rate that is within 75 psi/sec to 150 psi/sec (518 kPa/sec to 1034 kPa/sec). The stress rate determined at the interface depth of 3 inches (7.62 cm) from the pavement surface via numerical simulation carried out at 50°C for an 80-kN dual-tire vehicle at a speed of 1 mph (1.61 km/hour) induces 664 kPa/sec. In order to match the stress rate of the PATTI test with that determined from the numerical simulation, the PATTI test procedure proposed in this study recommends the stress rate confined between 90 psi/sec to 115 psi/sec (620 kPa/sec to 792 kPa/sec) and the test temperature of 50°C. Further, the MSR predicted at the interface depth of 3 inches (7.62 cm) can be extrapolated by establishing the variation in MSR with interface depth. Assuming that all the tack coats considered in this study are acceptable, an MSR that is less than 0.7 is considered a reasonable acceptance criterion for any tack coat for the selected warm mix surface layer. The MSR threshold value of 0.7 results in the BBS threshold value of 75 kPa at 50°C. However, if the layer above the tack coat is an open-graded friction course (OGFC), the cut-off is maintained at 750 kPa; [Chapter 6](#) provides details.

Major Conclusions

Despite the importance of applying a tack coat to enhance the bond strength at the asphalt interface and improve the long-term performance of the pavement structure, no standard QC test method is currently available to ensure the proper quality of tack coats. The current research approach and test results are used herein to propose a test procedure and criterion for acceptance of tack coats, which can be used for a tack coat QC program. This program incorporates a laboratory test procedure to determine the BBS of tack coats and the minimum BBS that is required for the acceptance of tack coat materials to ensure debonding resistance. In addition, a guideline for best practices and usage of tack coats is developed based on experience reported by different agencies in the United States and the test outcomes from the previous NCDOT project HWY-2013-04 and the current project RP 2018-03 on tack coats.

The following conclusions can be drawn based on the experimental work and computational analyses conducted in this research.

Experimental work

- The use of the t-TS principle to establish the ISS and BBS mastercurves was verified in this study. The t-T shift factors determined from axial compression dynamic modulus tests of the AC mixture were used successfully to develop ISS mastercurves. The t-T shift factors determined from dynamic shear rheometer tests of tack coat emulsions were used successfully to develop BBS mastercurves.
- The predictive model equation for ISS developed by Cho (2016) was fitted to obtain coefficients for the five different tack coat materials used in this study. This predictive model can be used to predict the shear strength at a specific pavement depth of interest, which can be in turn compared against the shear stress at that depth predicted from FlexPAVE™.
- The ISS decreases with an increase in the test temperature and a decrease in strain rate. This finding applies to all the tested MAST specimens, independent of the tack coat type.
- Three different confining pressures were applied to determine the effects of confinement on ISS. The results clearly indicate that the ISS is proportional to the applied confinement pressure. The mobilization of aggregate interlocking resulted in increased frictional resistance to the applied shear stress. Therefore, shear strength increases with an increase in confining pressure.
- MAST specimens were fabricated with three tack coat application rates (0.01 gal/yd², 0.03 gal/yd², and 0.05 gal/yd²) for the five different tack coats. The MAST test results did not indicate any effect of tack coat application rate on the ISS. Statistical analysis of the effect of the application rate on the ISS also supports this finding. However, the ISS test is a quick monotonic shear test that acts as a QC test and, hence, the real effects and performance of

the application rate cannot be completely captured with this test. A cyclic shear fatigue test is considered more reliable in terms of understanding the effects of application rate because the loading mode is similar to that found in field conditions.

- Tack coat type does not have a significant effect on ISS. Statistical analysis of all the outcomes under the different testing conditions supports this finding. However, the strain at failure and the strain at plateau stress for the non-tracking emulsions (NTCRS-1hM and Ultrafuse) were significantly greater than for the unmodified tack coats (CRS-2, CRS-1h), especially at temperatures higher than 35°C. This finding clearly indicates that focusing only on shear strength may lead to discrepancies with field performance. The energy that is dissipated during an ISS test could be a better indicator of debonding potential than shear strength. However, in this study, the dissipated energy up to failure could not be used to compare different tack coat materials because it was difficult to define the failure strain in the ISS test results for the non-tracking tack coats, especially at high temperatures. For these conditions, the shear stress reached an asymptotic behavior and the failure strain at the peak stress was difficult to determine and has a significant effect on the energy calculation.
- Therefore, it is unreasonable to conclude that the performance of non-tracking or modified emulsions is equivalent to that of unmodified emulsions based on shear strength. Cyclic shear fatigue tests may be a better method to capture the performance differences of various tack coat types than the monotonic shear strength test.
- Milled and unmilled are the two surface conditions considered in this study. The grooved surface of the laboratory specimens was created using a mechanical rotary milling machine that mimics the field-milled surface and matches the field-milled mean profile depth (MPD). The results show that the shear strength of the ungrooved surface is comparable to that of the grooved surface specimens. However, this finding may be related to the fact that the shear tests were carried out with the groove path aligned with the shearing direction. The smooth surface of the grooves that are aligned with the shearing direction facilitated easy slippage rather than resisting the shear displacement. Moreover, a grooved surface often weakens the strength of the pavement more than an ungrooved surface due to the damage caused by milling.
- In order to investigate whether or not the insignificant effect of the grooved surface on the ISS was due to the grooves and shearing orientation being in the same direction, additional tests were conducted with grooves at 30° and 90° angles from the shearing direction. Statistical analysis of the ISS results suggested no significant effect of the directional angle of the grooves on the ISS. This unexpected finding may be due to the damage that was induced on the bottom layer surface during the milling operation. Whether or not this finding would hold true in the field under actual milling operations remains unclear.
- A prediction equation for BBS, which is a function of the reduced tensile stress rate, was developed in this study. It was found that the BBS mastercurve construction typically

requires 13 different conditioning temperatures per tack coat, which consumes an enormous amount of time and effort. A new two-point method is proposed to predict the BBS mastercurve; that is, two tests conducted at two different temperatures. The proposed two-point method reduces the mastercurve construction time to within eight hours of testing, with a degree of accuracy that is comparable to the predictive model that uses the data from 13 temperatures.

- The ranking of the mastercurves that were constructed using the dynamic shear modulus values of each tack coat type follows the same ranking pattern as the predicted BBS mastercurves, thereby making the dynamic shear modulus a potential predictor of BBS.
- To identify the effects of the application rate on BBS, three residual application rates of 0.045 L/m² (0.01 gal/yd²), 0.14 L/m² (0.03 gal/yd²), and 0.23 L/m² (0.05 gal/yd²) were used at a single temperature, i.e., 44°C for NTCRS-1hM and 22°C for CRS-2 and CRS-1h. Even though no definite trend emerged among the different tack coat application rates for the different tack coats, the optimum residual application rate for the tested emulsions was below 0.14 L/m² (0.03 gal/yd²). Agencies, including the NCDOT, should specify the tack coat application rate as the residual application rate instead of the emulsion application rate in order to gain more consistent BBS test outcomes, thereby avoiding the residue variation within different emulsions that can affect the performance of the pavement system.

Numerical simulations

- In this research, ‘shear ratio’ is defined as the ratio between the shear stress at the interface under vehicular loading and the ISS. The maximum shear ratio (MSR) is determined by comparing the shear ratios at various locations in a pavement structure that are determined using the shear stress calculated from FlexPAVETM and the shear strength calculated from the ISS predictive model. A higher MSR implies greater potential for interface debonding that is due to repeated vehicular braking. An MSR that is greater than one indicates that debonding failure would occur due to the single braking of a dual tire at 80 kN. All the tack coats considered in this study generated sufficient shear strength to resist the shear stress in the field based on numerical simulations. Hence, the potential for interface debonding using these tack coats is minimal.
- The MSR typically is observed along the center of the longitudinal axis of the tire at 10 cm to 14 cm in front of the tire. The MSR location depends on the depth of the interface and the tack coat type.
- The worst field conditions expected in North Carolina for the interface to resist debonding during its service life are as follows: a thick pavement with a dual tire of 80 kN under the braking condition at a speed of 1 mph (1.61 km/hour) at 50°C.

Minimum required binder bond strength (BBS)

- Rigorous numerical simulations for different field conditions helped to develop a universal relationship between ISS and BBS followed by the MSR versus BBS relationship. The MSR-BBS relationship is presented as a function of interface depth and is used to determine the BBS threshold values for different interface depths.
- A methodology that can be used as part of the tack coat QC program is proposed to ensure the appropriate bonding of tack coat emulsions and provide acceptable field performance. This methodology uses the PATTI test to measure the BBS of the tack coat material tested at 50°C. The required stress rate during the test must be maintained at between 90 psi/sec and 115 psi/sec (620 kPa/sec and 792 kPa/sec).
- Assuming that all the tack coats considered in this study qualify for acceptance, an MSR that is less than 0.7 can be considered a reasonable acceptance criterion. Based on the MSR-BBS relationship, the BBS value at 50°C that corresponds to the MSR value of 0.7 was found to be 75 kPa. Therefore, if the BBS of a tack coat at 50°C is above 75 kPa, then the tack coat can be accepted for purchase. However, when tack coats are to be used for an open-graded friction course, the cut-off must be maintained at 750 kPa.

TABLE OF CONTENTS

Chapter 1. Introduction	1
1.1 Background	1
1.2 Research Needs and Significance.....	2
1.3 Research Objectives and Scope.....	3
1.4 Research Approach	3
1.5 Report Organization.....	6
Chapter 2. Materials and Properties.....	8
2.1 Asphalt Mixture	8
2.1.1 Dynamic Modulus ($ E^* $) Test	8
2.2 Tack Coat	10
2.2.1 Residue Recovery of Asphalt Emulsions	10
2.2.2 Curing Time for Asphalt Emulsions.....	11
2.2.3 Density of Emulsified Asphalt.....	11
2.2.4 Dynamic Shear Rheometer ($ G^* $) Test.....	12
Chapter 3. Test Methodology	14
3.1 Interlayer Shear Strength (ISS) Test.....	14
3.1.1 Laboratory Fabrication of MAST Specimens	14
3.1.2 Modified Advanced Shear Tester (MAST)	17
3.1.3 Digital Image Correlation (DIC) Technique	19
3.2 Understanding the Milled Pavement Surface and Fabrication in Laboratory.....	21
3.2.1 Field Core Milled Specimens.....	21
3.2.2 Milling Machine	23
3.2.3 Artificial Milled Surface Prototype Based on Field Cores	24
3.2.4 Field Milled Surface Investigation.....	25
3.2.5 Artificial Milled Surface Prototypes Based on Field Survey.....	26
3.3 Binder Bond Strength (BBS) Test.....	33
3.3.1 Pneumatic Adhesion Tensile Testing Instrument (PATTI) Test	33
3.3.2 Binder Bond Strength Test Methodology.....	35

3.3.3	Failure Modes in PATTI Test	39
Chapter 4.	Numerical Simulation of Pavement Response	41
4.1	Background	41
4.2	Parameters Used in the Numerical Simulations.....	41
4.2.1	Structure Information	41
4.2.2	Material Parameters for Each Pavement Layers	42
4.2.3	Climate Data.....	43
4.2.4	Traffic Data.....	43
4.2.5	Tire-Pavement Contact Pressure Configuration.....	43
Chapter 5.	Test Results and Discussion.....	45
5.1	Interface Shear Strength Results.....	45
5.1.1	Validation of Time-Temperature Superposition Principle for Interlayer System with Tack Coat	48
5.1.2	Effect of Tack Coat Type	49
5.1.3	Effect of Tack Coat Application Rate.....	50
5.1.4	Effect of Loading Rate and Temperature	60
5.1.5	Effect of Normal Confining Pressure	67
5.1.6	Effect of Surface Type	72
5.1.7	Effect of Groove Direction.....	73
5.1.8	Effect of Air Void Content and Compaction.....	81
5.1.9	Statistical Validation of the Effect of Various Parameters on ISS	82
5.2	Binder Bond Strength Test Results	89
5.2.1	Effect of Tack Coat Type.....	89
5.2.2	Effect of Tack Coat Application Rate.....	93
5.2.3	Validation of Time-Temperature Superposition Principle for Binder Bond Strength Using Different Tack Coats.....	96
5.2.4	Comparison of Mastercurves from PATTI Tests of Tensile Strength and Dynamic Shear Modulus of Asphalt Binder	105
Chapter 6.	Development of Tack Coat Selection Criteria.....	107
6.1	Development of Predictive Model for Interface Shear Strength	107
6.2	Development of Predictive Model for Binder Bond Strength.....	113

6.3	Identification of Interface Debonding Potential for Tack Coats Based on Numerical Simulation	114
6.4	Establishing a Universal Relationship between Maximum Shear Ratio and Binder Bonding Strength.....	117
6.5	Developing the MSR Failure Envelope	122
6.5.1	Measuring the Mix Parameter A.....	124
6.5.2	Measuring the BBS	129
6.6	Tack Coat Purchase Criteria	131
6.7	Project-specific Tack Coat Selection Criteria	132
Chapter 7.	Best Practices and Usage of Tack Coats in North Carolina.....	134
7.1	General	134
7.2	Tack Coat Terminology	135
7.3	Tack Coat Materials.....	136
7.3.1	Emulsified Asphalt.....	136
7.3.2	Asphalt Cement (Binder)	137
7.3.3	Cutback Asphalt	138
7.4	Selection of Tack Coat Materials	138
7.4.1	Approved Tack Coat Grades.....	138
7.4.2	Acceptance of Tack Coat Materials.....	139
7.5	Storage and Handling of Emulsions.....	141
7.5.1	Storage of Asphalt Emulsions.....	141
7.5.2	Handling of Asphalt Emulsions.....	142
7.5.3	Sampling of Asphalt Emulsions.....	143
7.6	Tack Coat Construction Practices	144
7.6.1	Surface Preparation and Cleaning.....	144
7.6.2	Tack Coat Application	146
7.6.3	Tack Coat Application Rates	148
7.6.4	Tack Coat Temperature during Application.....	149
7.6.5	Tack Coat Distributor.....	150
7.6.6	Tack Coat Tracking.....	158
7.7	Testing and Acceptance of In-place Tack Coat	160

7.7.1	Assessment of Tack Coat Coverage	160
7.7.2	Assessment of Tack Coat Binder Bond Strength	164
7.8	Method of Payment.....	164
Chapter 8.	Conclusions and Recommendations	165
8.1	Experimental Work.....	165
8.1.1	Interface Shear Strength.....	165
8.1.2	Binder Bond Strength.....	166
8.2	Numerical Simulation	167
8.3	The Minimum Required Binder Bond Strength (BBS).....	167
8.4	Recommendations for Further Research	167
REFERENCES.....		169
Appendix A.	Literature Review	177
A.1.	Factors that Affect Interface Bond Strength	177
A.1.1	Type of Tack Coat Materials	177
A.1.1	Application Rate.....	177
A.1.2	Existing Surface Conditions.....	179
A.1.3	Temperature.....	179
A.1.4	Normal Confining Pressure.....	179
A.1.5	Other Factors	180
A.2.	Debonding Performance Evaluation Methods	180
A.3.	Substantial Literature Review	182
A.3.1	Wisconsin DOT Research.....	182
A.3.2	NCHRP Report 712.....	186
A.3.3	FHWA-OK-18-02 Project.....	187
A.3.4	Research from Louisiana (Das et al. 2017)	189
A.3.5	Research from Illinois (Leng et al. 2008).....	190
A.3.6	Research from China (Hu et al. 2017).....	192
A.3.7	Research from Tennessee (Song et al. 2015)	193
A.3.8	Research from Oregon (Coleri et al. 2020)	193
A.4.	Critical Summary	196

A.4.1	Binder Bond Strength.....	197
A.4.2	Factors That Affect Bond Strength.....	198
Appendix B.	Numerical Simulation.....	203
B.1.	Analysis of Stress Distribution at Interface.....	203
Appendix C.	Test Methodology.....	207
C.1.	Roller Compactor for ISS Test Specimens	207
C.2.	Milling Procedure	208
Appendix D.	Best Practices and Usage of Tack Coats in North Carolina.....	209
D.1.	Section 1020.....	209
D.2.	M&T Form 605.....	211
D.3.	Asphalt Delivery Tickets for Emulsified Asphalt.....	212
D.4.	Temperature-Volume Corrections for Emulsified Asphalt	214

LIST OF FIGURES

Figure I-1. Schematic illustrations for (a) MAST test setup and (b) PATTI test setup.	vi
Figure I-2. Thick pavement section.	vii
Figure I-3. Flow chart for research approach.	viii
Figure 1-1. Field mechanism of bond failures.	1
Figure 1-2. Delamination and exposure of underlying layer. (Source: http://www.defence.gov.au/demg/7technical_guidance/aircraft_pavement_manual/part_a/a4.htm)	2
Figure 1-3. Flow chart for research approach.	4
Figure 2-1. Aggregate gradation of RS9.5B mixture.	8
Figure 2-2. Dynamic modulus mastercurve for RS9.5B.	10
Figure 2-3. Dynamic shear modulus mastercurves for various tack coats.	13
Figure 3-1. Specimen preparation steps: (a) compaction of bottom layer, (b) tack coat application, (c) curing process, (d) placement of the bottom layer in the mold, (e) compaction of top and bottom layers, and (f) completed gyratory-compacted specimens (Cho 2016).	16
Figure 3-2 MAST specimens.	17
Figure 3-3. Illustrations of the Modified Advanced Shear Tester (MAST).	18
Figure 3-4. Gluing procedure of MAST specimen: (a) MAST specimen, (b) glue on steel shoes, (c) specimen laid on half steel shoes, (d) second half of steel shoes on top of specimen, (e) shoe with specimen fastened inside gluing frame, and (f) completed assembly.	18
Figure 3-5. MAST test setup: (a) schematic diagram, (b) loading MAST shoes into loading jig, and (c) test setup with DIC system.	19
Figure 3-6. Digital image correlation analysis of differences between initial image and deformed image (Seo et al.2002).	20
Figure 3-7. Milled surface field cores.	21
Figure 3-8. Two milled surface gyratory-compacted specimens.	22
Figure 3-9. Three-dimensional laser scanner.	22
Figure 3-10. Effects of perpendicularity of field core samples on shear tests.	23
Figure 3-11. Milling machine: teeth details.	24
Figure 3-12. Drilling machine used for artificial milled surfaces.	24
Figure 3-13. Prototype artificial field cores with different groove widths.	25
Figure 3-14. Field milled surfaces on Hillsborough Street, Raleigh, NC.	26
Figure 3-15. Artificial milled surfaces: (a) high, (b) medium, and (c) low walls between grooves.	27
Figure 3-16. 3-D laser profiler on Maynard Rd., Cary, NC.	27
Figure 3-17. Schematic diagram of mean profile depth determination.	28
Figure 3-18. Field-milled surfaces on Maynard Road, Cary, NC.	29

Figure 3-19. Profiles of lab-fabricated milled surfaces (transverse direction): (a) high, (b) medium, and (c) low walls between grooves.....	30
Figure 3-20. Profile depths of actual field-milled surfaces (transverse direction): (a) Field 1, (b) Field 2, (c) Field 3, (d) Field 4, and (e) Field 5.	31
Figure 3-21. Mean profile depths: (a) laboratory milled surfaces and (b) field milled surfaces. .	32
Figure 3-22. 3-D renderings: (a) lab ‘mid’, (b) Field 2, and (c) Field 4.	33
Figure 3-23. (a) Type IV self-alignment adhesion tester (PATTI) and (b) cross-sectional schematic of self-aligning piston assemblies (ASTM D4541-17 (2017)).	35
Figure 3-24. Step-by-step procedure for PATTI testing.	36
Figure 3-25. Test set-up for hot spray gun usage.....	37
Figure 3-26. Metal caps on pull-off stubs to apply setting pressure.	38
Figure 3-27. Stress rates measured using PATTI for rotation and fixed dial conditions.....	39
Figure 3-28. (a) Ideal cohesive failure of binder, (b) mixture of cohesive failure and adhesive failure of the pull stub, and (c) adhesive failure of the pull stub.	40
Figure 4-1 Thick pavement structure used in computational simulations.	42
Figure 5-1. Shear strain measured based on crosshead LVDT and DIC technique for ISS test at 50.8 mm/min, 19°C, 483 kPa confining, and Ultrafuse.....	46
Figure 5-2. Pure power form-fitting method to evaluate strain rate (k') at 50.8 mm/min, 19°C, 483 kPa confining, and Ultrafuse.....	47
Figure 5-3. Verification of t-TS principle for construction of ISS mastercurve.....	48
Figure 5-4. Comparison of shear strength values of CRS-2 and CRS-1h via line of equality.	50
Figure 5-5. Shear strength mastercurves of CRS-2 at various application rates under unmilled condition: (a) 69 kPa, (b) 276 kPa, and (c) 483 kPa.	52
Figure 5-6. Shear strength mastercurves of CRS-2 at various application rates under milled condition: (a) 69 kPa, (b) 276 kPa, and (c) 483 kPa.	53
Figure 5-7. Comparisons of shear strength values of CRS-2 at two different application rates via line of equality: (a) 0.03 gal/yd ² vs. 0.01 gal/yd ² , (b) 0.05 gal/yd ² vs. 0.01 gal/yd ² , and (c) 0.05 gal/yd ² vs. 0.03 gal/yd ²	55
Figure 5-8. Shear strength mastercurves of CRS-1h at various application rates at 483 kPa under milled condition.	56
Figure 5-9. Comparisons of shear strength values of CRS-1h at two different application rates under milled condition via line of equality: (a) 0.03 gal/yd ² vs. 0.01 gal/yd ² , (b) 0.05 gal/yd ² vs. 0.01 gal/yd ² , and (c) 0.05 gal/yd ² vs. 0.03 gal/yd ²	57
Figure 5-10. Variations in interface shear strength with temperature for Ultrafuse specimens fabricated using different tack coat application rates at 483 kPa confining pressure and with an ungrooved interface surface.	58
Figure 5-11. Interface shear strength of CRS-2 (Source 2) applied at various application rates on ungrooved interface surface at (a) 69 kPa confining pressure, and (b) 483 kPa confining pressure.	59

Figure 5-12. Shear strength mastercurves of CRS-2 at various confining pressures under unmilled condition using different tack coat application rates of (a) 0.01 gal/yd ² , (b) 0.03 gal/yd ² , and (c) 0.05 gal/yd ² .	61
Figure 5-13. Shear strength mastercurves of CRS-2 at various confining pressures under milled condition using different tack coat application rates of (a) 0.01 gal/yd ² , (b) 0.03 gal/yd ² , and (c) 0.05 gal/yd ² .	63
Figure 5-14. Shear strength mastercurves of CRS-1h at various confining pressures and 0.03 gal/yd ² application rate under unmilled condition.	64
Figure 5-15. Shear strength mastercurves of CRS-1h at various confining pressures and 0.03 gal/yd ² application rate under milled condition.	64
Figure 5-16. Shear strength mastercurves for Ultrafuse at various tack coat application rates under 483 kPa confining pressure and with an ungrooved interface surface.	65
Figure 5-17. Interface shear strength mastercurves for CRS-2 (Source 2) at various application rates for ungrooved surface at (a) 69 kPa confining pressure and (b) 483 kPa confining pressure.	66
Figure 5-18. Comparisons of shear strength of CRS-2 under unmilled and milled conditions at two different confining pressures via line of equality: (a) 276 kPa vs. 69 kPa, (b) 483 kPa vs. 69 kPa, and (c) 483 kPa vs. 276 kPa.	68
Figure 5-19. Comparisons of shear strength values of CRS-1h at two different confining pressures via line of equality: (a) 276 kPa vs. 69 kPa, (b) 483 kPa vs. 69 kPa, and (c) 483 kPa vs. 276 kPa.	70
Figure 5-20. Effect of confining pressure at application rate of 0.03 gal/yd ² of CRS-2 (Source 2): (a) mastercurve for interface shear strength and (b) at three confining pressure levels.	71
Figure 5-21. Comparison of shear strength values of CRS-2 between milled and unmilled conditions via line of equality.	72
Figure 5-22. Comparison of shear strength values of CRS-1h under milled and unmilled conditions via line of equality.	73
Figure 5-23. MAST specimen loading configuration with different angles of the grooves.	74
Figure 5-24. Interface shear strength mastercurves of NTCRS-1hM for three groove directions/angles and 0.05 gal/yd ² application rate.	74
Figure 5-25. Failed grooved surfaces with different groove orientations at three temperatures and loading rates.	76
Figure 5-26. Comparison of interface shear strength of specimens fabricated using two different compaction methods.	81
Figure 5-27. Comparison of interface shear strength values of specimens made with the same CRS-2 emulsion obtained from two different sources.	82
Figure 5-28. Failure mode of CRS-2 (left) compared to CRS-1h (right) at 5°C.	90
Figure 5-29. PATTI test results for (a) CRS-2 (Source 1) (b) CRS-2 (Source 2), (c) CRS-1h, (d) NTCRS-1hM, and (e) Ultrafuse at 0.14 L/m ² (0.03 gal/yd ²) residual application rate.	93

Figure 5-30. Residual application rate comparison of (a) CRS-2 (Source 1), (b) CRS-1h at 22°C, and (c) NTCRS-1hM at 44°C.	96
Figure 5-31. Mastercurves for (a) CRS-2 (Source 1), (b) CRS-2 (Source 2), (c) CRS-1h, (d) NTCRS-1hM, and (e) Ultrafuse at 0.14 L/m ² (0.03 gal/yd ²) residual application rate.	99
Figure 5-32. Mastercurve comparison of all tack coats tested at 0.14 L/m ² (0.03 gal/yd ²) residual application rate.	100
Figure 5-33. Predicted tensile strength values for (a) CRS-2 (Source 1), (b) CRS-2 (Source 2), (c) CRS-1h, (d) NTCRS-1hM, and (e) Ultrafuse at 0.14 L/m ² (0.03 gal/yd ²) residual application rate along the line of equality for the all-point (AP) method and two-point (2P) method.	104
Figure 5-34. Predictions of tensile strength using all-point and two-point methods for all tack coat materials used in this study.	105
Figure 5-35. Comparison of mastercurves for (a) pull-off tensile strength and (b) dynamic shear modulus values.	106
Figure 6-1. ISS and BBS mastercurves of (a) CRS-2 (Source 1), (b) CRS-1h, and (c) NTCRS-1hM, and (d) Ultrafuse.	109
Figure 6-2 Comparison of interface shear strength values predicted by Equation (30) and actual shear strength data sets for tack coats: (a) CRS-2 (Source 1), (b) CRS-1h, (c) NTCRS-1hM, (d) CRS-2 (Source 2), slab-compacted, and (e) Ultrafuse.	113
Figure 6-3. Shear ratio, shear strength (CRS-2 (Source1)), and shear and normal stress levels in longitudinal direction under central axis of tire at layer interface.	115
Figure 6-4. Typical interface layer shear strain history.	116
Figure 6-5. Typical interface layer shear stress history.	117
Figure 6-6. Flowchart showing step-by-step procedure to establish universal relationship between interface shear strength (ISS) and binder bond strength (BBS).	118
Figure 6-7. Relationship between ISS and BBS for the tack coats considered in this study at various depths in the pavement section: (a) 1 in., (b) 1.5 in., (c) 2 in., (d) 2.5 in., and (e) 3 in.	121
Figure 6-8. MSR failure envelope for different mixtures.	122
Figure 6-9. Change in MSR with depth.	123
Figure 6-10. Interface shear strength variation with cohesion component at different depths for (a) WM-WM and (b) HM-HM.	126
Figure 6-11. Time-temperature shift factor function for different mixtures and tack coats.	127
Figure 6-12 Variation of field shear stress at MSR location for different tack coats.	128
Figure 6-13. Typical variation in confining pressure at MSR location.	129
Figure 6-14. Verification of predicted MSR using various levels of BBS measurements.	131
Figure 6-15. Failure envelope for various AC mixture layers.	132
Figure 7-1. Distress due to improper bonding: (a) debonding and (b) fatigue cracking (FHWA 2016).	134
Figure 7-2. Asphalt binder sampling: (a) typical submerged sampling device and (b) sampling asphalt binder from a tanker.	143

Figure 7-3. Rotary broom eliminating milling debris and loading the truck (courtesy: https://www.forconstructionpros.com/pavement-maintenance/sweepers/article/11237578/how-to-reduce-costly-delays-in-mill-and-fill-asphalt-road-repair).	146
Figure 7-4. Uniform tack application (FHWA 2016).	147
Figure 7-5. Tack coat ‘break’ (FHWA 2016).	148
Figure 7-6. Asphalt distributor (NCDOT 2018a).	150
Figure 7-7. Examples of streaks: “Zebra Tack” or “Corn Rows.”	151
Figure 7-8. Examples of different nozzle sizes for different application rates (FHWA 2016).	152
Figure 7-9. Nozzle orientation: (a) fan coverage for different nozzle orientations and (b) field spraying with different nozzle orientations.	153
Figure 7-10. Recommended angle of emulsion spray from spray bar: (a) top view of distributor spray bar, (b) nozzles on spray bar set at manufacturer’s recommended angle (ground view to spray bar), (c) view of distributor bar from rear of distributor, and (d) typical uniform asphalt distribution (courtesy: https://roadresource.org/treatment_resources/tack_coat?page=about_process).	153
Figure 7-11. Non-uniform tack coat: streaks (Mohammad et al. 2012).	154
Figure 7-12. Spray bar height: (a) fan overlap based on spray bar height (NCDOT 2015) and (b) proper overlap to mitigate effect of clogged nozzle.	155
Figure 7-13. Inappropriate use of spray wand to apply tack coat.	156
Figure 7-14. Calibrating distributor in accordance with ASTM D2995 (2014) (FHWA 2016) using calibration pads: (a) distributor truck spraying tack coat onto calibration pads and (b) detail of sprayed calibration pads.	157
ASTM Method B uses containers that are placed under each nozzle of the spray bar, as pictured in Figure 7-15. The distributor then discharges material into the containers for a set period. The volume of the material in the containers is then calculated. Transverse uniformity of the application can be verified by checking the consistency of the material in each container, and the application rate becomes a function of the truck’s ground speed.	157
Figure 7-16. Calibrating distributor volumetrically (courtesy: http://onlinemanuals.txdot.gov/txdotmanuals/scm/asphalt_distributor.htm#i1007776).	157
Figure 7-17. Tack coat tracking by haul vehicles in work zone (courtesy: https://roadresource.org/treatment_resources/tack_coat?page=about_process).	158
Figure 7-18. Tack coat tracking due to allowed traffic.	159
Figure 7-19. Volume gauges on distributor tanks (NCDOT 2012).	160
The tack coat application rate gauge and temperature gauge, shown in Figure 7-20 (a) and (b), respectively, also should be checked regularly. The tack coat rate must be checked regularly by the DOT technician to determine that the specified amount of tack is being placed. The rate of application may be obtained at intervals by using the total gallons applied divided by the square yards upon which the tack coat is placed. At the end of each operation, a technician must compute the actual rate of the tack coat applied and record this rate on the Asphalt Roadway	

Technician's Daily Report (M&T Form 605). The rate of application should be calculated separately for each individual application or 'shot'. Also, the technician should check the temperature gauge on the outside of the truck for the proper application temperature of the tack coat. 160

Figure 7-21. Distributor gauges: (a) application rate gauge inside distributor truck and (b) temperature gauge on distributor tank (NCDOT 2012). 161

Strapping the distributor is important for pay purposes and also for determining the average asphalt application rate for each shot, which allows for immediate information to be obtained to make adjustments from one shot to the next. The following procedure may be used to strap the distributor. Immediately before and after the asphalt shot, the operator should stop the distributor truck on a level spot such that the tank is as level as possible. Some distributors have a level attached to the tank; if not, then a 3- to 4-foot carpenter's level may be used. The strap stick should be clean so that the level of asphalt can be read easily. The manhole cover at the top of the tank, shown in Figure 7-22 (a), should be opened, and the strap stick inserted into the tank and held as nearly vertical as possible. The strap stick, shown in Figure 7-23 (b), should be lowered into the asphalt until it touches the bottom of the tank. The strap stick then should be removed from the tank. The number of gallons is read at the top of the line that is covered by asphalt. On some distributor models, the strap stick itself is not graduated and must be held against a graduated scale mounted on the side of the tank in order to be read. 161

Figure 7-24. Strapping the distributor: (a) manhole cover on top of distributor tank and (b) strap stick used to measure quantity of asphalt in distributor tank (courtesy: http://onlinemanuals.txdot.gov/txdotmanuals/scm/asphalt_distributor.htm#i1007629). 162

Figure A1. Test devices used in Washington Center for Asphalt Technology research. 181

Figure A2. List of factors and level descriptions for laboratory shear testing study (Bahia et al. 2019). 183

Figure A3. High texture (left) and low texture (right) mixtures (Bahia et al. 2019). 183

Figure A4. Effect of surface texture and application rate at various tack coats: (a) 0.02 gal/yd², (b) 0.05 gal/yd² (Bahia et al. 2019). 184

Figure A5. ANOVA for ISS main factors: (a) trackless included and (b) without trackless (Bahia et al. 2019). 185

Figure A6. Comparison of lab and field ISS for field validation study (Bahia et al. 2019). 185

Figure A7. Effects of residual application rate on ISS for lab-compacted samples (Mohammad et al. 2012). 186

Figure A8. Effects of sample preparation methods on ISS (Mohammad et al. 2012). 187

Figure A9. Mean interface shear bond strengths for the OGFC, sand, and SMA mixtures (Mohammad et al. 2012). 187

Figure A10. Effect of residual application rate on ISS: unaged HMA layer (Ghabchi et al. 2018). 188

Figure A11. ISS values for different surface types and optimum residual application rates of tack coats (Ghabchi et al. 2018).	188
Figure A12. Surface mean texture depths in field projects (Das et al. 2017).	189
Figure A13. Effects of pavement surface type on ISS in all projects (Das et al. 2017).	189
Figure A14. Effect of tack coat material type on ISS in all projects (Das et al. 2017).....	190
Figure A15. Effect of residual application rate on ISS on existing HMA pavement surface in the Florida project (Das et al. 2017).	190
Figure A16. Effects of HMA, tack coat, and tack coat application rate (Leng et al. 2008).	191
Figure A17. PCC surface texture (Leng et al. 2008).	191
Figure A18. Effect of PCC surface texture (Leng et al. 2008).	192
Figure A19. The ISS by different material and application rates at different temperatures: (a) 25 °C and (b) 50°C (Hu et al. 2017).....	192
Figure A20. Effect of underlying layer on shear strength at different temperatures (Song et al. 2015).	193
Figure A21. Average ISS results for all tack coats (Coleri et al. 2020).	194
Figure A22. ISS versus MTD for each tack (Coleri et al. 2020).	195
Figure A23. Milled surface tack response (Coleri et al. 2020).	195
Figure A24. ISS versus application rate for field and lab samples (Coleri et al. 2020).	195
Figure A25. Behavior of pavement layers during bending under different bond conditions: (a) fully bonded, (b) partially bonded, and (c) no bond (Kim et al. 2011).....	198
Figure B1. Shear stress distribution throughout pavement depth at various temperatures (thin pavement, 106.8 kN, 88 km/h, 0.55 braking condition).	203
Figure B2. Critical conditions according to several factors.....	204
Figure B3. Effect of axle load on maximum shear ratio.....	205

LIST OF TABLES

Table I-1. Testing Conditions for MAST Tests	vi
Table 2-1 Shift Factor Coefficients of RS9.5B Mixture Used in the Study	10
Table 2-2. Material Properties of Tack Coats Used in the Current Study	12
Table 2-3. Shift Factor Coefficients of Different Tack Coats Used in the Current Study.....	13
Table 3-1. Interlayer Shear Strength Test Conditions	14
Table 3-2 Air Void Content Data for MAST Specimens	14
Table 3-3. Mean Profile Depth Values of Three Laboratory Milled Surfaces and Five Field Milled Surfaces	32
Table 4-1. Prony Coefficients for Relaxation Modulus.....	43
Table 5-1. Selected Actuator Strain Rate and Corresponding Reduced DIC Strain Rate and Interface Shear Strength.....	49
Table 5-2. <i>P</i> -values Obtained from Multiple Linear Regression Analysis of Effect of Groove Angle on Interface Shear Strength.....	77
Table 5-3. Summary of Major Findings Related to Interface Shear Strength of Milled Pavements	79
Table 5-4. <i>P</i> -value Results for Multiple Linear Regression Model during Iteration and Coefficients of Determination (<i>R</i> ²)	84
Table 5-5. Coefficients of Multiple Linear Regression Model during Iteration.....	85
Table 5-6 Results of Multiple Linear Regression Model for Gyratory-Compacted Specimens...	87
Table 5-7 Coefficients of Interface Shear Strength Prediction Equation Obtained from Multiple Linear Regression Model.....	87
Table 5-8 Results of Multiple Linear Regression Model for Diverse Specimens	88
Table 5-9 Results of Multiple Linear Regression Model for Angle Effect	89
Table 6-1. Coefficients of Interface Shear Strength Prediction Equation for Different Asphalt Layer Interface Conditions at Reference Temperature of 20°C	110
Table 6-2. Coefficients of Interface Shear Strength Prediction Equation for Different Asphalt Layer Interface Conditions at Reference Temperature of 5°C (Cho 2016).....	110
Table 6-3. Coefficients of Binder Bond Strength Prediction Equation for Different Tack Coats	114
Table 6-4. Material Parameter <i>A</i> for Standard Asphalt Mixtures	125
Table 7-1. Abbreviations Used for Typical Emulsion Designations	137
Table 7-2. Nomenclature of Approved Emulsions at NCDOT with Their Corresponding Split-Up Abbreviations (see Table 7-1).....	137
Table 7-3. Storage Temperatures for Asphalt Emulsions (Gierhart and Johnson 2018).....	142
Table 7-4. Application Rates for Tack Coats (NCDOT 2018a)	149
Table 7-5. Distributor Tank Application Temperature Ranges for Tack Coats	150

Table A1. Summary of Agency Tack Coat Specifications (Cross and Shrestha 2005).....	178
Table A2. Recommended Tack Coat Application Rates (Cross and Shrestha 2005).....	179
Table A3. Test Methods: Washington Center for Asphalt Technology Study	182
Table A4. Recommended Application Rates Used by Various Industries	199
Table A5. Different Recommended Curing Times.....	201
Table B1. Maximum Shear Ratios According to Different Conditions.....	205

SYMBOLS AND ABBREVIATIONS

A	=	Constant, asphalt concrete mix material parameter used for maximum shear ratio predictive equation
a_1, a_2, a_3	=	Functions of temperature
a_B, n_B	=	Material parameter constants for binder bond strength predictive equation
A_{cs}	=	Cross-sectional area of specimen, m^2
a_I, b_I, c_I, d_I, e_I	=	Material parameter constants for interface shear strength predictive equation
a_T	=	Time-temperature shift factor
b, c	=	Constants, shape parameters used for maximum shear ratio predictive equation
BBS	=	Binder bond strength, kPa
d	=	Depth of interface from asphalt surface, inches
DIC	=	Digital image correlation
E_∞	=	Equilibrium modulus, MPa
$E(t)$	=	Relaxation modulus, MPa
E^*	=	Dynamic modulus, MPa
E_i	=	Relaxation strength, MPa
F_A	=	Axial force, kN
F_c	=	Confining force, kN
f	=	Loading frequency, Hz
f_R	=	Reduced frequency, Hz
G^*	=	Dynamic shear modulus, MPa
G_g^*	=	Glassy dynamic shear modulus when frequency tends to infinite
ISS	=	Interface shear strength, kPa
k	=	Reduced strain rate at reference temperature
k'	=	Slope of strain vs. time at temperature T
m	=	Number of Maxwell elements
m_e, ν	=	Constant, dimensionless, shape parameter
MPD	=	Mean profile depth, mm
MSR	=	Maximum shear ratio
PATTI	=	Pneumatic Adhesion Tension Testing Instrument
SG	=	shear gap, mm
t	=	time, s
u_{A-act}	=	Actuator-based axial displacement, mm
u_{A-DIC}	=	Digital image correlation-based axial displacement, mm
x_i	=	Independent predictor, or explanatory variable.
\hat{Y}	=	Dependent or response variable

W_A	=	Weight of beaker, rod, and residue, g
W_B	=	tare weight of beaker and rod, g
$\hat{\beta}_i$	=	Regression model parameter
β, γ	=	Constant, material parameters for the sigmoidal function
δ	=	Minimum value of $ E^* $, MPa
$\delta + \alpha$	=	Maximum value of $ E^* $, MPa
ε	=	Strain
ρ_i	=	Relaxation times, s
$\dot{\gamma}$	=	Shear strain rate
$\dot{\gamma}_R$	=	Reduced shear strain rate
γ_{yz}	=	Shear strain in the longitudinal direction under the tire
γ_{xz}	=	Shear strain in the transverse direction under the tire
σ_c	=	Normal confining stress, kPa.
$\dot{\sigma}$	=	Axial stress rate, kPa/s
$\dot{\sigma}_R$	=	Reduced axial stress rate, kPa/s
σ_t	=	Tensile strength / binder bond strength, kPa
$\sigma_{t-crit.}$	=	Critical tensile strength / binder bond strength at 50°C, kPa
τ_s	=	Shear stress, kPa
τ_f	=	Shear strength at the layer interface, kPa
$\tau_{cohesion}$	=	Cohesion component of shear strength, kPa
τ_{yz}	=	Shear stress in longitudinal direction under the tire, kPa
τ_{xz}	=	Shear stress in transverse direction under the tire, kPa
ω	=	Angular loading frequency, Hz
ω_c	=	Constant, location parameter where loss modulus equals storage modulus
ω_R	=	Reduced angular frequency, Hz
ξ	=	Reduced time at reference temperature, s

Chapter 1. Introduction

1.1 Background

The desirable design thickness of surface layers in the flexible pavement is constructed through multiple-layers. The layered construction eases the overall procedure, improves the quality control, and is economical than using a single pavement layer. Prior to paving, the top surface of the existing layer is cleaned to make the surface dust and moisture-free. Further, a thin layer of tack coat is applied to provide a sufficient bond between the new surface and the existing layer. Tack coat is usually in the form of an emulsion or hot binder. For optimal performance, the tack coat should be thin and uniform and should 'break' just before the new asphalt concrete layer/overlay is paved. The process of breaking the emulsion is characterized by the separation of liquid asphalt and water into two separate phases. After the water evaporates, the residual asphalt forms a bond with the underlying surface. For the pavement to be structurally and functionally sound, a proper bond between the structural layers is essential. Lack of interface bonding may lead to several premature distresses because the debonded layers no longer act as a monolithic pavement section. Debonding/delamination occurs at the interface of two asphalt layers when the shear or tensile stress exceeds the shear or tensile strength of the tack coat. Therefore, the prevention of debonding requires a good understanding of the stress that acts on the bonded interface. Figure 1-1 shows the debonding failure mechanism observed in the field. Figure 1-2 exemplifies the delamination of a surface layer with cracking in the underlying layer.

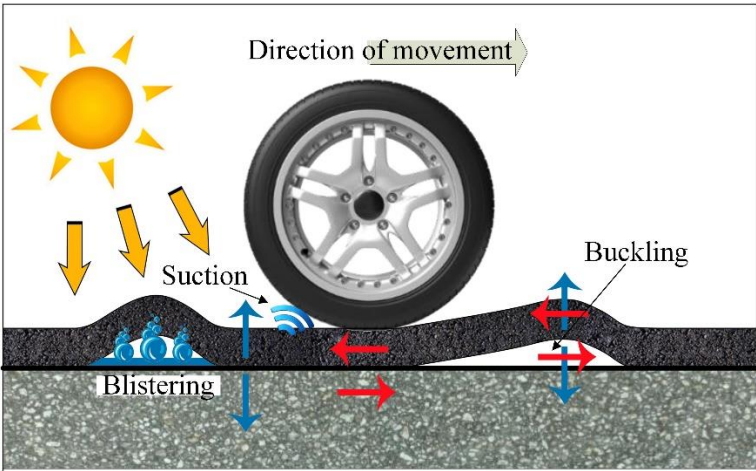


Figure 1-1. Field mechanism of bond failures.



Figure 1-2 Delamination and exposure of underlying layer. (Source: http://www.defence.gov.au/demg/7technical_guidance/aircraft_pavement_manual/part_a/a4.htm)

1.2 Research Needs and Significance

The forensic investigation of the pavement failures in North Carolina apparently shows the occurrence of premature debonding/delamination distresses. The weak bond among the adjacent concrete layers is the contributing factor for such failures (Park 2013, and Tayebali et al. 2004). It is debatable that cracking or debonding occurred first; however, it is clear that the debonding aggravates the rate of pavement failure.

Although there are many numerical analysis tools available to model the asphalt concrete materials, similar attention is not given in modeling and understanding the interface behavior. The current pavement design method lacks a systematic and mechanistic approach in designing the pavement interfaces. Thus, the tack coat selection procedure is based on empirical methods and manufacturers' recommendations (Karshenas 2015).

Two significant factors that ensure adequate bond strength between the pavement layers are a proper tack coat application rate and good tack coat quality. Although control of the tack coat application rate can be achieved through various methods, the minimum tack coat rate that is needed to ensure adequate bond strength for a given situation is currently unknown. The rate required is dependent on material type, interface conditions, structural design, and the service conditions of the pavement in question.

In order to have proper control over the tack coat quality and its application, an evaluation of the effects of various factors on the interface shear strength (ISS) of tack coated applied asphaltic layers need to be studied. Modified asphalt shear tester (MAST), a direct shear test device with normal confinement, is found to successfully mimic the field condition and help to predict the field ISS (Cho 2016). Besides, more research is required to refine and validate a tack coat quality control methodology for various tack coats and conditions in the field. Consequently, a quick and

in-situ test method and selection criteria need to be proposed, that could provide the quality control measurement of tack coats that is set based on rigorous numerical and experimental relations. A comprehensive literature review is reported in [Appendix A](#), and the major research gaps were noted. In summary, a tack coat quality control (QC) program is needed that accounts for the effects of the overlay mixture to be used, the type of the tack coat material and its application rate, and the milling conditions on the debonding potential of asphalt overlay over asphalt pavements.

1.3 Research Objectives and Scope

The primary objective of this proposed research is to develop a set of test procedure and acceptance criterion that can be used in a tack coat quality control (QC) program. ISS and Binder Bond Strength (BBS) were measured from double-layered AC specimens with five different tack coat materials at the interface and tack coat materials, respectively. Several factors that affect ISS, including material type, application rate, surface conditions, temperature, normal pressure, were considered in the ISS testing. Specifically, the application rate, which is the only factor that engineers can readily control to mitigate debonding in asphalt pavements, was evaluated in detail. Moreover, a particular investigation for surface conditions was conducted because surface condition as a factor for ISS is a controversial issue for engineers and contractors.

Numerical analysis of various pavement structures and vehicular loading conditions were performed to calculate the critical stresses that govern the debonding and compared against the predicted ISS of different tack coat in the field to evaluate the debonding potential of each tack coat. Eventually, all the information from the ISS and BBS tests and numerical simulations was used to develop universal relationships between ISS and BBS and between the maximum shear ratio (MSR) versus BBS. These relationships serve the basis for the acceptance criterion for BBS in a tack coat quality control (QC) program.

1.4 Research Approach

The research approach for the current project is outlined in Figure 1-3. This approach eventually aids in finding the minimum required BBS values for acceptance of a tack coat. There are four phases for achieving this goal.

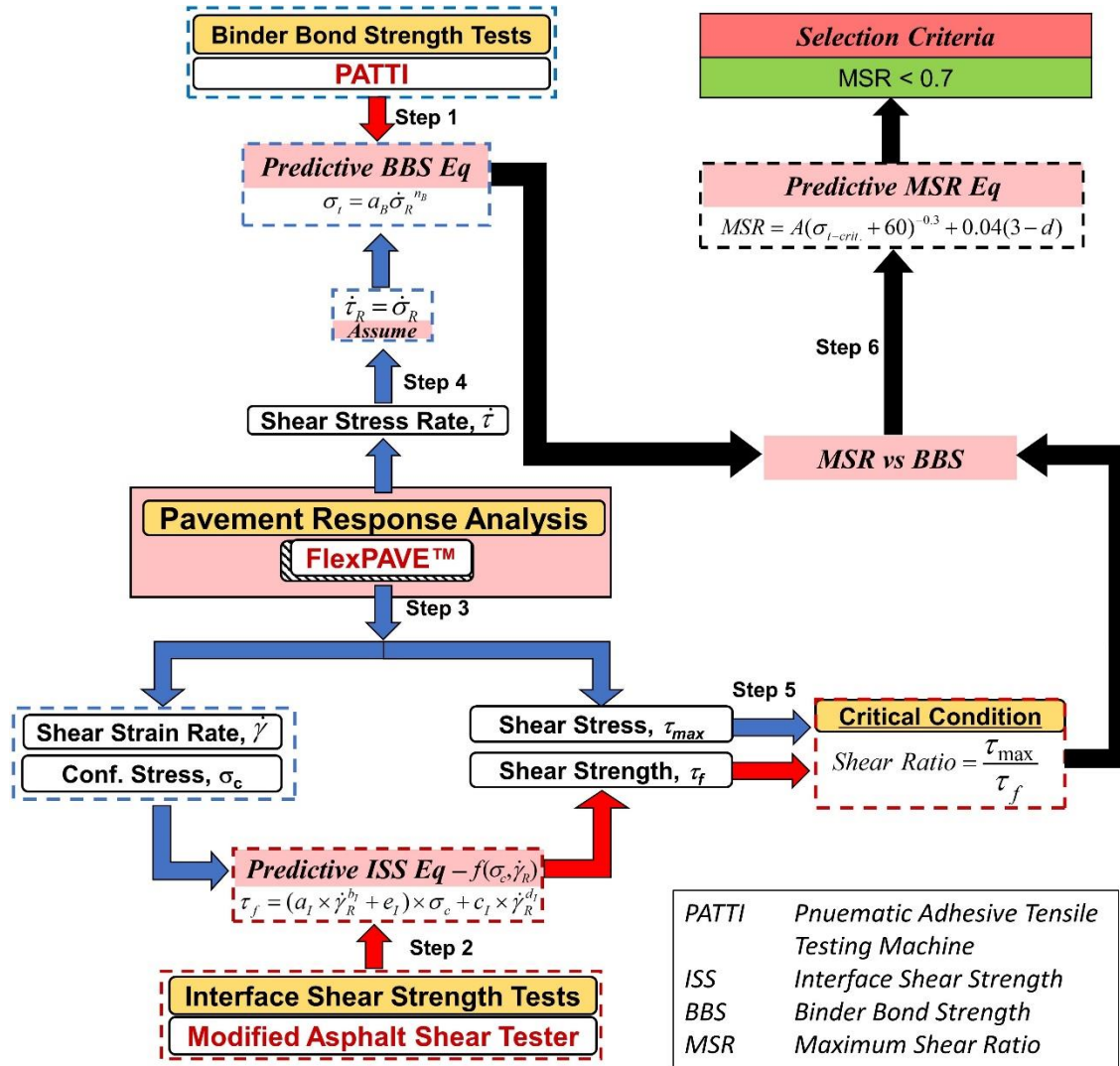


Figure 1-3. Flow chart for research approach.

Phase 1: Development of Predictive Equations for the Interface Shear Strength (ISS) and Binder Bond Strength (BBS) Based on Laboratory Tests.

Phase 1 measures the ISS of double-layered AC specimens with different tack coat materials at the interface using a Modified Asphalt Shear Tester (MAST). The tests were carried out at various confining pressures, temperatures, and strain rates (monotonic). [Chapter 5](#) critically evaluates the outcome of the ISS test results. Analyzing all the outcomes establishes a relation in measuring the ISS based on confining pressure and reduced strain rate, as shown in Equation (4).

$$\tau_f = (a_I \times \dot{\gamma}_R^{b_I} + e_I) \times \sigma_c + c_I \times \dot{\gamma}_R^{d_I} \quad (4)$$

where

$$\tau_f = \text{ISS, kPa,}$$

$\dot{\gamma}_R$ = reduced shear strain rate, and
 σ_c = normal confining stress, kPa.

The parameters a_i , b_i , c_i , d_i , and e_i for all the five tack coats were found and reported in Table 6-1.

Similarly, The BBS test was conducted at 13 different temperatures. Further, the results were successfully used to verify the validity of the time-Temperature superposition principle on the BBS. Consequently, a relationship between BBS and reduced stress rate was derived, as shown in the Equation (5).

$$\sigma_t = a_B \dot{\sigma}_R^{n_B} \quad (5)$$

where

σ_t = BBS,
 $\dot{\sigma}_R$ = reduced stress rates, and
 a_B, n_B = material parameters.

Phase 2: Numerical Simulation of Pavement Response

The pavement response analysis is carried out on a typically found thin pavement structure in North Carolina using a finite element program known as FlexPAVE™. The normal stresses, shear strains, and shear stresses observed at the interface during the analysis were extracted and reported. The details of the numerical simulation results are in [Chapter 2](#).

Phase 3: Identifying the Interface Debonding Potential based on Maximum Shear Ratio (MSR)

The debonding potential of an interface depends on the tack coat material's ability to resist the maximum shear stresses at the interface induced due to vehicular loads. Thereby, the debonding potential is defined by a factor known as the maximum shear ratio (MSR). Shear Ratio is the ratio of shear stress over shear strength along with the interface. The maximum value of the shear ratio along the interface is considered as the MSR and indicator for debonding. If the maximum shear ratio along the interface exceeds one, then the interface fails in shear and debonding occurs.

The maximum shear stresses at the interface are derived from the FlexPAVE simulations, whereas the shear strength of a specific tack coat along the interface in the field is predicted using Equation (4). The normal pressure (confining pressure) and reduced strain rate used in Equation (4) are obtained from the numerical simulations. Thereby, the MSR value for different tack coats was found out for the critical field conditions. The MSR analysis shows that all five tack coats considered for the current study passed the MSR criterion.

Meanwhile, the reduced shear stress rate during simulation aids in predicting the expected BBS using the Equation (2) (Step 4) while the reduced shear strain rate at the same simulation condition

predicts the ISS using Equation (1). These rigorous numerical simulations at numerous field condition aid in establishing a universal relationship between the ISS and BBS irrespective of the tack coat type. The details of this development are provided in [Chapter 6](#). The bridging factors for constructing the universal relationship between the ISS and BBS are the shear strain rate and shear stress rate determined from the numerical simulation.

Phase 4: Evaluating the Minimum BBS Requirement for Tack Coat Acceptance

The universal relationship between ISS and BBS leads to develop a predictive model for MSR as a function of BBS and depth of the interface. Typically, PATTI test procedure recommends carrying out the test at a tensile stress rate within 75 to 150 psi/sec (518 to 1034 kPa/sec). The new test procedure proposed in this study recommends the stress rate ranging between 90 to 115 psi/sec (620 to 792 kPa/sec). The stress rate measured at an interface depth of 3 inches (7.62 cm) from the pavement surface using numerical simulation carried out at 50°C for an 80 kN dual tire vehicle at a speed of 1 mph induces 664 kPa/sec. The field stress rate of 664 kPa/sec falls within the typical stress rate range observed during the BBS tests. Henceforth, the test protocol recommends to carry out the BBS test at 50°C. Further, the MSR predicted at 3 inch (76.2 mm) depth interface is extrapolated by establishing the variation of MSR with the interface depth. Assuming all the tack coats considered for the current study is acceptable for selection, the MSR value less than 0.7 is considered as a reasonable acceptance criterion for any tack coats for the selected warm mix surface layer. If the BBS value measured at 50°C is above 75 kPa then the tack coat can be accepted for purchase. However, for open-graded friction course the cut-off is kept at 750 kPa. The details are provided in [Chapter 6](#).

1.5 Report Organization

[Chapter 1](#) is an introductory chapter that provides background information about the research needs, highlights the importance of proper bonding at the asphalt concrete layer interface, and lists the objectives of this research. [Chapter 2](#) provides the details of materials and their properties used for the current research. [Chapter 3](#) shows different test methods, the experimental program, and the testing methodology used for this research. Information about the materials used for the current study is also presented. It also aids in understanding the various approaches that are used to provide information about milled surfaces in the field. [Chapter 4](#) presents the numerical simulation conditions considered for the current analysis, the material models, and the parameters. [Chapter 5](#) provides a discussion of the test results of ISS and BBS under various conditions and the effects of each influential factor. [Chapter 6](#) explains the step-by-step procedure followed to develop the tack coat selection criteria in detail. It also presents a pavement response analysis that describes the comprehensive distribution of the stress intensity at the layer interface under actual loading conditions. In order to determine the critical conditions, results from the stress distribution analysis conducted using FlexPAVE™ under various conditions are evaluated. [Chapter 7](#) proposes the best practices and usage of tack coats in North Carolina based on extensive review of various

specifications, research reports, articles and the current research experience. [Chapter 8](#) concludes the findings of the current research and the recommendations for the future work. The details of the supportive test results for the respective chapters including literature review are provided in various appendices.

Chapter 2. Materials and Properties

2.1 Asphalt Mixture

The AC material used in the current project for the fabrication of MAST specimens were obtained as loose mix from the Fred Smith Company Knightdale plant in US 64 at Wake Stone Quarry. The procured AC loose mix was designated as RS9.5B where the letter 'R' indicates the presence of reclaimed asphalt pavement (RAP), 'S' stands for the surface mixture on the pavement, the number 9.5 reflects the nominal maximum aggregate size, and 'B' represents the middle level of traffic (3-30 million ESAL). The current mix is categorized by the manufacturer as a warm mix material and Evotherm 3G is used as an additive agent. Besides, it contains 35% of fractionated RAP. The total binder content of the mix is 5.5%. Figure 2-1 presents the aggregate gradation of RS9.5B. The theoretical specific gravity and the bulk specific gravity of the loose mix RS9.5B were measured as per AASHTO T 209-20 (AASHTO 2020a) and AASHTO T 331-17 (AASHTO 2017a) respectively. It is found that G_{mm} for the mix is 2.43 g/cm^3 .

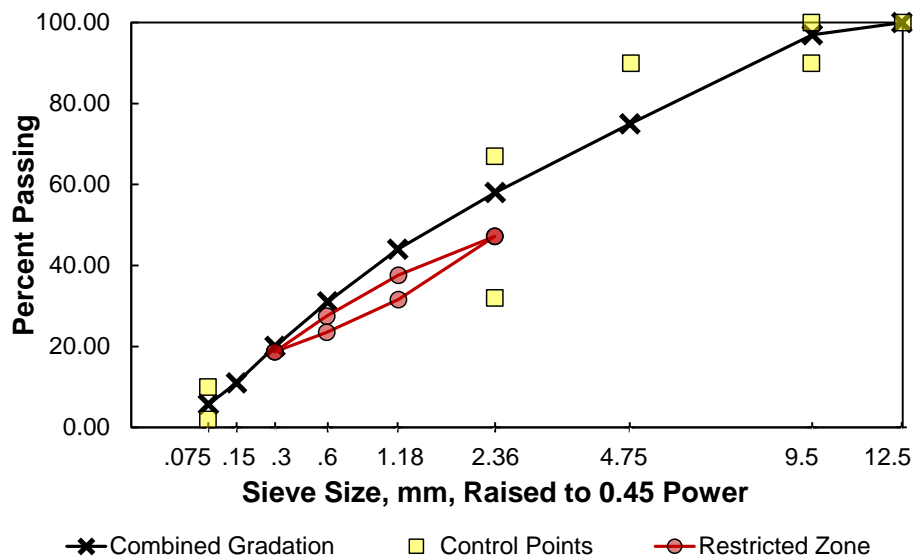


Figure 2-1. Aggregate gradation of RS9.5B mixture.

2.1.1 Dynamic Modulus ($|E^*|$) Test

The linear viscoelastic properties of asphalt concrete mixtures can be determined by dynamic modulus ($|E^*|$) tests that measure a specimen's stress-strain relationship under continuous sinusoidal loading. The parameters obtained are the complex modulus values and time-temperature (t - T) shift factors. Shift factor (a_T) aids in representing the effect of time and temperature by a unique parameter referred to as reduced time/frequency, f_R with Equation (6). Figure 2-2 presents the dynamic modulus test results for three replicates each of the RS9.5B mixtures at different temperature/frequency combinations conducted as per AASHTO TP 132-19 (AASHTO 2019).

The test specimens were 38 mm in diameter and 110 mm high cylindrical specimen cored and cut from a gyratory sample of 180 mm height. The air void of each specimen obtained from gyratory sample was 6%.

An Asphalt Mixture Performance Tester (AMPT) Pro was used as the testing device, and the tests were performed at three temperatures, 4°C, 20°C, and 40°C, and six frequencies, 25, 10, 5, 1, 0.5 and 0.1 Hz. A mastercurve was developed by shifting the data points of each replicate horizontally at an arbitrarily selected reference temperature; in this case, 20°C. Table 2-1 presents the t - T shift factor function coefficients for the mixture obtained while fitting a sigmoidal function (Equation (7)). The Prony series coefficients are obtained by fitting the storage modulus with the function shown in Equation (9) using the collocation method (Park et al. 1996, Schapery 1962).

$$f_R = f \times a_T \quad (6)$$

$$\log|E^*| = \delta + \frac{\alpha}{1 + \frac{1}{e^{\beta + \gamma \log(f_R)}}} \quad (7)$$

$$\log(a_T) = a_1 T^2 + a_2 T + a_3 \quad (8)$$

$$E(t) = E_\infty + \sum_{i=1}^m E_i e^{-t/\rho_i} \quad (9)$$

where

- a_1, a_2, a_3 = regression coefficients,
- a_T = time-temperature shift factor,
- f = loading frequency, Hz,
- f_R = reduced frequency, Hz,
- $|E^*|$ = dynamic modulus, MPa,
- δ = minimum value of $|E^*|$,
- $\delta + \alpha$ = maximum value of $|E^*|$,
- β, γ = material constants describing the shape of the sigmoidal function,
- $E(t)$ = the relaxation modulus, MPa,
- E_∞ = the equilibrium modulus, MPa,
- E_i = the relaxation strength, MPa,
- ρ_i = the relaxation times, s,
- m = the number of Maxwell elements, and
- t = time, s.

An Excel solver developed at NCSU, named as FlexMATTM, automates the above steps, and provide the Prony series representation of relaxation modulus. The output parameters obtained are used as material model property input for the numerical modeling software, FlexPAVETM 1.1.

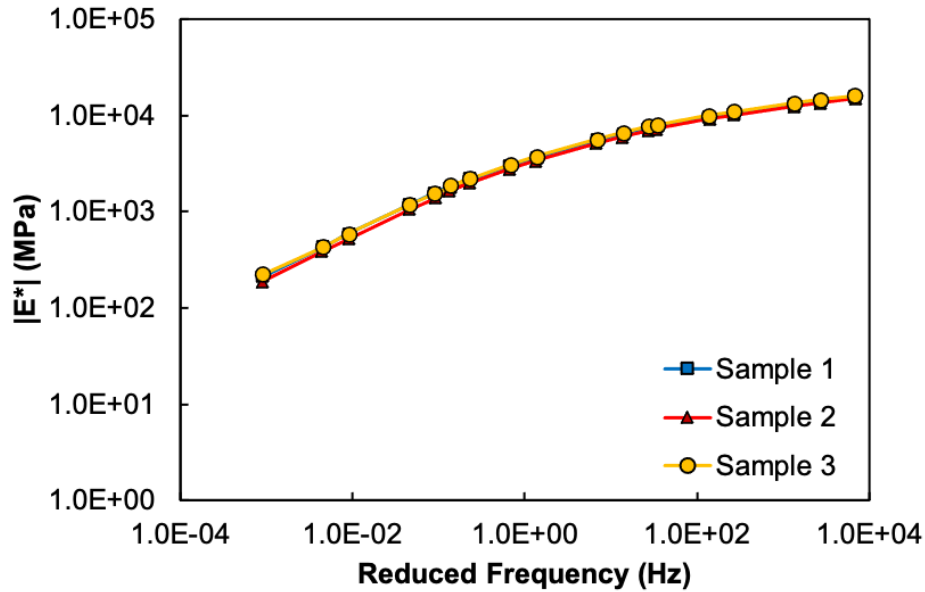


Figure 2-2. Dynamic modulus mastercurve for RS9.5B.

Table 2-1 Shift Factor Coefficients of RS9.5B Mixture Used in the Study

Shift Factor Coefficient	Value
a₁	9.63E-04
a₂	-0.167
a₃	3.084

2.2 Tack Coat

Three emulsion types, CRS-2 (2 sources), CRS-1h and NTCRS-1hM, and one hot binder, Ultrafuse, were selected as tack coat material for the current project. In order to avoid the storage instability, only two out of four tack coat materials (CRS-2 and CRS-1h) were obtained initially. The experimental plan was designed in such a way that the duration from material acquisition to sample testing through fabrication was kept minimal. As the sample fabrication for Interlayer shear strength (ISS) and binder bond strength (BBS) tests using the two tack coats progresses, the remaining three tack coat materials, CRS-2 (Source 2), NTCRS-1hM, and Ultrafuse were acquired.

2.2.1 Residue Recovery of Asphalt Emulsions

The residual application rate for each tack coat was estimated based on the results from residue recovery tests. ASTM D6937-16 (ASTM 2016a) guidelines were followed in this study to recover the residue. The method stipulates heating 50 ± 0.1 grams of asphalt emulsion in an air-forced oven at $163^\circ\text{C} \pm 3.0^\circ\text{C}$ for two hours. Each emulsion was placed inside an oven in 140-mm diameter open beakers made from glass or metal along with a glass rod used for stirring. After two hours,

each beaker was removed from the oven and its contents were stirred thoroughly using the glass rod. The samples were returned to the oven for another one hour and then allowed to cool to room temperature. Finally, the percentage of residue was calculated by weighing the samples using Equation (10).

$$\text{Residue, \%} = 2(W_A - W_B) \quad (10)$$

where

W_A = weight of beaker, rod, and residue (g) and

W_B = tare weight of beaker and rod (g).

2.2.2 Curing Time for Asphalt Emulsions

Breaking and setting are the two stages of the emulsion curing process. During breaking, the dispersed state of the emulsion is altered to its base asphalt binder form; i.e., this phase differentiates the liquid asphalt and water as two different entities. The setting stage allows this separated water to evaporate, thereby curing the emulsion. An evaporation test typically is carried out to determine the curing time that is required for the water to escape by monitoring the water loss with time. In this research, each type of emulsion was placed in an environmental chamber at 25°C for the evaporation tests. The test temperature was determined based on the normal ambient temperature in the North Carolina State University (NCSU) laboratory. Three replicates for each emulsion were prepared and subjected to the same test conditions. The tack coat application rate of 0.181 L/m² (0.04 gal/yd²) was used to distribute the tack coat material uniformly in a 140-mm diameter container at 25°C. The curing time was determined to be when the percentage of water loss reached asymptotic trends, that is, the point at which no more water loss occurred. The curing time of all emulsions were approximately 30 minutes.

2.2.3 Density of Emulsified Asphalt

The density of the emulsified asphalt was determined in order to convert the volume unit per unit area of the tack coat application rate (or the tack coat residual application rate) to the weight unit per unit area. These tests were performed according to ASTM D6937-16 (ASTM 2016a). The density values obtained from these tests and residue recovery outcomes were used to calculate the weight of the tack coat (g) needed to fabricate laboratory samples. Table 2-2 presents the material properties of the study emulsions.

Table 2-2. Material Properties of Tack Coats Used in the Current Study

Property	Unit	Type of Tack Coat				
		CRS-2 (Source 1)	CRS-2 (Source 2)	CRS-1h	NTCRS- 1hM	Ultrafuse (Hot Binder)
Residual Asphalt Content	%	56.91	66.17	53.75	48.15	100
Density	kg/L	1.010	1.010	1.016	1.018	1.014
Base Binder		PG 58-22	PG 58-22	PG 64-22	PG 64-22 Modified	Polymer Modified
Curing Time	Min	30				NA
Residual Application Rate	L/m ²	0.14	0.14	0.14	0.14	0.14
	gal/yd ²	0.30	0.30	0.30	0.30	0.30
Tack Coat Application Rate	L/m ²	0.20	0.19	0.20	0.21	0.14
	gal/yd ²	0.43	0.40	0.44	0.46	0.30

2.2.4 Dynamic Shear Rheometer ($|G^*|$) Test

The DSR measures the dynamic shear modulus ($|G^*|$) and determines the t-T shift factors of asphalt binders. The DSR model used in the current study is an Anton Paar MCR 302. The MCR 302 is a user-friendly device that is capable of reaching wide temperature ranges, as low as -160°C to as high as 1000°C in minutes, for any type or combination of rheological tests. These mechanical tests were performed as frequency sweep tests at 5°C, 20°C, 35°C, 50°C, and 64°C. The loading frequency ranged from 0.1 Hz to 30 Hz at 1% shear strain amplitude. The frequency sweep tests were designed to enable the construction of mastercurves of the dynamic shear modulus values and to obtain t-T shift factors for the binder and emulsion residue used in this study. The asphalt residue used for DSR testing was recovered according to AASHTO R78-16 (AASHTO 2020b) Method B.

Analysis of DSR test outcomes is a simple process due to the long-established standards and practice of the device. If the results of any two tests of the same emulsion type exceed the recommended 6.4% difference specified in AASHTO T315-12 (AASHTO 2020c), then neither results should be used and the emulsion must be retested. In this study, the results from the DSR tests were averaged per each emulsion and input into a mastercurve template builder using an Excel spreadsheet. This Excel spreadsheet uses the dynamic shear modulus, frequency, and temperature from the DSR tests to calculate the shift factors for each emulsion by fitting the data points to the Christenson–Anderson–Marasteanu (CAM) model (Christensen and Anderson 1992) at a reference temperature, as given in Equation (11). The general form of the t-T shift factor equation is shown in Equation (12), where $|G^*|_g$ is the glassy dynamic shear modulus and is equal to 1 GPa for asphalt binder. ω_c , m , and ν are the CAM model fitting parameters for the $|G^*|$ mastercurve. Equation (12) describes the reduced frequency, ω_R , where a_T is the shift factor at temperature T and ω is the actual testing angular frequency.

$$|G^*|(\omega_R) = |G^*|_g \left[1 + \left(\frac{\omega_c}{\omega_R} \right)^\nu \right]^{-\frac{m_e}{\nu}} \quad (11)$$

$$\omega_R = a_T \times \omega \quad (12)$$

where

$|G^*|$ = dynamic shear modulus,

$|G^*|_g$ = glassy dynamic shear modulus when frequency tends to infinite,

ω_c = constant, location parameter where loss modulus equals to storage modulus, and

m_e, ν = constant, dimensionless shape parameter.

Table 2-3 presents the shift factor coefficients for each emulsion in this study that were measured at the reference temperature of 20°C. Figure 2-3 shows the master curve for dynamic shear modulus for various tack coats.

Table 2-3. Shift Factor Coefficients of Different Tack Coats Used in the Current Study

Shift Factor Coefficients	CRS-2 (Source 1)	CRS-2 (Source 2)	CRS-1h	NTCRS-1hM	Ultrafuse
a1	7.82E-04	1.40E-12	7.68E-04	7.12E-04	2.94E-04
a2	-0.146	-0.134	-0.150	-0.160	-0.116
a3	2.618	2.675	2.701	2.913	2.198

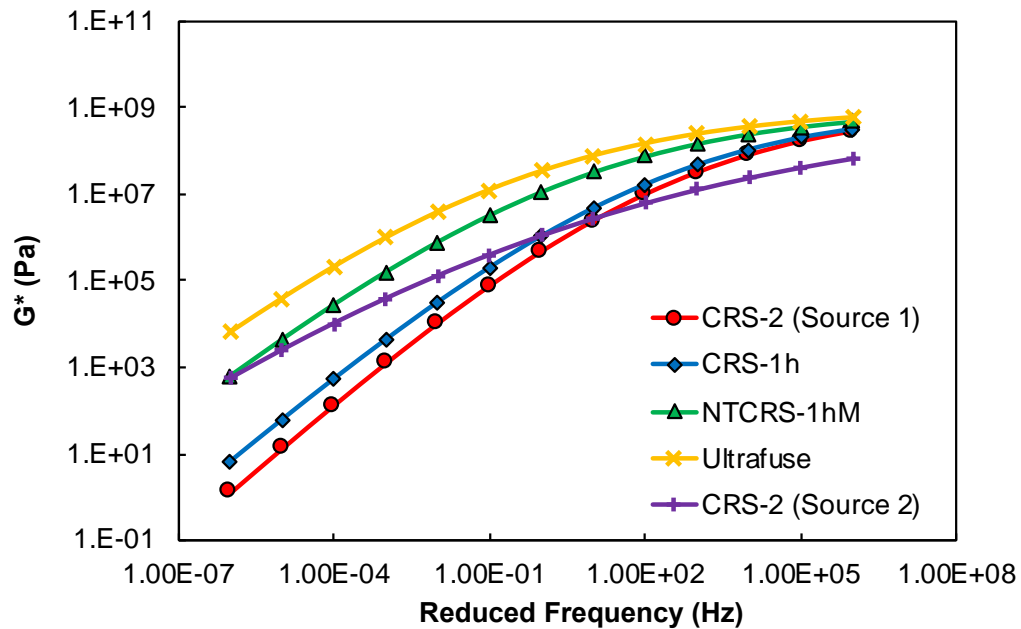


Figure 2-3. Dynamic shear modulus mastercurves for various tack coats.

Chapter 3. Test Methodology

3.1 Interlayer Shear Strength (ISS) Test

Five different tack coat materials were tested for ISS under various test conditions. Modified Asphalt Shear Tester (MAST) is employed to measure the ISS of various tack coat interfaces. All the MAST specimens were loaded in monotonic mode in shear to investigate the effects of temperature, loading rate, confining pressure, application rate, and surface conditions on the ISS of the materials. Table 5.2 presents the factors and parameters that were used to create the various ISS test conditions.

Table 3-1. Interlayer Shear Strength Test Conditions

Factors	Number of Levels
Tack Coat	2 (CRS-2, CRS-1h, NTCRS-1hM, Ultrafuse and CRS-2 (Source 2))
Temperature	4 (5°C, 19°C, 35°C, 53°C)
Loading Rate	3 (0.02, 0.2, 2 in./min)
Confining Pressure (Normal Stress)	3 (69, 276, 483 kPa)
Application Rate (Residual)	3 (0.01, 0.03, 0.05 gal/yd ²)
Surface Condition	2 (Unmilled, Milled)
Compaction Method	2 (Gyratory, Slab)

3.1.1 Laboratory Fabrication of MAST Specimens

Several steps are involved in the fabrication of double-layered MAST specimens. A detailed study on air voids was carried out on MAST specimens to find the optimal mass of AC to achieve 6% air voids for the top and bottom layers. Table 3-2 shows the results of the air void study.

Table 3-2 Air Void Content Data for MAST Specimens

Design Air Void (%)	Layer	Dimension (mm)		
		150 (D) × 50.8 (H)*	150 (D) × 50.8 (H)*	101.6 (D) × 38.1 (H)
7.5	Bottom	6.8	6.4	6.1
	Top	-	7.4	6.4
8.0	Bottom	7.3	6.8	6.7
	Top	-	7.7	6.8

The initial step of specimen fabrication is to make the MAST samples. The necessary quantity of AC for the respective layers (top/bottom) was batched and heated to the compaction temperature [145°C (293°F)]. The gyratory compaction molds were heated to 155°C (311°F). The primary stage is to create a one-layered cylindrical sample that is 150 mm (6 in.) in diameter and 50.8 mm (2 in.) in height. Typically, a cooling period of 24 hours is allowed before the application of a tack

coat. Further, a tack coat is applied uniformly to achieve a consistent thickness on the top of the bottom layer. A foam brush is used to spread the emulsified asphalt above the bottom layer while a metal canister with a perforated cap was used to pour the hot binder (application rates are reported in Table 3-1). The hot binder was spread at the interface using a spatula and a hot gun. If the tack coat used is an emulsified asphalt, then the tack coat is allowed to cure. A curing period of 30 min to 1 hour is ideal before proceeding to the top layer compaction. During the curing period, the water evaporates, leaving the residual asphalt on the surface. If a hot asphalt is used as a tack coat, then no curing period is required. After curing, the bottom layer with the tack coat layer on the top is placed into the gyratory mold again. The same compaction process that was followed for the bottom layer is repeated on top of the bottom layer in order to produce the upper AC layer that also has a thickness of 50.8 mm (2 in.). Thus, the final MAST sample of 150 mm (6 in.) diameter and 101.2 mm (4 in.) height is produced. The presence of air void gradient along the sample periphery in contact with the hot mold is well known (Chehab et al. 2000). Henceforth, to maintain a consistent air void distribution throughout the specimens, the samples were cored and cut to a height of 76.2 mm (3 in.) and a diameter of 101.6 mm (4 in.) before testing. Figure 3-1 and Figure 3-2 show the sample preparation steps (Cho 2016) and the final MAST specimens, respectively.



(a)



(b)



(c)



(d)



(e)



(f)

Figure 3-1. Specimen preparation steps: (a) compaction of bottom layer, (b) tack coat application, (c) curing process, (d) placement of the bottom layer in the mold, (e) compaction of top and bottom layers, and (f) completed gyratory-compacted specimens (Cho 2016).



Figure 3-2 MAST specimens.

3.1.2 Modified Advanced Shear Tester (MAST)

The MAST was designed to investigate the shear properties of uniform asphalt mixtures as well as interlayer interfaces. A thorough study about the pros and cons of the existing interface direct shear testing devices around the globe was carried out by the previous researchers at NCSU. Further to which a rigorously designed shear testing device was developed, tagged as modified asphalt shear tester (MAST), that address the problems inherent to many of the current devices used for shear testing. Figure 3-3 presents illustrations of the MAST, which is a direct shear apparatus that is capable of testing 6-inch and 4-inch square specimens as well as 4-inch diameter cylindrical specimens for direct shear. This device can perform not only a simple shear bond strength test but can also test for shear fatigue resistance under different loading and environmental conditions (i.e., load- or displacement-controlled mode at various temperatures).

The initial step in the MAST test set-up is to glue the specimen, shown in Figure 3-4(a) to steel shoes using Devcon steel putty. Each steel shoe has grooves to provide a sufficient bond between the shoe and the specimen, as shown in Figure 3-4(b). Extreme care was taken to clean the shoes before each glue application to prevent failure at the glued area. A special guiding frame was employed to ensure proper alignment of the specimen during gluing, thus minimizing any eccentricity that might occur during the test. Figure 3-4(c) show the specimen placed in the shoes. Once the specimen was properly glued into the shoes, it was cured for 24 hours.

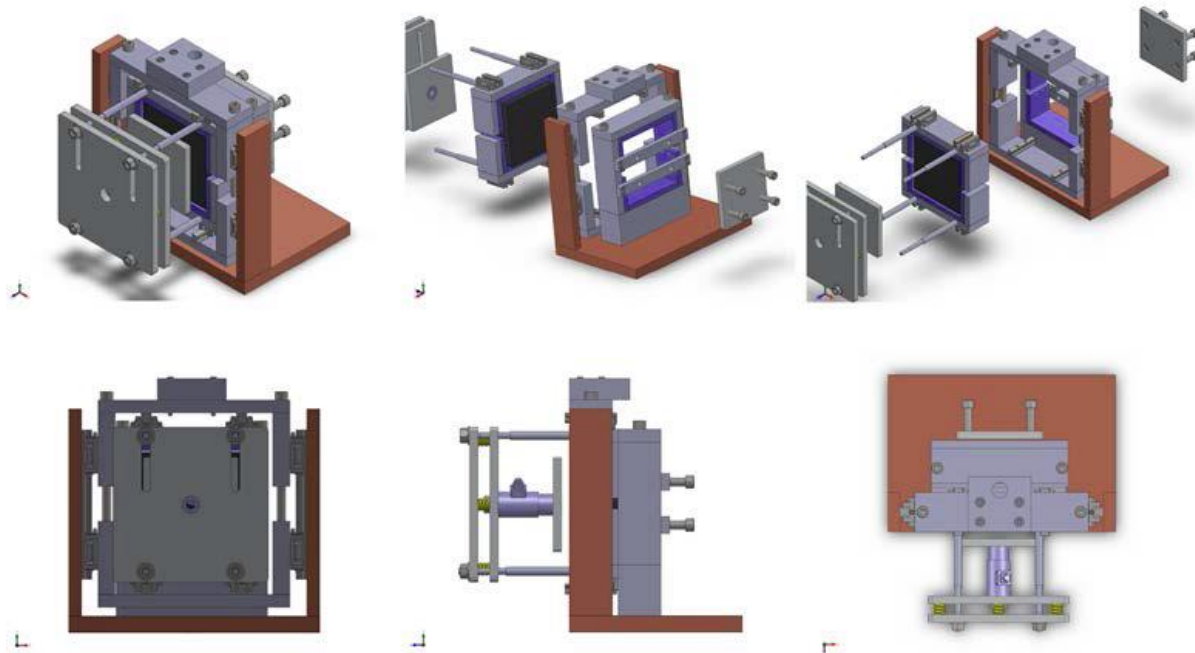


Figure 3-3. Illustrations of the Modified Advanced Shear Tester (MAST).

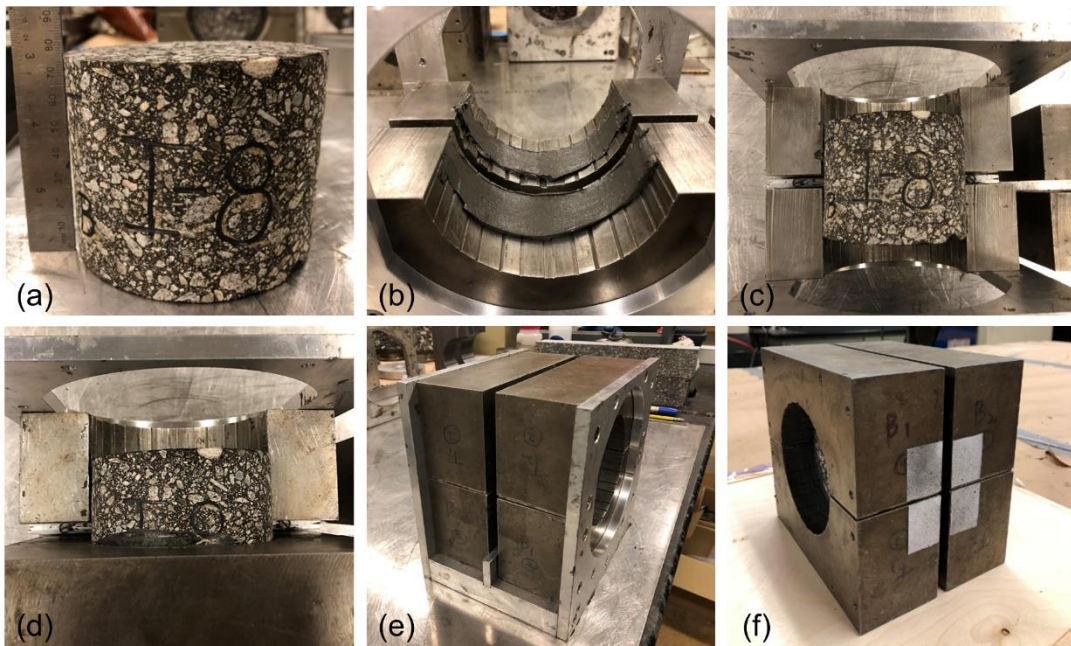


Figure 3-4. Gluing procedure of MAST specimen: (a) MAST specimen, (b) glue on steel shoes, (c) specimen laid on half steel shoes, (d) second half of steel shoes on top of specimen, (e) shoe with specimen fastened inside gluing frame, and (f) completed assembly.

The MAST consists of a loading jig, which is a metal box frame bisected into two sections separated by a gap of 8 mm. One section of the loading jig is fixed while the other side is movable. The movable side is free to travel vertically (parallel to the interface) as well as horizontally

(perpendicular to the interface). This unconstrained movement is provided by linear roller tracks. One of the distinctive features of the MAST is that the initial normal confining stress that is applied to a specimen can be controlled by tightening a set of bolts while simultaneously monitoring the load level using an in-line load cell. This application method for normal confining stress was inspired by Adam Zofka’s shearing device (Zofka et al. 2015), the Advanced Shear Tester.

Figure 3-5 shows the specimen in the loading shoes being mounted and fastened to the MAST loading jig through multiple screws. Once the MAST with specimen is ready, the jig is installed to the MTS machine allow for temperature conditioning. The specimens were conditioned at the respective test temperature for at least three hours before testing. A closed-loop feedback climatic chamber, fueled with liquid nitrogen as the coolant, was employed to control and maintain a constant temperature during conditioning and testing. After which the ISS test is commenced at a specific displacement amplitude planned as per the experimental design.

Figure 3-5 also shows the speckled paper and opening that are used in the digital image correlation (DIC) set-up, and Figure 3-5 shows the lighting and camera used in the DIC system to capture images of the MAST specimen.

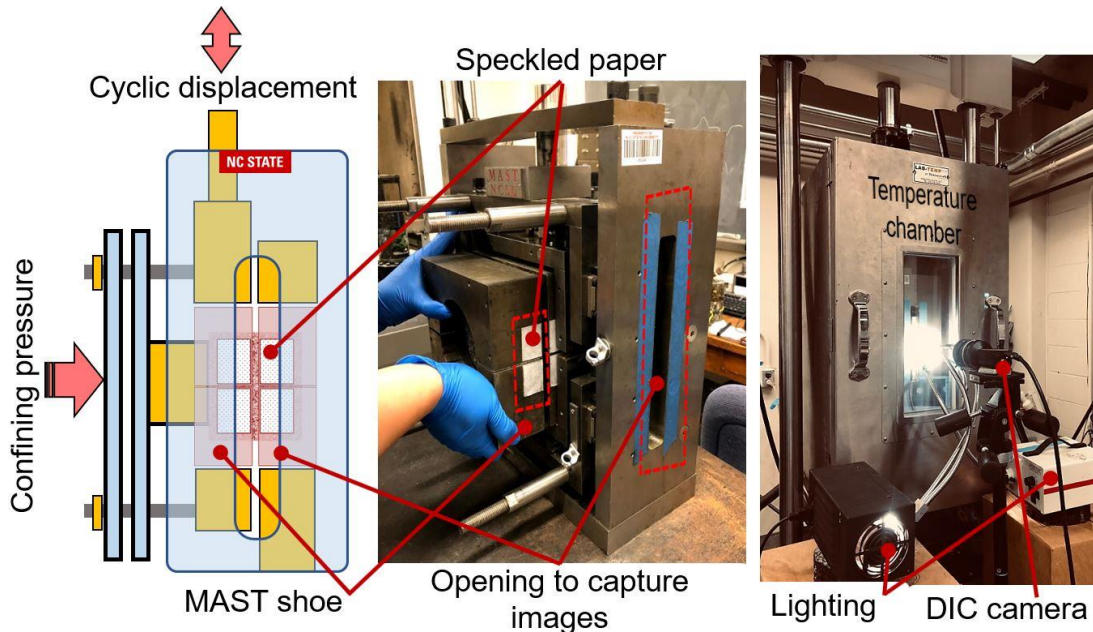


Figure 3-5. MAST test setup: (a) schematic diagram, (b) loading MAST shoes into loading jig, and (c) test setup with DIC system.

3.1.3 Digital Image Correlation (DIC) Technique

Even though the principle behind a monotonic asphalt shear test is simple, the MAST is a sophisticated device. It has numerous components that must be assembled and disassembled during specimen loading and unloading. The major challenge during MAST testing is to ensure that

shearing occurs only along with the interface, which is achieved by securely attaching shoes to the jig through threaded bolts and screw fasteners. Even then, the moment that is induced on the shoe is so high during the test that it causes a rocking action. The degree of the rocking movement depends on the temperature at which the analysis is carried out, thus indicating that the cause of the rocking is a machine compliance issue. Furthermore, many connections and bearings are located between the actuator and the MAST, which also adds deformation to the actuator linear variable differential transformer (LVDT) measurements. At a glance, an on-specimen LVDT should be a quick solution, but the rocking action makes those measurements inaccurate. Hence, the on-specimen displacement of the shear test is measured using an external non-contact DIC system.

A digital image correlation (DIC) system can be employed to compute the relative displacements and strains at the layer interface through the comparison of images of a deformed specimen with the images of an initial, undeformed reference specimen using advanced mathematical techniques. To implement the DIC analysis of the differences between the initial image and the deformed images, the undeformed reference image is divided into small subsets, and then the corresponding locations of these subsets in the deformed images are tracked by matching their grayscale pixel levels, as shown in Figure 3-6. By tracking the location of the subsets, the horizontal and vertical displacements of the center point of each subset in the pixels can be determined at different stages in the testing (Seo et al. 2002).

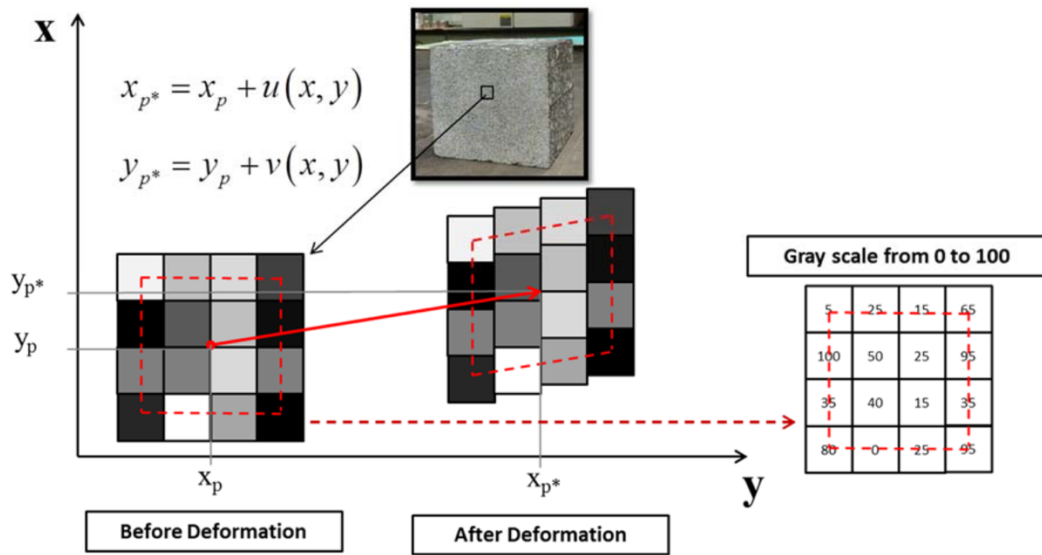


Figure 3-6. Digital image correlation analysis of differences between initial image and deformed image (Seo et al.2002).

The DIC system set-up includes a 5-megapixel camera along with a 35–75 mm f: 3.3–4.5 manual focus lens to capture images. Two dual-fiber optical gooseneck lights were used to provide consistent, cool, and sufficient lighting on the specimen surface. An adjustable tripod stand with

built-in bubble levels was used to level the camera and place it at an approximate distance of 75 cm from the specimen and at the same height and lateral position as the specimen. A relatively high shutter speed of 1.5 ms was used to prevent blurry images. An f-stop of 3.3, which is a relatively wide lens aperture size, was used to let in the maximum possible light to hit the camera sensor. A relatively low gain setting close to -3.9 db was used to prevent unwanted image noise. The DIC camera was connected to a computer that was installed with two commercially available DIC software packages developed by Correlated Solutions, Inc: Vic-Snap and Vic-2D. Vic-Snap is used to acquire images during testing and also aid in controlling the camera shutter speed, position, and lighting levels. VIC-2D is two-dimensional DIC analysis software that is used to calibrate the scale, analyze the captured images, and calculate the displacements and strains through comparisons of images using advanced mathematical algorithms. Key aspects and details regarding DIC analysis can be found in Safavizadeh and Kim (2017).

3.2 Understanding the Milled Pavement Surface and Fabrication in Laboratory

3.2.1 Field Core Milled Specimens

Surface condition of pavements, milled and unmilled surfaces, is one of the factors considered in this research project. Therefore, a few field core samples were obtained as part of the project. Further, the top layer was fabricated following the procedure detailed in Section 3.1.1. Figure 3-7 shows the two milled surfaces with different shapes, heights, and widths of grooves. At first, these differences were considered to be ignorable, but after the fabrication of the milled surface specimens, these differences led to different volumes of the samples and thus two different test specimens.



Figure 3-7. Milled surface field cores.

Also, when the same amount of top layer material was applied on two different milled bottom layers to achieve the same height of the top layers, the density values of these two top layers were

completely different. Visual observation of the two specimens shows that asphalt binder from specimen no 2 has extruded out of specimen indicating excess compaction, hence, different density as shown in Figure 3-8.



Figure 3-8. Two milled surface gyratory-compacted specimens.

Following the fabrication of specimens using milled surface field core samples, the need to obtain more information about milled surfaces emerged. Given the difficulties that were encountered for precise specimen fabrication, a three-dimensional (3D) laser scanner, depicted in Figure 3-9, was utilized to measure specific information about the milled surfaces. Typically, a 3D laser scanner is used to measure the rut depths of a pavement. Although many efforts have been tried to obtain information about milled surfaces, until now, the 3D laser scanner method has been considered as the best way to estimate mill surface measurements. However, this method offers almost no consistency, and the surfaces of the field core samples show significant variation.

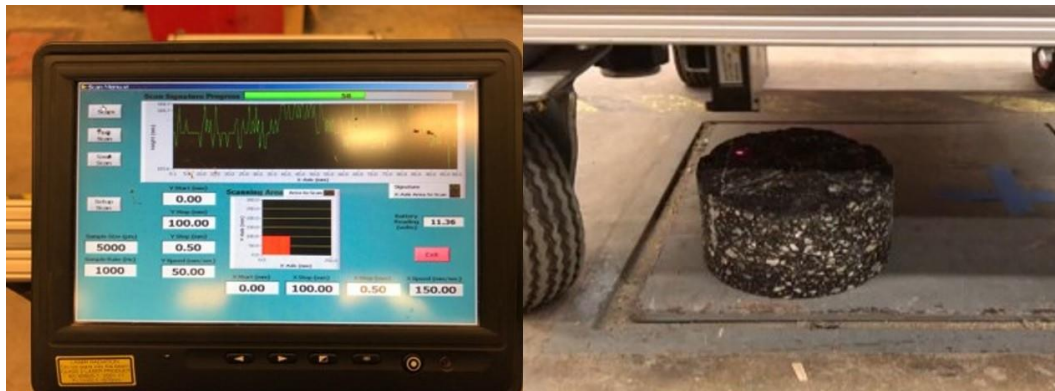


Figure 3-9. Three-dimensional laser scanner.

The investigation using the 3D laser scanner was focused on the milled surfaces of field core samples because the milled surface affects the specimen fabrication process and was expected to affect the test results also. The 3D laser scanner was used to measure the milled surfaces, but the uncertainties surrounding the sample geometries and inconsistency of the grooves led to skepticism about using field cores. The main concern came from the observation that the milled surface was not perpendicular to the side of the field core. This problem would cause the shear loading plane, which is perpendicular to the side of the core, not to be even with the interface of the milled surface and overlay. Figure 3-10 shows that field core samples that do not have perpendicular geometries can affect the results of shear tests.

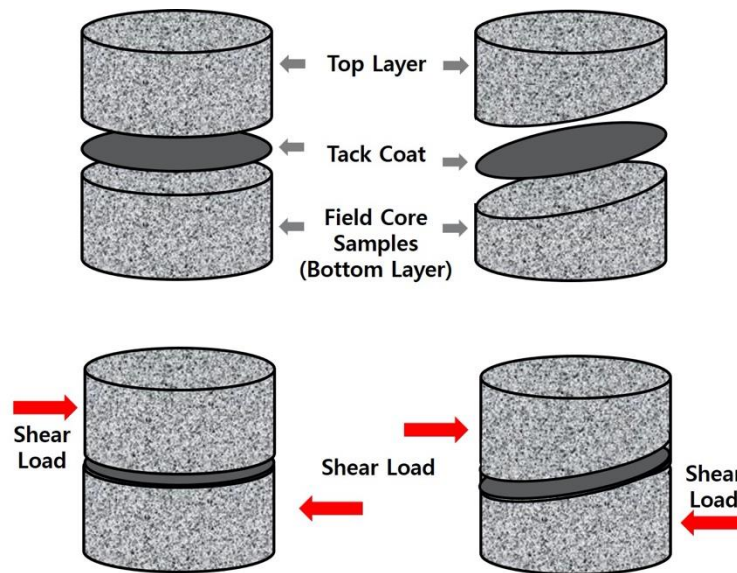


Figure 3-10. Effects of perpendicularity of field core samples on shear tests.

The texture or perpendicularity of a milled surface can significantly impact the fabrication of a specimen and even the shear strength test results. An alternative to field core samples tries by producing an artificial milled surface in the laboratory that mimics the actual milled surfaces of field core samples. This artificial surface has more consistent grooves on the surface and also guarantees perpendicularity between the top and side surfaces.

3.2.2 Milling Machine

To make the artificial milled surfaces as similar as possible to actual milled surfaces, the NCSU research team visited a milling machine company, Delta, to obtain information about the milling process. Figure 3-11 shows details of a milling machine, in particular the teeth that determine the texture of the milled surface. Each tooth rotates to prevent one-sided wear or uneven wear. When the teeth contact the surface for milling, they are at acute angles, not right angles, to the pavement surface. Usually, milled pavements have grooves that are wider than a tooth width, which has a range of 10 mm to 13 mm (0.4 in. to 0.5 in.). The distance between the centerlines of two teeth is 5/8 inch.



Figure 3-11. Milling machine: teeth details.

3.2.3 Artificial Milled Surface Prototype Based on Field Cores

In order to fabricate an artificial milled surface bottom-layer sample, the drilling machine shown in Figure 3-12 was chosen because it has a mechanism that makes a groove using a rotation that is similar to that found in the Delta milling machines. The machine shown in Figure 3-12 is able to make rounded grooves using round-tip drill bits that are similar to the grooves made by a milling machine. Figure 3-13 presents specimen prototypes with different groove widths.



Figure 3-12. Drilling machine used for artificial milled surfaces.

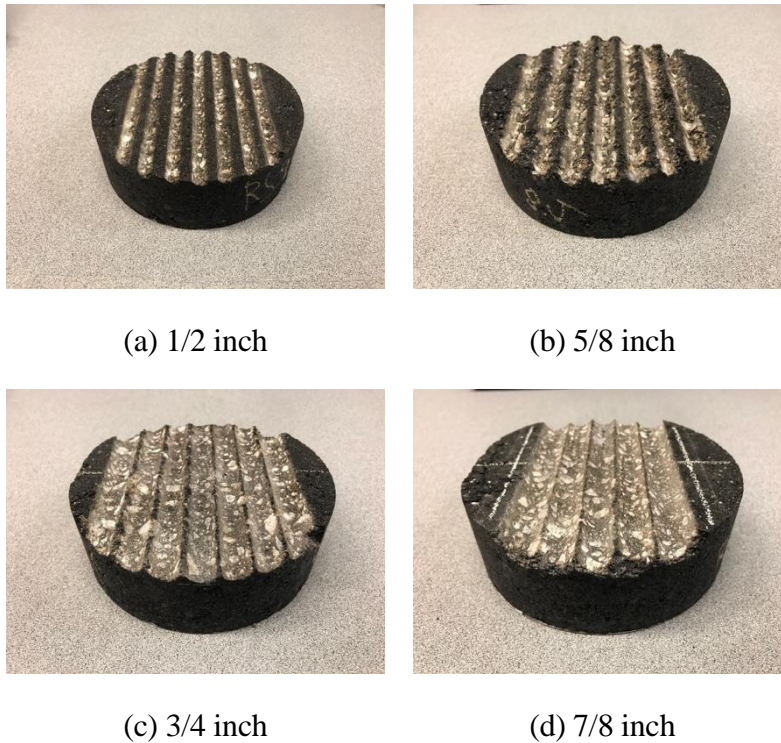


Figure 3-13. Prototype artificial field cores with different groove widths.

Using field core samples is considered the best way to reflect field conditions and real pavements, but it involves many uncertainties and possibly large variations. Laboratory-milled samples would reduce the variations in the test results; however, whether the shear strength measured from such laboratory-milled samples is representative of the shear strength of field cores remains in question.

3.2.4 Field Milled Surface Investigation

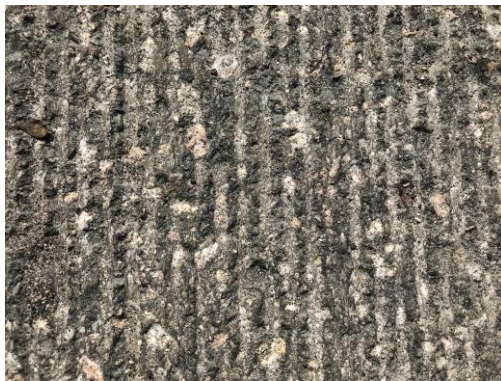
The investigation into milled surfaces utilized the Hillsborough Street pavement construction project in Raleigh, NC, as the milled surface field. The surface grooves were almost the same width as the distance between the centerline of two teeth in the milling machine. However, the actual groove width of approximately 3/8 inch was narrower than the tooth width, which has a range of 0.4 inches to 0.5 inches. Importantly, no asphalt binder material was evident on top of the walls that separated two grooves because the milling machine obviously and randomly crushed the top of the walls. Figure 3-14 shows the overall conditions and texture of the Hillsborough Street milled surfaces.



(a)



(b)



(c)



(d)

Figure 3-14. Field milled surfaces on Hillsborough Street, Raleigh, NC.

3.2.5 Artificial Milled Surface Prototypes Based on Field Survey

Based on the Hillsborough Street field investigation, the NCSU research team fabricated new versions of an artificial milled surface bottom-layer sample. The previous samples could have any amount of asphalt binder material on top of the walls between the grooves and appeared as a new pavement surface with the grooves full of asphalt binder material. However, the actual field- milled surface on Hillsborough Street did not have much asphalt binder material on the top of the walls between the grooves. So, the NCSU research team made additional prototypes with various heights of groove walls; Figure 3-15 (a), (b), and (c) present these prototypes with high, medium, and low walls, respectively.



(a)

(b)

(c)

Figure 3-15. Artificial milled surfaces: (a) high, (b) medium, and (c) low walls between grooves. A visual inspection of the surface conditions of the Hillsborough Street field pavement was unable to validate the intended similarity of the laboratory-fabricated samples to the actual milled surface. In order to obtain accurate texture depth measurements, a second investigation was conducted at a pavement construction site at Maynard Road in Cary, NC to inspect the pavement's milled surface using a 3-D laser profiler, as shown in Figure 3-16. This profiler employs the innovative RoLine line laser, produced by LMI Selcom. This laser has been used successfully in developing RoboTex, a 3-D laser sensor for measuring the surface texture of concrete pavement, as part of a research effort under the sponsorship of the Federal Highway Administration. The RoLine laser measures the distance between the laser sensor and pavement surface in both the longitudinal and transverse directions and produces a 3-D map of the pavement's surface texture (Kim and Adams 2011). Thus, by using this 3-D laser profiler, the NCSU research team was able to obtain more accurate field data about the surface texture and then could measure the mean profile depth (MPD), a parameter that indicates a pavement's surface condition.



Figure 3-16. 3-D laser profiler on Maynard Rd., Cary, NC.

Mean Profile Depth Definition

The MPD represents the exposed texture depth of a pavement surface. Transit New Zealand (2005) defines the MPD as expressed here by Equation (13):

$$MPD = \frac{\text{Peak level (1st)} - \text{Peak level (2nd)}}{2} - \text{Average level} \quad (13)$$

Figure 3-17 schematically explains the variables used in Equation (13). In the diagram, the MPD clearly indicates the roughness (i.e., macro-surface texture) and exposure depth of the milled surface.

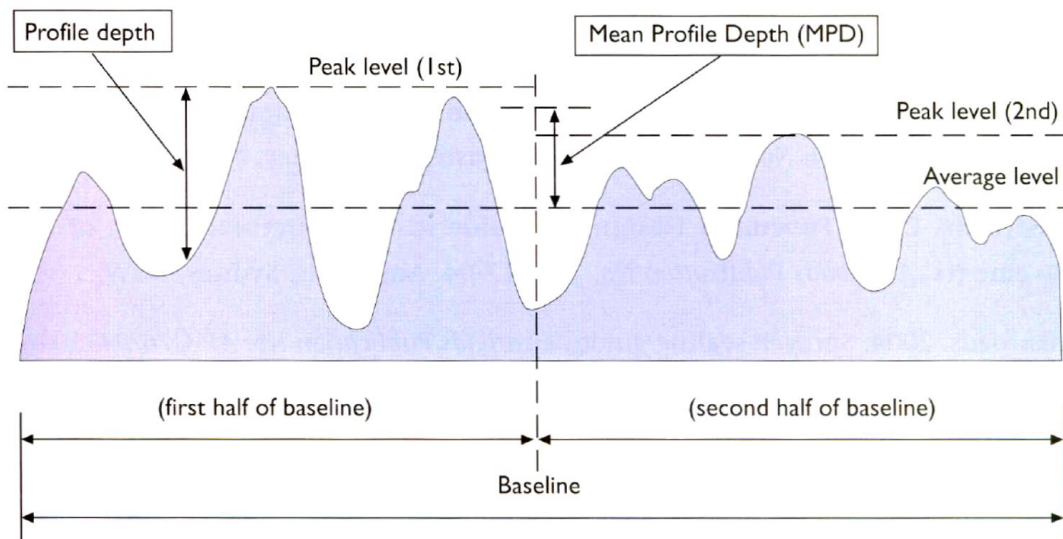


Figure 3-17. Schematic diagram of mean profile depth determination.

In addition to using a 3-D laser profiler, the NCSU research team also visually inspected the surface conditions of the pavement section at Maynard Road in Cary, NC. The surface grooves appeared as dotted lines in some sections. In most cases, the distance (width) between the grooves was the same as the distance (width) between the centerlines of two teeth in a milling machine. Figure 3-18 shows the overall conditions and texture of the milled surfaces at the Maynard Road site. Figure 3-18 (a) and (b) are photos taken perpendicular to the pavement surface, whereas Figure 3-18 (c) and (d) are photos taken at an angle. Figure 3-18 (a) and (c) show the milled surface with more straight grooves, whereas Figure 3-18 (b) and (d) show more dotted patterns in the grooves.



(a)



(b)

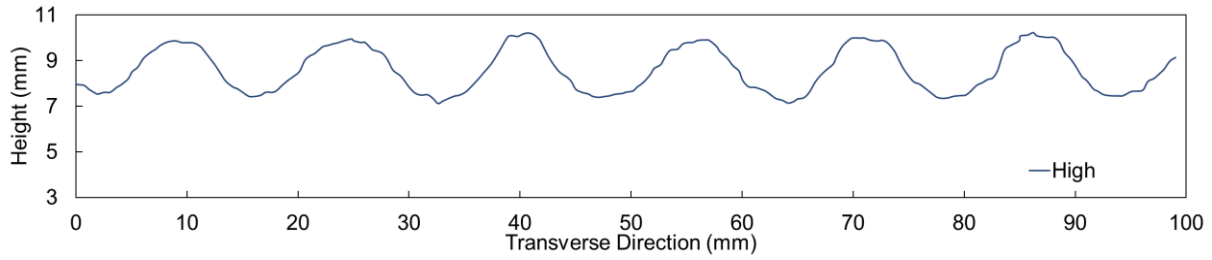


(c)

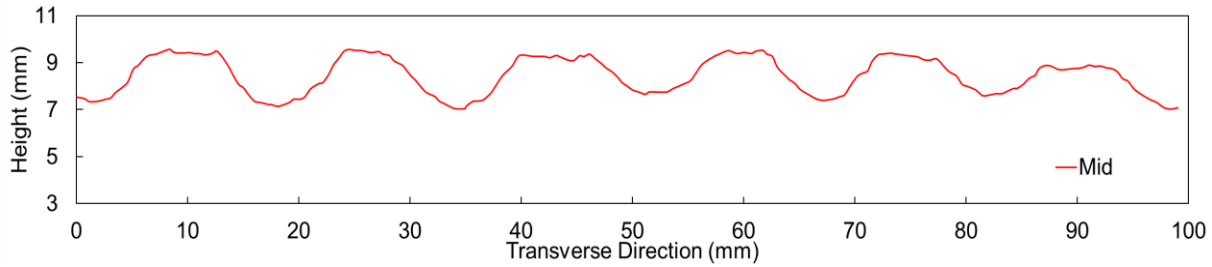


(d)

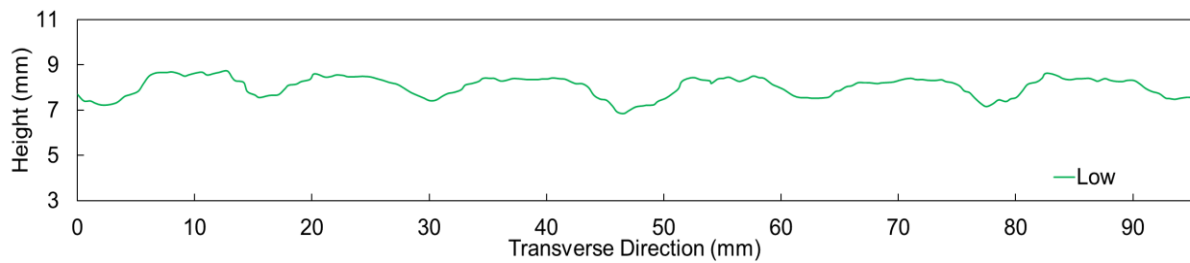
Figure 3-18. Field-milled surfaces on Maynard Road, Cary, NC.



(a)



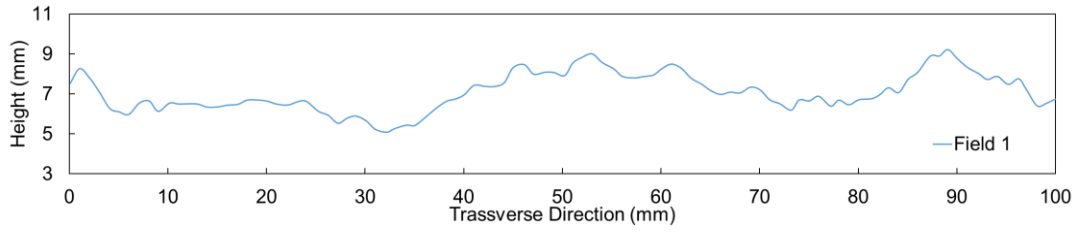
(b)



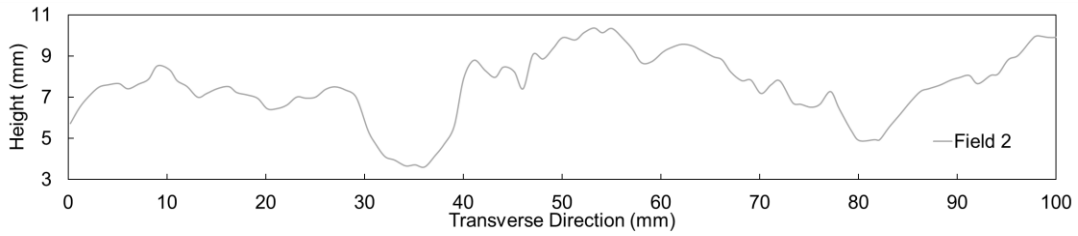
(c)

Figure 3-19. Profiles of lab-fabricated milled surfaces (transverse direction): (a) high, (b) medium, and (c) low walls between grooves.

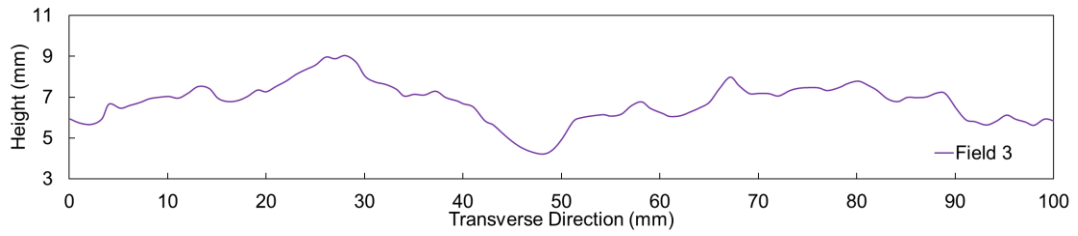
The NCSU research team was able to obtain profile data for five different field sections at the Maynard Road site in Cary, NC. Figure 3-20 shows the five different profiles of these field-milled surfaces.



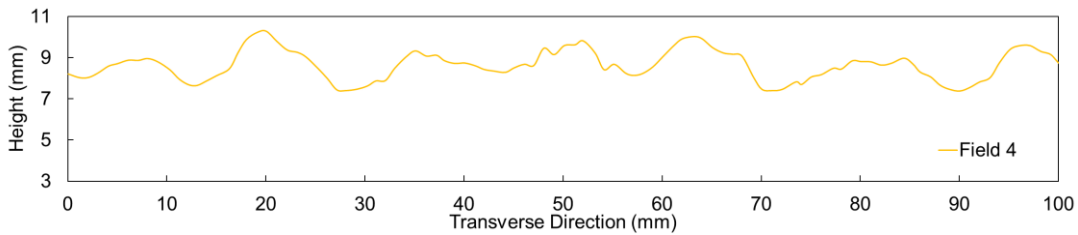
(a)



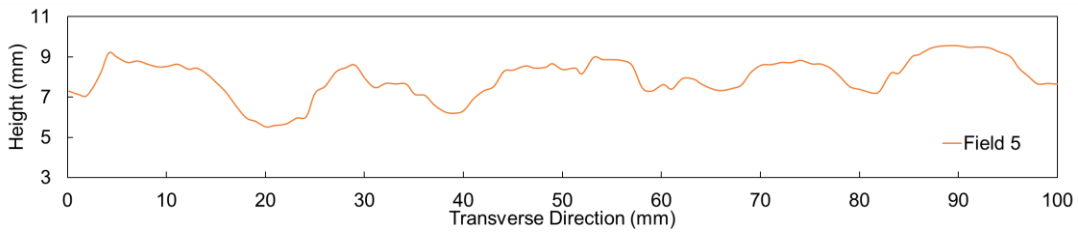
(b)



(c)



(d)



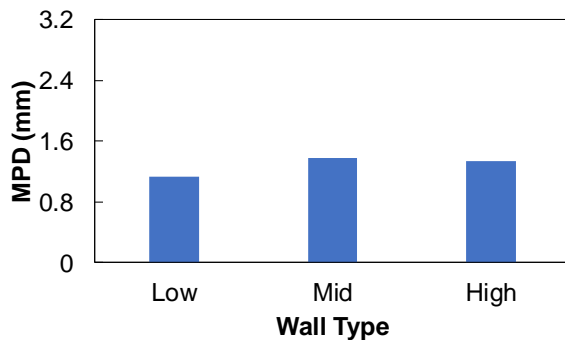
(e)

Figure 3-20. Profile depths of actual field-milled surfaces (transverse direction): (a) Field 1, (b) Field 2, (c) Field 3, (d) Field 4, and (e) Field 5.

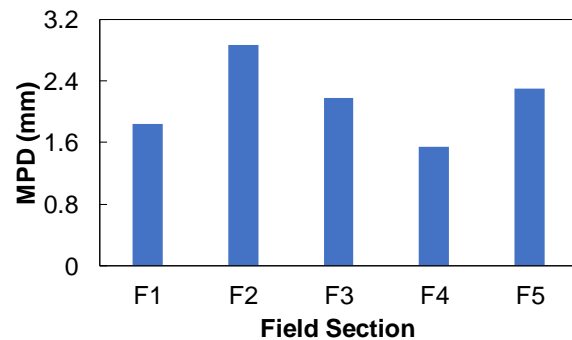
The NCSU research team had difficulty in determining the differences between the laboratory-fabricated (Figure 3-19) and field-milled (Figure 3-20) surfaces using profile data alone. Therefore, the team used the 3-D laser profiler to analyze the profiles of laboratory-fabricated and field milled surfaces. The MPD values were used to find the sample that most closely resembled field conditions. Table 3-3 presents the MPD values of the three laboratory-fabricated samples and five field milled surfaces. Figure 3-21 (a) and (b) indicate the MPDs for the laboratory and field milled surfaces, respectively.

Table 3-3. Mean Profile Depth Values of Three Laboratory Milled Surfaces and Five Field Milled Surfaces

Place	Type	MPD (mm)			
		Avg.	Max	Min	SD
Lab	Low	1.13	1.37	0.93	0.10
	Mid	1.37	1.52	1.23	0.06
	High	1.34	1.46	1.19	0.05
Field	F1	1.84	2.84	1.20	0.37
	F2	2.87	3.78	2.22	0.35
	F3	2.18	3.56	1.47	0.43
	F4	1.54	2.09	1.15	0.22
	F5	2.30	3.13	1.66	0.36



(a)

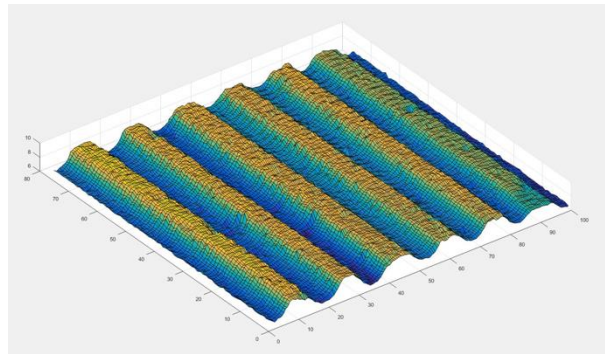


(b)

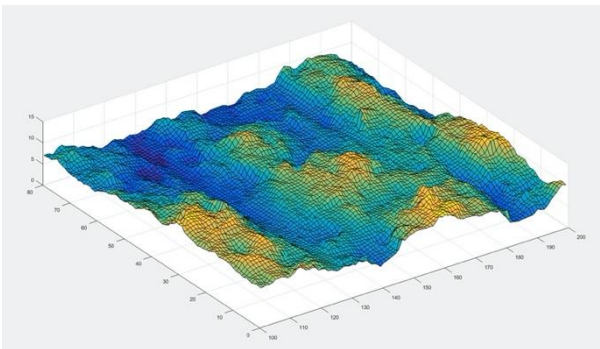
Figure 3-21. Mean profile depths: (a) laboratory milled surfaces and (b) field milled surfaces.

Based on a comparison of the MPD results, the ‘mid’ wall laboratory milled sample had the highest MPD value among the three laboratory samples with a depth of 1.37 mm. Among the field sections, Section F4 had the lowest MPD of 1.54 mm. The other field sections had 1.2 to 1.9 times higher MPD values with a standard deviation of 15% to 20 percent. Also, all the other field surfaces were more uneven than Section F2. Figure 3-22 presents 3-D rendered images that show the profile depths of the laboratory ‘mid’ wall sample and field sections F2 and F4. The groove pattern on the milled surface of Section F2, shown as Figure 3-22 (b), is highly irregular compared to that of Section F4, shown in Figure 3-22 (c), as justified by Section F2’s standard deviation of

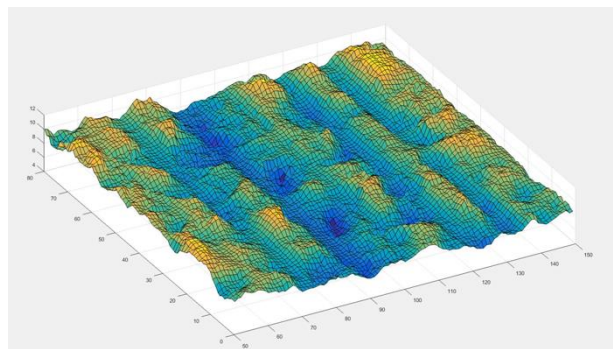
its MPD value. Also, the ‘mid’ wall laboratory sample and field section F4 have similar groove patterns according to their 3-D images. Therefore, among the laboratory samples, the ‘mid’ wall sample is the most representative of a field milled surface and used for all milled MAST specimen. However, such specimens are tagged as grooved specimens hereafter. The MPD value of the ‘mid’ wall sample is lower than the MPD values of the field milled surfaces; however, a lower MPD value would result in less shear strength in a Modified Advanced Shear Tester (MAST) test, which provides relatively conservative shear strength data.



(a)



(b)



(c)

Figure 3-22. 3-D renderings: (a) lab ‘mid’, (b) Field 2, and (c) Field 4.

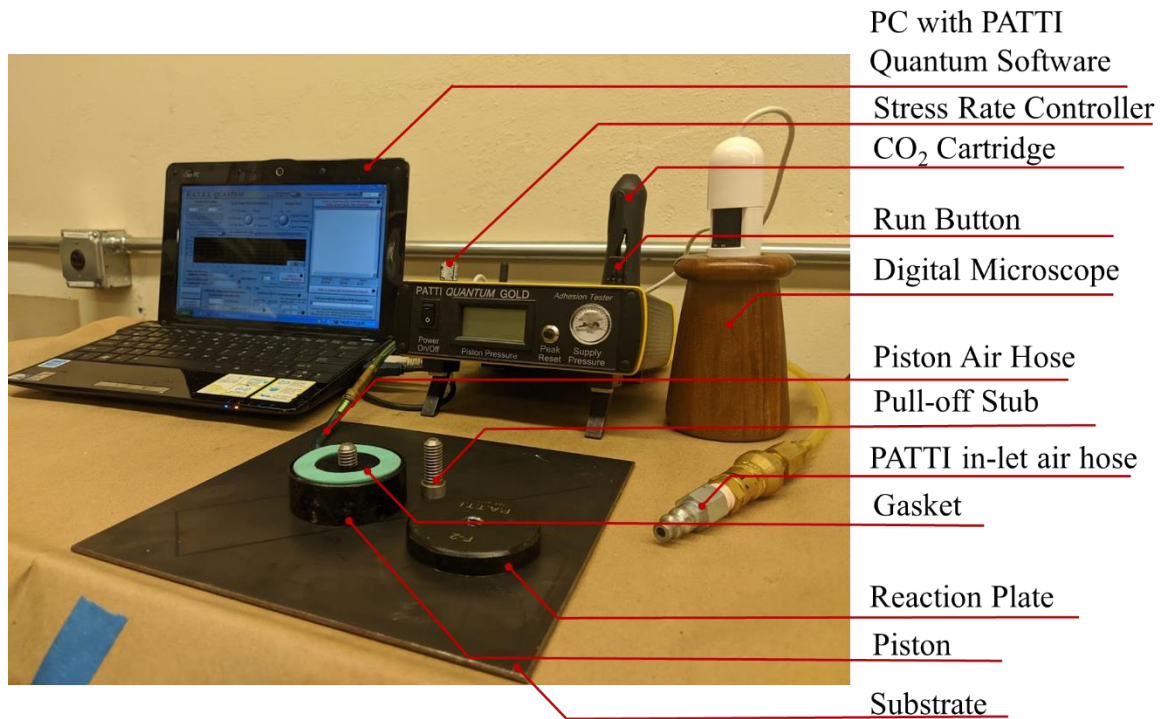
3.3 Binder Bond Strength (BBS) Test

3.3.1 Pneumatic Adhesion Tensile Testing Instrument (PATTI) Test

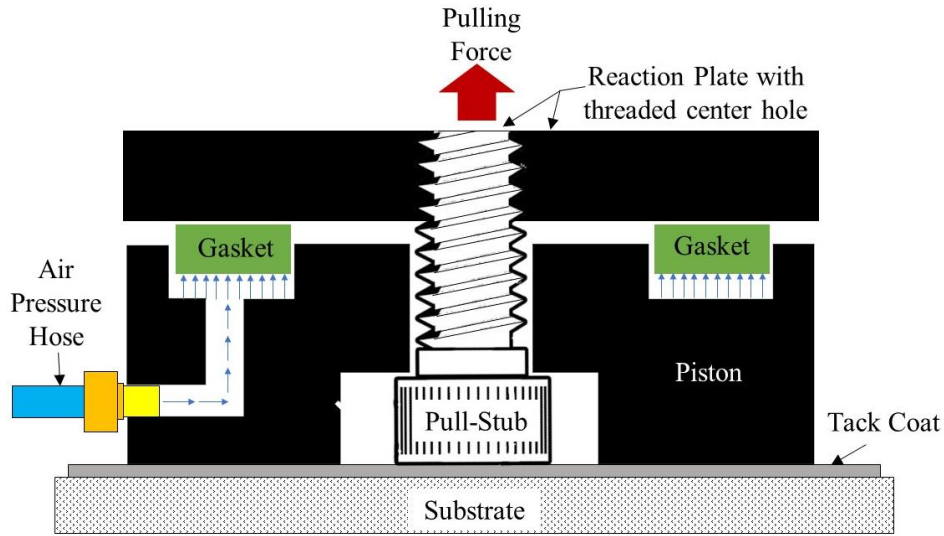
AASHTO T361-16 (AASHTO 2020d) details the laboratory test procedure for adhesion testing but does not consider different application rates and cannot be used for field testing. In response, Karshenas (2015) developed a new procedure based on AASHTO T361-16 (AASHTO 2020d) and describes the use of an adhesion tester in the field and in the laboratory. Karshenas (2015) also

established a strong prediction relationship between BBS and bond shear strength of asphalt concrete specimens. The current research extends the Karshenas research by investigating the possibility of applying the time-temperature (t-T) superposition principle to the measured tensile strength to build mastercurves.

In this study, the PATTI is used to measure the BBS of asphalt binders. PATTI is a self-aligning, pneumatic device that is used to measure the pull-off tensile strength of tack coats and the corresponding stress rate at different test temperatures. Figure 3-23 shows the PATTI used in this study. It is a Quantum Series Gold model, categorized as a Type IV/ Method D test device in ASTM D4541-17 (ASTM 2017). The system applies a true axial force relative to the pull stub to obtain a tensile strength value. This value can quantitatively represent the tensile bond strength between the tack coat and substrate. The PATTI test is not limited to asphalt binder but also can be used to test paint, film, coatings, or most adhesives on a smooth, rough, porous, flat, or curved substrate. The PATTI system can test bond strength levels up to 68,948 kPa (10,000 psi).



(a)



(b)

Figure 3-23. (a) Type IV self-alignment adhesion tester (PATTI) and (b) cross-sectional schematic of self-aligning piston assemblies (ASTM D4541-17 (2017)).

3.3.2 Binder Bond Strength Test Methodology

The PATTI test procedure that is described in this section draws from previous research conducted at NCSU (Cho 2016, Karshenas 2015). The fundamental procedure is derived from ASTM D4541-17 (ASTM 2017) and later AASHTO TP-91-13, now AASHTO T361-16 (AASHTO 2020d). The goal of this guideline is to allow both laboratory and field testing using PATTI. Figure 3-24 illustrates the step-by-step procedure for conducting PATTI pull-off tests.

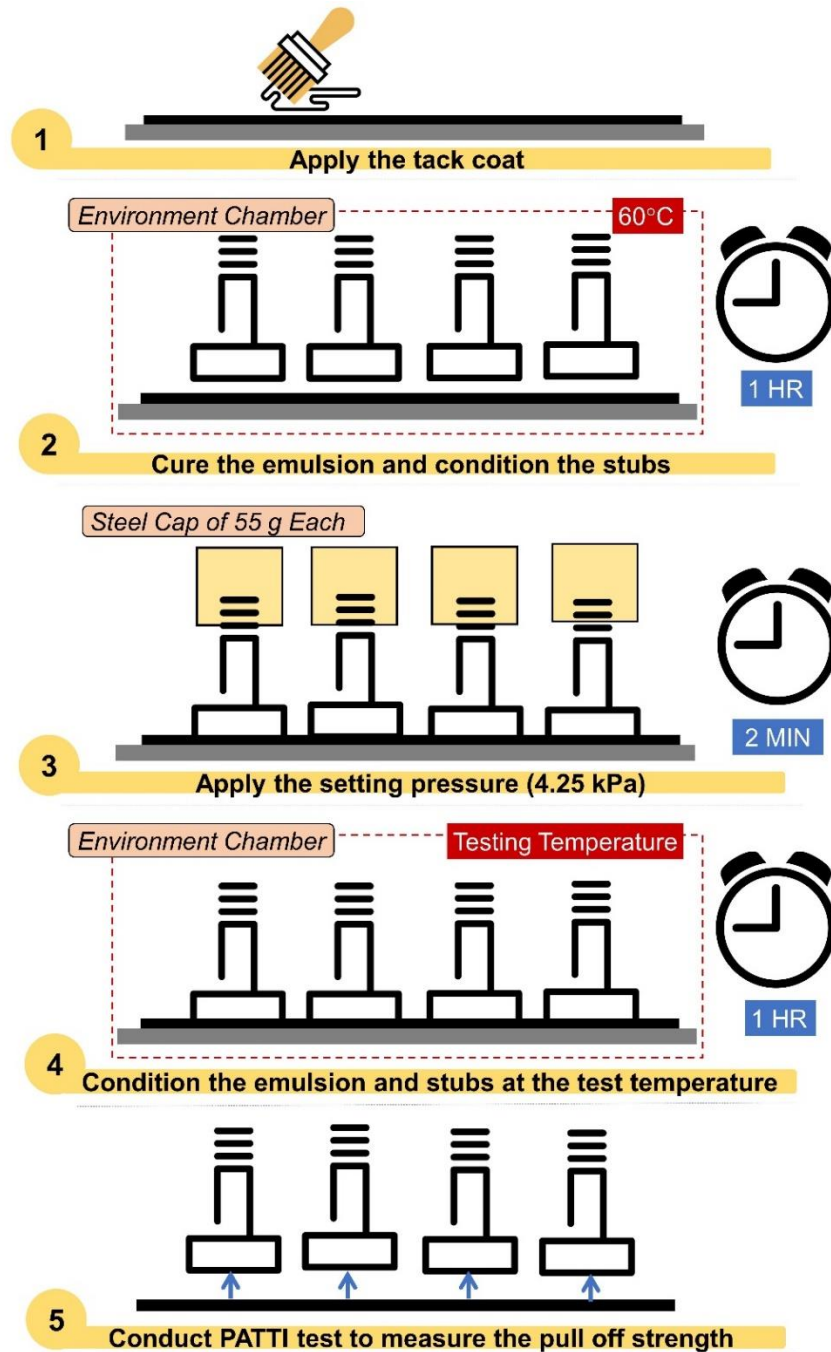


Figure 3-24. Step-by-step procedure for PATTI testing.

Step 1: Tack Coat Sample Preparation

The tack coat sample used for PATTI tests can be obtained either by placing a metal plate (substrate) on the existing asphalt surface prior to the application of the tack coat at the construction site or by applying a tack coat with the specified application rate using a foam paintbrush in the laboratory. According to ASTM D4541 (ASTM 2017), a metal substrate should be used when testing pull-off strength. However, the rigidity and surface texture of the substrate

will affect the results of the test, and these characteristics are not controllable variables in field measurements. In this study, the research team used the recommended standard substrate, which is an 11-gauge cold-rolled steel plate with matte finish, in accordance with ASTM A568/A568M-17a (ASTM 2019). The team used this specific plate because of its availability and ease of production and standardization. The foam paintbrush is to be used only for emulsions, and a hot spray gun is employed to apply hot binder onto the substrate in the lab. Figure 3-25 shows the hot spray gun that was used to spray Ultrafuse hot binder onto a metal substrate in this study. The metal template is used to confine the spray within the testing area.

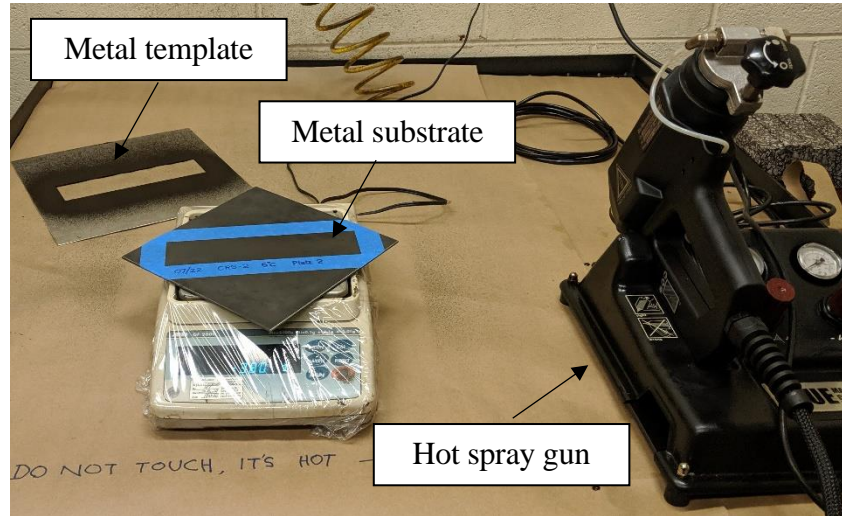


Figure 3-25. Test set-up for hot spray gun usage.

Step 2: Curing the Emulsion

Improper curing of emulsions causes weak bonding. Therefore, allowing sufficient curing time is crucial for gaining inherent strength, and the length of the curing time depends on the tack coat type. For example, rapid-setting emulsions require a curing period of 30 minutes, whereas slow-setting emulsions need at least an hour to cure. For either case, the pull stubs and substrate with tack coat are heated to the application temperature of 60°C in an oven for their respective curing time. Each substrate sample requires at least three pull stubs or replicates. In the case of hot binders, the substrate with tack coat and pull stubs are heated to the compaction temperature (typically 145°C) for ten minutes to liquefy the binder and to activate the tackiness of the binder to bond with the pull-off stub. This heating time of ten minutes was found to be the most appropriate time for this purpose based on the outcome consistency of all the stubs placed after different heating times.

Step 3: Application of Setting Pressure

During preliminary testing, once a sample has cured, the heated pull stubs are placed on the tack coat sample, and the pull-off strength is measured after conditioning. In this study, the dominant

adhesive failure that was observed for the hard and non-tracking tack coats. To mitigate this problem, a metal cap weighing $55.0 \text{ g} \pm 1.0 \text{ g}$ was placed on top of each pull stub for two minutes at the ambient temperature of the laboratory to ensure the formation of a good bond with the tack coat, as shown in Figure 3-26. This overburden weight was intended to mimic the dead load (stress) of typical surface layers.

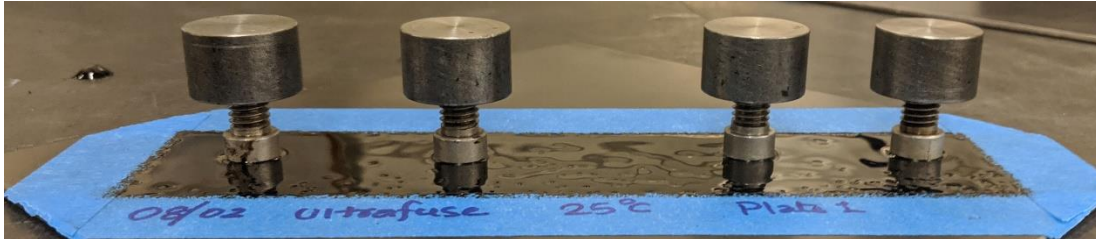


Figure 3-26. Metal caps on pull-off stubs to apply setting pressure.

Step 4: Conditioning the Plate and Stub

After two minutes of setting pressure application, the metal caps are removed, and the tack coat sample is conditioned in an environmental chamber at the testing temperature for one hour. Asphalt binder properties are highly dependent on temperature. ASTM D4541-17 (ASTM 2017) recommends that the stress rate range should fall within a small bandwidth of 345 kPa/s to 1,034 kPa/s (50 psi/s to 150 psi/s) such that the PATTI test is conducted at numerous temperatures to obtain the necessary overlap among the pull-off strength values, which in turn aids the mastercurve construction. For the present study, tests were run at 5°C, 7°C, 10°C, 13°C, 15°C, 17°C, 19°C, 22°C, 25°C, 30°C, 35°C, 44°C, and 53°C using the residual application rate of 0.14 L/m^2 (0.03 gal/yd^2).

Step 5: Pull-off Tensile Testing

The standard practice specified in ASTM D4541-17 (ASTM 2017) is to pull off the stubs for at least three substrate replicates (four stubs per substrate) at the same conditioning temperature. The PATTI Quantum software that accompanies the device records the peak tensile strength and changes in stress with time. However, this tensile strength value may not be a legitimate result because it depends on the failure mode of the pull stub, the load rate, and the repeatability.

The PATTI system can apply only a limited range of loading rates during BBS tests of asphalt binder to meet acceptability standards. ASTM D4541-17 (ASTM 2017) and the PATTI owner's manual state that the load rate shall not exceed 1,034 kPa/s (150 psi/s), as the variability in the measured BBS values for asphalt binders is too high after this point. Therefore, most of the load rates used in this research fell within 345 kPa/s to 1,034 kPa/s (50 psi/s to 150 psi/s). The procedure, according to ASTM D4541-17 (ASTM 2017), is to start with the load dial in the 'off' position and slowly turn the dial counterclockwise to release the air pressure after pressing the

‘Run’ button until the desired stress rate is achieved. The major difficulty of the stipulated procedure is maintaining a constant stress rate. In fact, a nonlinear stress-growth curve was observed, as shown in Figure 3-27. An alternative to this procedure is to set the load dial to a specific position prior to running the test. This position is determined based on multiple trials and is usually below the quarter of the dial circle. The dial is left at this position for the entire test series. As shown in Figure 3-27 this alternative method resulted in a linear stress-growth curve that is both repeatable and eases the calculation of the stress rate (the slope of the line). Hence, this alternative method was used throughout the study.

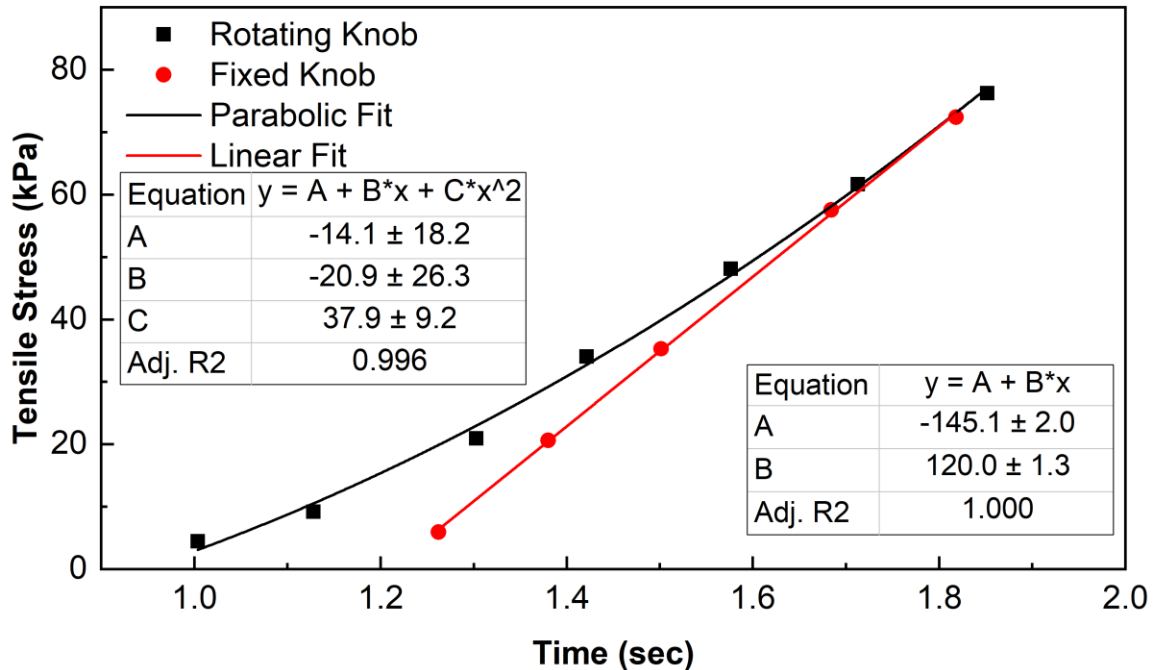


Figure 3-27. Stress rates measured using PATTI for rotation and fixed dial conditions.

3.3.3 Failure Modes in PATTI Test

Once the binder achieves its tensile strength under specific PATTI test conditions, the pull-off stub detaches from the substrate. This detachment is considered pull-stub failure and occurs in three primary ways that define the failure modes. Cohesive failure mode occurs within the asphalt binder, leaving a uniform layer of binder on the stub and substrate, as shown in Figure 3-28 (a). Adhesive failure mode occurs when the pull stub completely detaches from the binder, leaving the binder entirely on the substrate. Or, the pull stub pulls the binder layer along with the stub, leaving no trace of the binder on the substrate, as shown in Figure 3-28 (c). A test can also fail in a combination of these two modes, as seen in Figure 3-28 (b), which is termed ‘mixed failure.’ During mixed failure, some portion of the asphalt binder remains on either the stub or substrate. Other miscellaneous types of failure are possible when sliding or twisting occurs during the initial application of the pull stub or during placement of the piston. The ideal type of failure for this

research is a cohesive failure because it demonstrates the tensile strength of the binder itself and not its adhesive capabilities. During the data analysis performed in this study, if the failure was outside the cohesive type of failure, then the results were dismissed.

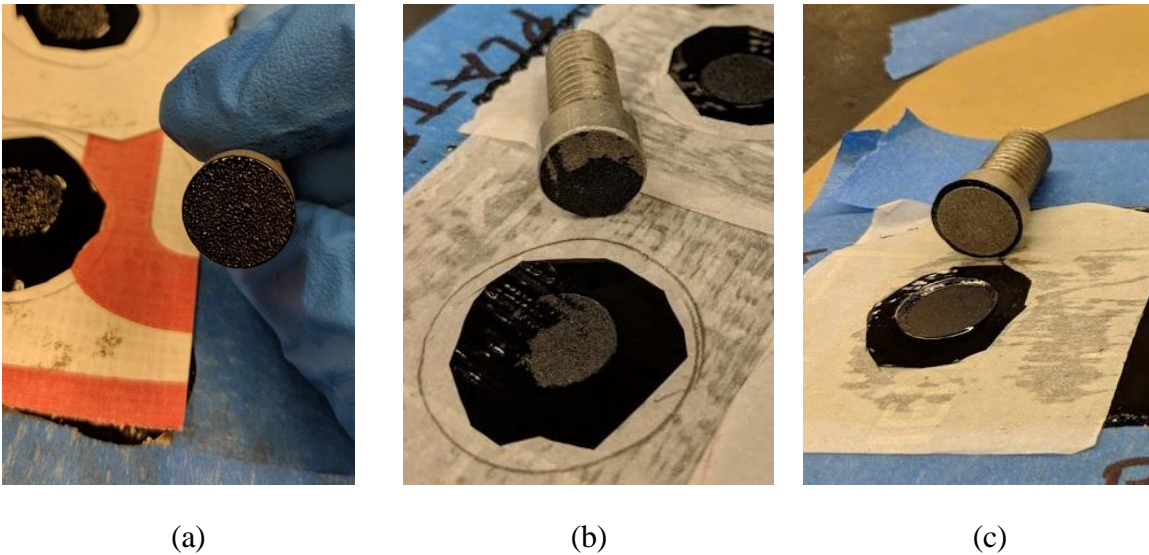


Figure 3-28. (a) Ideal cohesive failure of binder, (b) mixture of cohesive failure and adhesive failure of the pull stub, and (c) adhesive failure of the pull stub.

The final stage of PATTI test analysis should follow the repeatability criteria stipulated by ASTM D4541-17 (ASTM 2017). According to the standard, the difference between each test in terms of intra-laboratory results should be less than 14.8%, and the difference in inter-laboratory test results should be a maximum of 28.4% for a D-type tester. In this research, if the results were found to differ more than 14.8%, then they were dismissed as outliers.

Chapter 4. Numerical Simulation of Pavement Response

4.1 Background

The presence of sufficient interface bond strength among the pavement layers is evaluated by understanding and quantifying the distribution of the stresses within the pavement section under realistic traffic conditions. NCSU research group has developed a fast Fourier transform-based three-dimensional (3D) viscoelastic finite element (FE) analysis tool known as FlexPAVE™ (formerly known as the LVECD program) to evaluate the pavement response under moving vehicle loads. It can simulate actual climatic conditions as generated by the Enhanced Integrated Climatic Model (EICM). Besides, the software is zipped with the Simplified ViscoElastic Continuum Damage (S-VECD) and permanent deformation shift model that could predict the pavement response and distresses viz. fatigue cracking and rutting for any temperature and any traffic conditions. In this study, FlexPAVE™ was used to determine the critical stresses involved in debonding.

Cho (2016) has conducted extensive pavement response analysis on three typical pavement sections constructed in North Carolina, categorized as thin, intermediate, and thick structures. The analysis was carried out at 5°C, 20°C, 40°C, and 60°C, three different speeds, 8 km/hour (5 mph), 40 km/hour (25 mph), and 88 km/hour (55 mph), three axle loads, 106.8 kN (24 kips), 160 kN (36 kips), and 213.6 kN (48 kips), and two types of tire rolling conditions, i.e., free rolling and Braking to measure the critical debonding condition. The outcome shows that the most critical stress state condition that leads to debonding is created by a thick pavement structure ran over by a single tire with a single – axle single - tire load of 213.6 kN (48 kips) at a fixed vehicular speed of 8 km/hour (5 mph) under braking condition. Henceforth, that specific condition is considered for the current study except that the tire loading is assumed as 80 kN (18 kips) single-axle dual-tire configuration. All the conditions considered by Cho (2016) were simulated using the current study's mixture properties and tack coat predictive equation. The outcomes are reported in [Appendix B](#).

4.2 Parameters Used in the Numerical Simulations

4.2.1 Structure Information

Among the typical pavement sections in North Carolina, a thick pavement has higher vulnerable chances to debonding (Cho 2016). Figure 4-1 shows the cross-section view and provides the thickness of each layer assumed for the thick pavement structure for the present study. The top three layers i.e., surface, intermediate, and base layers, are asphalt concrete mixtures with different gradations. The standard thickness for surface course constructed with asphalt mixture's having 9.5 mm nominal maximum aggregate size usually ranges between 38.1 mm (1.5 in.) and 63.5 mm (2.5 in.). Henceforth, in the present study, a thickness of 25.4 mm (1 in.), 38.1 mm (1.5 in.), 50.8 mm (2 in.), 63.5 mm (2.5 in.) and 76.2 mm (3 in.) was chosen to analyze the critical loading condition.

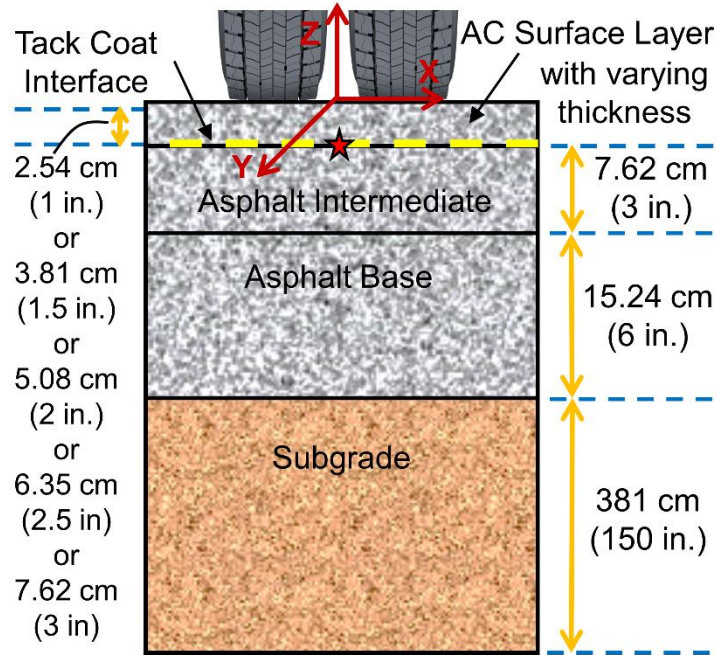


Figure 4-1 Thick pavement structure used in computational simulations.

4.2.2 Material Parameters for Each Pavement Layers

Asphalt Concrete

The three top layers of the thick pavement structure are assigned with the material properties of asphalt concrete. The surface course is assigned with either Warm Mix (RS9.5B-RAP35%) or Hot Mix (RS9.5B-RAP30%) depending mixture under consideration, while the intermediate and base layers with properties of mixtures I19B and B25B, respectively.

The viscoelastic nature of asphalt concrete is defined with the aid of Prony series coefficients/parameters in the FlexPAVE™. It is achieved through the interconversion from dynamic modulus to relaxation modulus over a wide time region using the generalized Maxwell model using the Equation (9). The number of Maxwell elements decides the prediction accuracy, more elements, high accuracy but leads to more complexity at the same time. FlexMAT™, an excel based software, is used to analyze the dynamic modulus outcomes to calculate the Prony series coefficients, as shown in Table 4-1. The material properties for I19B and B25B were adopted from Cho (2016).

Subgrade

The subgrade is assumed as linear elastic material in the FlexPAVE™ simulations and the modulus value used in the current analysis is 68.95 MPa (10,000 psi).

Table 4-1. Prony Coefficients for Relaxation Modulus

ρ_i (sec)	E_i (MPa)			
	WM	HM	I19B	B25B
2.00E+08	8.202168	13.42	15.86	10.71
2.00E+07	6.853888	25.71	31.18	21.24
2.00E+06	21.46807	52.45	65.98	45.3
2.00E+05	61.20037	115.27	150.13	105.76
2.00E+04	184.5173	270.18	356.33	268.88
2.00E+03	519.327	641.43	823.24	702.8
2.00E+02	1219.639	1401.35	1685.67	1676.39
2.00E+01	2218.648	2533.1	2821.99	3194.19
2.00E+00	3079.913	3595.62	3759.34	4550.7
2.00E-01	3370.041	3173.76	3476.25	4160.3
2.00E-02	3067.792	3761.12	3756.6	4357.92
2.00E-03	2451.163	3104.72	3081.01	3337.35
2.00E-04	1793.888	2497.32	2440.15	2452.81
2.00E-05	1239.69	1851.65	1802	1669.18
2.00E-06	825.7544	1323.71	1286.44	1099.82
2.00E-07	536.8434	917.49	893.45	705.84
2.00E-08	355.599	624.31	610.14	446.61
E_∞	2.859034	60.49	38.24	51.59
Ref Temp (°C)	5	5	5	5

4.2.3 Climate Data

Although FlexPAVE™ has the ability to simulate the pavement behavior under changing temperature as a function of time and pavement depth, the isothermal temperature profile at 50°C was used in this study as it acts as the critical condition for debonding.

4.2.4 Traffic Data

The design vehicle configuration for the response analysis is chosen as a dual-tire system to replicate the tire loading condition of a half of a single-axle dual-tire condition. An axle load of 80 kN is used, which is distributed through the dual tire configuration as 40-kN (9 kips) with 827.4-kPa (120 psi) tire-pavement contact pressure.

4.2.5 Tire-Pavement Contact Pressure Configuration

The tire-pavement contact pressure distribution is non-uniform and mimicking it is essential in accurate pavement response computations. Moreover, the tire-pavement contact pressure distribution is affected significantly by tire inflation pressure, tire type, and tire load. NCSU

research team determined the FlexPAVE™ tire-pavement contact area on the Stress-In-Motion (SIM) technology under the moving load (De Beer et al. 2004). The rectangular shape with an aspect ratio of 11/7 (length/width) is assumed in FlexPAVE™. The tire-pavement contact pressure distribution is based on fitting a quadratic function to the actual pressure in both the longitudinal and transverse directions. The test outcomes after carrying out different combination of numerical simulations are reported in [Chapter 6](#).

Chapter 5. Test Results and Discussion

5.1 Interface Shear Strength Results

During the MAST test, four measurements were recorded to analyze the ISS results. They are the actuator displacement, actuator force, confining force, and the on-specimen displacement using DIC. Actuator displacement, actuator force and confinement loads were acquired using a 16-bit National Instruments data acquisition board and recorded using LabVIEW software. VIC-2D software is employed to measure the on-specimen displacements.

The measured actuator force is used to calculate the shear stress (τ_s) at any time during the test, as shown in Equation (14).

$$\tau_s = \frac{F_A}{A_{cs}} \quad (14)$$

where

F_A = axial force, kN and
 A_{cs} = cross-sectional area of the specimen, m².

The actuator displacement is only used to verify the input constant displacement rate for the test and is not used for the analysis. The on-specimen displacement measured using DIC is used to calculate the DIC shear strain (γ) to avoid the effect of machine compliance on the actuator strain.

$$\gamma = \frac{u_{A-DIC}}{SG} \quad (15)$$

where

u_{A-DIC} = DIC based axial displacement and
 SG = shear gap (8 mm in this study).

The confining force measured using the load cell placed in the platen parallel to the specimen is used to measure the normal stress that mimics the real field conditions.

$$\sigma_c = \frac{F_c}{A_{cs}} \quad (16)$$

where

F_c = confining force.

The on-specimen strain values are lower than the crosshead LVDT's (actuator) measured strain values and differ depending upon the stiffness of the specimen due to the machine compliance. As

shown in Figure 5-1, the crosshead strain rate is constant through the test, while the DIC strain rate follows a non-linear trend. Chehab et al. (2002) proposed a pure power form-fitting method to measure the strain rates of such non-linear responses. The on-specimen strain rate in a power form is shown in Equations (17), (18), and (19) .

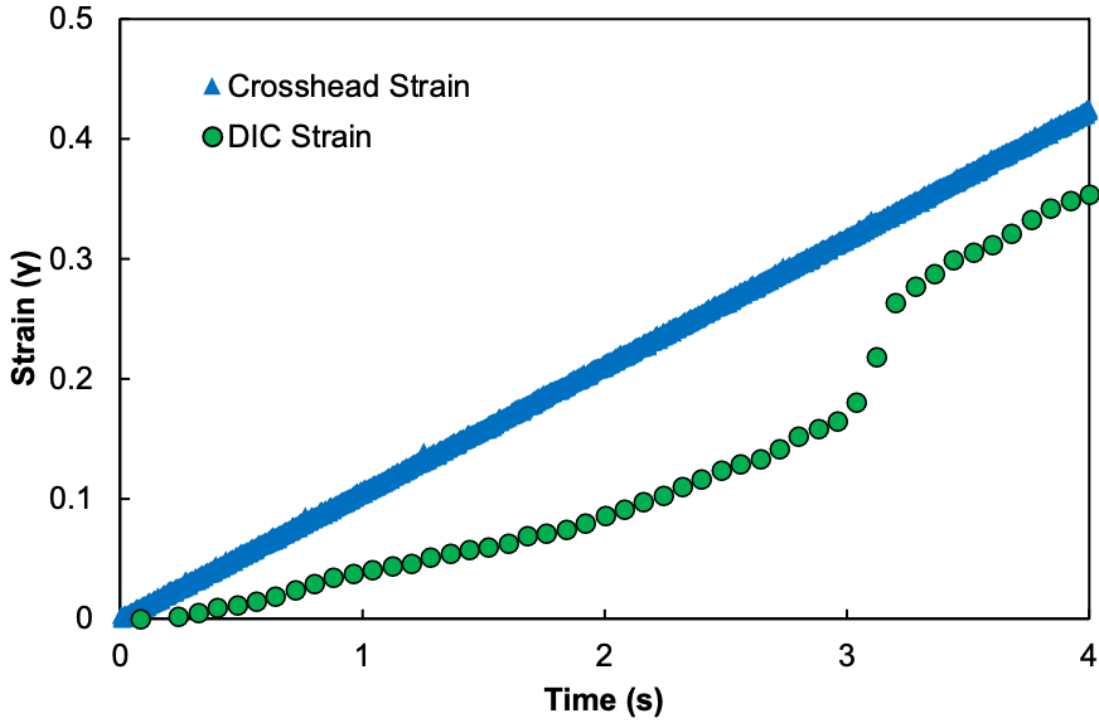


Figure 5-1. Shear strain measured based on crosshead LVDT and DIC technique for ISS test at 50.8 mm/min, 19°C, 483 kPa confining, and Ultrafuse.

$$\varepsilon = k' \times t^n \quad (17)$$

$$\varepsilon = k' \times a_T^n \times \left(\frac{t}{a_T} \right)^n \quad (18)$$

$$\varepsilon = k \times \xi^n \quad (19)$$

where

- ε = strain,
- k' = slope of strain vs. time at temperature T,
- ξ = reduced time at reference temperature, and
- k = reduced strain rate at reference temperature.

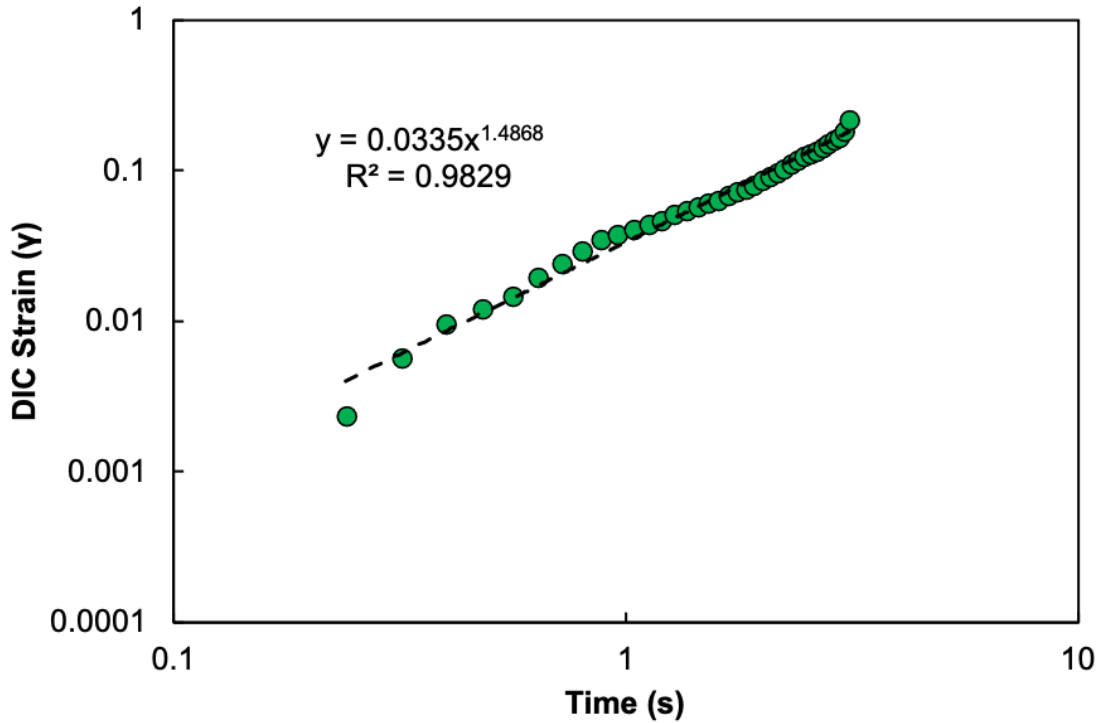


Figure 5-2. Pure power form-fitting method to evaluate strain rate (k') at 50.8 mm/min, 19°C, 483 kPa confining, and Ultrafuse.

Figure 5-2 shows the fitting technique used to obtain the strain rate. For this process, only the data before failure were used. In other words, if the data deviate from a power law, they are excluded from the fitting process for the acquisition of strain rate.

In this research, k' is considered as the DIC shear strain rate ($\dot{\gamma}$) measured based on the proposed method by Chehab et al. (2002). Further, the reduced shear strain rate ($\dot{\gamma}_R$) was calculated by multiplying the DIC shear strain rate with the shift factor (a_T) measured from dynamic shear modulus tests of the corresponding tack coat material used within the MAST specimen, as shown in Equation (20).

$$\dot{\gamma}_R = \dot{\gamma} \times a_T \quad (20)$$

where

- $\dot{\gamma}_R$ = reduced shear strain rate and
- $\dot{\gamma}$ = shear strain rate.

5.1.1 Validation of Time-Temperature Superposition Principle for Interlayer System with Tack Coat

Cho (2016) demonstrated that the time-temperature superposition principle is valid for the construction of an ISS mastercurve based on the MAST and DSR test results. Following the same methodology, in this research, 11 different reduced shear strain rates were selected to verify the applicability of t-T principle to construct a smooth mastercurve. The MAST specimens and test conditions selected for the verification are CRS-2 tack coat, 276 kPa confining pressure, 0.03 gal/yd² residual application rate, and unmilled surface. Cho (2016) approach is verified to ascertain the reproducibility of the approach with a different user.

The shift factors of each tack coat materials were measured by carrying out temperature-frequency sweep tests using DSR. The time-temperature shift factor function shown in Equation (8) was fitted to the measured data points to get the model coefficients. The model coefficients for each tack coat materials at 20°C reference temperature are shown in Table 2-3.

The coefficients of the shift factors that were measured for each tack coat type at a standard reference temperature of 20°C using the DSR were substituted in the t-T shift factor formula shown in Equation (8) to obtain the shift factors at the respective conditioning temperatures used in the MAST tests. Further, using Equation (20), the reduced shear strain rate at the MAST testing temperature was calculated.

Table 5-1 presents the selected actuator shear strain rates, measured DIC shear strain rates and corresponding ISS results, respectively.

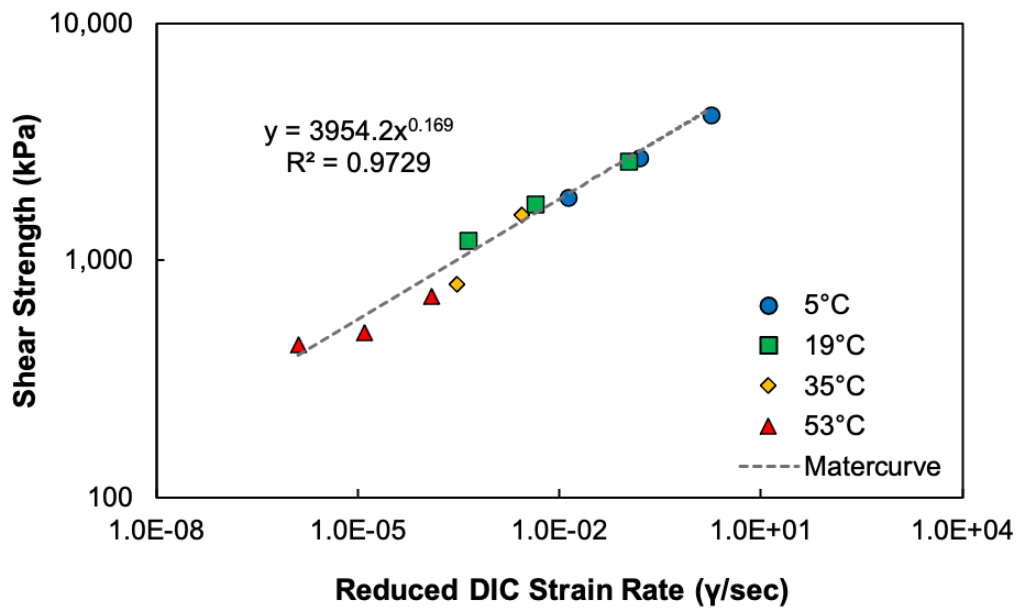


Figure 5-3. Verification of t-TS principle for construction of ISS mastercurve.

Table 5-1. Selected Actuator Strain Rate and Corresponding Reduced DIC Strain Rate and Interface Shear Strength

Temperature (°C)	Loading Rate (mm/min)	DIC Strain Rate (γ /sec)	Reduced DIC Strain rate (γ /sec)	Interlayer Shear Strength (kPa)
5	50.8	4.116E-02	2.136E-02	4113.75
	5.08	3.644E-03	1.891E-03	2692.72
	0.508	3.072E-04	1.594E-04	1846.98
19	50.8	7.800E-02	1.274E-03	2623.51
	5.08	3.215E-03	5.249E-05	1722.16
	0.508	3.182E-04	5.196E-06	1219.68
35	50.8	7.232E-02	3.246E-05	1555.34
	5.08	7.914E-03	3.552E-06	793.61
53	50.8	7.289E-02	1.484E-06	706.40
	5.08	7.325E-03	1.491E-07	495.96
	0.508	7.591E-04	1.546E-08	441.55

The ISS values from two adjacent reduced strain rates, tested at different temperatures and strain rates, overlaps/align to draw the mastercurve as shown in Figure 5-3. The fitted function of the ISS mastercurve has a power form. Thereby, the t-TS principle was validated by creating a smooth mastercurve for ISS.

Further to the verification, the number of test combinations with regard to loading rate and temperature was reduced from 12 (4 rates \times 3 temperatures) to four: 0.02 in./min (53°C), 0.2 in./min (35°C), 2 in./min (19°C), and 2 in./min (5°C) from hereafter. Some tests exhibited the failure within the mixture (rather than at the interface), and the data from these tests were discarded in the analysis.

5.1.2 Effect of Tack Coat Type

Figure 5-4 presents an overall comparison of the CRS-2 and CRS-1h emulsions based on all the ISS test results. As shown, the CRS-2 tack coat provides greater shear strength than the CRS-1h tack coat.

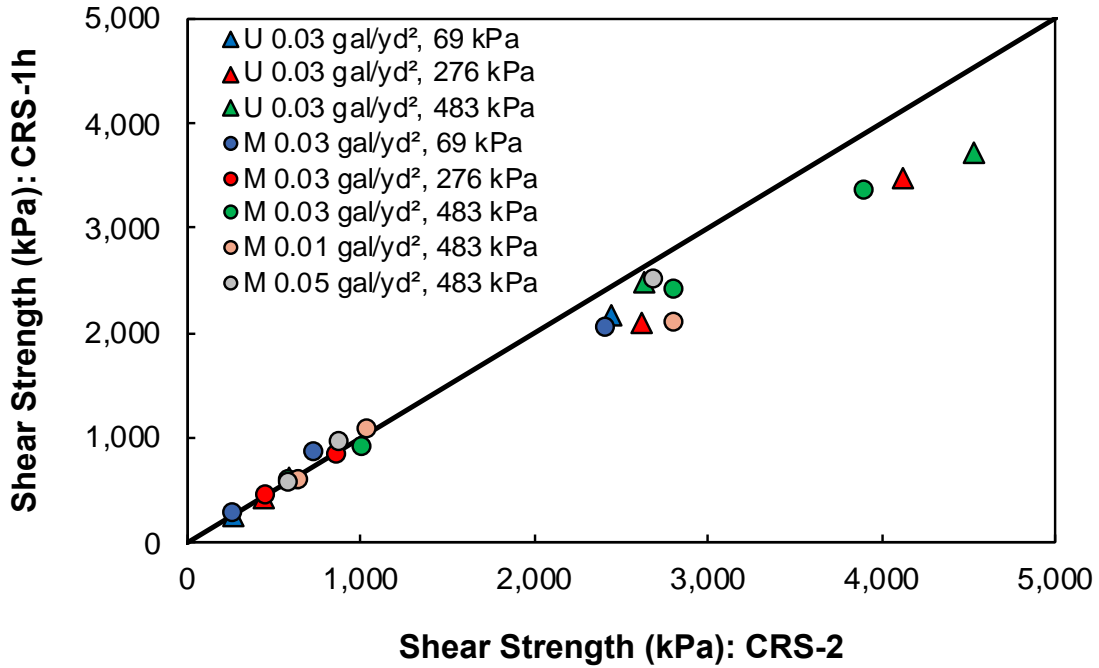
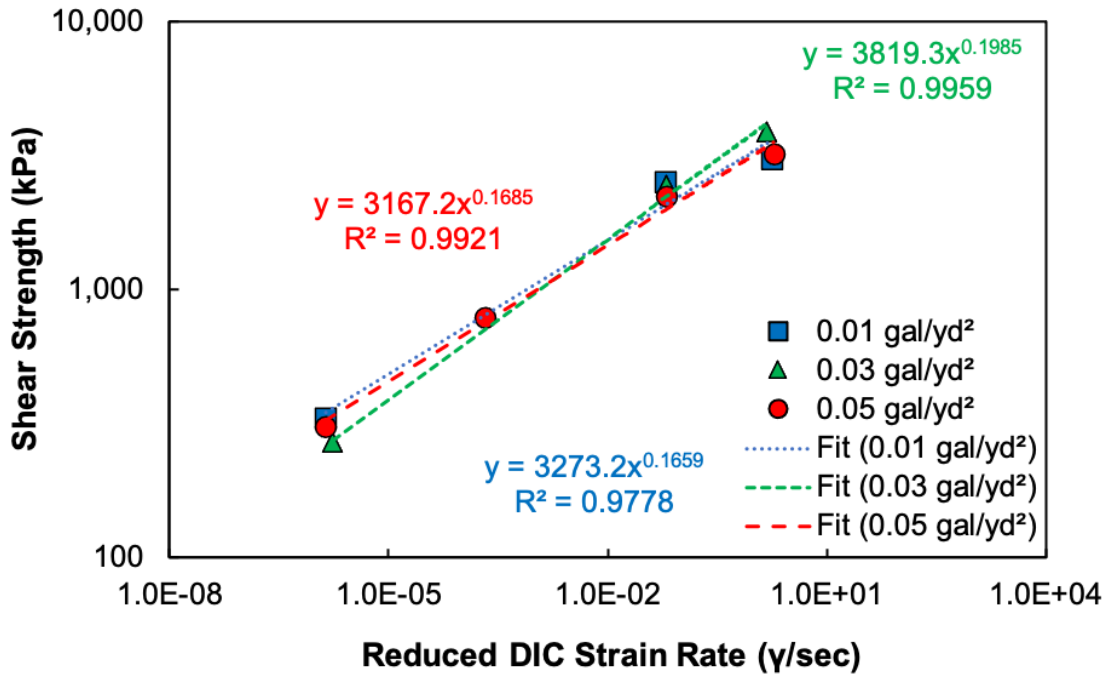


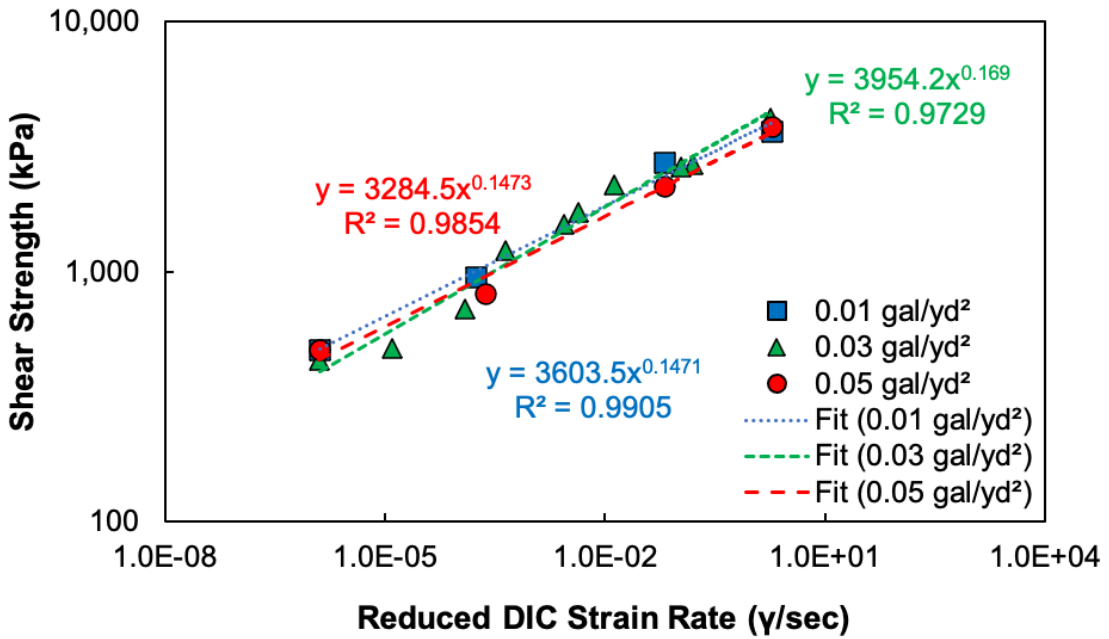
Figure 5-4. Comparison of shear strength values of CRS-2 and CRS-1h via line of equality.

5.1.3 Effect of Tack Coat Application Rate

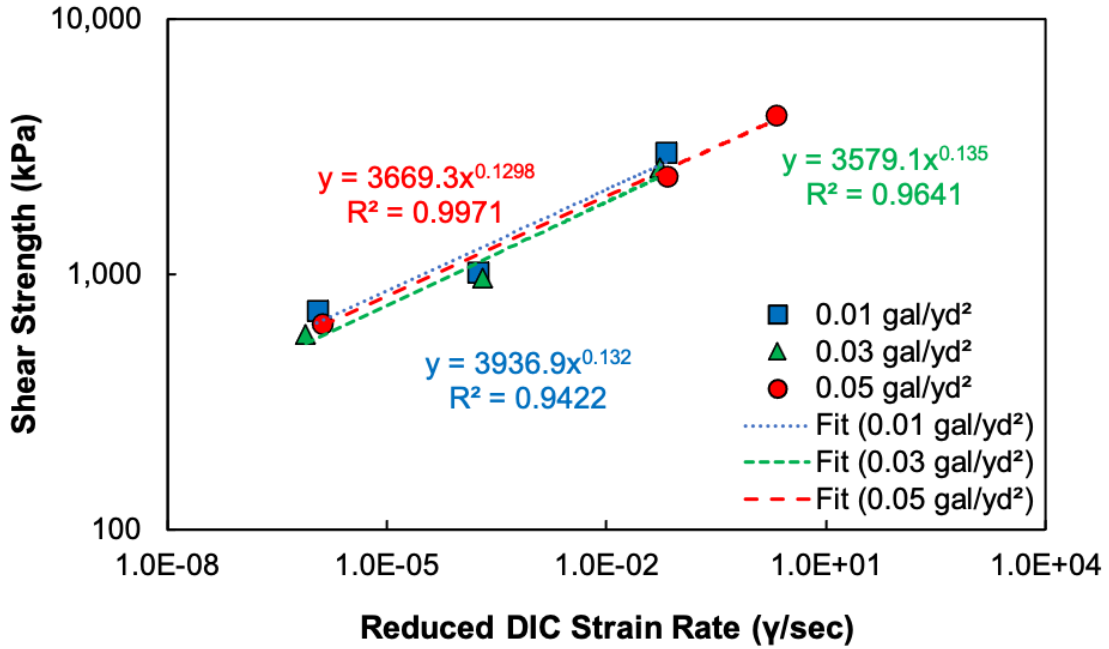
Figure 5-5 and Figure 5-6 present the shear strength mastercurves of CRS-2 under unmilled and milled conditions, respectively. The shear strength mastercurves were developed at three different application rates: 0.01 gal/yd², 0.03 gal/yd², and 0.05 gal/yd². Each figure consists of three graphs with the different confining pressures: 69 kPa, 276 kPa, and 483 kPa.



(a)

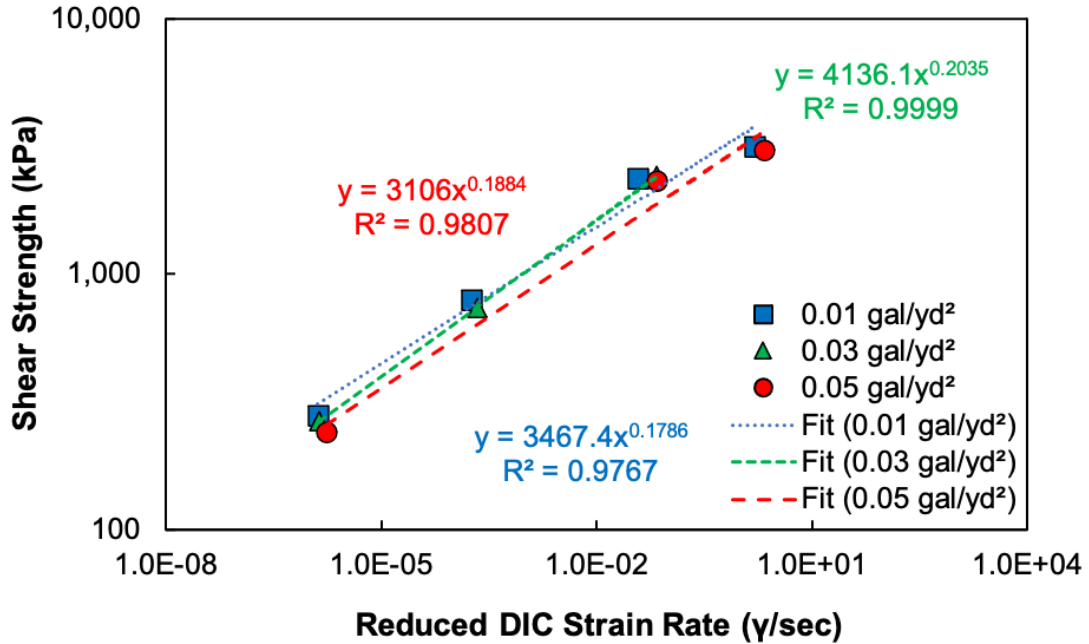


(b)

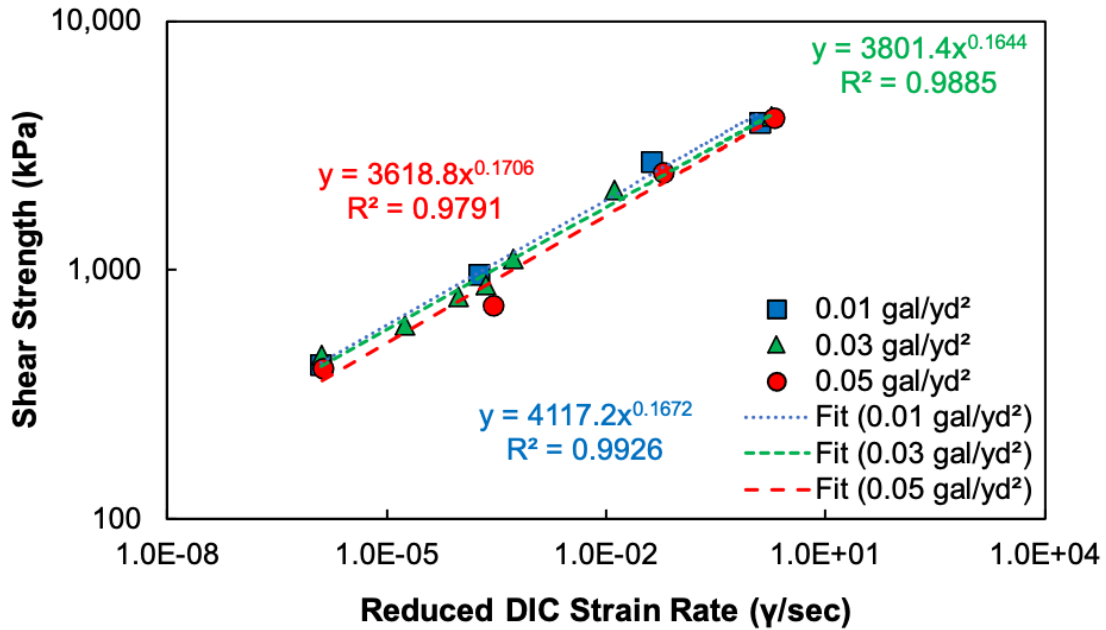


(c)

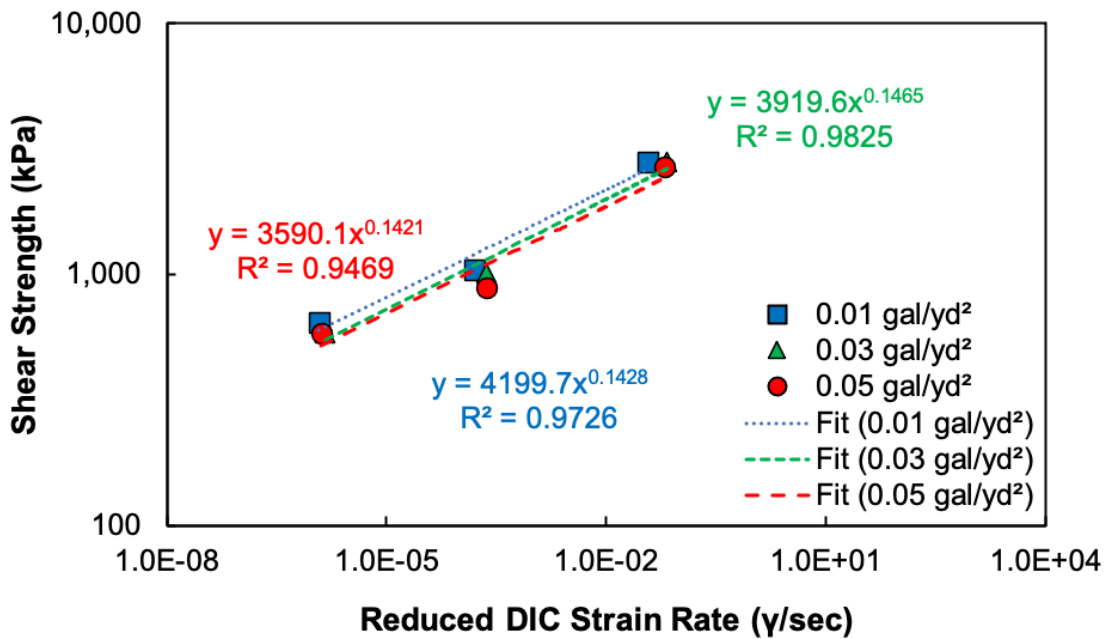
Figure 5-5. Shear strength mastercurves of CRS-2 at various application rates under unmilled condition: (a) 69 kPa, (b) 276 kPa, and (c) 483 kPa.



(a)



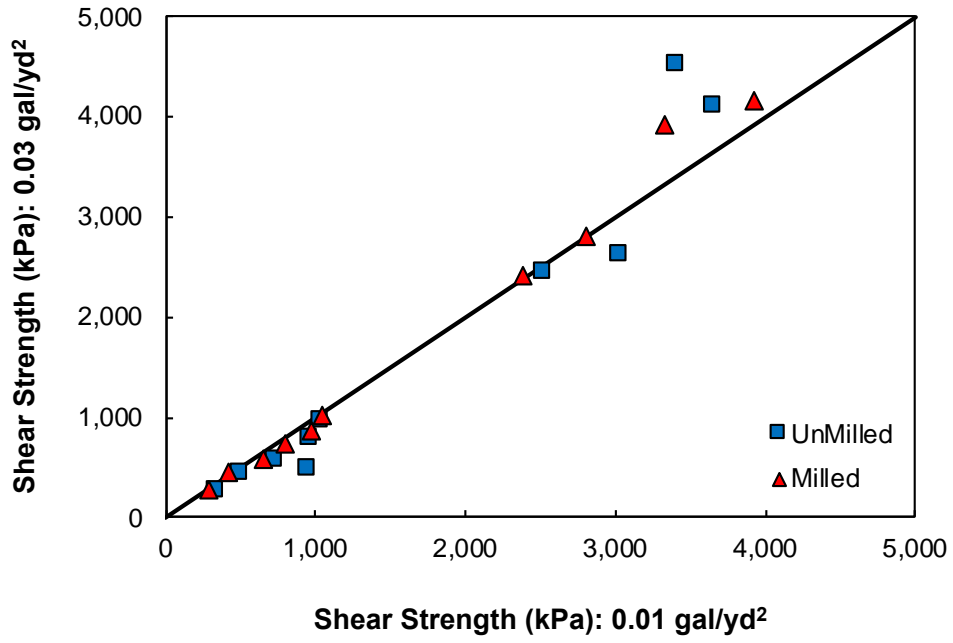
(b)



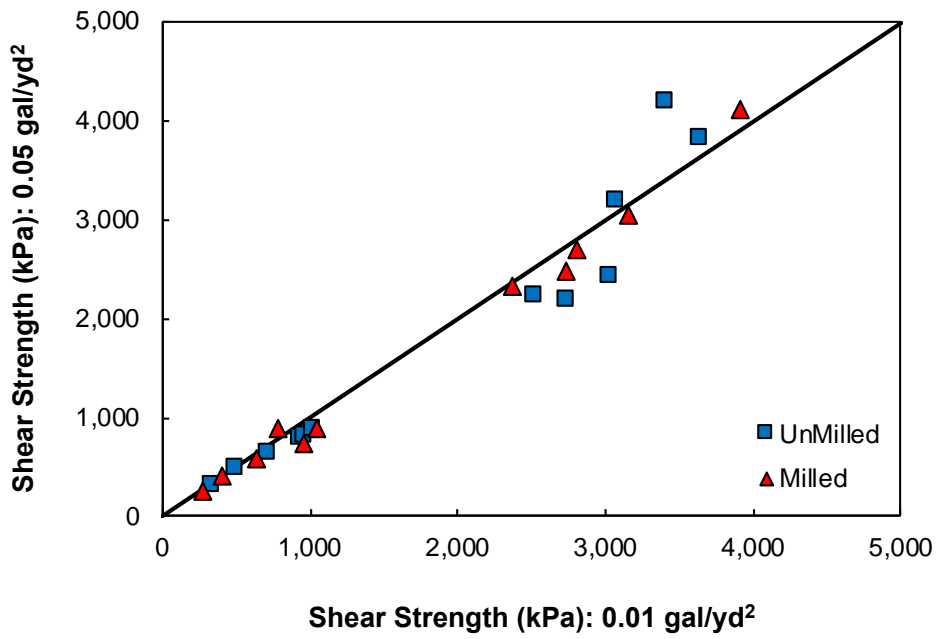
(c)

Figure 5-6. Shear strength mastercurves of CRS-2 at various application rates under milled condition: (a) 69 kPa, (b) 276 kPa, and (c) 483 kPa.

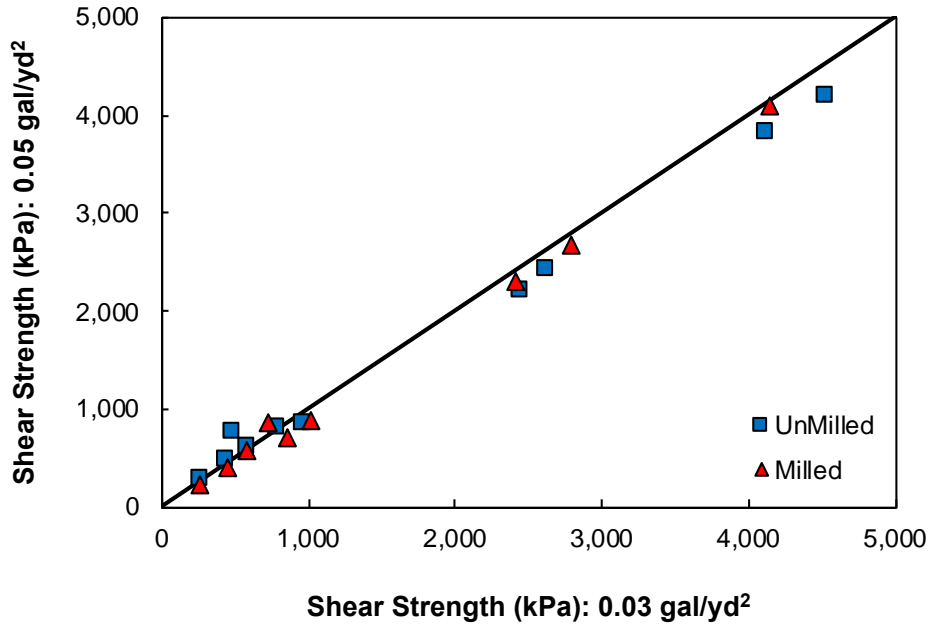
Similar to the comparisons of the shear strength values at two different confining pressures (Figure 6.7), Figure 5-7 presents comparisons of the shear strength values at two different application rates. In general, the effects of the tack coat application rate on the ISS are insignificant.



(a)



(b)



(c)

Figure 5-7. Comparisons of shear strength values of CRS-2 at two different application rates via line of equality: (a) 0.03 gal/yd² vs. 0.01 gal/yd², (b) 0.05 gal/yd² vs. 0.01 gal/yd², and (c) 0.05 gal/yd² vs. 0.03 gal/yd².

In order to examine the effects of the application rate, shear strength mastercurves were developed at three different application rates: 0.01 gal/yd², 0.03 gal/yd², and 0.05 gal/yd² at 483 kPa under the milled condition, as shown in Figure 5-8. Figure 5-9 presents comparisons of the shear strength values of CRS-1h at two different application rates under the milled condition. As was the case for the CRS-2 tack coat results, the effect of different application rates on the ISS is insignificant.

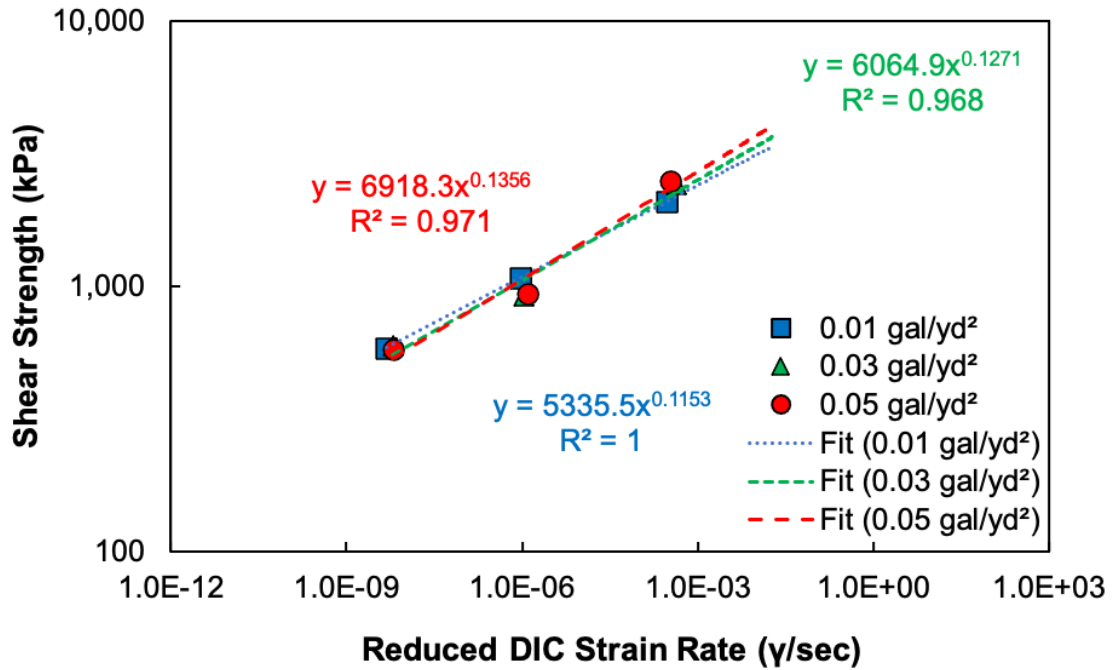
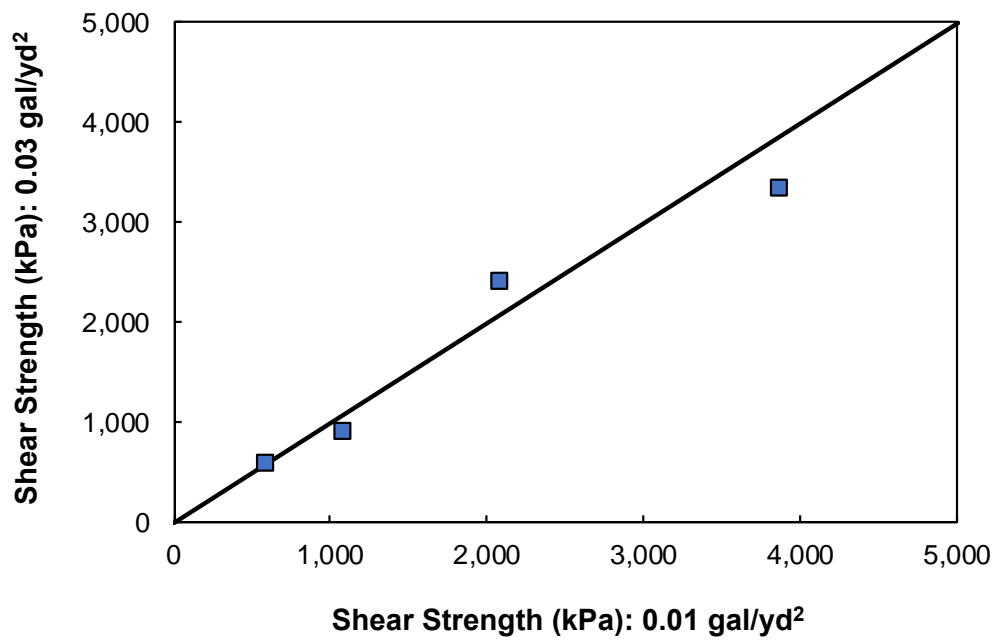
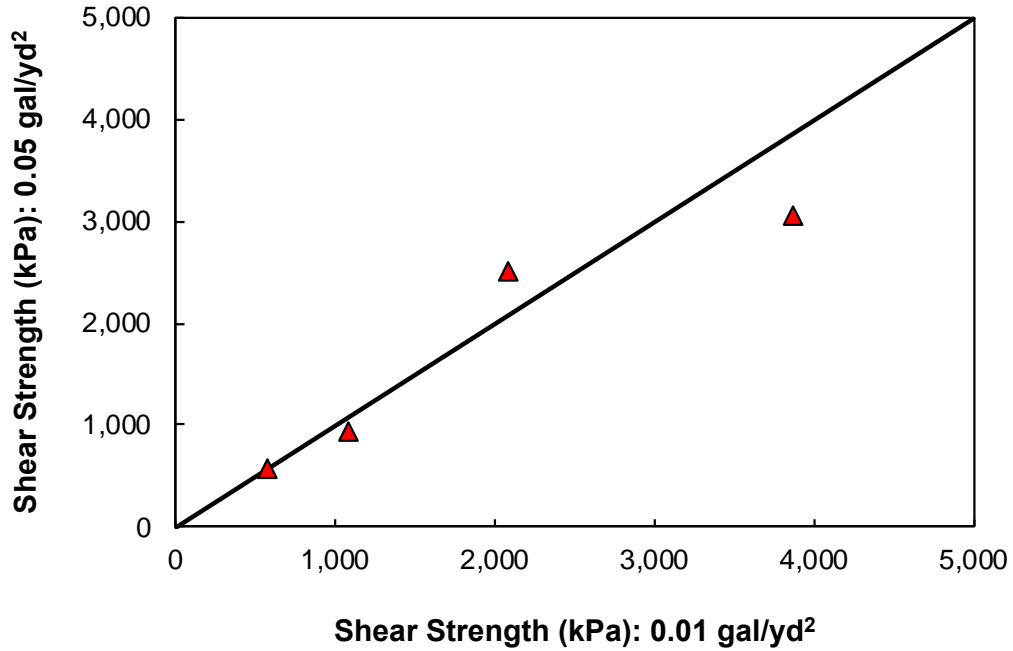


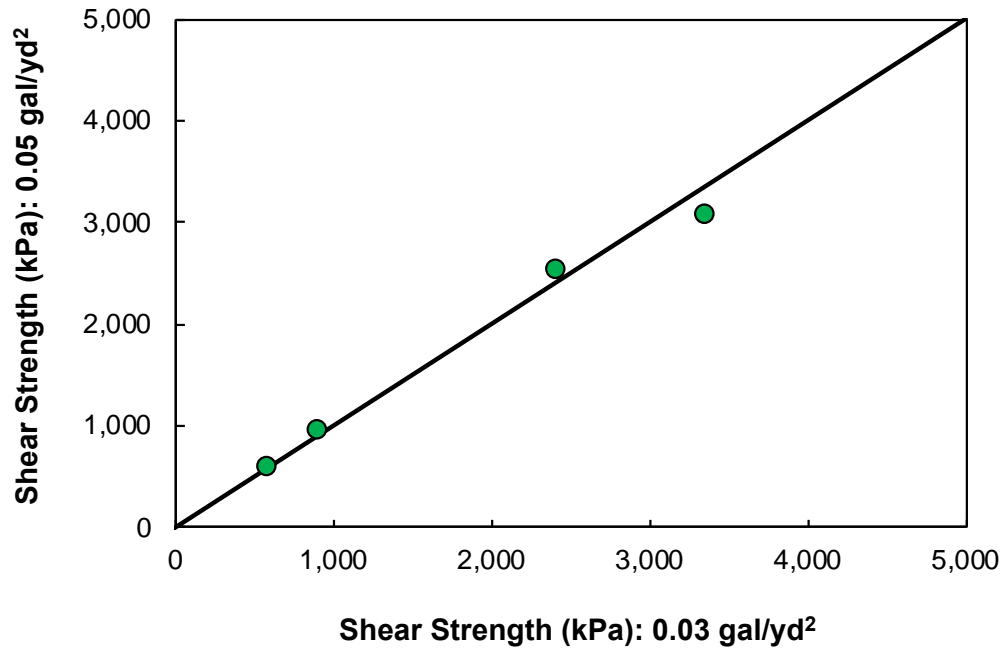
Figure 5-8. Shear strength mastercurves of CRS-1h at various application rates at 483 kPa under milled condition.



(a)



(b)



(c)

Figure 5-9. Comparisons of shear strength values of CRS-1h at two different application rates under milled condition via line of equality: (a) 0.03 gal/yd² vs. 0.01 gal/yd², (b) 0.05 gal/yd² vs. 0.01 gal/yd², and (c) 0.05 gal/yd² vs. 0.03 gal/yd².

Figure 5-10 shows the ISS values of specimens that were fabricated using the Ultrafuse tack coat with various tack coat application rates and at different temperatures. These results indicate that no definite trend could be established to demonstrate the effect of application rate. Figure 5-10 also shows that, when tested at 19°C, the specimen with an application rate of 0.03 gal/yd² has a marginally higher shear strength value than the other two ISS test specimens with application rates of 0.01 gal/yd² and 0.05 gal/yd².

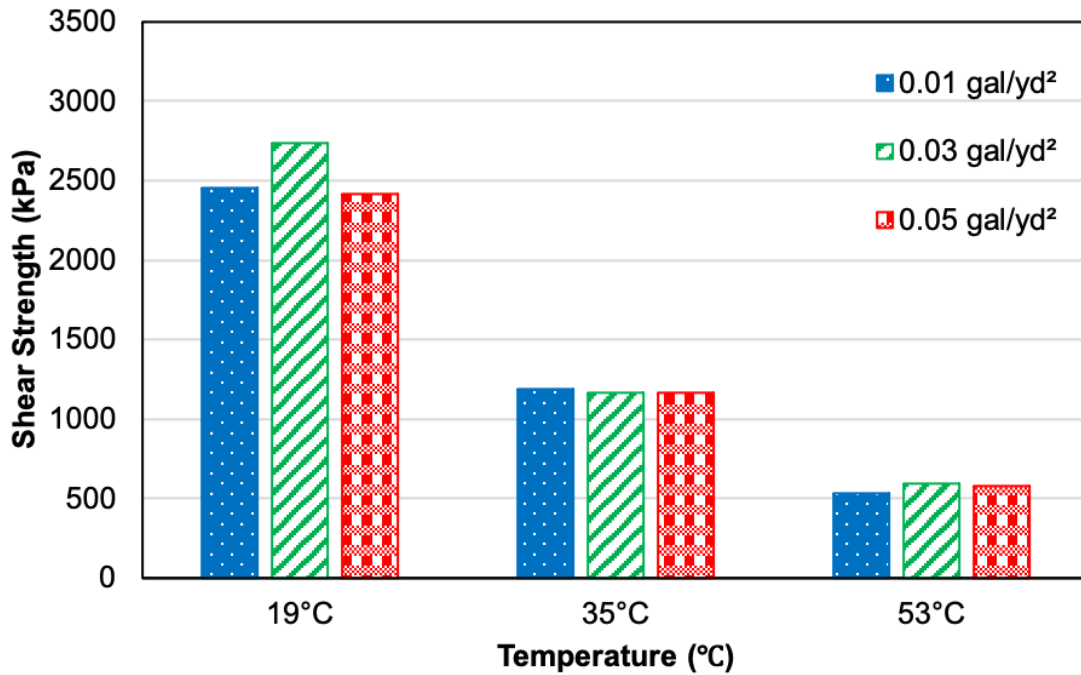
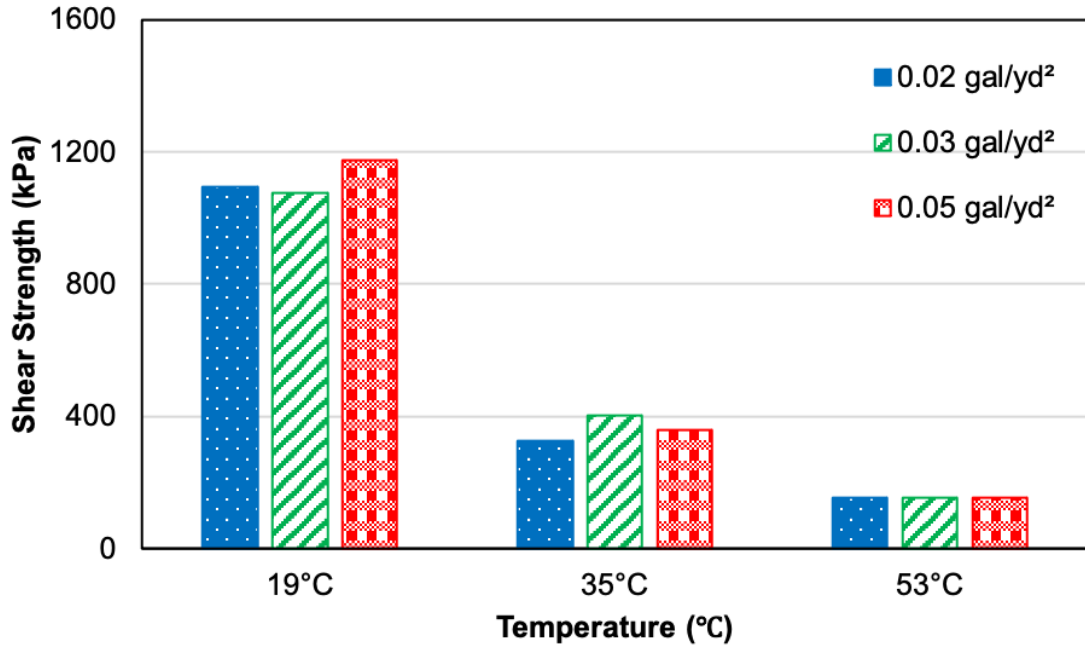
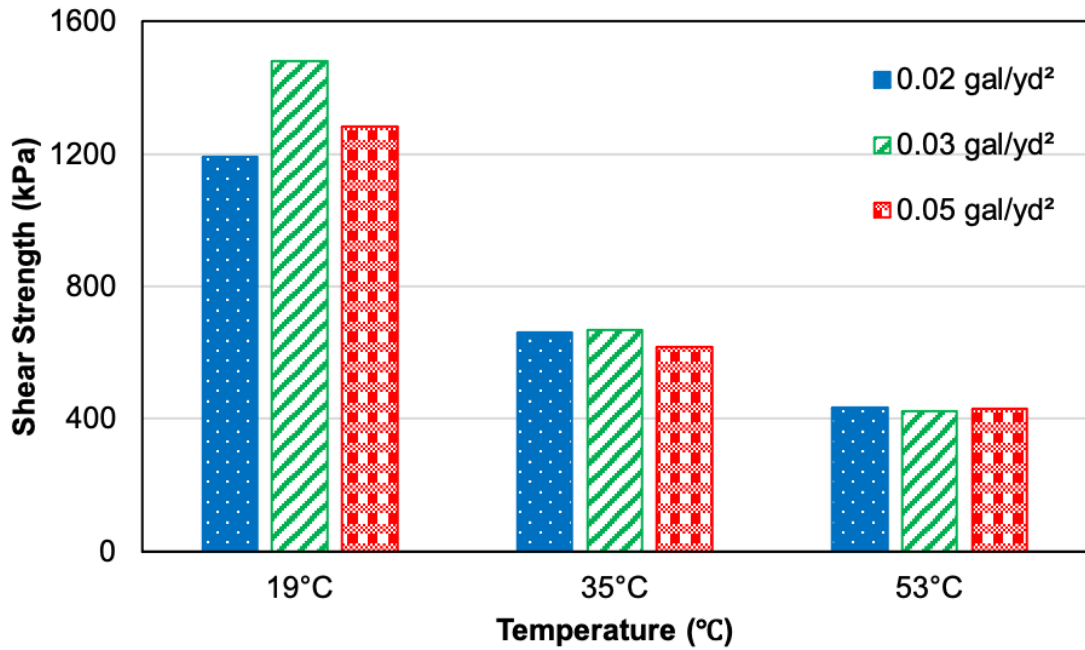


Figure 5-10. Variations in interface shear strength with temperature for Ultrafuse specimens fabricated using different tack coat application rates at 483 kPa confining pressure and with an ungrooved interface surface.

Similar to the study of the Ultrafuse test specimens, the CRS-2 (Source 2) test specimens with various tack coat application rates indicate no definite trend to justify the efficacy of the monotonic ISS test to differentiate the effects of tack coat application rate on the ISS. Figure 5-11 presents a comparison of the ISS test results for CRS-2 at different temperatures with 69 kPa and 483 kPa confining pressure.



(a)

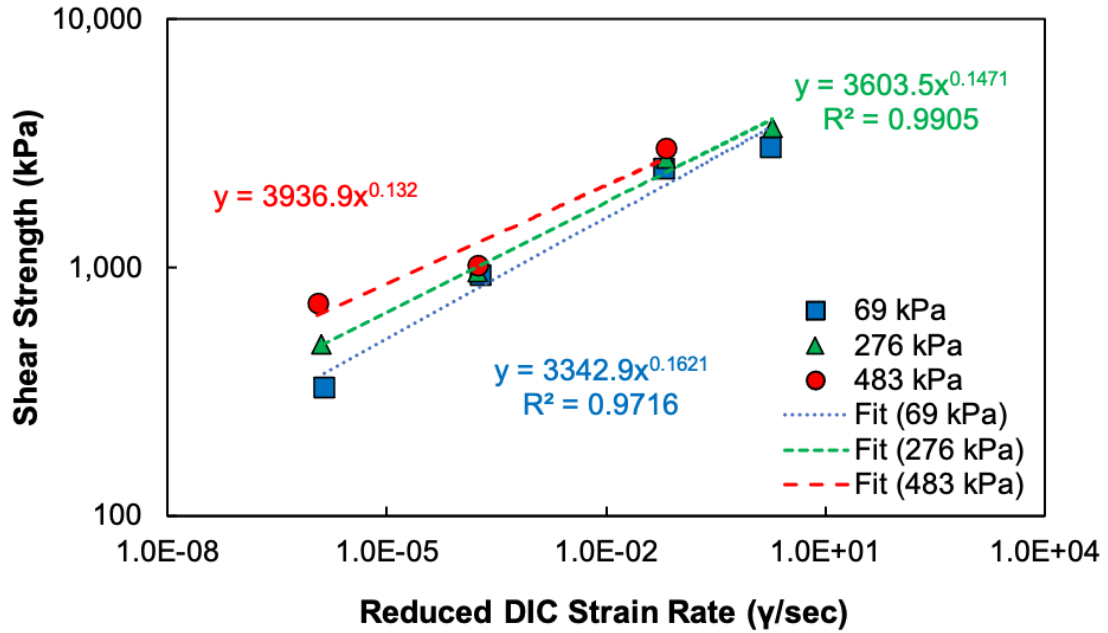


(b)

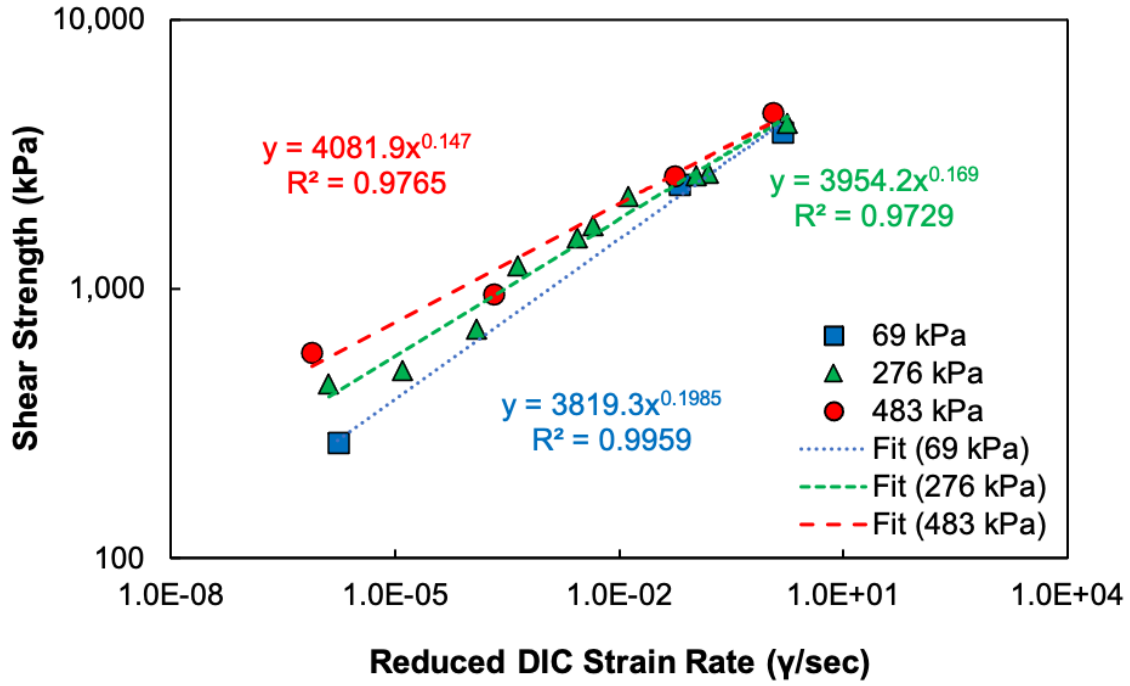
Figure 5-11. Interface shear strength of CRS-2 (Source 2) applied at various application rates on ungrooved interface surface at (a) 69 kPa confining pressure, and (b) 483 kPa confining pressure.

5.1.4 Effect of Loading Rate and Temperature

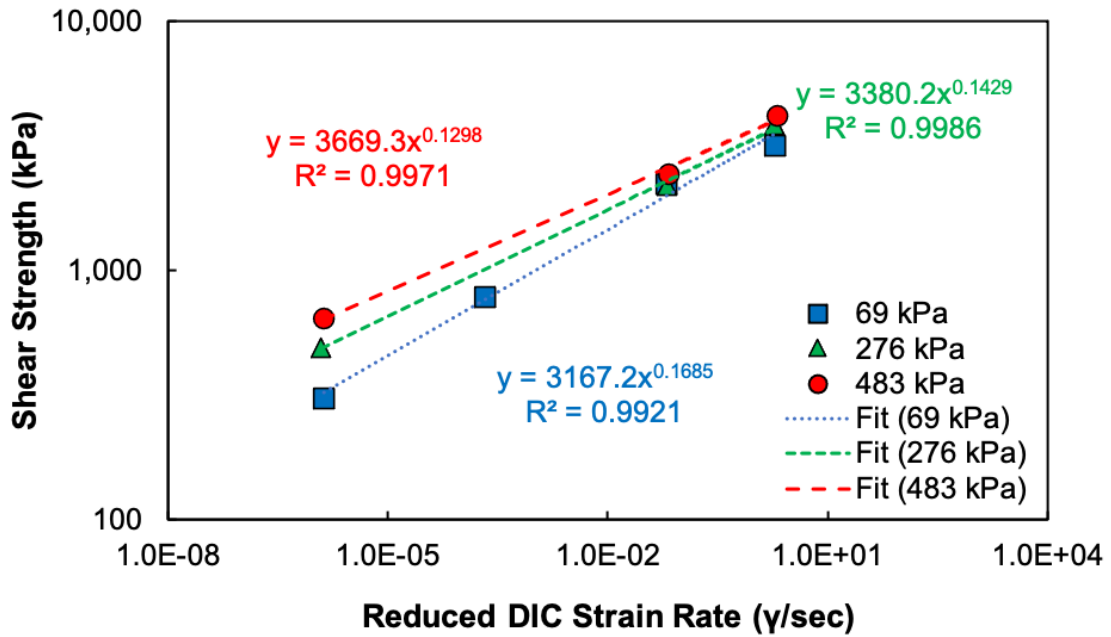
CRS-2 was applied as the first tack coat material to be tested. Figure 5-12 and Figure 5-13 present the shear strength mastercurves for the unmilled and milled conditions, respectively. Each figure consists of three graphs with the three tack coat application rates: 0.01 gal/yd², 0.03 gal/yd², and 0.05 gal/yd².



(a)

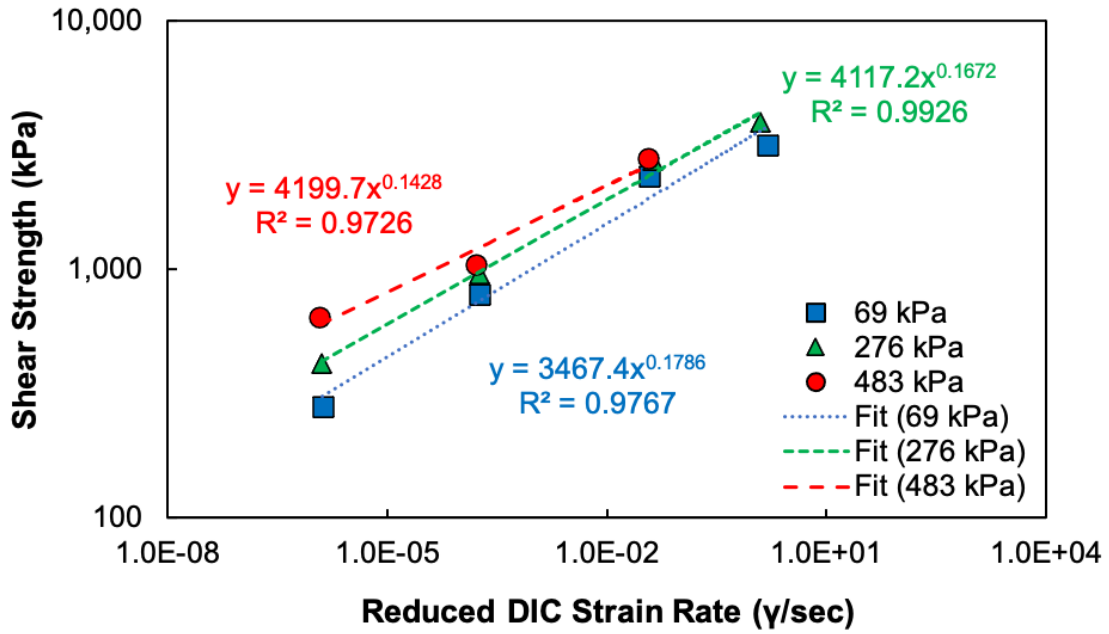


(b)

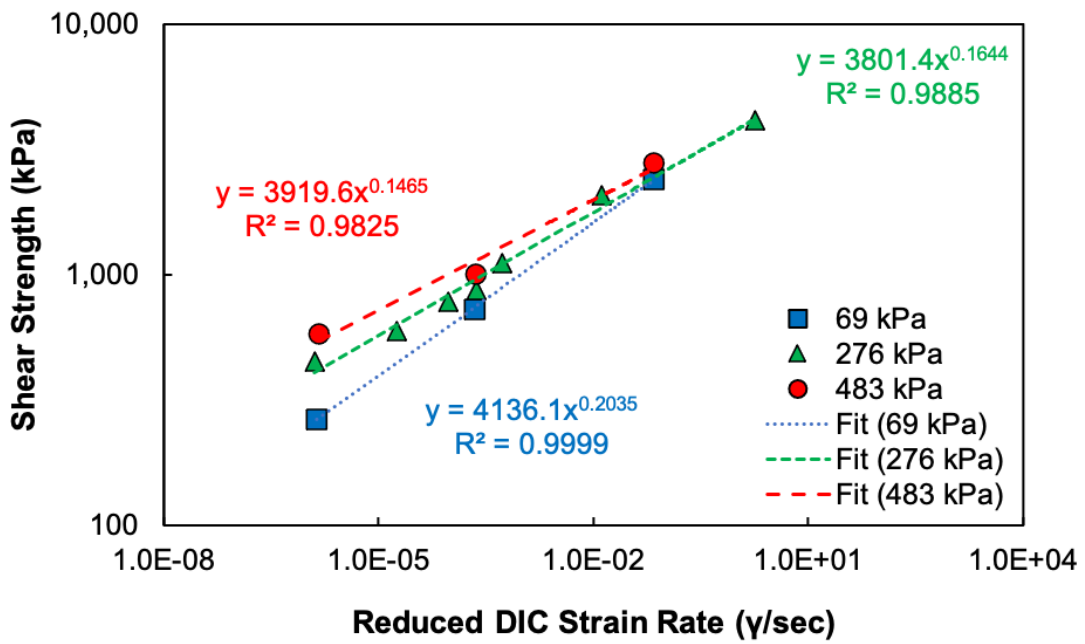


(c)

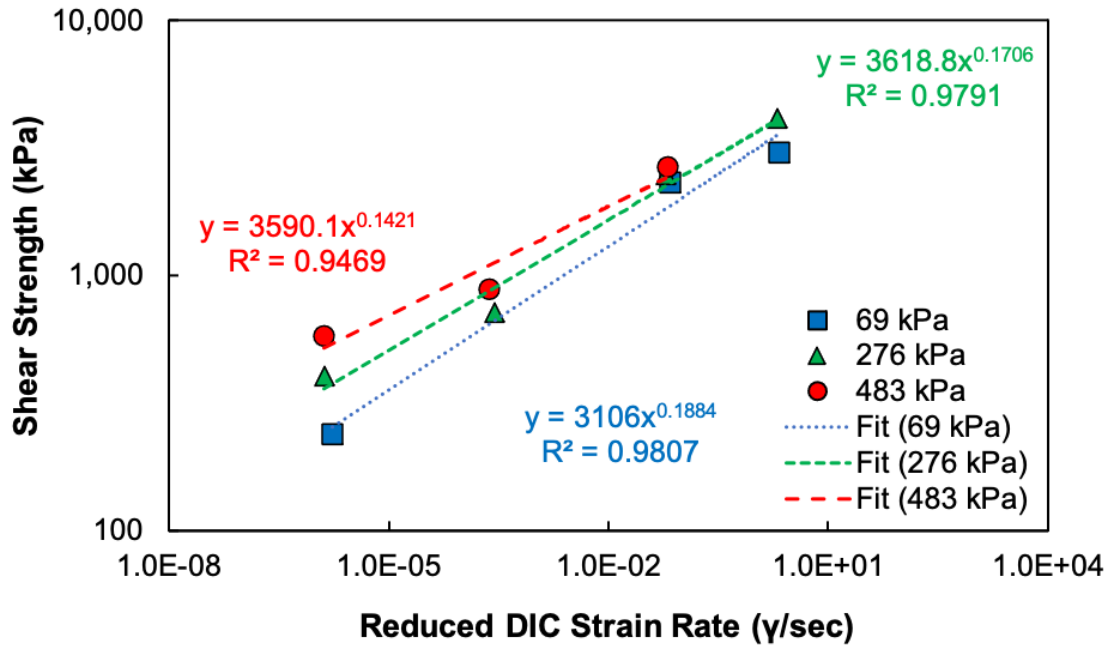
Figure 5-12. Shear strength mastercurves of CRS-2 at various confining pressures under unmilled condition using different tack coat application rates of (a) 0.01 gal/yd², (b) 0.03 gal/yd², and (c) 0.05 gal/yd².



(a)



(b)



(c)

Figure 5-13. Shear strength mastercurves of CRS-2 at various confining pressures under milled condition using different tack coat application rates of (a) 0.01 gal/yd², (b) 0.03 gal/yd², and (c) 0.05 gal/yd².

CRS-1h emulsion was applied as the second tack coat material to be tested. Figure 5-14 and Figure 5-15 present the shear strength mastercurves at the application rate of 0.03 gal/yd² under unmilled and milled conditions, respectively.

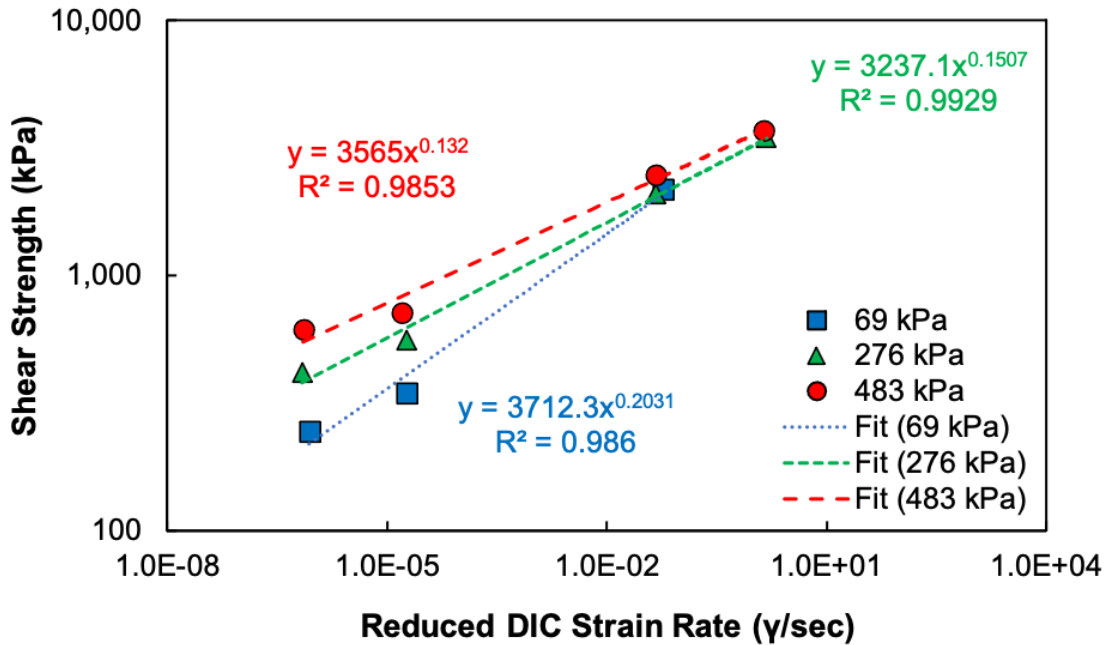


Figure 5-14. Shear strength mastercurves of CRS-1h at various confining pressures and 0.03 gal/yd² application rate under unmilled condition.

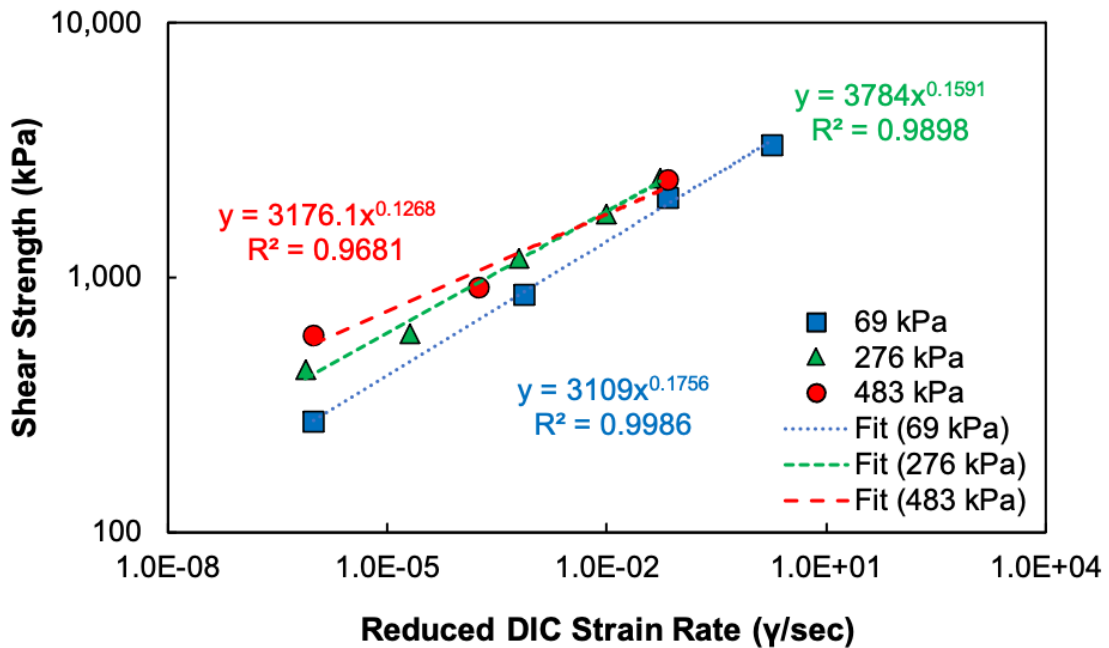


Figure 5-15. Shear strength mastercurves of CRS-1h at various confining pressures and 0.03 gal/yd² application rate under milled condition.

Gyratory-compacted MAST specimens fabricated with Ultrafuse as the tack coat material were applied at three rates of 0.01 gal/yd², 0.03 gal/yd², and 0.05 gal/yd² to evaluate their ISS. These

specimens were subjected to a constant displacement rate of 50.8 mm/min at three temperatures (19°C, 35°C, and 53°C) under normal confining pressure of 483 kPa to measure the effects of temperature and loading rate on the ISS. The specimen interface surface texture was ungrooved. The temperature and loading rate, represented as reduced strain rate, are significant factors that determined the ISS test results, as shown in Figure 5-16. These results indicate a trend; i.e., with an increase in reduced strain rate, the ISS increases. The same trend was observed for specimens fabricated using the other types of emulsions, CRS-2, NTCRS-1hM, and CRS-1h.

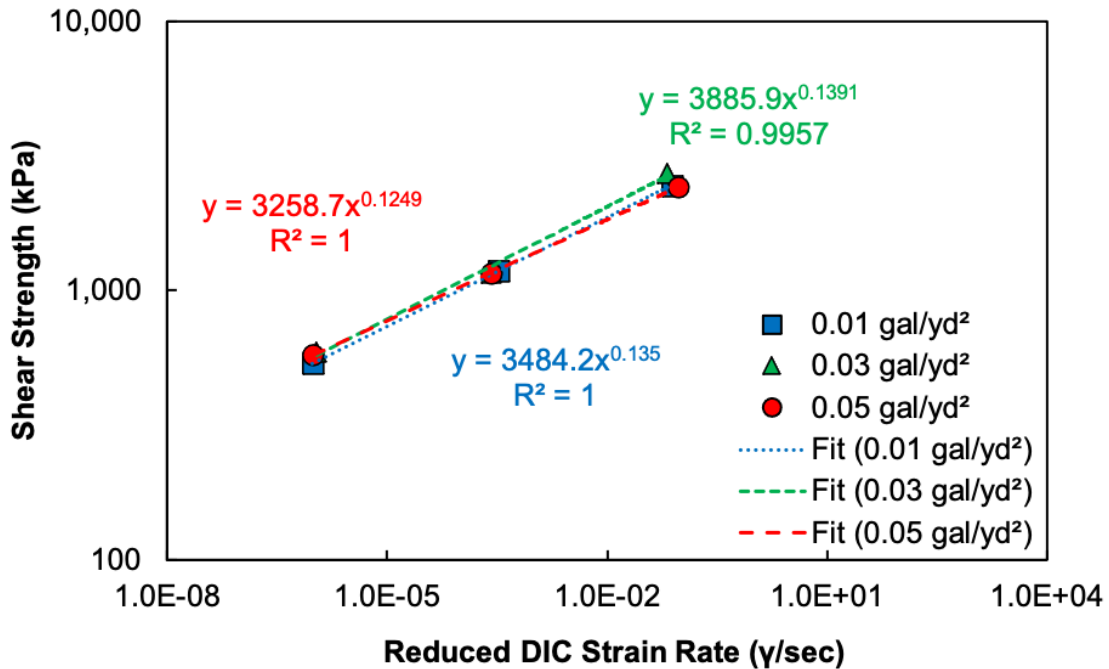
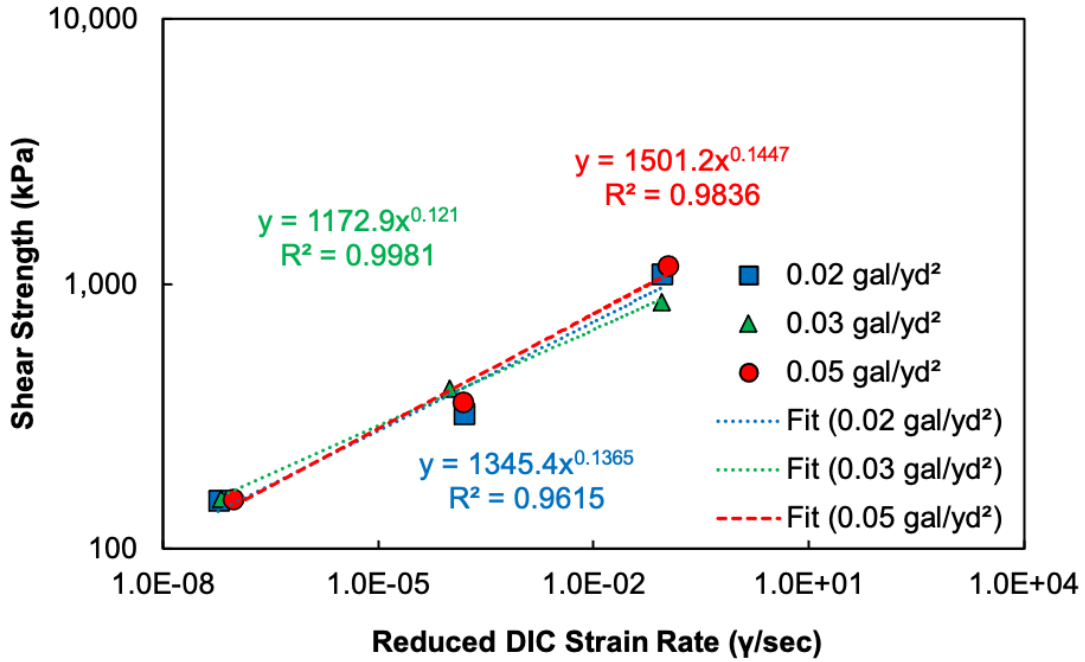
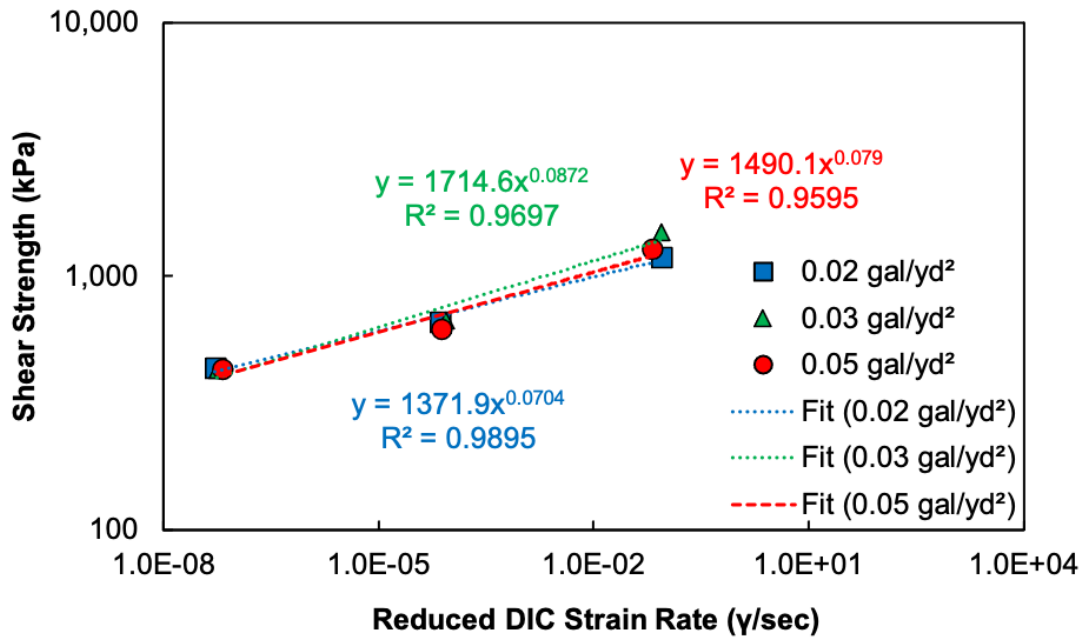


Figure 5-16. Shear strength mastercurves for Ultrafuse at various tack coat application rates under 483 kPa confining pressure and with an ungrooved interface surface.

MAST specimens with the newly obtained CRS-2 (Source 2) as the tack coat were fabricated using a slab compactor to resemble field compaction conditions. The details of the fabrication were detailed in [Appendix C](#). Figure 5-17 presents the shear strength mastercurves of the specimens with an ungrooved interface surface with different tack coat application rates: 0.02 gal/yd², 0.03 gal/yd², and 0.05 gal/yd² tested under 69 kPa and 483 kPa confining pressure, respectively. The test results for the slab-compacted specimens clearly show that the reduced strain rate is a primary factor that controls the ISS.



(a)

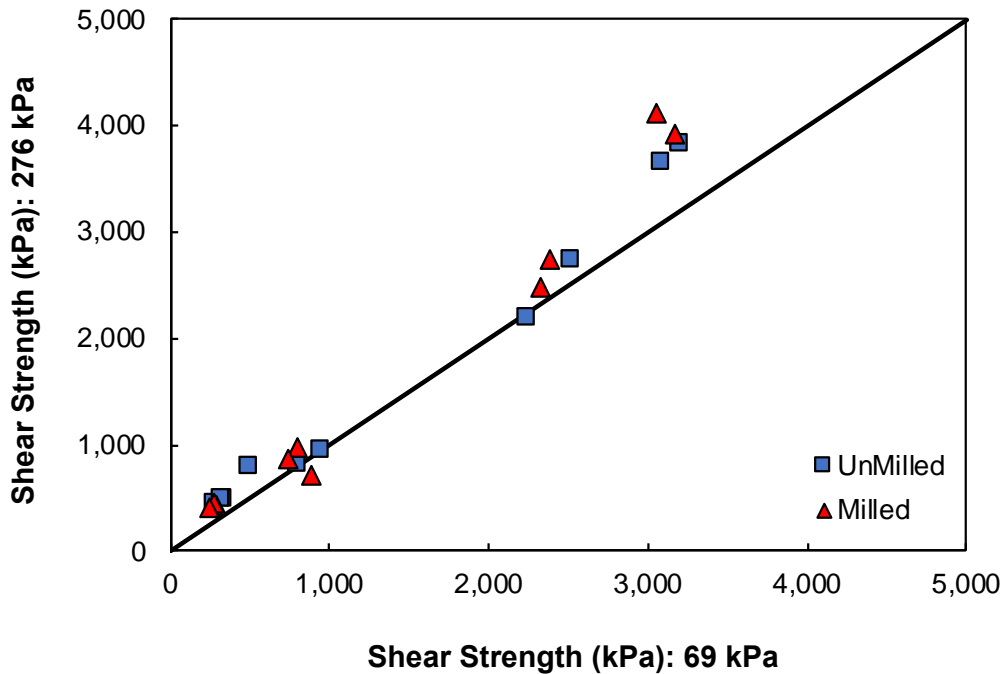


(b)

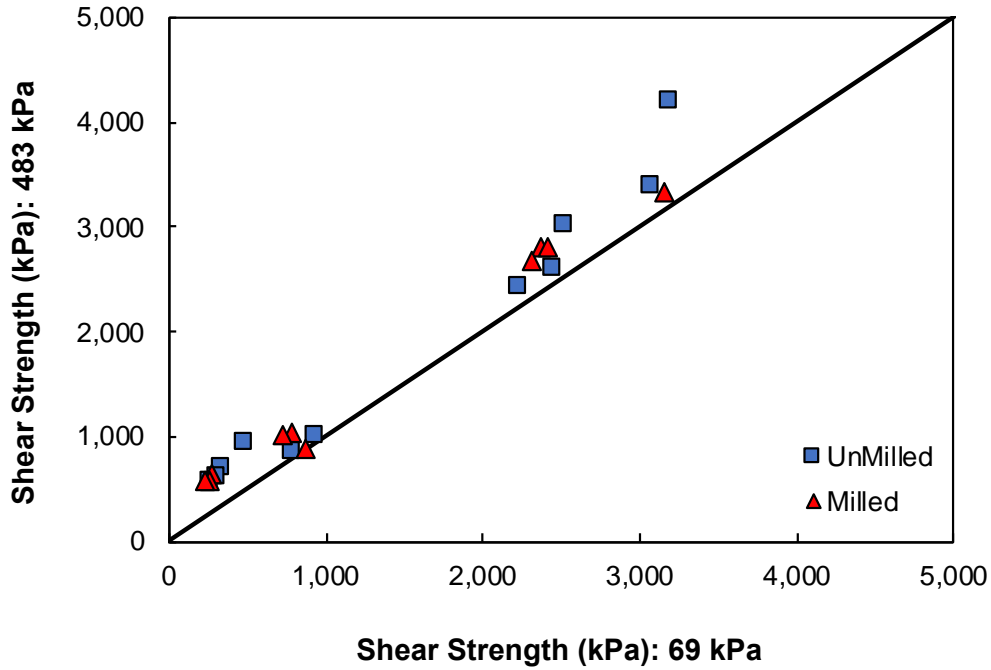
Figure 5-17. Interface shear strength mastercurves for CRS-2 (Source 2) at various application rates for ungrooved surface at (a) 69 kPa confining pressure and (b) 483 kPa confining pressure.

5.1.5 Effect of Normal Confining Pressure

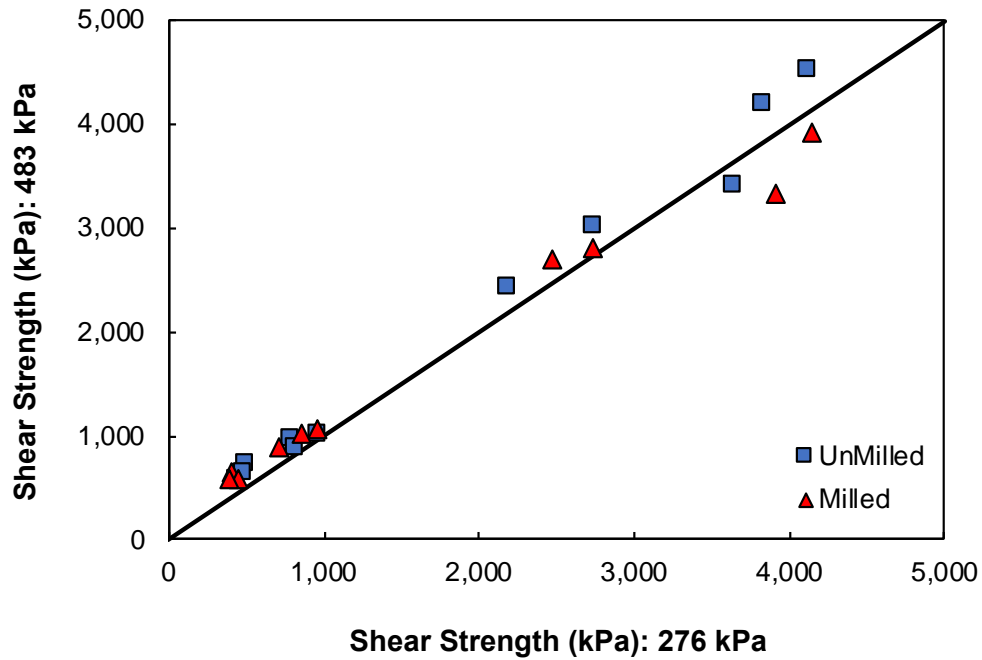
The figures shown in Section 5.1.5 also show the effects of confining pressure via the plots of the shear strength mastercurves. Moreover, Figure 5-18 presents comparisons of the shear strength values at two different confining pressures under milled and unmilled conditions. The largest difference in ISS between the two confining pressures is shown in Figure 5-18 (b) for 483 kPa vs. 69 kPa. Most data points are located above the line of equality, indicating greater ISS from the 483 kPa confining pressure than from 69 kPa. Figure 5-18 (a) shows that the difference in ISS between 276 kPa and 69 kPa is less than between 483 kPa and 69 kPa, whereas the difference in ISS between 483 kPa and 276 kPa is the least, as shown in Figure 5-18 (c). These observations clearly demonstrate the effects of confining pressure on ISS; that is, greater confining pressure results in greater ISS.



(a)



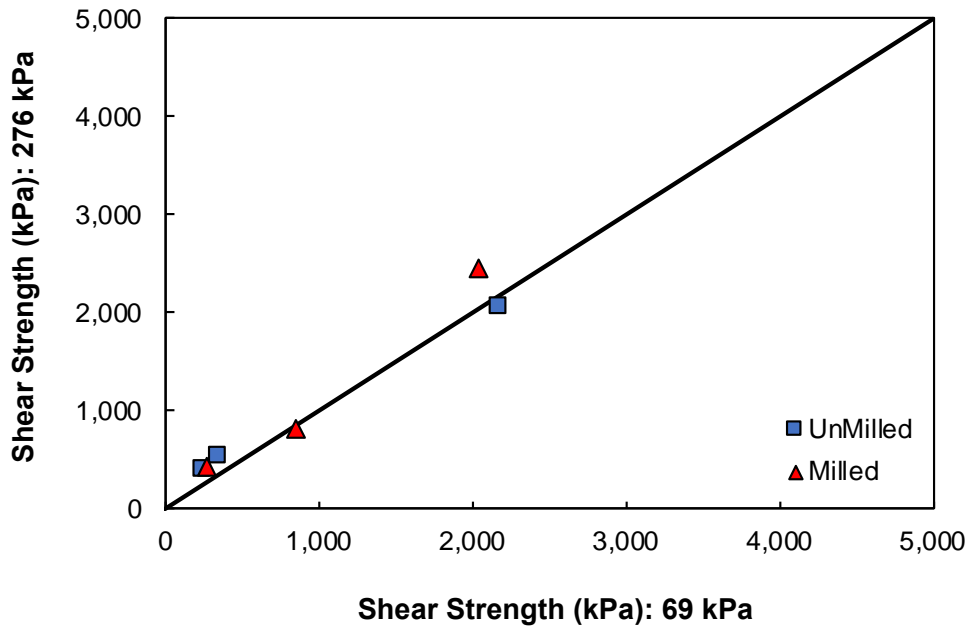
(b)



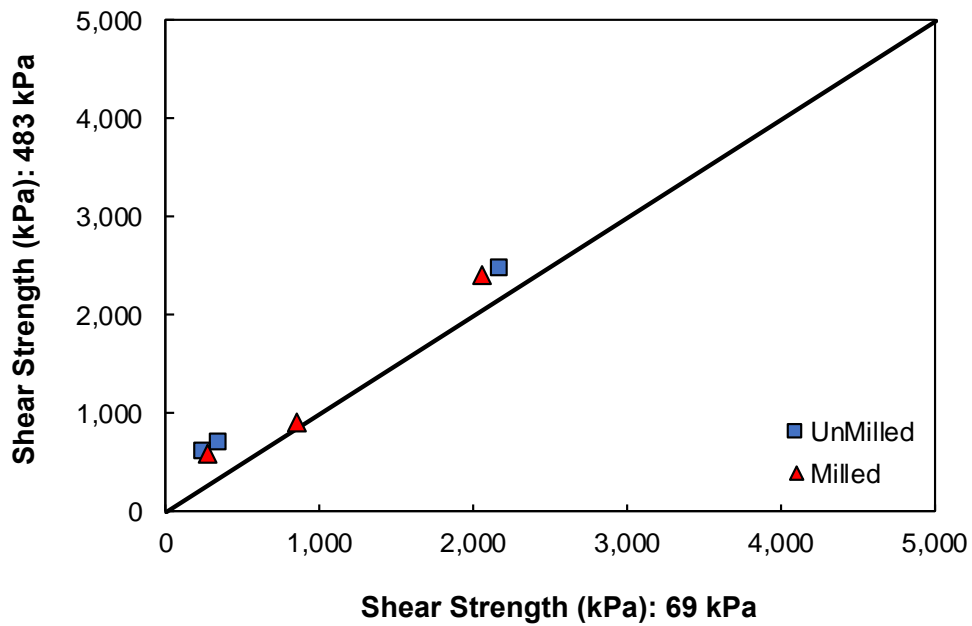
(c)

Figure 5-18. Comparisons of shear strength of CRS-2 under unmilled and milled conditions at two different confining pressures via line of equality: (a) 276 kPa vs. 69 kPa, (b) 483 kPa vs. 69 kPa, and (c) 483 kPa vs. 276 kPa.

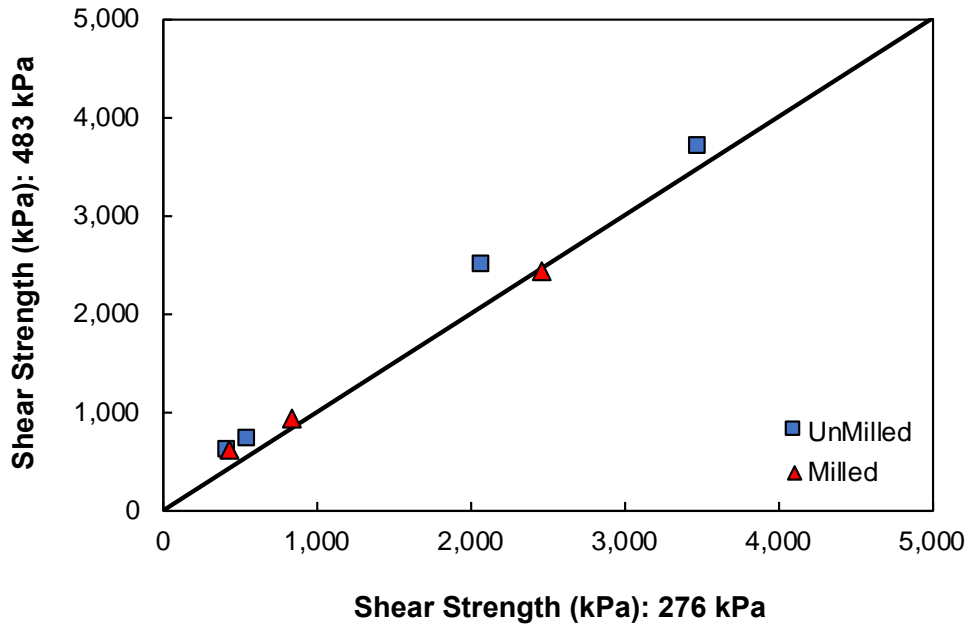
In order to examine specific differences, Figure 5-19 presents comparisons of the shear strength values of CRS-1h at two different confining pressures. The trends seen in Figure 5-19 for CRS-1h are the same as those seen in Figure 5-18 for the CRS-2 tack coat; that is, the confining pressure of 483 kPa results in the greatest ISS, followed by 276 kPa and finally 69 kPa.



(a)



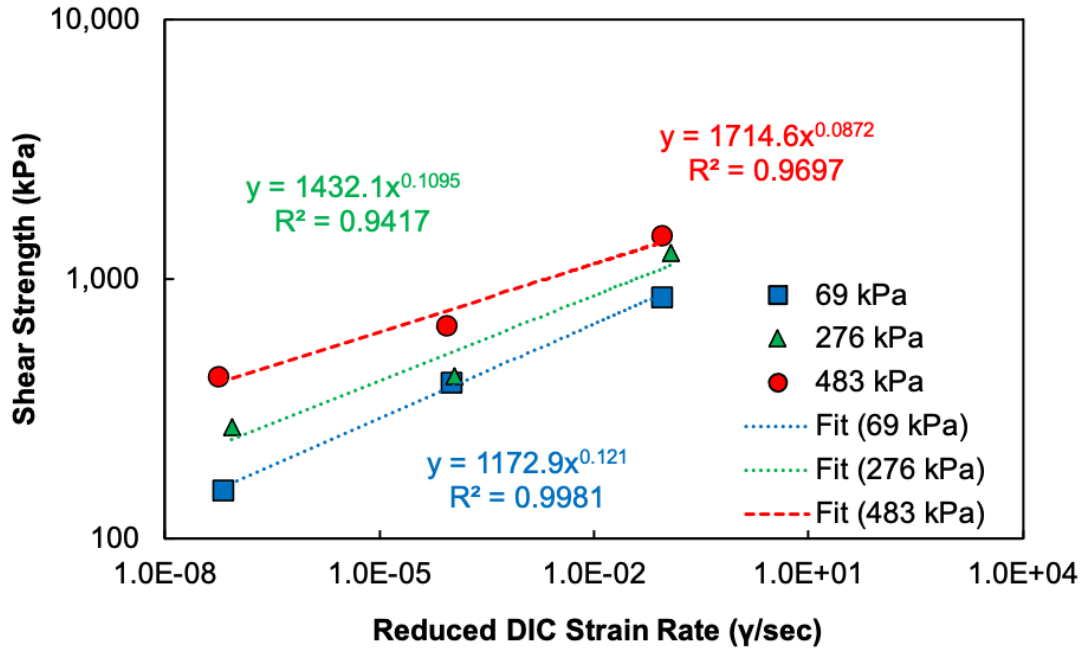
(b)



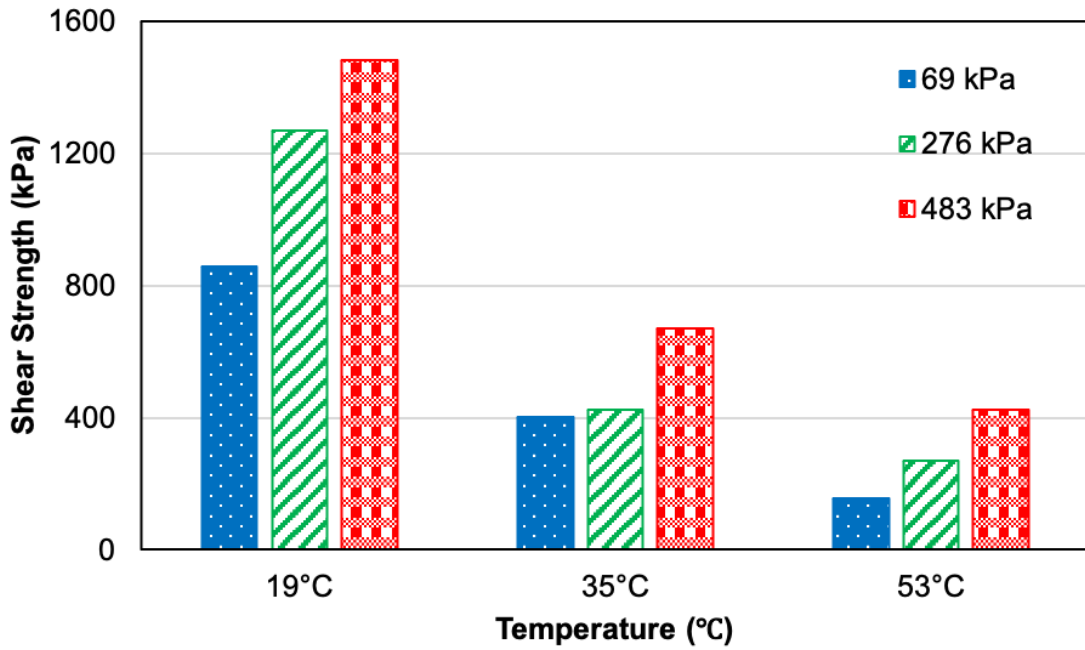
(c)

Figure 5-19. Comparisons of shear strength values of CRS-1h at two different confining pressures via line of equality: (a) 276 kPa vs. 69 kPa, (b) 483 kPa vs. 69 kPa, and (c) 483 kPa vs. 276 kPa.

The effect of confinement on the ISS is evident for the slab-compacted specimens with the CRS-2 (Source 2) tack coat. The outcomes indicate that, with an increase in confinement, the mobilization of frictional stress at the interface occurs, thereby increasing the ISS. In order to complete the test matrix, additional tests were carried out at a confining pressure of 276 kPa; Figure 5-20 presents the results.



(a)



(b)

Figure 5-20. Effect of confining pressure at application rate of 0.03 gal/yd² of CRS-2 (Source 2): (a) mastercurve for interface shear strength and (b) at three confining pressure levels.

5.1.6 Effect of Surface Type

Figure 5-21 presents a comparison of the shear strength values of CRS-2 under two different surface conditions to show the effects of surface conditions on shear strength. This figure shows that the ISS values obtained from a milled surface are close to those from an unmilled surface. This finding is somewhat unexpected because the milled surface would provide more friction under shear loading and thus greater ISS than an unmilled surface. However, the shear loading was applied in the direction of the grooves on the milled surface and therefore would not necessarily provide additional friction during the shear test. In the field, the grooves are oriented in relatively random directions and, thus, greater shear strength is expected from the milled surface. The effect of the angle between the loading direction and the groove direction on ISS is investigated.

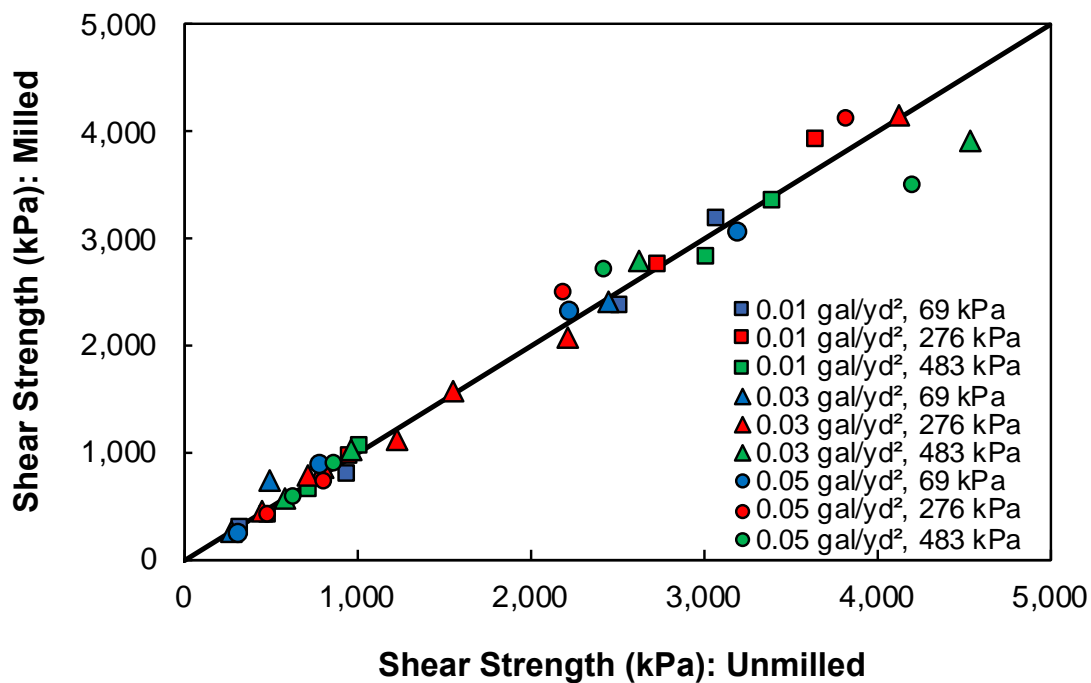


Figure 5-21. Comparison of shear strength values of CRS-2 between milled and unmilled conditions via line of equality.

Figure 5-22 indicates the effects of surface conditions on shear strength by comparing the shear strength values of CRS-1h under the two surface conditions. Figure 5-22 also provides information about the difference in shear strength for CRS-1h under milled and unmilled conditions. As in the CRS-2 cases, no significant difference in ISS as a function of surface conditions is evident.

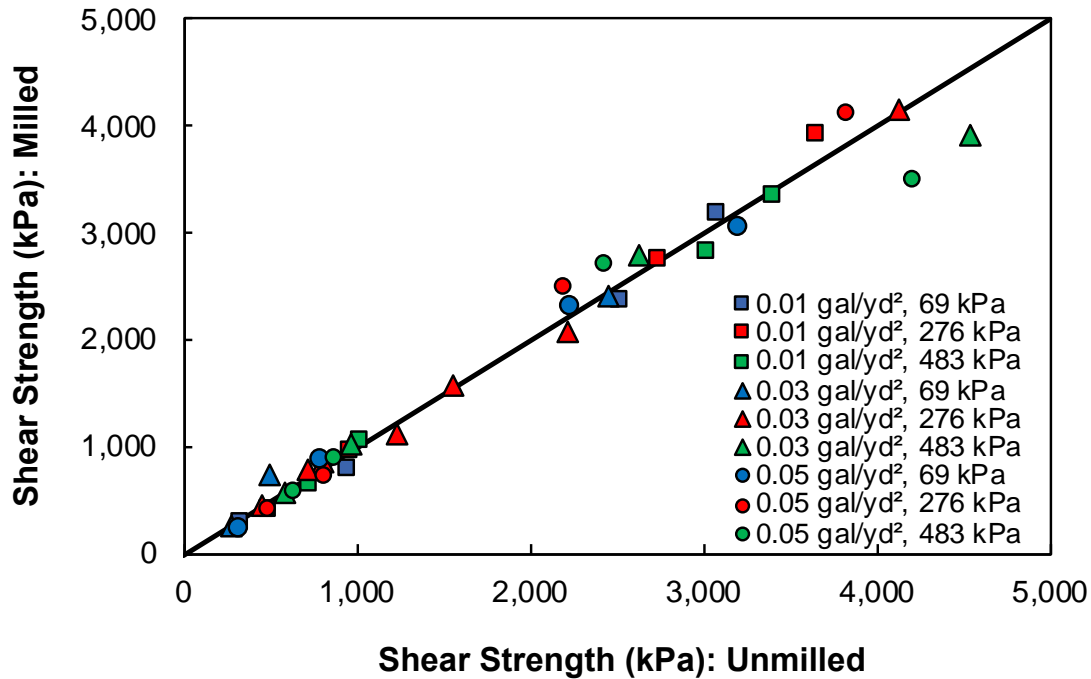


Figure 5-22. Comparison of shear strength values of CRS-1h under milled and unmilled conditions via line of equality.

5.1.7 Effect of Groove Direction

The study of the effects of surface type revealed that a milled surface does not improve the ISS compared to an unmilled surface. During the tests, the grooves of the milled specimens were oriented in the shear loading direction. The alignment of the loading direction and groove orientation and well-defined grooves made in the laboratory are the suspected cause for the insignificant effect of surface type on the ISS. Note that milled surfaces in the field are far more random and uneven. The contrary response to the anticipated performance of the milled surface led to a study of the effect of the groove direction/orientation on the ISS. Three angles, 0°, 30°, and 90°, were considered for the study and were set between the loading and groove directions, as depicted in Figure 5-23.

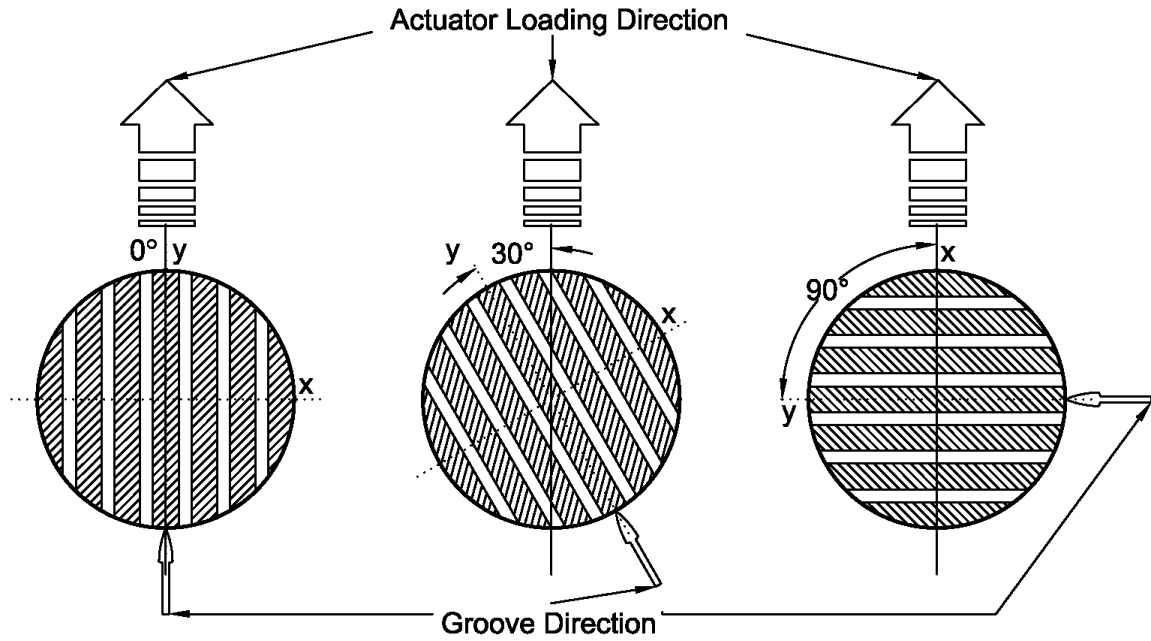


Figure 5-23. MAST specimen loading configuration with different angles of the grooves.

NTCRS-1hM sprayed specimens were selected for this study. The confining pressure of 25 psi was applied for the tests. Three actuator strain rates of 2, 0.2, and 0.02 in./min were applied to the specimens that had been conditioned at three different temperatures (19°C, 35°C, and 53°C). Figure 5-24 shows the ISS mastercurves of NTCRS-1hM for the three groove directions. The results clearly show that the change in groove direction has a negligible effect on the ISS.

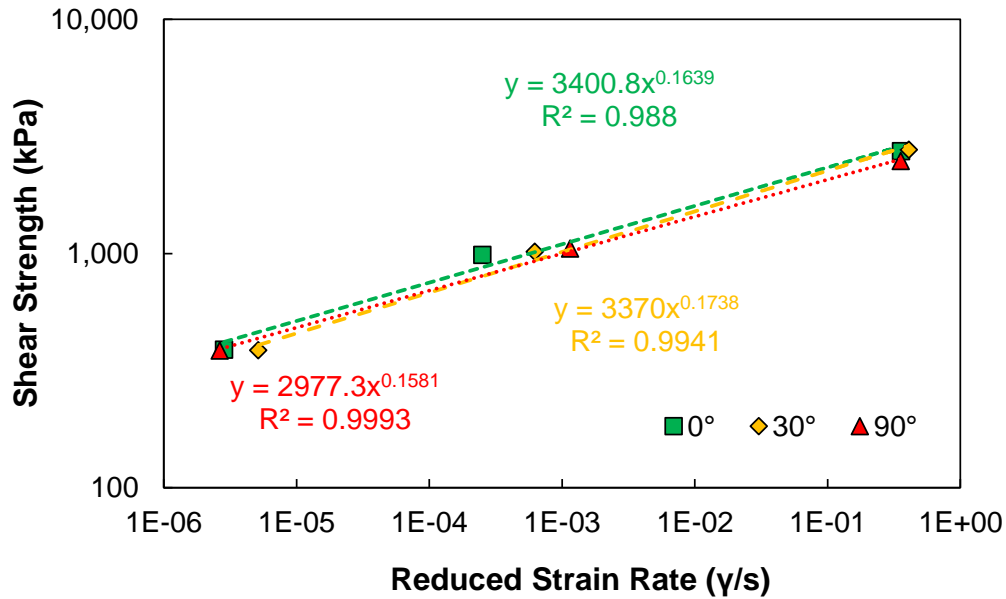


Figure 5-24. Interface shear strength mastercurves of NTCRS-1hM for three groove directions/angles and 0.05 gal/yd² application rate.

In order to investigate the reason for the insignificant effect of the groove direction on the ISS, the failed grooved surfaces were examined to determine their fracture patterns, as shown in Figure 5-25. The failed surfaces of the grooved specimens at the 19°C, 2 in./min condition show white spots that indicate aggregate fracture. These white spots appear at the top half of the specimen surface because the shear crack starts from the bottom of the specimen and, as the crack propagates, a smaller area of the specimen takes the load, which in turn increases the stress in the remaining area. This increased stress in the top half of the specimen seems to be the cause of the aggregate fracture. Another observation that can be made from Figure 5-25 is that the groove pattern can be seen after failure for the specimen surfaces at the 30° groove angle at 35°C and 53°C, but not for the specimens with the 0° and 90° groove angles. In other words, the 30° angle groove specimens at 35°C and 53°C show the presence of grooves on the failed surface, which is not observed in the other cases. Although it is premature to pinpoint the reason(s) that different failure patterns are seen in specimens with the 30° angle grooves using the results from one replicate test per condition, the distribution of the shear stress along and perpendicular to the ribs seems to have caused the observed patterns. In short, the areas of the ribs that contribute to bearing the load are the same in the 0° and 90° cases. The only difference is the direction/orientation of the stress in the yz and xz planes, respectively. In the 30° angle case, τ_{yz} and τ_{xz} acted together in every rib, thereby reducing the stress experienced by the ribs in each shear plane (yz and xz) by resolving the force component. As a result, the ribs did not shear, but rather allowed the specimen to dilate, which unhinged the interlock of the ribs and then left the groove patterns on the specimen surface.

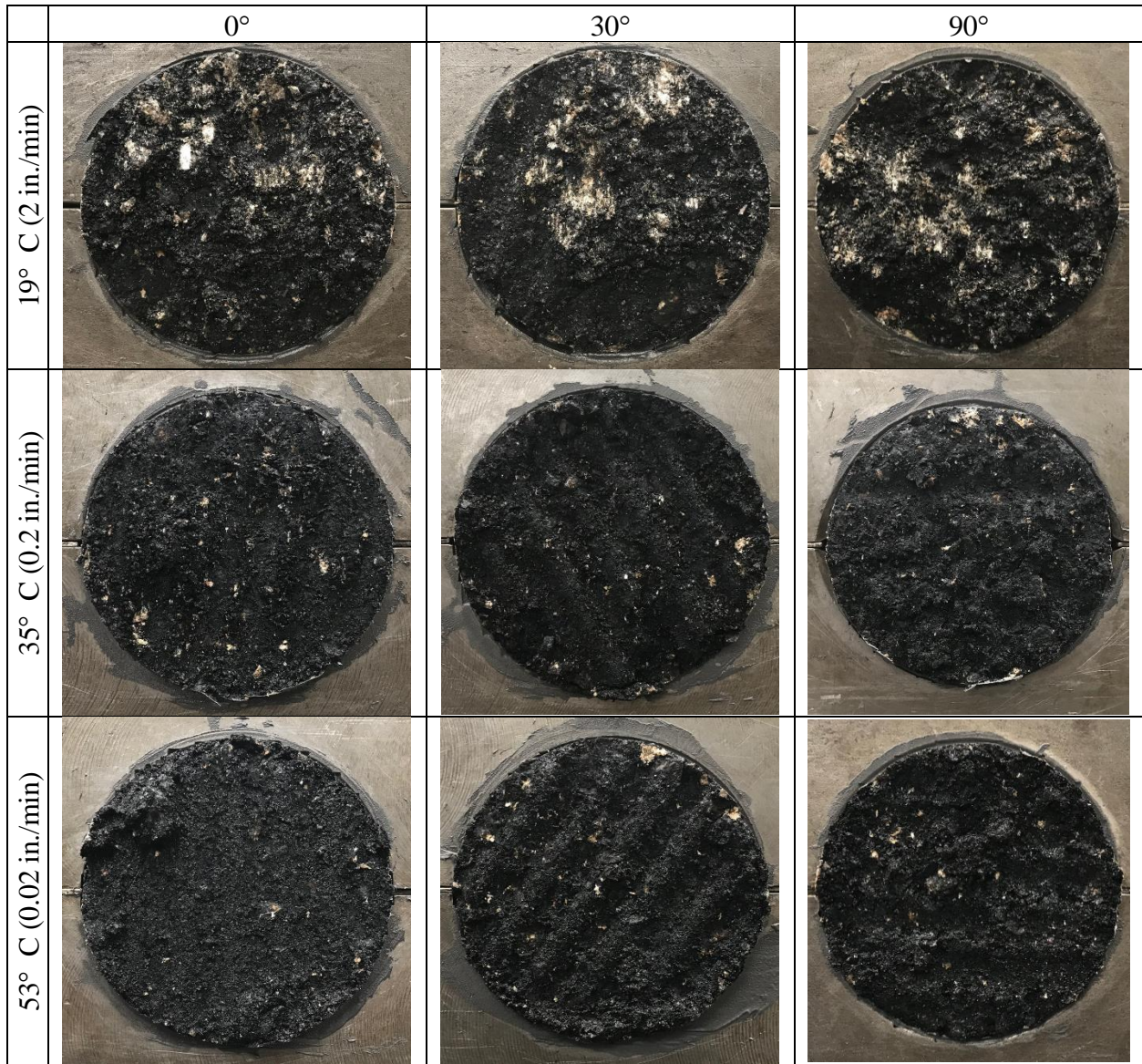


Figure 5-25. Failed grooved surfaces with different groove orientations at three temperatures and loading rates.

Statistical multiple regression analysis was carried out using Rstudio software to determine the effects of various parameters considered for the study. The null hypothesis assumed here is that no effect is evident from the parameter/parameters in question. The decision rule adopted here is that, if the p -value < 0.05 , then the null hypothesis is rejected (i.e., a parameter has an effect on the ISS). If the p -value > 0.05 , then the rejection of the null hypothesis fails (i.e., a parameter does not affect the ISS). Table 5-2 shows the p -values for the various parameters considered in the study and that the reduced strain rate is the only parameter that influences the ISS.

Table 5-2. *P*-values Obtained from Multiple Linear Regression Analysis of Effect of Groove Angle on Interface Shear Strength

Parameters	<i>F</i>-value	<i>P</i>-value
Reduced strain rate	8725.24	0.007
Confinement	0.01	0.949
Groove angle	18.17	0.147
Reduced strain rate × confinement	9.58	0.199
Confinement × groove angle	1.48	0.438
Reduced strain rate × groove angle	18.84	0.144
Reduced strain rate × confinement × groove angle	43.35	0.096

In order to reiterate the observations made regarding milled surfaces, the findings of other researchers are reported in Table 5-3. The different project findings are contradictory in many aspects because of differences in the test specimen fabrication method and the tack coat type employed in making the specimen. However, certain observations are in common. Even though no study listed in Table 5-3 explicitly investigated the effect of groove direction on ISS, the studies that were carried out using field and laboratory-made specimens are considered for discussion. Bahia et al. (2019) reported that the ISS of field milled specimens is comparable to that of field unmilled specimens, whereas laboratory-fabricated unmilled specimens show a big improvement in ISS compared to unmilled field specimens. Therefore, Bahia et al. did not recommend using laboratory specimens to predict ISS in the field. Also noteworthy is that the laboratory specimens used in the Bahia et al. study were fabricated using a gyratory compactor, yet the laboratory and field milled specimens showed comparable ISS values. The probable cause for the similar strength results may be attributable to the fact that the bottom layer of both the lab and field specimens used milled specimens cored from the field. The ISS of the laboratory and field specimens measured by Coleri et al. (2020) in their study also yielded comparable results. This outcome may be due to the use of a slab compactor to make both the milled and unmilled specimens in the laboratory in the Coleri et al. (2020) study. Therefore, the conclusion is that the compaction method has an effect on the ISS. Coleri et al. also found that different MTDs do not affect the ISS and that laboratory milling practices do not create any differences in ISS. These findings indicate that the ISS of laboratory-fabricated specimens is less likely to be affected by groove patterns and directions.

These observations lead to the conclusion that milled surfaces do not have an effect on bond strength during ISS tests; however, this conclusion does not imply that milled surfaces do not affect pavement performance. In order to evaluate the performance of milled pavement surfaces, field loading conditions must be simulated in the laboratory by applying cyclic loading. The fatigue decay rate of the interface modulus for the milled and unmilled surfaces will dictate the resistance against debonding. Even though debonding is assumed to be caused by a single event (e.g., while a vehicle is braking), the chances of that event causing a detrimental effect on the

pavement will increase with post construction traffic. The delay time that the interface condition takes to reach that critical bond condition depends on the surface type, i.e., milled or unmilled. Therefore, researching the effects of milled surfaces under cyclic loading on the reduction in the interface modulus and bond strength is highly recommended.

Table 5-3. Summary of Major Findings Related to Interface Shear Strength of Milled Pavements

Reference	Fabrication Method		MTD	Tack Coat Type	TC App. Rate	Equipment for Testing			
	Bottom Layer	Top Layer				Name	LR	σ_c (psi)	Temp.
			mm		gal/yd ²		mm/min	psi	°C
Mohammad et al. (2012)	Field	Field	NA	SS-1h	0.055	LISST	2.54	20	25
Major Conclusion: The milled surface performed better than new or existing HMA pavement (unmilled surface).									
Mohammad et al. (2018)	Field	Field	1.62	Non-tracking SS-1H	0.05	LISST	2.54	--	25
	Field	Field	1.56	Non-tracking SS-1	0.05				
	Field	Field	1.92	CBC-1h, NTSS-1hM, CSS-1h	0.05				
	Field	Field	1.83	CSS-1H, CBC-1H	0.03-0.07				
Major Conclusion: The milled HMA surface yielded the highest ISS, followed by new HMA, existing HMA, and PCC surface types.									
Ghanchi et al. (2018)	Field	Field	NA	CRS-1, CRS-1S, SS-1, CBC-1H, NTQS-1HH, NTHAP	0.031-0.155	LISST	2.54	0	25
Major Conclusions: For the milled specimens, CRS-1S led to a reduction in ISS with an increase in the TC application rate compared to the no tack coat condition, whereas other TCs led to an increase in the ISS with an increase in the application rate. Compared to the unaged, unmilled HMA surface, the ISS of the milled specimen was lower for the no-tack coat condition. At the optimum application rate, the milled surfaces showed higher ISS values compared to the unaged, unmilled HMA surfaces in all TC cases.									
Bahia et al. (2019)	Field	Field/Lab (SGC)	NA	SS-1h and QS-1h	0.05	LISST	2.54	7 & 20	25
	Field	Field/Lab (SGC)	NA	SS-1h and QS-1h	0.025				
Major Conclusions: Lab and field specimens with an unmilled surface exhibit different ISS values and cannot be used to predict field ISS values using lab-measured ISS values for the same materials. The ISS of the field milled specimens was comparable to that of the unmilled field specimens.									

Coleri et al. (2020)	Lab (SC)	Lab (SC)	1.82-2.6	CSS1H, ENGR	0.06-0.12	LISST	2.54	30	25
	Field	Field	NA	CSS1H, ENGR	0.075-0.16				

Major Conclusions:

Different MTDs did not affect the ISS, and laboratory milling practices did not create bias in the results.

The laboratory-produced ISS results are similar to those observed for field specimens.

The ISS response of field milled samples is highly variable because there is less control over construction issues such as non-uniform tack coat coverage.

The ISS values of the lab-prepared milled and overlay (unmilled) specimens were comparable.

Note: MTD is mean texture depth; TC is tack coat; LR is loading rate; σ_c is confining pressure; LISST is Louisiana Interlayer Shear Strength Tester, HMA is hot mix asphalt; PCC is Portland concrete cement; ISS is interface shear strength; NA is not available; SGC is Superpave Gyratory Compactor; SC is slab compactor.

5.1.8 Effect of Air Void Content and Compaction

The typical laboratory method used for ISS test specimen fabrication involves a gyratory compactor. The primary goal of using the alternative slab compactor is to study the effect of the compaction method on the specimen's ISS. Therefore, for this study, both a gyratory compactor and a slab compactor were used to make ISS test specimens with CRS-2 (Source 2) at an application rate of 0.03 gal/yd². Figure 5-26 shows that the ISS values of the specimens fabricated using the two different compaction methods differ at all temperatures. In addition, the measured air void content of the specimens made using the slab compactor is 8.5%, whereas it is 6% when fabricated with the gyratory compactor. Therefore, the difference in ISS is attributable not only to the compactor type but also to the overall air void content of the specimen itself.

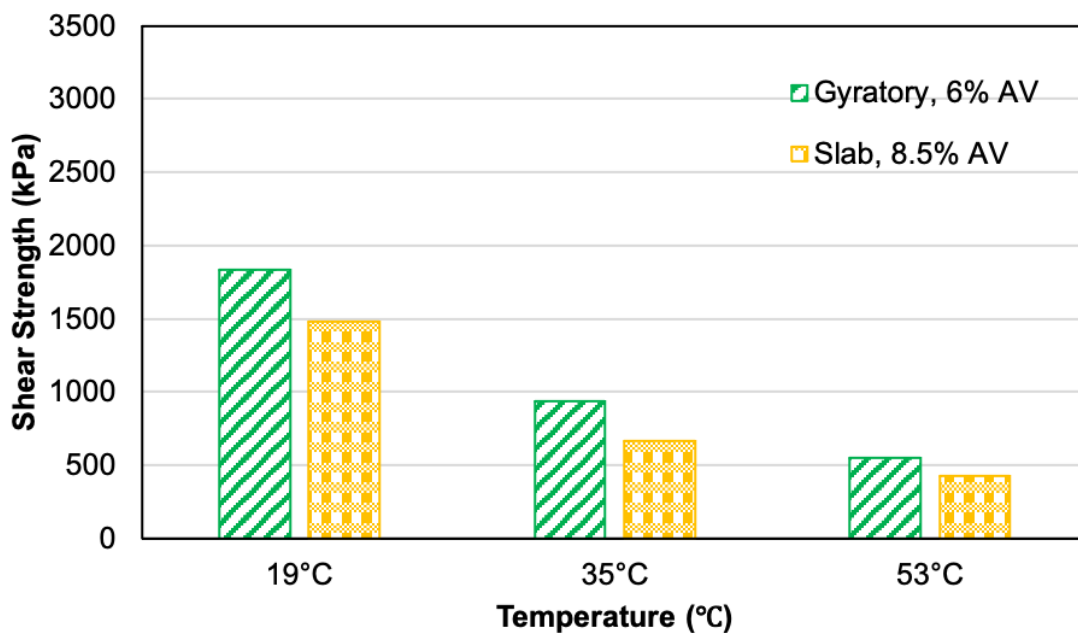


Figure 5-26. Comparison of interface shear strength of specimens fabricated using two different compaction methods.

The effect of tack coat source is another major factor that is considered in this study. Here, the same tack coat, CRS-2, obtained from two different sources (Source 1 and Source 2), was used to investigate the effects of tack coat source on the ISS of the specimens. Figure 5-27 presents the results of a comparative study based on the same test conditions. The figure shows that, depending on the emulsion source, the same type of emulsion can exhibit different ISS values at low temperatures.

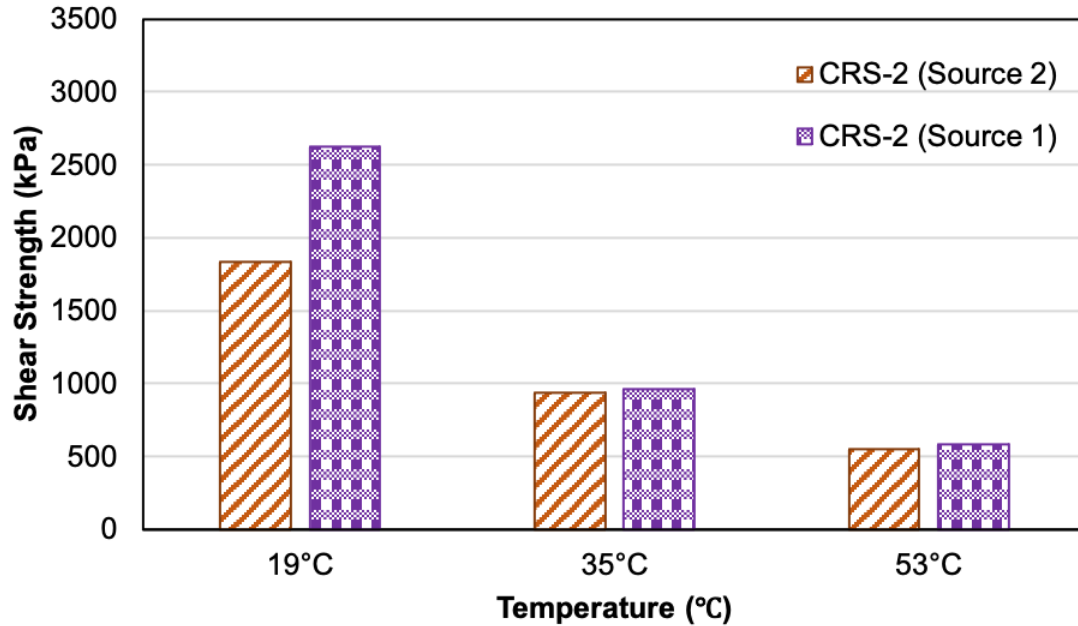


Figure 5-27. Comparison of interface shear strength values of specimens made with the same CRS-2 emulsion obtained from two different sources.

5.1.9 Statistical Validation of the Effect of Various Parameters on ISS

The previous sections show that ISS is a power function governed by reduced DIC shear strain rates. In order to evaluate the significances of each factor for ISS, multiple linear regression (MLR) model is as shown in Equation (21). In this research, Equation (22) was chosen for the analysis because it presents the effect of factors when they interact.

$$\hat{Y} = \hat{\beta}_0 + \hat{\beta}_1 x_1 + \hat{\beta}_2 x_2 + \hat{\beta}_p x_p + Error \quad (21)$$

$$\hat{Y} = \hat{\beta}_0 + \hat{\beta}_1 x_1 + \hat{\beta}_2 x_2 + \hat{\beta}_3 x_1 x_2 \quad (22)$$

where

- \hat{Y} = dependent or response variable,
- $\hat{\beta}_i$ = model parameter, and
- x_i = independent, predictor, or explanatory variable.

Statistical Analysis of Gyratory-Compacted Specimens

All the specimens that were fabricated by gyratory compaction and at the unmilled condition were chosen to see the effects of all the factors. R-studio software was used for this analysis. Equation

(23) is a regression model that was created for this analysis as well. Several factors (parameters) and combination of factors serve as interaction parameters that present the significance of themselves. The ISS and reduced DIC shear strain rates are in log scale because they have a power function relationship.

$$\log_{10}(ISS) = \hat{\beta}_0 + \hat{\beta}_1 x_1 + \hat{\beta}_2 x_2 + \dots + \hat{\beta}_i x_i \quad (23)$$

where

- $\hat{\beta}_0$ = intercept,
- $\hat{\beta}_1$ = log (reduced strain rate),
- $\hat{\beta}_2$ = confinement,
- $\hat{\beta}_3$ = application rate,
- $\hat{\beta}_4$ = log(reduced strain rate) × Confinement,
- $\hat{\beta}_5$ = log(reduced strain rate) × Application rate,
- $\hat{\beta}_6$ = confinement × application rate,
- $\hat{\beta}_7$ = log(reduced strain rate) × confinement × application rate,
- $\hat{\beta}_8, \hat{\beta}_9, \hat{\beta}_{10}, \text{ and } \hat{\beta}_{11}$ = Type (CRS-2, CRS-1h, NTCRS-1hM, Ultrafuse)

For statistical analysis using MLR, iterations of elimination of insignificant factors were conducted to evaluate the change in the significant factors. Table 5-4 presents the *p*-value of each parameter at each iteration step. The process of eliminating the least significant factors preceded the iteration process. Table 5-5 shows all the model coefficients used in the iteration process.

Table 5-4. P-value Results for Multiple Linear Regression Model during Iteration and Coefficients of Determination (R²)

Parameter	<i>p</i>-value					
Coefficient of determination	0.9606	0.9606	0.9605	0.9604	0.9548	0.9514
Reduced strain rate	8.150E-28	1.715E-28	3.826E-29	8.722E-30	3.056E-31	3.505E-31
Confinement	4.964E-11	2.802E-11	1.649E-11	9.855E-12	7.494E-12	1.336E-11
Application rate	7.838E-02	7.462E-02	7.145E-02	6.856E-02	7.338E-02	
Reduced strain rate × confinement	1.998E-07	1.390E-07	9.989E-08	7.260E-08	5.831E-08	9.834E-08
Reduced strain rate × application rate	6.970E-01	6.932E-01	6.900E-01			
Confinement × application rate	7.335E-01	7.302E-01				
Reduced strain rate × confinement × application rate	9.670E-01					
Type	1.882E-01	1.776E-01	1.687E-01	1.605E-01		

Table 5-5. Coefficients of Multiple Linear Regression Model during Iteration

Parameter		Coefficient					
Intercept		3.678E+00	3.674E+00	3.660E+00	3.643E+00	3.655E+00	3.614E+00
Reduced strain rate		2.122E-01	2.113E-01	2.113E-01	2.069E-01	2.076E-01	2.074E-01
Confinement		-2.692E-04	-2.589E-04	-2.140E-04	-2.138E-04	-1.810E-04	-1.798E-04
Application rate		-2.500E+00	-2.386E+00	-1.904E+00	-1.355E+00	-1.355E+00	
Reduced strain rate × confinement		-1.900E-04	-1.872E-04	-1.872E-04	-1.872E-04	-1.890E-04	-1.887E-04
Reduced strain rate × application rate		-1.784E-01	-1.474E-01	-1.482E-01			
Confinement × application rate		1.831E-03	1.488E-03				
Reduced strain rate × confinement × application rate		9.357E-05					
Type	CRS-2 (1)	1.948E-02	1.948E-02	1.942E-02			
	CRS-2 (2)	3.944E-03	3.923E-03	3.873E-03			
	NTCRS- 1hM	1.126E-01	1.125E-01	1.125E-01			
	Ultrafuse	3.131E-02	3.131E-02	3.111E-02			

Eventually, all the insignificant factors were removed using the significant level, or *p*-value, of 0.05.

Table 5-6 shows the final model coefficients and their p -values to indicate the significance of the coefficients. Moreover, the coefficients for confinement and for the combination of reduced strain rate and confinement are still negative because the regression model consists of several log forms of the variables and a dependent/response variable, as shown in Equation (23).

Table 5-6 Results of Multiple Linear Regression Model for Gyratory-Compacted Specimens

Parameter	Coefficient	p-value
Intercept	3.614E+00	$R^2 = 0.9514$
Reduced strain rate	2.074E-01	3.505E-31
Confinement	-1.798E-04	1.336E-11
Reduced strain rate × confinement	-1.887E-04	9.834E-08

Additionally, an ISS prediction equation was developed from the statistical MLR analysis model. Equation (24) and Table 5-7 present the ISS prediction equation obtained using MLR and the equation's coefficients, respectively. (Section 6.1 provides details.)

$$\tau_f = \dot{\gamma}_R^{(a_I + b_I \times \sigma_c)} \times 10^{(c_I \times \sigma_c + d_I)} \quad (24)$$

Where

- τ_f = interface shear strength (kPa),
- $\dot{\gamma}_R$ = reduced strain rate (γ/s),
- σ_c = normal confining pressure (kPa), and
- $a_I, b_I, c_I,$ and d_I = model coefficients for interface shear strength.

Table 5-7 Coefficients of Interface Shear Strength Prediction Equation Obtained from Multiple Linear Regression Model

Condition	Interface Shear Strength Model Coefficients			
	a_I	b_I	c_I	d_I
Gyratory Specimen	2.074E-01	-1.798E-04	-1.887E-04	3.614E+00

Statistical Analysis of Effects of Compaction and Surface Condition

Because the insignificance of the application rate and tack coat type on ISS became known in this study, additional statistical analysis was conducted to find the (in)significance of the other factors, i.e., compaction method and surface condition. The same form of the MLR model that was used to analyze the application rate and tack coat type also was used for this analysis, but the application and tack coat type parameters were replaced with compaction method and surface condition. The reduced strain rate, confinement, and combination of reduced strain rate and confinement were maintained for this analysis because they were determined to be the significant factors for the ISS. Equation (25) presents the details and parameters. Note that the factors, compaction method and surface condition, do not possess any combined factor because they are categorical predictors.

$$\log_{10}(ISS) = \hat{\beta}_0 + \hat{\beta}_1 x_1 + \hat{\beta}_2 x_2 + \dots + \hat{\beta}_i x_i \quad (25)$$

where

- $\hat{\beta}_0$ = intercept,
- $\hat{\beta}_1$ = log (reduced strain rate),
- $\hat{\beta}_2$ = confinement,
- $\hat{\beta}_3$ = log (reduced strain rate) * confinement,
- $\hat{\beta}_4$ = compaction, and
- $\hat{\beta}_5$ = surface.

Table 5-8 presents additional statistical analysis results obtained using the MLR model. All the parameters except the surface condition in this analysis are significant for ISS as the p -values are mostly lower than the common criterion value of 0.05. The effect of the compaction method on ISS is clear whereas the effect of the surface condition is subtle.

Table 5-8 Results of Multiple Linear Regression Model for Diverse Specimens

Parameter	Coefficient	p -value
Intercept	3.526E+00	$R^2 = 0.922$
Reduced strain rate	1.674E-01	8.900E-78
Confinement	2.015E-05	4.117E-19
Reduced strain rate * confinement	-1.159E-04	1.189E-08
Compaction	-2.272E-01	7.132E-25
Surface	-1.604E-02	4.702E-01

Statistical Analysis of Effect of Groove Angle

Statistical analysis was performed to investigate the effect of the groove direction angle on the ISS. For this analysis, only the NTCRS-1hM tack coat material at 0.23 L/m² (0.05 gal/yd²) and 172 kPa (25 psi) confining pressure was used. The tests were conducted under the three main reduced strain rates used for the MLR linear model. Equation (26) was composed to show effect of the groove directional angle on the ISS is not critical and

Table 5-9 presents the analysis results with p -values.

$$\log_{10}(ISS) = \hat{\beta}_0 + \hat{\beta}_1 x_1 + \hat{\beta}_2 x_2 + \dots + \hat{\beta}_i x_i \quad (26)$$

where

$\hat{\beta}_0$ = intercept,

$\hat{\beta}_1$ = log (reduced strain rate),

$\hat{\beta}_2$ = angle, and

$\hat{\beta}_3$ = log (reduced strain rate) * angle.

Table 5-9 Results of Multiple Linear Regression Model for Angle Effect

Parameter	Coefficient	p-value
Intercept	3.537E+00	$R^2 = 0.9919$
Reduced strain rate	1.683E-01	2.053E-06
Angle	-6.697E-04	3.249E-01
Reduced strain rate * angle	-8.668E-05	6.439E-01

5.2 Binder Bond Strength Test Results

PATTI was able to show consistent results within a single tack coat type as well as identify distinctive outcomes for each tack coat. During the course of these tests, limitations and challenges were discovered and are discussed in the following sections.

5.2.1 Effect of Tack Coat Type

All the tack coats investigated in this study exhibited an inverse proportional relationship between tensile strength and temperature; i.e., with an increase in temperature, the tensile strength decreased. However, in the case of CRS-1h, NTCRS-1hM, and Ultrafuse, the tensile strength followed this inverse proportionality relationship until it hit a specific level at a specific temperature. This temperature is hereafter referred to as the ‘ceiling temperature.’ Further testing at temperatures lower than the ceiling temperature resulted in the tensile strength remaining either constant or weakening, which is contrary to an expected surge in strength.

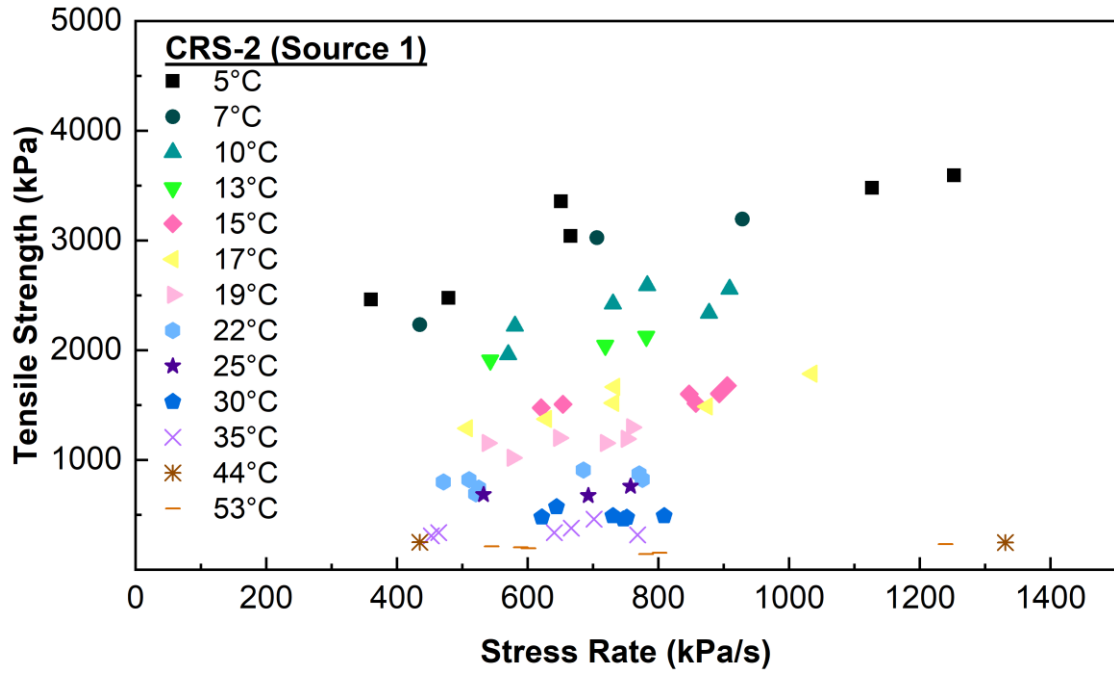
Among the five emulsions tested, the most consistent cohesive failure mode was observed for CRS-2 (Source 1 and Source 2) and CRS-1h. However, for CRS-1h, starting at 15°C and below, most tests resulted in adhesive failure at the pull-off stub. This occurrence was found during the CRS-1h tests initially at 5°C and, to ensure that the observed response was not due to a malfunction of PATTI or a systematic error in the test procedure, comparison tests were repeated using CRS-2 at 5°C. The CRS-2 emulsion consistently failed in cohesion, whereas CRS-1h failed in adhesion or a combination of cohesion and adhesion. Figure 5-28 shows the stubs that were used in these two tests that were run at 5°C with a residual application rate of 0.14 L/m² (0.03 gal/yd²).

The verification test results demonstrate that the adhesive failure was not caused by a flaw of PATTI or the PATTI test protocol, but rather that the cohesive strength of the tack coat exceeded the adhesive strength between the tack coat and pull-off stubs. Visual inspection of the failure as well as tensile strength trends helped to identify the critical ceiling temperature for a specific tack coat, below which an adhesive response would be expected. Therefore, the results under adhesive failure do not truly represent the tensile strength at that specific temperature.

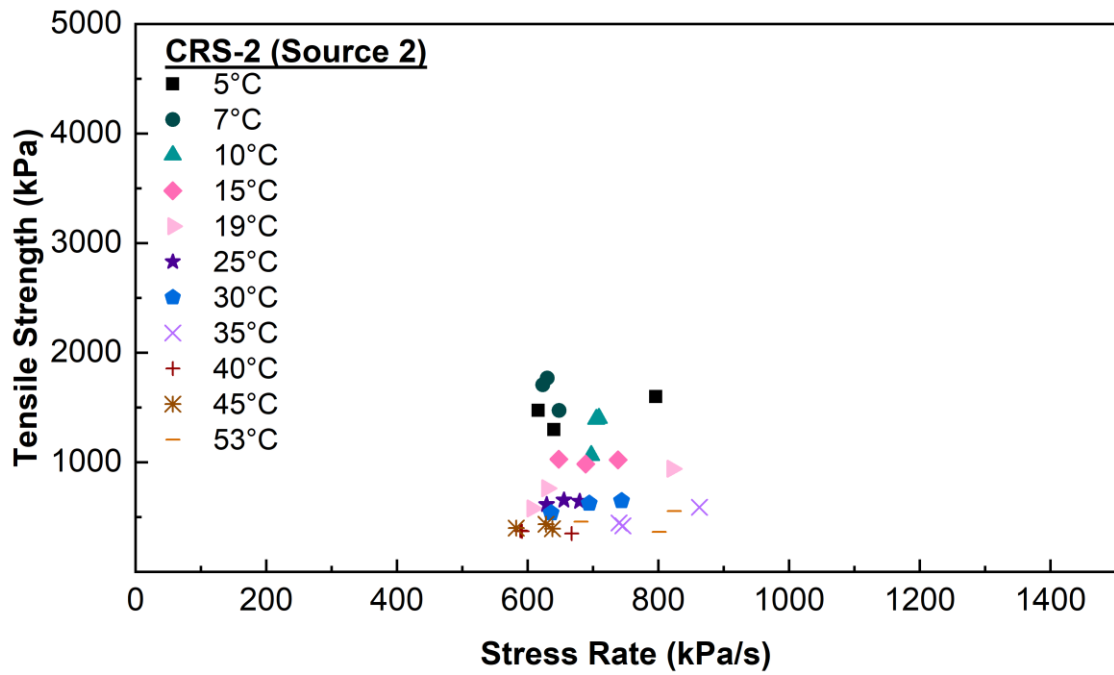


Figure 5-28. Failure mode of CRS-2 (left) compared to CRS-1h (right) at 5°C.

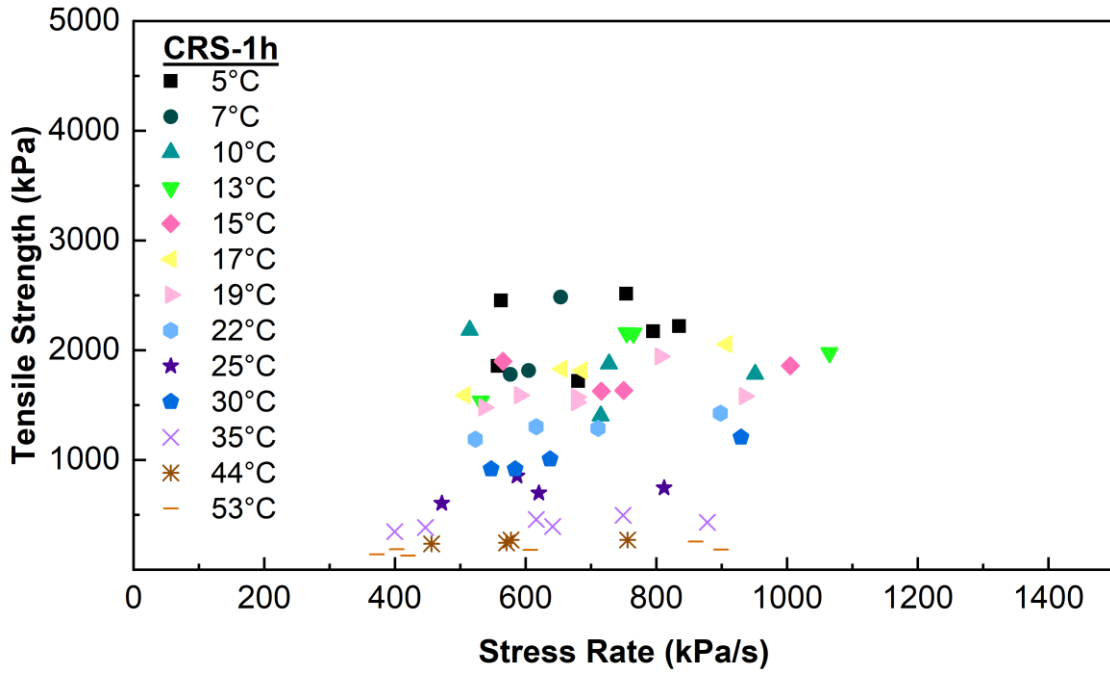
The two non-tracking tack coats, NTCRS-1hM (emulsion) and Ultrafuse (hot binder) showed an adhesive failure of the pull-off stubs even at the high temperatures of 44°C and 30°C, respectively. The debonding responses at the high temperatures verify that these tack coats are non-tracking materials. These two non-tracking tack coats are chemically formulated to resist the wheel-tracking of construction vehicles during construction that can lead to a weak bond between the asphalt concrete layers. However, when a new asphalt concrete mixture is placed on top of a non-tracking tack coat at the compaction temperature, the tacking nature of the binder reactivates and glues the old and new layers together. Hence, non-tracking tack coats must be heated to 145°C (a typical compaction temperature) prior to placing the pull stubs and metal caps during testing. The metal caps mimic actual field conditions with regard to setting pressure and allow the non-tracking emulsion to stick to the pull stubs. Even then, temperatures below 30°C will result in mixed failure or adhesive failure due to the excessive cohesive strength of the tack coat. Figure 5-29 presents the pull-off strength values of all the tack coats tested at different temperatures.



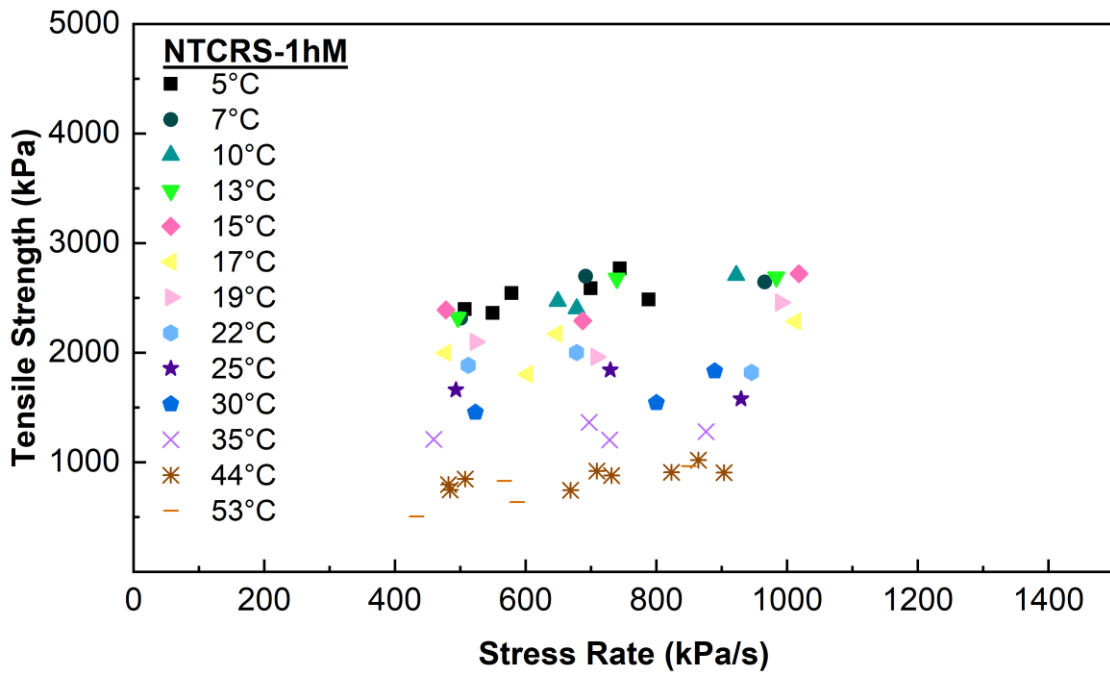
(a)



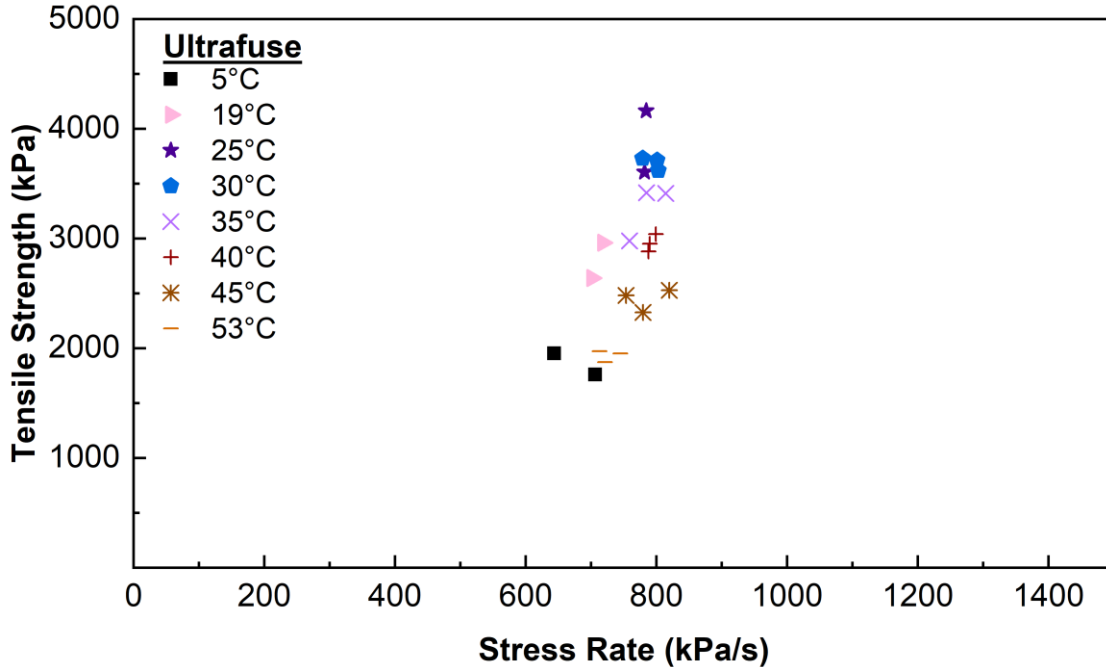
(b)



(c)



(d)



(e)

Figure 5-29. PATTI test results for (a) CRS-2 (Source 1) (b) CRS-2 (Source 2), (c) CRS-1h, (d) NTCRS-1hM, and (e) Ultrafuse at 0.14 L/m² (0.03 gal/yd²) residual application rate.

5.2.2 Effect of Tack Coat Application Rate

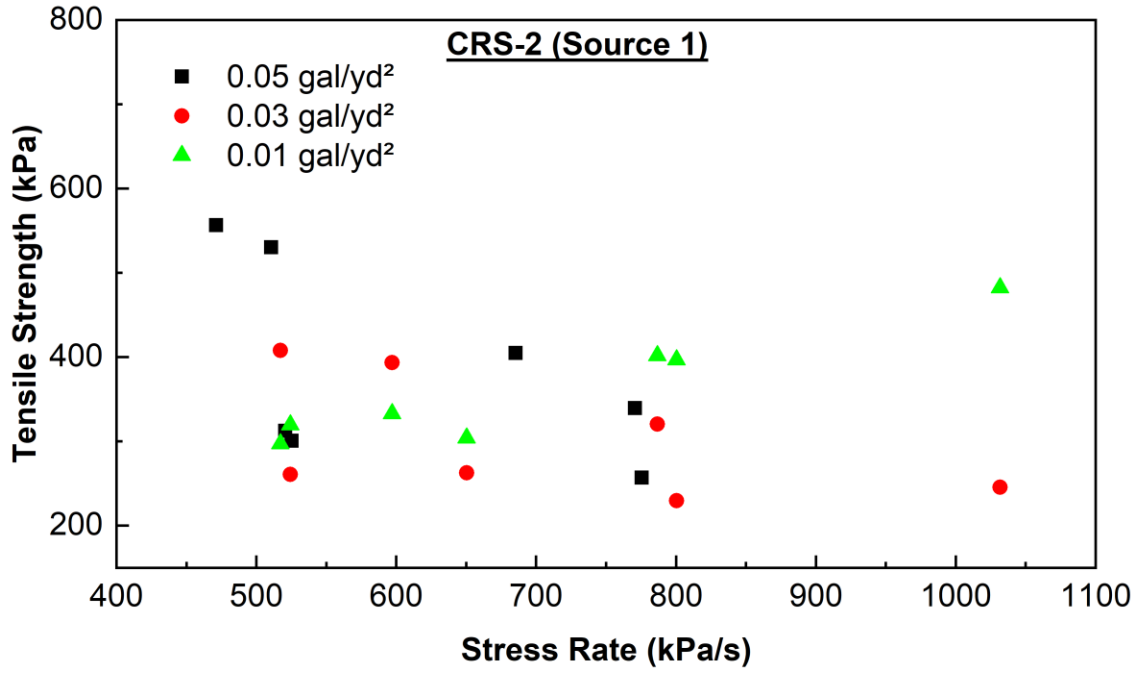
PATTI tests were conducted using CRS-2 (Source 1), CRS-1h, and NTCRS-1hM at three tack coat application rates, 0.045 L/m² (0.01 gal/yd²), 0.14 L/m² (0.03 gal/yd²), and 0.23 L/m² (0.05 gal/yd²), to investigate the effects of application rate on the BBS. The test temperatures used for CRS-2 (Source 1), CRS-1h, and NTCRS-1hM were 22°C, 22°C, and 44°C, respectively. The effects of the tack coat application rate were studied by comparing the BBS values that were measured when the pull-off stubs failed under cohesive mode. For non-tracking tack coats, adhesive bond failure was prominent below a certain temperature. In the case of NTCRS-1h, this temperature was 30°C. In order to achieve consistent cohesive failure at different application rates, the research team decided, based on experience, to run the test at 44°C for the non-tracking emulsions. Also, for any user, running a PATTI test at a temperature that is close to the ambient room temperature is easy, because this protocol allows more time to conduct the test using four pull-off stubs on a metal substrate. If the test temperature is not close to the ambient room temperature (higher or lower), the test procedure that uses four stubs must be completed within 90 seconds; otherwise, the temperature of the tack coat will drop or increase quickly in order to reach the ambient temperature, which would cause unreasonable results. Hence, testing at temperatures that are not close to the ambient temperature is allowed only for two stubs at a time (within 90 seconds), and

the metal substrate with the remaining two pull-off stubs must be returned to the conditioner for another 30 minutes. Therefore, the research team decided to test CRS-2 and CRS-1h at 22°C because both of these tack coats exhibited cohesive failure at that temperature.

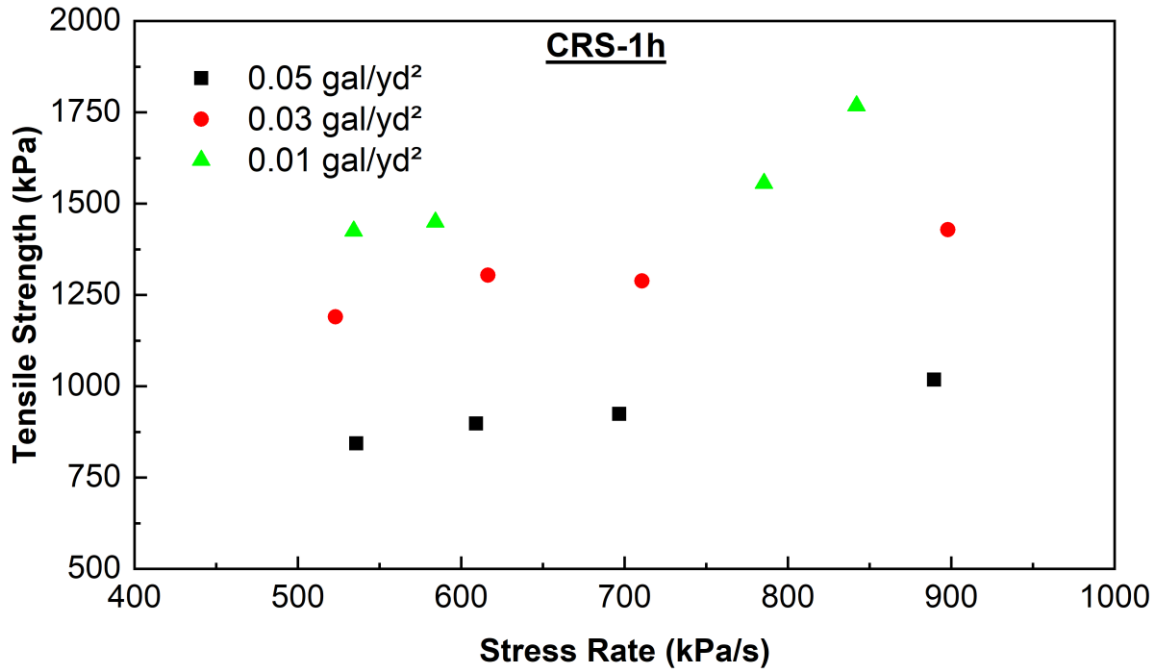
Figure 5-30 (a) shows that CRS-2 (Source 1) tested at 22°C does not exhibit definitive trends at the lowest residual application rate of 0.045 L/m² (0.01 gal/yd²), which appears to result in the highest tensile strength, whereas any difference in the tensile strength between 0.14 L/m² (0.03 gal/yd²) and 0.23 L/m² (0.05 gal/yd²) is difficult to find. One of the significant problems with the tests conducted at 0.23 L/m² (0.05 gal/yd²) was that many of the pull stubs would slip or shear off either as the test was being conducted or when the pull stub was applied after curing. This problem was likely due to the applied tack coat quantity, as this issue was not seen at the lower application rates.

Similar to CRS-2 (Source 1), CRS-1h was tested at three different application rates at 22°C. Unlike CRS-2, however, the CRS-1h results indicate distinct responses to the different application rates, as shown in Figure 5-30 (b). For example, the application rate of 0.045 L/m² (0.01 gal/yd²) consistently resulted in the highest tensile strength, whereas 0.23 L/m² (0.05 gal/yd²) resulted in the lowest tensile strength among the three rates. A possible reason for the discrepancy in these results is the failure mode at each application rate. The low application rate consistently led to cohesive failure, whereas the high application rate led to more adhesive failure.

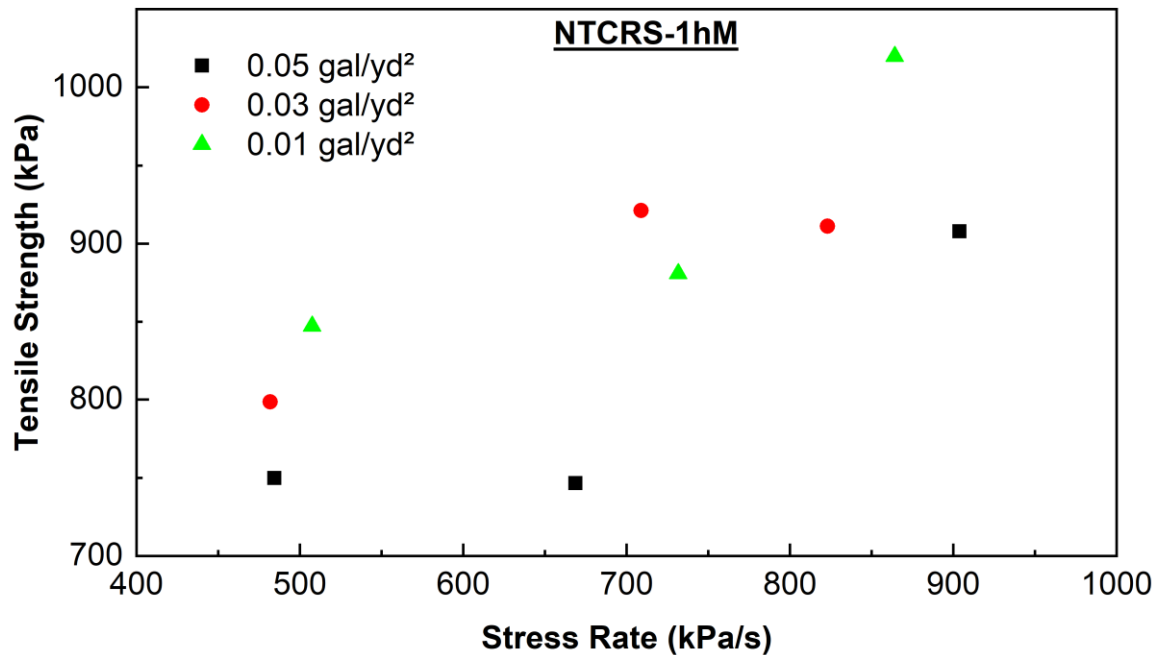
Figure 5-30 (c) shows the effects of the application rate on NTCRS-1hM at 44°C. This temperature was the lowest temperature that led to consistent cohesive failure. Similar to CRS-2, the trend is not as definitive as for CRS-1h, but the low residual application rate of 0.045 L/m² (0.01 gal/yd²) still corresponds to the highest tensile strength and the high rate of 0.23 L/m² (0.05 gal/yd²) still corresponds to the lowest tensile strength.



(a)



(b)



(c)

Figure 5-30. Residual application rate comparison of (a) CRS-2 (Source 1), (b) CRS-1h at 22°C, and (c) NTCRS-1hM at 44°C.

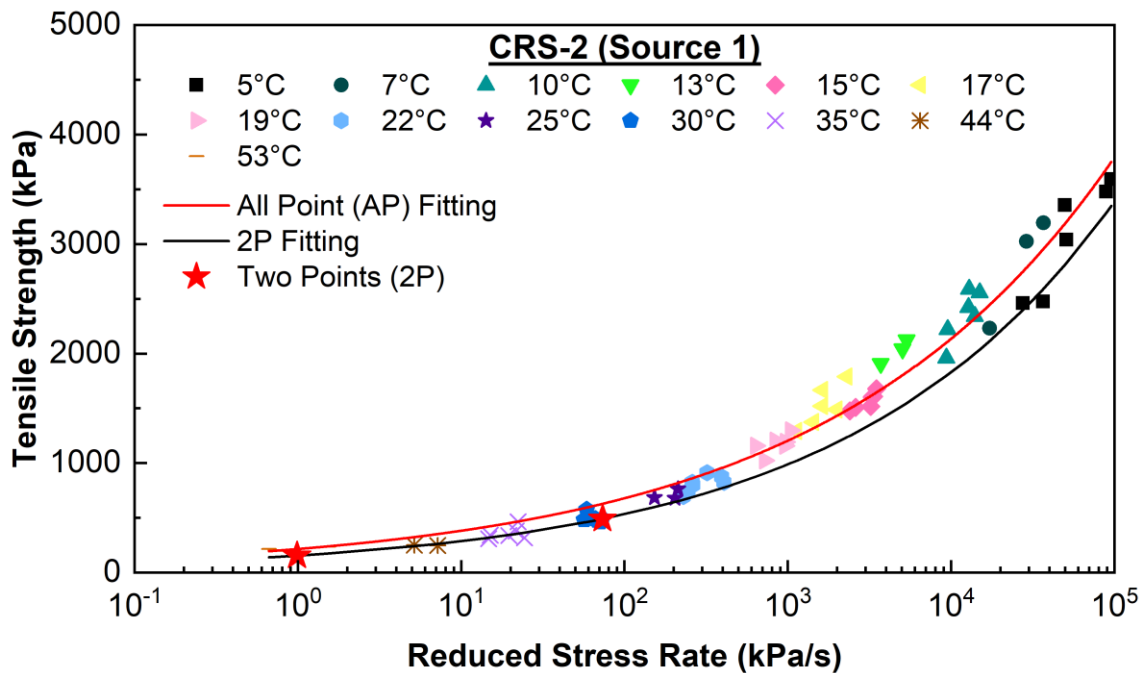
Consequently, a specific trend for BBS could not be established among the different tack coat application rates. The Quality Management System manual for the NCDOT specifies the optimal emulsion application rate of 0.04 gal/yd². Therefore, based on the estimated residue of typical emulsions, the residual application rate of 0.14 L/m² (0.03 gal/yd²) was chosen in this study for the remaining PATTI tests at various temperatures.

5.2.3 Validation of Time-Temperature Superposition Principle for Binder Bond Strength Using Different Tack Coats

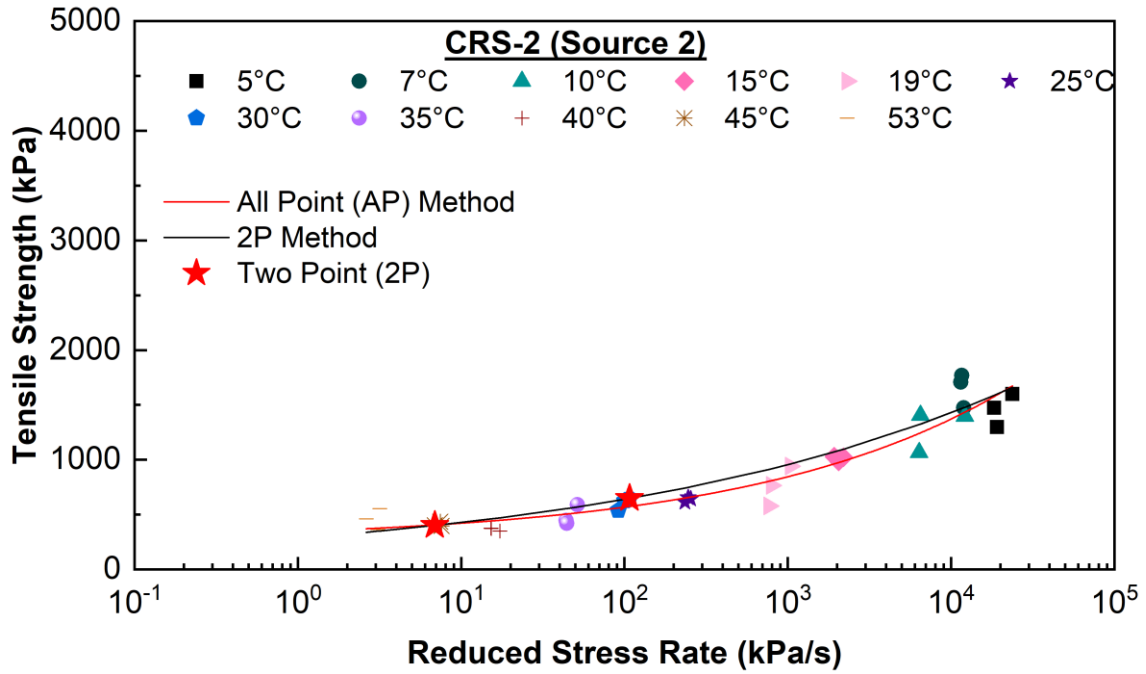
In this study, the PATTI and DSR test results were used to validate the application of the t-T superposition principle for the pull-off tensile strength of the asphalt tack coats. The coefficients of the shift factors that were measured for each tack coat type using the DSR were substituted in the t-T shift factor formula, Equation (8), to obtain the shift factors at the respective conditioning temperatures used in the PATTI tests. The shift factor imposes a quantum of horizontal drift for the pull-off tensile strength value that occurs when the shift factor is multiplied by the stress rate used in the PATTI test. This process results in a ‘reduced stress rate’ scale that allows the construction of mastercurves. The reference temperature used for the calculation of the shift factor coefficients obtained from the DSR is considered also as the reference temperature for the PATTI test mastercurves. For the current study, the predicted PATTI mastercurves were constructed at the

reference temperature of 20°C because the DSR shift factor coefficients were calculated at that same temperature.

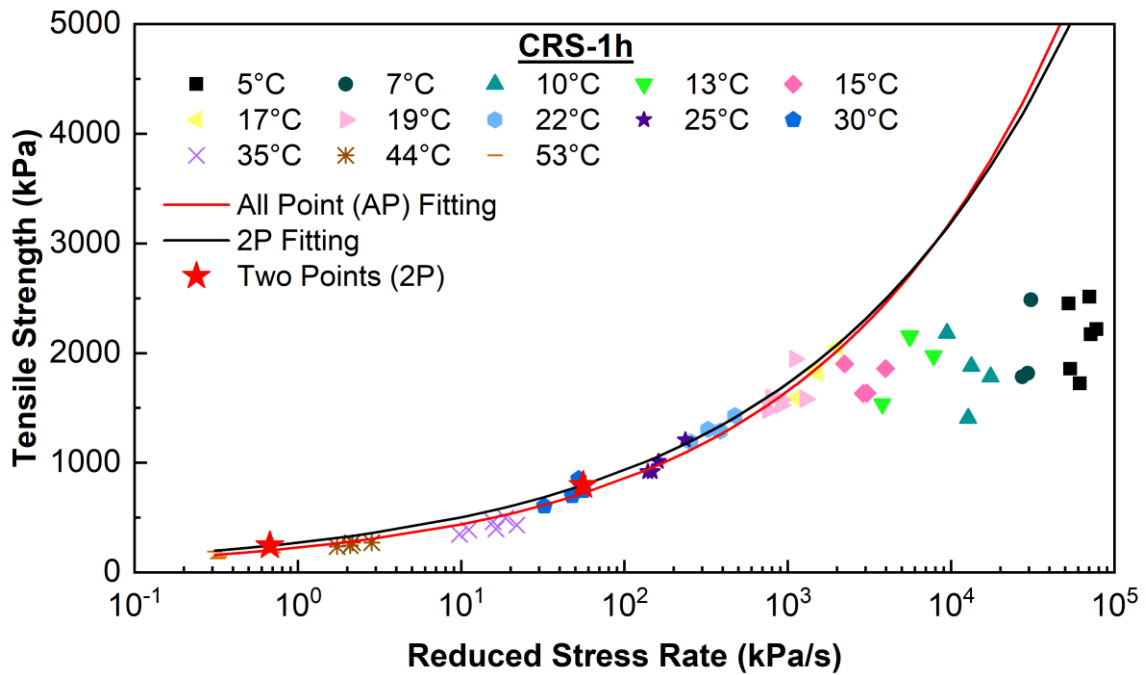
Figure 5-31 (a) and (b) present the PATTI test results for CRS-2 from Source 1 and Source 2, respectively. The resultant mastercurves have a tight grouping of tensile strength data points for all temperatures, and good data overlap at the lower temperatures. If more tests at higher temperatures were to be used in this research, the results would likely be similar. The effects of adhesive failure for CRS-1h are clearly observed in Figure 5-31 (c). For the temperature range of 53°C to 17°C, all the tensile strength data points follow a definite trend, but when the material begins to fail adhesively, the data points spread, and the trend flattens horizontally. The difficulties in stub adhesion for NTCRS-1hM and Ultrafuse are even more evident in Figure 5-31 (d) and (e), respectively, as the data point spread is higher in their respective mastercurves compared to the other emulsions. In the case of NTCRS-1hM, the pull-off strength ceiling of 2,758 kPa (400 psi) is shown in the mastercurve starting from 15°C to 5°C. For Ultrafuse, the degradation of the strength is observed from 25°C to 5°C after reaching the ceiling strength at 4,215 kPa (611 psi). The trend in pull-off strength above the ceiling temperature is inversely proportional to the temperature change. In contrast, testing at temperatures below the ceiling temperature resulted in the tensile strength either reaching a plateau or decreasing.



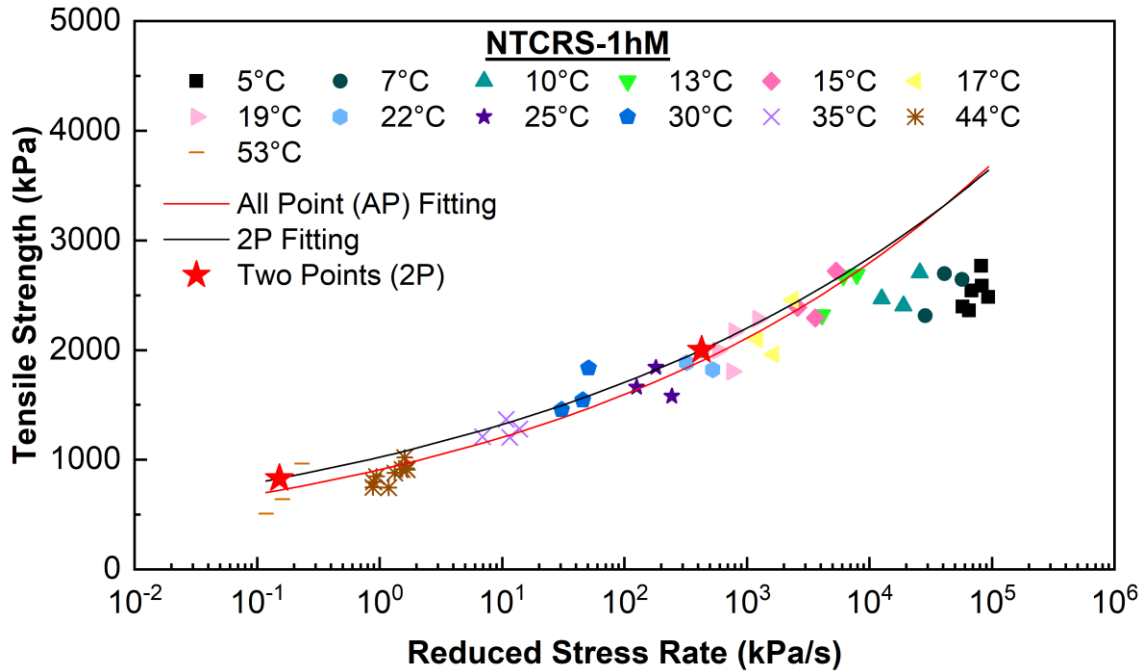
(a)



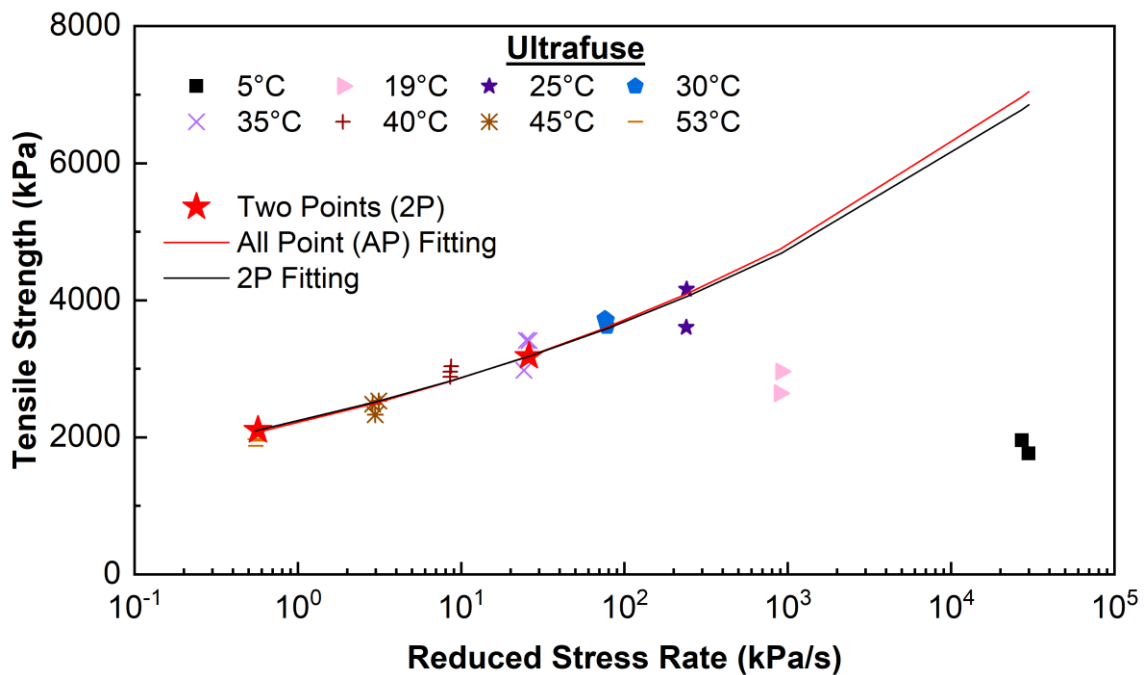
(b)



(c)



(d)



(e)

Figure 5-31. Mastercurves for (a) CRS-2 (Source 1), (b) CRS-2 (Source 2), (c) CRS-1h, (d) NTCRS-1hM, and (e) Ultrafuse at 0.14 L/m² (0.03 gal/yd²) residual application rate.

Figure 5-32 shows that, when all five mastercurves are placed on the same scale, Ultrafuse displays significantly greater tensile strength at all reduced stress rates compared to all the other tack coats investigated in this study. NTCRS-1hM has the second highest curve, as its tensile strength surpasses that of the other three tack coats, CRS-1h and CRS-2 (both sources). Although CRS-2 (both sources) and CRS-1h have very low tensile strength values at the lower reduced load rates, these strength values are shown to increase quickly as the reduced load rate increases. CRS-2 (Source 1) and CRS-2 (Source 2) have the highest tensile strength values at the highest reduced load rates (lower temperatures and higher load rates).

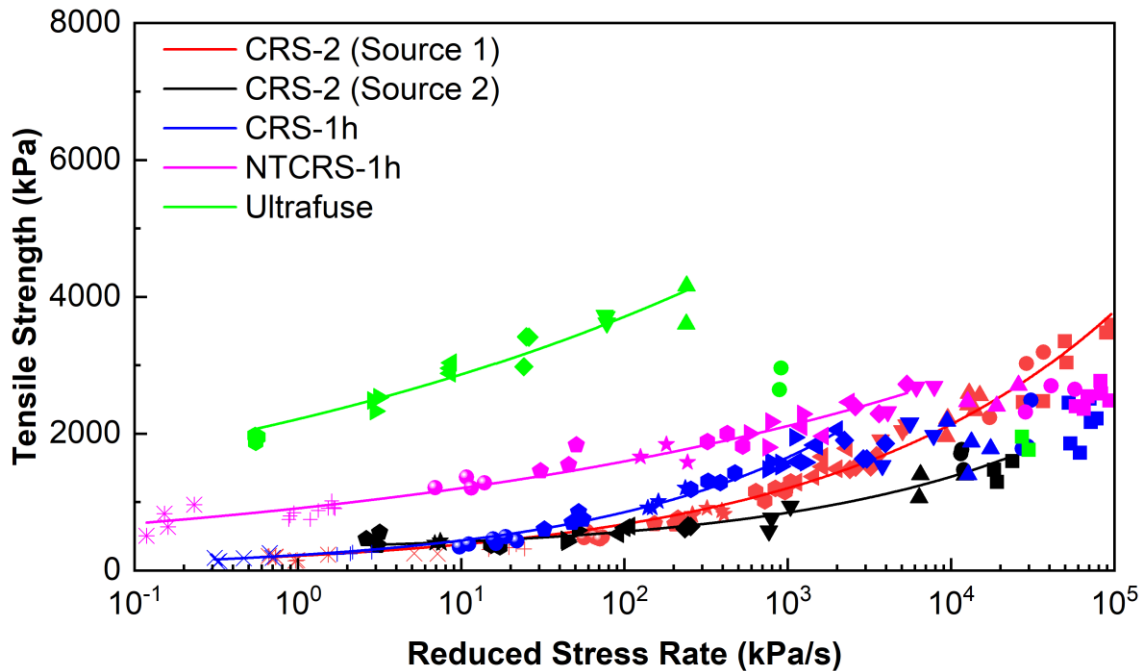


Figure 5-32. Mastercurve comparison of all tack coats tested at 0.14 L/m² (0.03 gal/yd²) residual application rate.

All-Point Method

The mastercurves in semi-log scale that were constructed using the tensile strength data points of each tack coat response were fitted using a power-law function (Figure 5-32). CRS-2 (Source 1) and CRS-2 (Source 2) show the best fit, whereas the trend lines for CRS-1h, NTCRS-1hM, and Ultrafuse are skewed due to the sudden change in failure mode at and below the ceiling temperature. The responses of CRS-1h, NTCRS-1hM, and Ultrafuse at and below the ceiling temperature led to the need to plot a second mastercurve for these three tack coats by eliminating the data points that exhibited mixed failure or adhesive failure. Then, the only data points left in the mastercurves were the data points for cohesive failure. The trend lines for CRS-1h, NTCRS-1hM,

and Ultrafuse fit the data better once the data points below the ceiling temperatures were eliminated.

Based on the fitted power-law functions developed from the data, theoretical mastercurves were constructed to predict the tack coat performance without any adhesive failure. The strength predictions show that NTCRS-1hM starts with a high tensile strength value at a low reduced load rate but that such strength would be overtaken by the two emulsions (CRS-2 (Source 1) and CRS-1h) as the reduced load rate increases. CRS-2 (both sources) and CRS-1h would start with very similar tensile strength values at the lower reduced load rates, but CRS-1h would increase in strength faster, ending with the greatest tensile strength of the three emulsions at the high reduced load rates. Again, this trend theoretically would hold true only if the cohesive failure occurred at all temperatures and load rates and thus should be viewed only as such.

Two-Point Method

Mastercurves for the different tack coats can be constructed based on PATTI tests carried out at 13 temperatures. The reason for carrying out multiple PATTI tests is that the acceptable stress rate range specified in ASTM D4541-17 (ASTM 2017) is limited to within 345 kPa/s to 1,034 kPa/s (50 psi/s to 150 psi/s). Therefore, the reduced stress rate measured at a specific temperature contributes to only a small region in the mastercurve. Furthermore, at lower temperatures, the pull stubs often fail in adhesive mode, which eventually leads to discarding those results. Consequently, considerable time must be spent testing at numerous temperatures to complete each mastercurve.

In order to avoid such extensive effort and time spent testing at 13 different temperatures, a two-point analysis method is proposed here. This method purports carrying out PATTI tests at two different temperatures, preferably at temperatures above 30°C to avoid adhesive failure. The shift factors obtained from the DSR test results are applied to the two calculated stress rates to measure the reduced stress rates that correspond to the test temperatures. Equations (27) and (28) express the typical power form at two temperatures at the corresponding reduced stress rates.

$$(\sigma_t)_{\dot{\sigma}_{R_1}} = a_B \dot{\sigma}_{R_1}^{n_B} \quad (27)$$

$$(\sigma_t)_{\dot{\sigma}_{R_2}} = a_B \dot{\sigma}_{R_2}^{n_B} \quad (28)$$

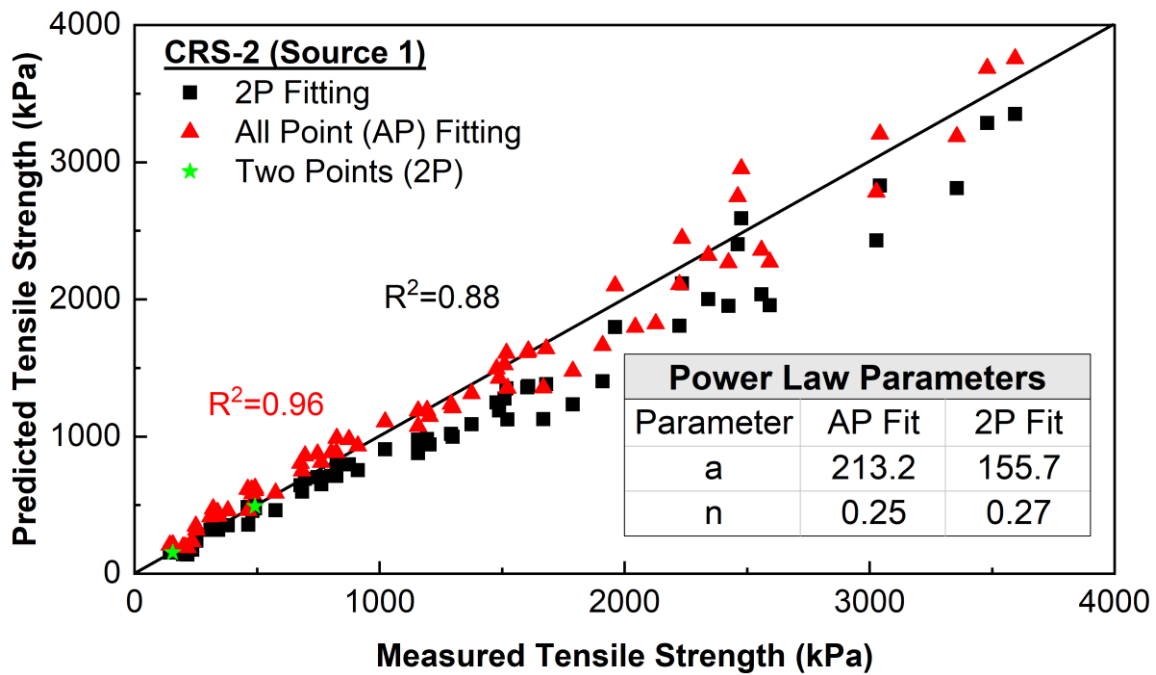
where

$\dot{\sigma}_{R_1}$, $\dot{\sigma}_{R_2}$ = reduced stress rates,
 σ_t = tensile strength, and
 a_B , n_B = material parameters.

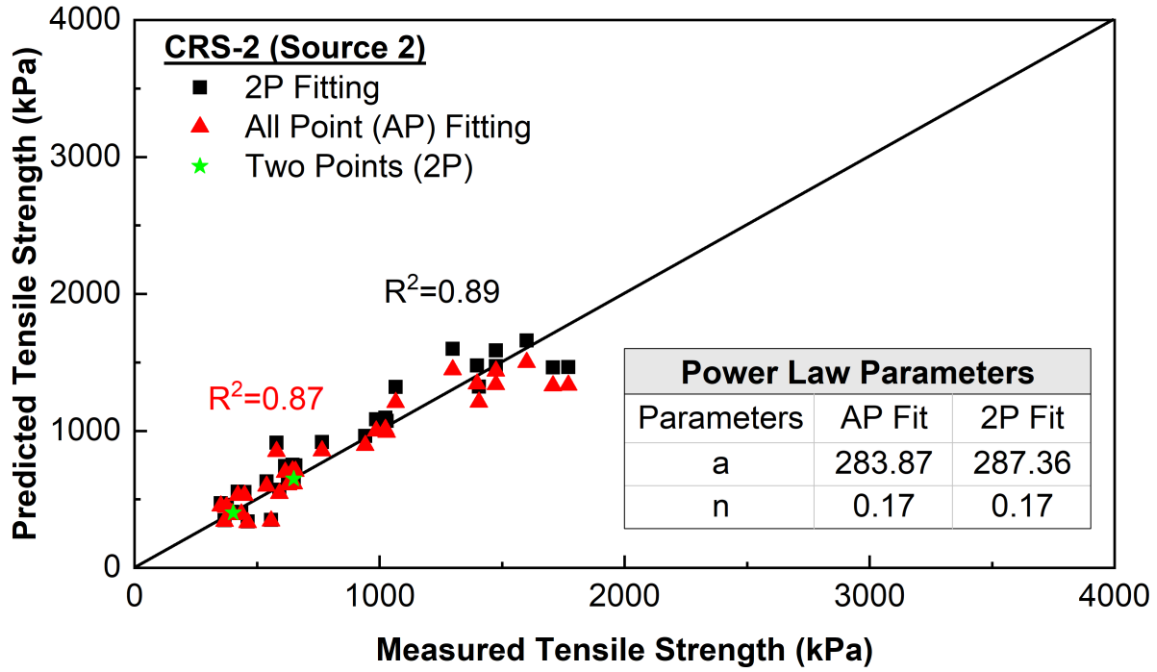
The ratio of the selected two points produces the relationship expressed as Equation (29).

$$\frac{(\sigma_t)_{\dot{\sigma}_{R_1}}}{(\sigma_t)_{\dot{\sigma}_{R_2}}} = \left(\frac{\dot{\sigma}_{R_1}}{\dot{\sigma}_{R_2}} \right)^{n_B} \quad (29)$$

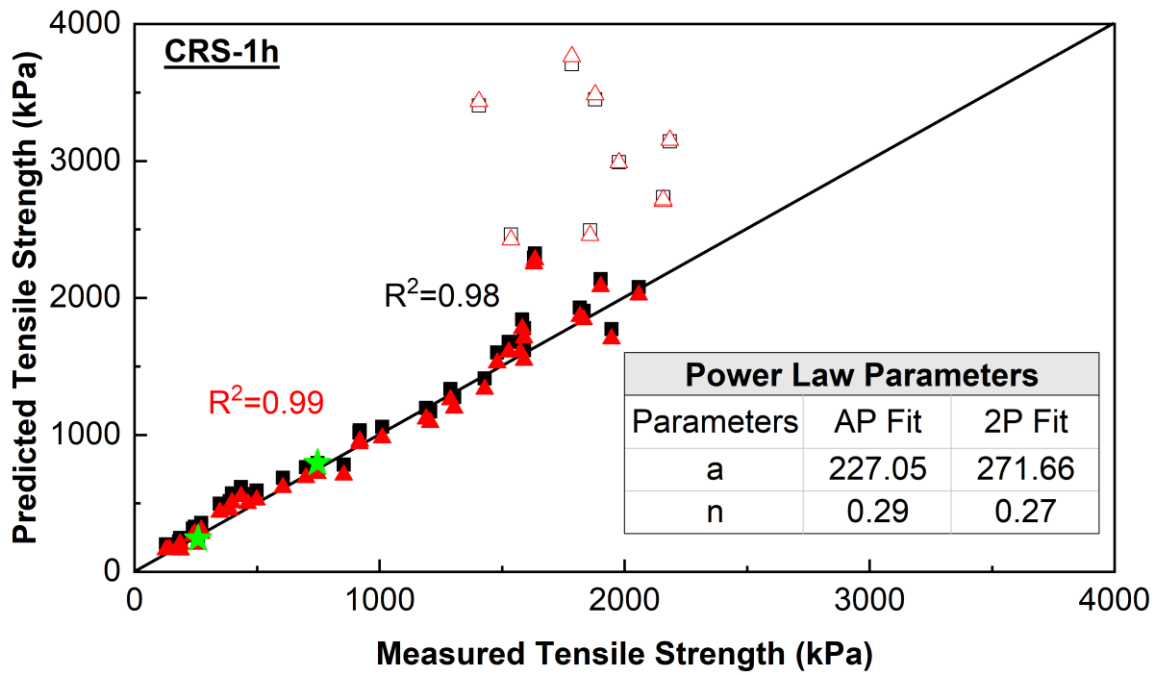
Equation (29) is solved to find the value of n_B , which is then substituted in Equations (27) and (28) to obtain a_B . The measured material parameters derived using the proposed two-point method produce predictions that are comparable to those derived using the all-point method for all tack coat materials, as shown in Figure 5-33 and Figure 5-34. In order to achieve reasonable predictions using the two-point method, the tensile strength value of each chosen point should be maintained and the average of the pull-off tensile strengths from three plates that hold four pull stubs per plate (12 tests in total for each temperature) should be within the intra-laboratory variance of 14.8 percent. This protocol will improve the reliability of the tensile strength predictions when using the two-point method.



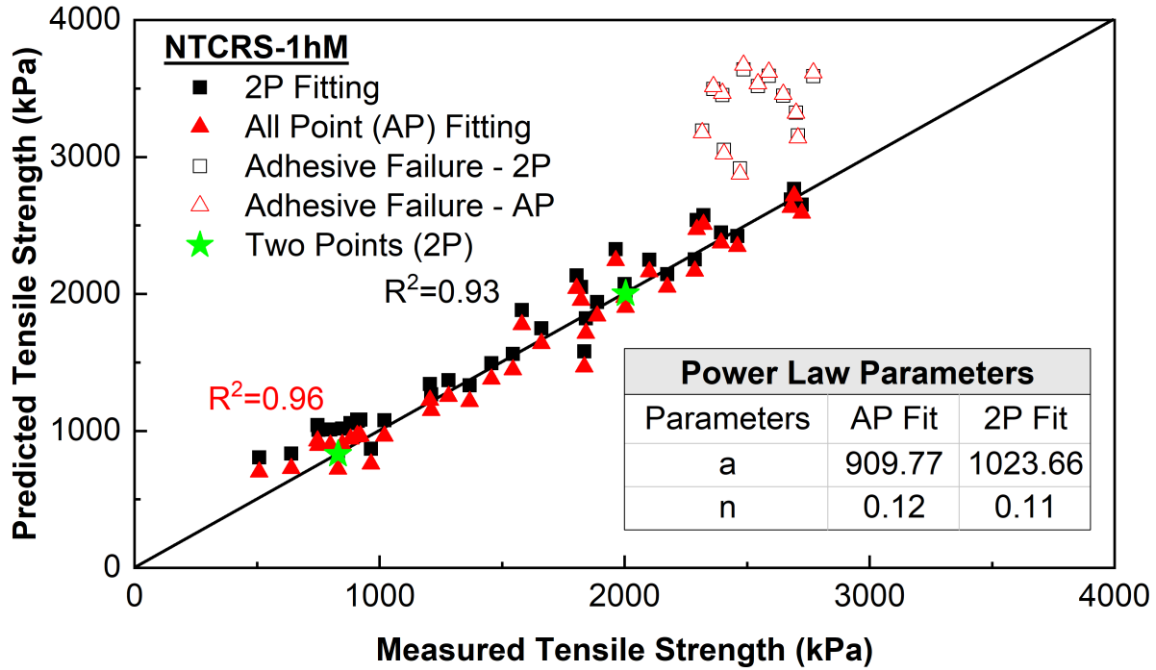
(a)



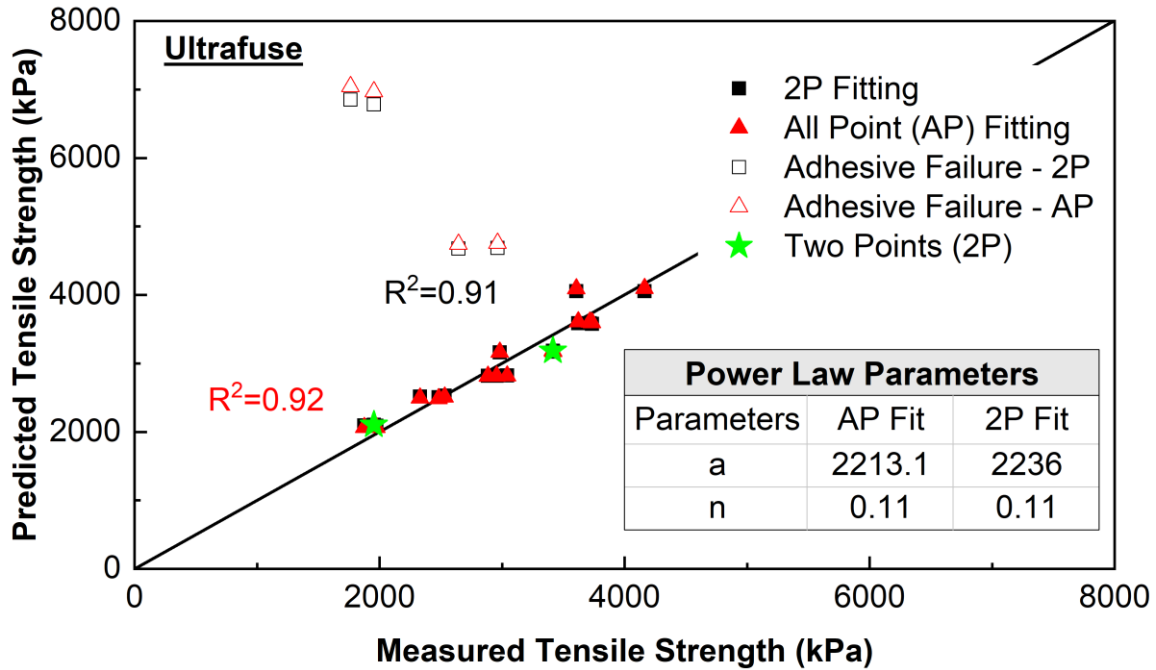
(b)



(c)



(d)



(e)

Figure 5-33. Predicted tensile strength values for (a) CRS-2 (Source 1), (b) CRS-2 (Source 2), (c) CRS-1h, (d) NTCRS-1hM, and (e) Ultrafuse at 0.14 L/m² (0.03 gal/yd²) residual application rate along the line of equality for the all-point (AP) method and two-point (2P) method.

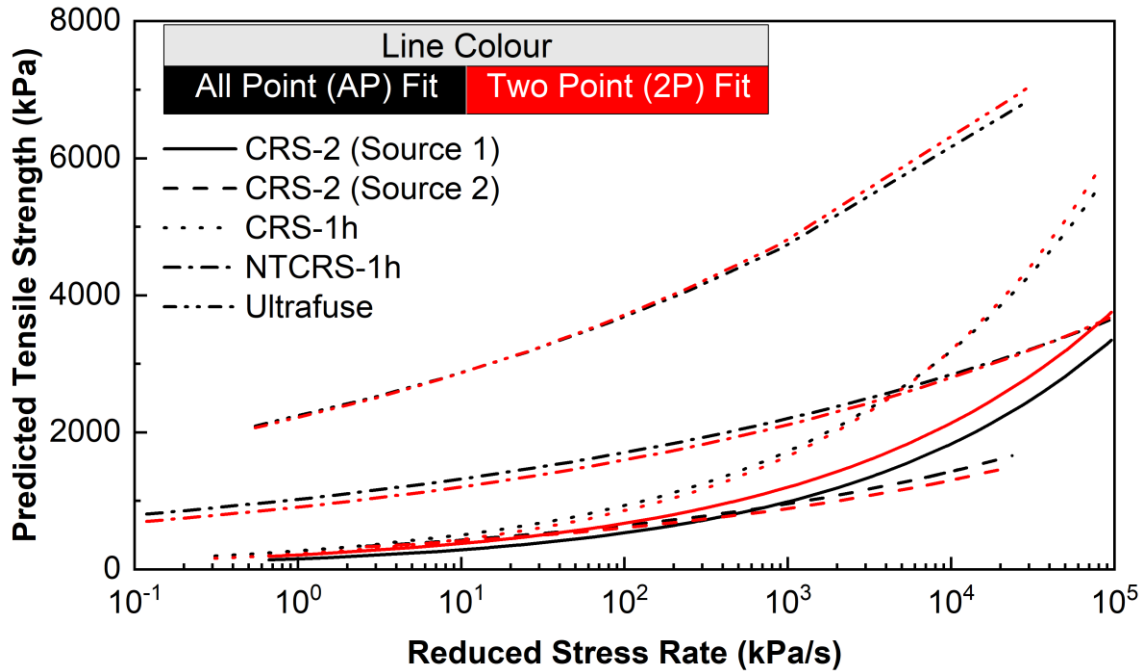
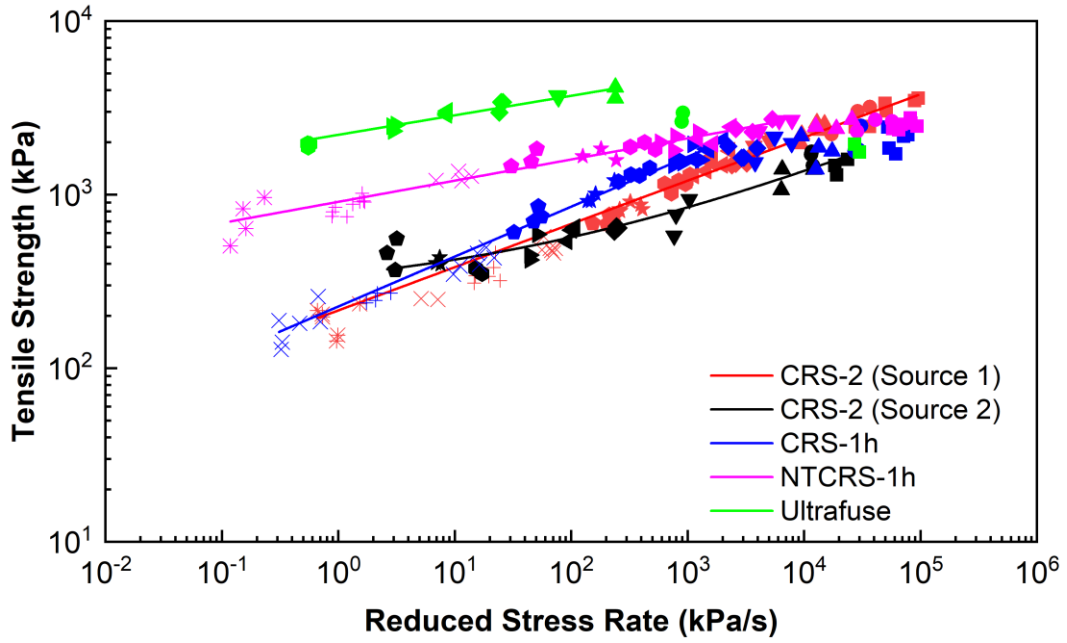


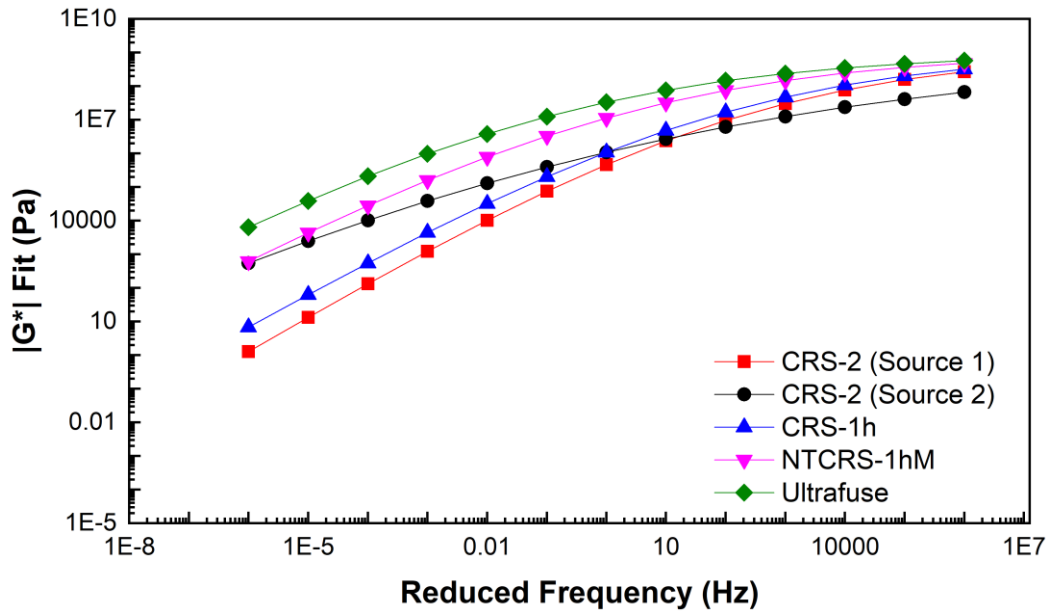
Figure 5-34. Predictions of tensile strength using all-point and two-point methods for all tack coat materials used in this study.

5.2.4 Comparison of Mastercurves from PATTI Tests of Tensile Strength and Dynamic Shear Modulus of Asphalt Binder

The reliability of the theoretical PATTI tensile strength mastercurves was examined by comparing the mastercurves developed using the dynamic shear modulus $|G^*|$ values of the asphalt binder. The dynamic shear modulus values of each tack coat were measured via DSR tests. The resultant dynamic shear modulus mastercurves show that Ultrafuse surpasses all the other tack coats in terms of quality, followed by NTCRS-1hM. Two other emulsions, CRS-2 (Source 1) and CRS-1h, have similar strength curves, as shown in Figure 5-35 (a). The ranking of the developed dynamic shear modulus mastercurves is the same as the ranking of the pull-off tensile strength mastercurves after removing the adhesive failure stubs, as shown in Figure 5-35 (b). It is worth noting that adhesive failure often was observed for the non-tracking tack coats while carrying out the DSR tests at lower temperatures. Therefore, the inherent nature of the tack coat to cause adhesive failure is due to its non-tracking characteristic at service temperatures.



(a)



(b)

Figure 5-35. Comparison of mastercurves for (a) pull-off tensile strength and (b) dynamic shear modulus values.

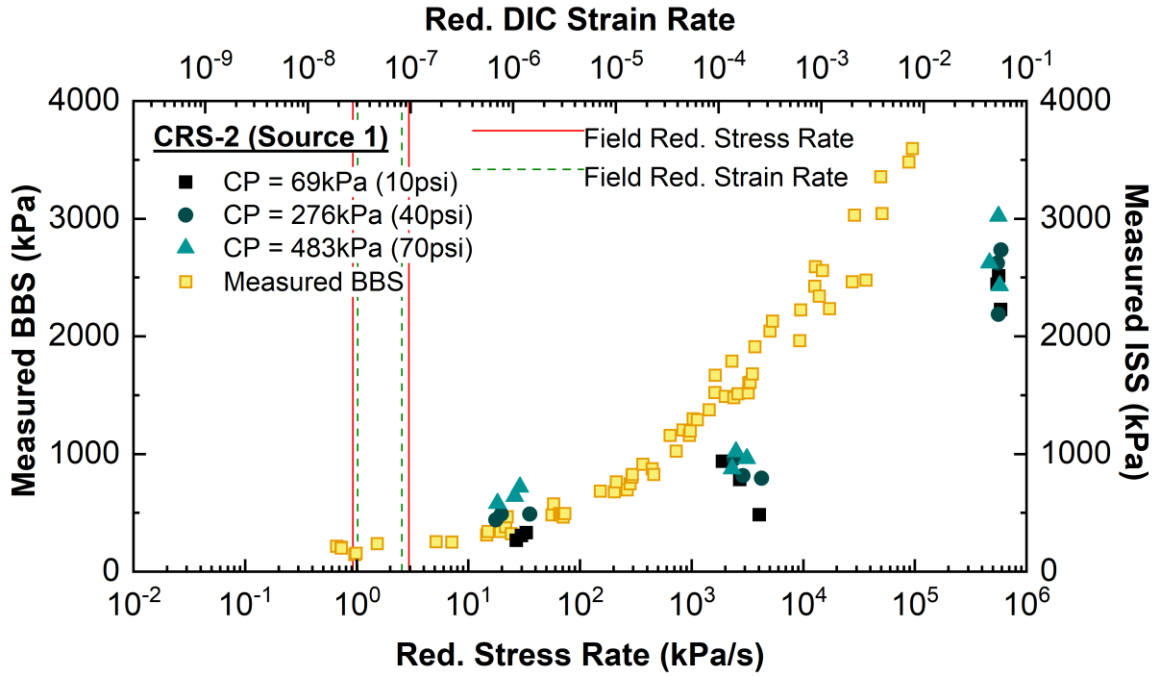
Chapter 6. Development of Tack Coat Selection Criteria

6.1 Development of Predictive Model for Interface Shear Strength

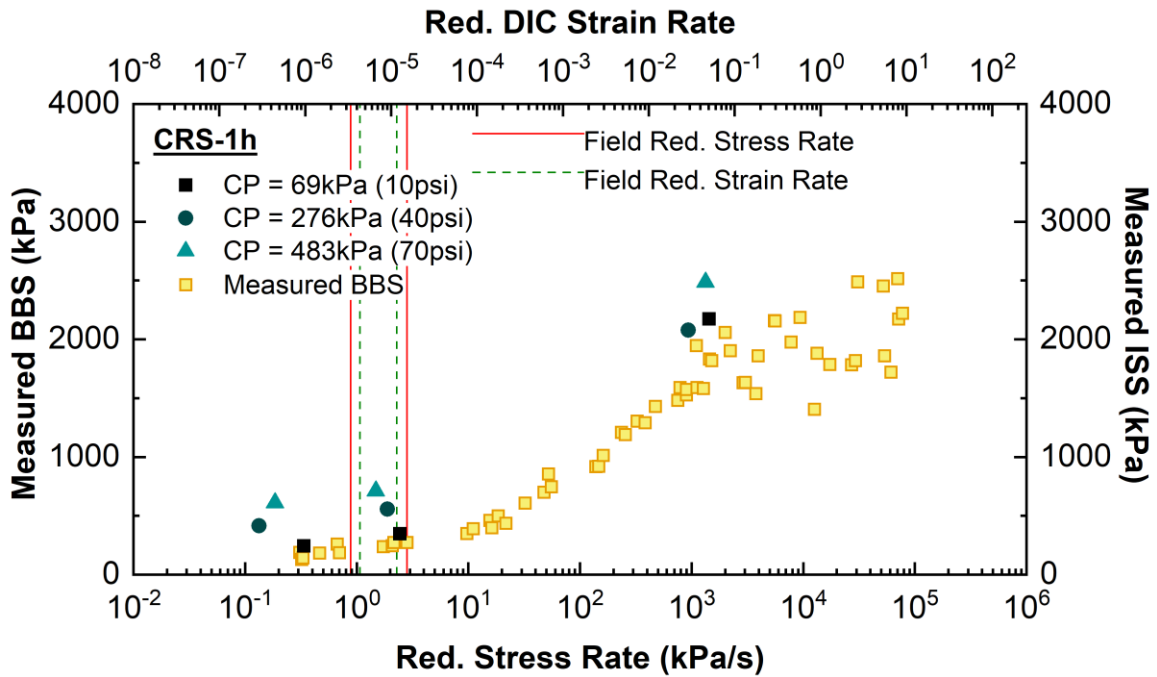
In this chapter, the research team's efforts to develop a universal relationship between interface shear strength (ISS) and binder bond strength (BBS) for different tack coat materials are described. In order to compare these two parameters, the initial step was to develop a prediction equation for ISS. The test parameters that govern the ISS prediction equation are the reduced strain rate (a combination of temperature and loading rate) and normal confining stress. The prediction equation follows the same form proposed in the NCDOT HWY 2013-04 research project, presented here as Equation (30).

$$\tau_f = (a_I \times \dot{\gamma}_R^{b_I} + e_I) \times \sigma_c + c_I \times \dot{\gamma}_R^{d_I} \quad (30)$$

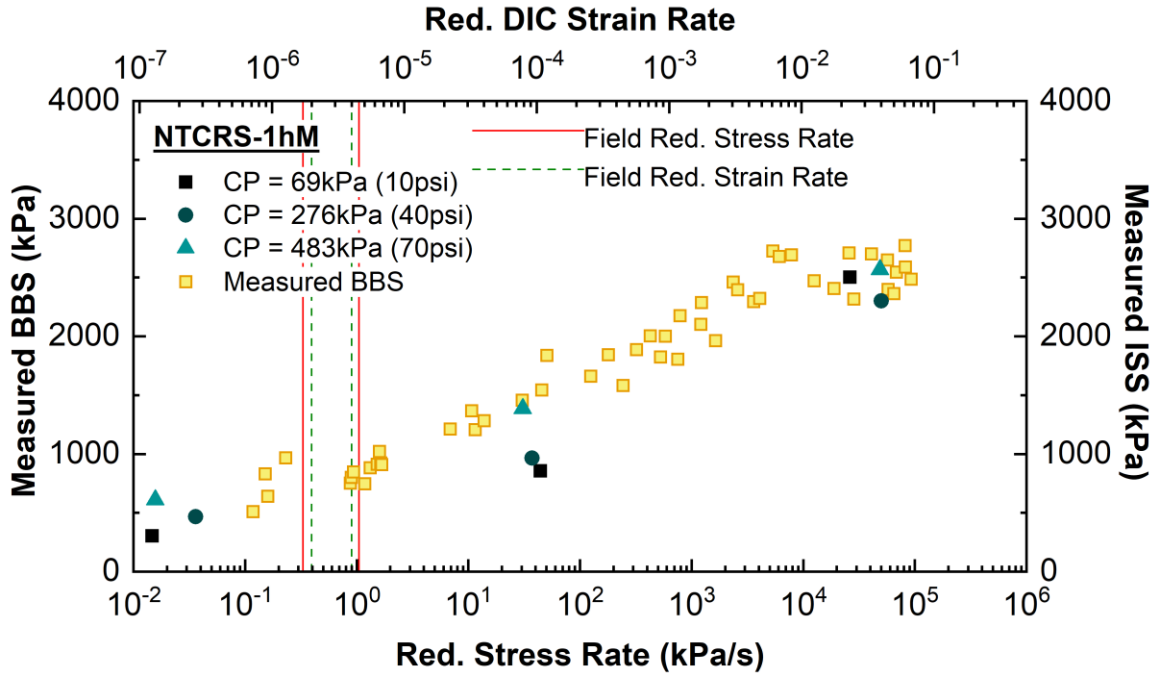
The research team conducted a fitting analysis using MATLAB software on the data presented in Figure 6-1. The corresponding coefficients a_I , b_I , c_I , d_I , and e_I of the prediction model presented in Equation (30) are shown in Table 6-1 for different tack coat material interface conditions. In addition, Table 6-2 presents the master curve coefficients for three different tack coat applied specimens calculated during the HWY 2013-04 project. The coefficients are verified and presented in the final report of HWY 2013-04 and therefore is used for developing the universal relation between ISS and BBS. Note that the two values for b_I in Table 6-1 have a minus sign, which indicates the opposite trend of decreasing ISS as the reduced strain rate increases. However, the effect of reduced strain rate on ISS is reflected through both b_I and d_I . The d_I value with a positive sign is much larger than the b_I value with a negative sign, and therefore the overall effect of the reduced strain rate on ISS is correctly represented (i.e., increase in the reduced strain rate results in the increase in ISS) by the coefficient values shown in Table 6-1.



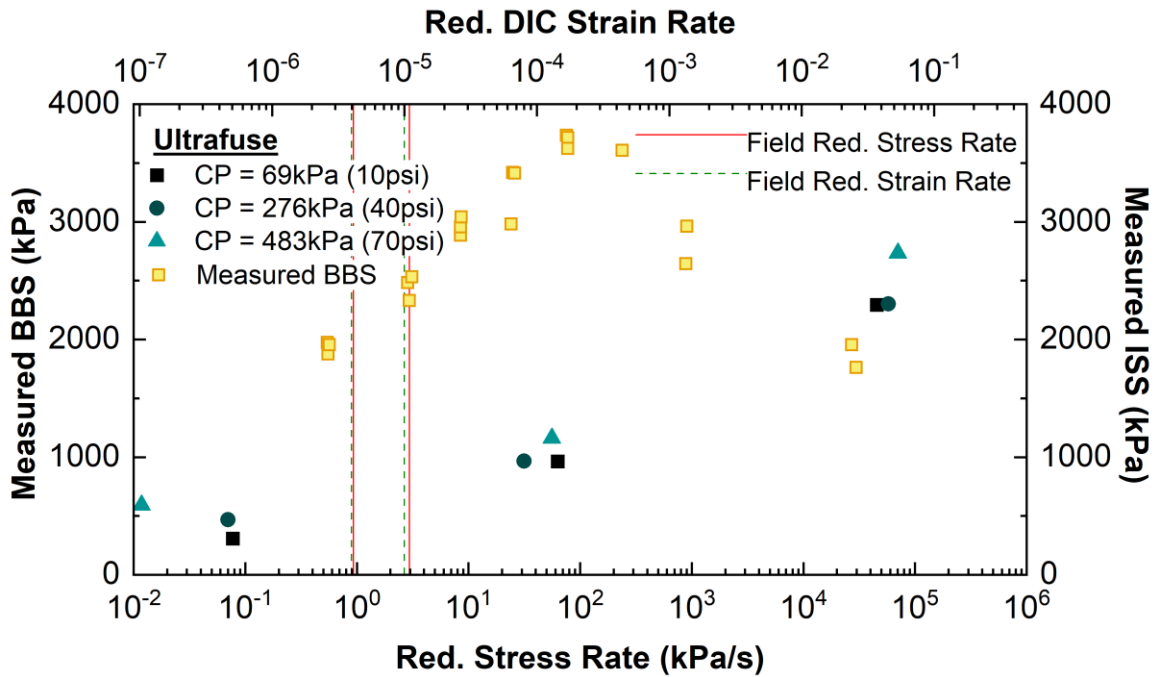
(a)



(b)



(c)



(d)

Figure 6-1. ISS and BBS mastercurves of (a) CRS-2 (Source 1), (b) CRS-1h, and (c) NTCRS-1hM, and (d) Ultrafuse.

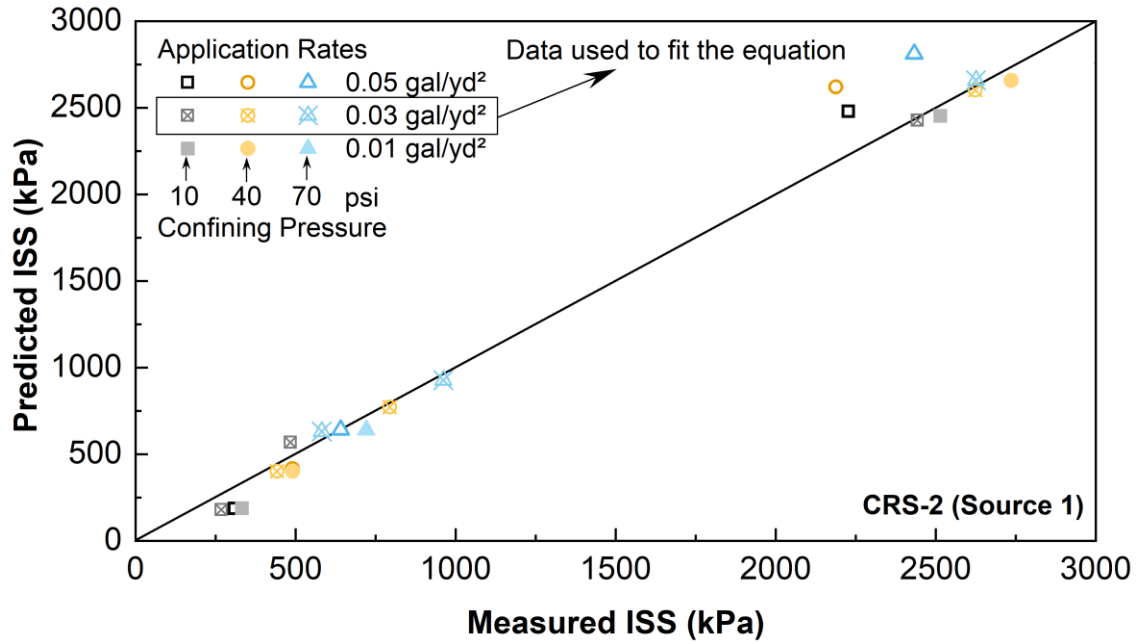
Table 6-1. Coefficients of Interface Shear Strength Prediction Equation for Different Asphalt Layer Interface Conditions at Reference Temperature of 20°C

Tack Coats	ISS Model Coefficients					
	a_I	b_I	c_I	d_I	e_I	R^2
CRS-2 (Source 1)	0.7683	-0.02659	5606	0.2907	1.64E-05	0.99
CRS-1h (Source 1)	4.41E-08	0.000618	4173	0.2322	9.58E-01	0.99
NTCRS-1hM	0.3656	-0.03963	4029	0.1603	6.63E-08	0.97
Ultrafuse	0.8000	0.9810	3779	0.1672	6.90E-01	0.99
CRS-2 (Source 2)	3.7130	0.4716	1065	0.1302	6.52E-01	0.99

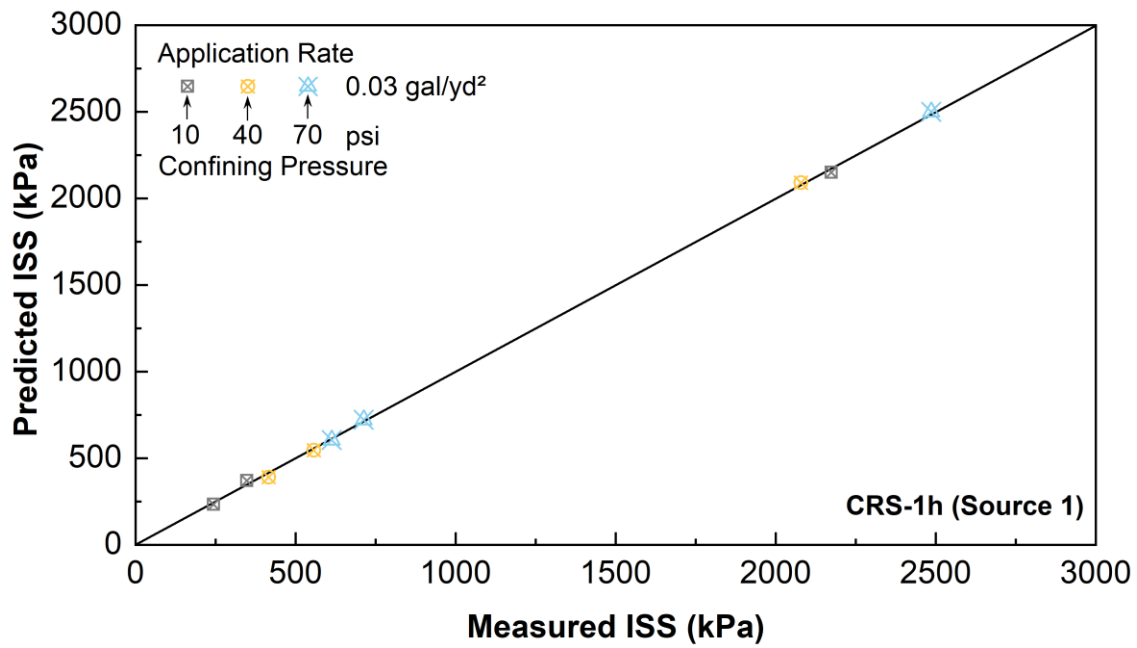
Table 6-2. Coefficients of Interface Shear Strength Prediction Equation for Different Asphalt Layer Interface Conditions at Reference Temperature of 5°C (Cho 2016)

Tack Coats	ISS Model Coefficients					
	a_I	b_I	c_I	d_I	e_I	R^2
CRS-2 (Source 3)	2.6116	0.0685	6140.4	0.1564	0.18	0.99
CRS-1h (Source 2)	1.8174	0.0564	6075.3	0.1566	0.16	0.99
No Tack Coat	1.2058	0.0329	5229.5	0.1612	0.15	0.99

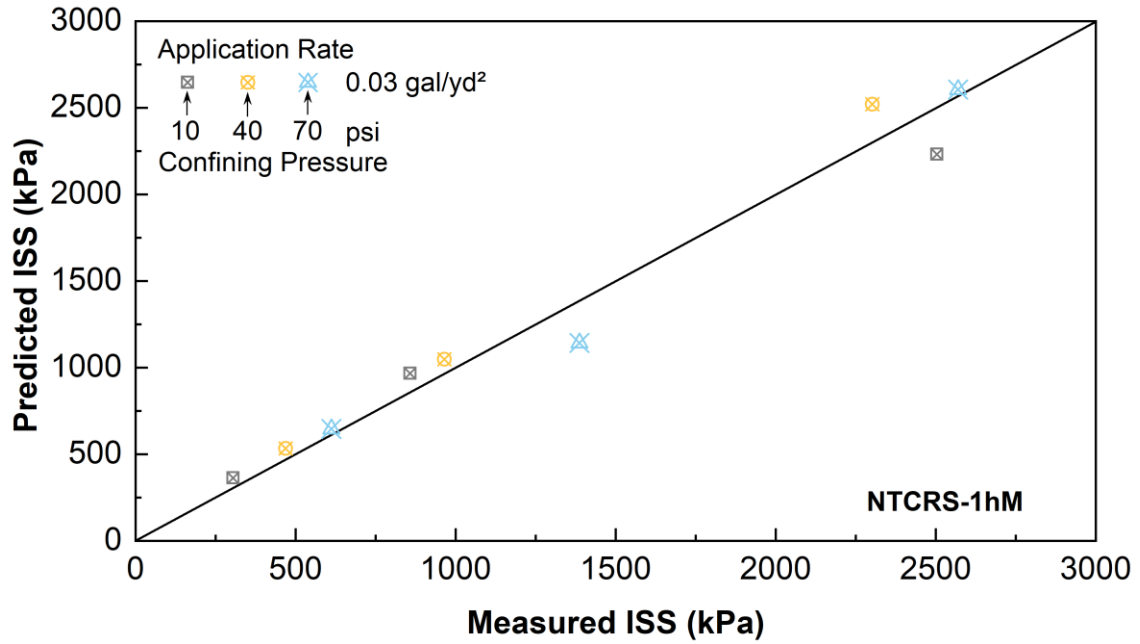
Figure 6-2 presents a comparison of the shear strength values that were predicted using the prediction equation, Equation (30), and the shear strength values that were measured via MAST tests. The MAST specimens were tested using various tack coats at the interface and at three application rates (0.01, 0.03, 0.05 gal/yd²); note that only CRS-2 (Source 2) used the application rate of 0.02 gal/yd² instead of 0.01 gal/yd². As the effect of the application rate was insignificant, the verification of the prediction equation was conducted by using the prediction equation calibrated by the ISS data at the application rate of 0.03 gal/yd² to predict the ISS data at the other application rates. These predicted ISS data are compared against the measured ISS data in Figure 6-2. The distribution of predicted points along the line of equity and the R-square values of fit that range from 0.97 to 0.99 clearly show that the proposed model equation delivers high prediction accuracy.



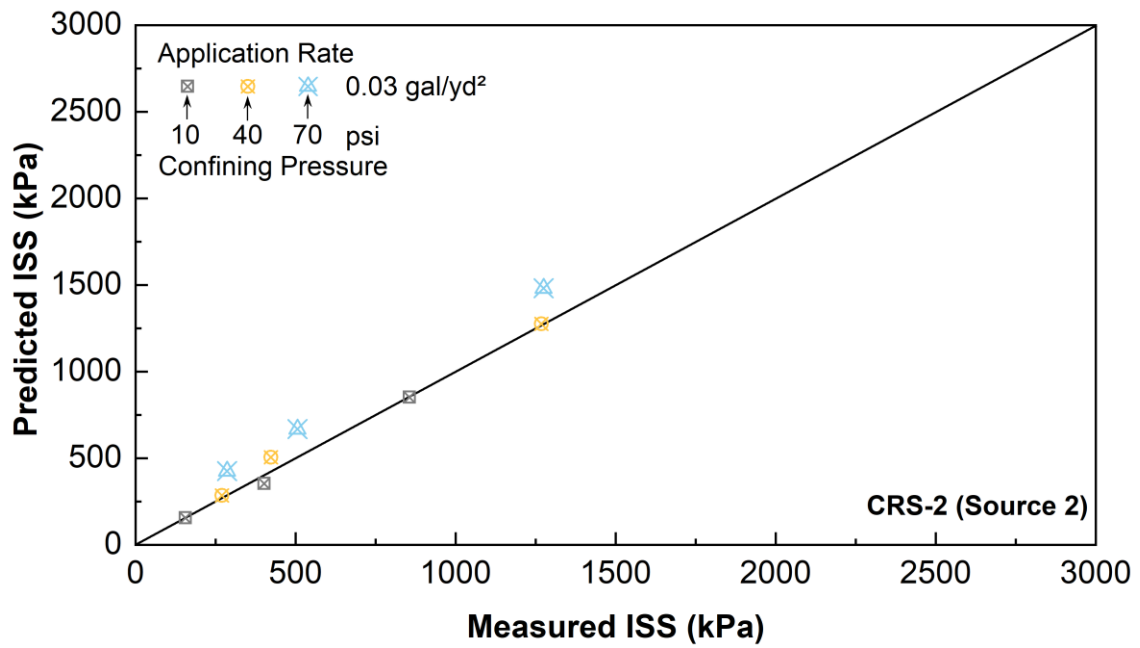
(a)



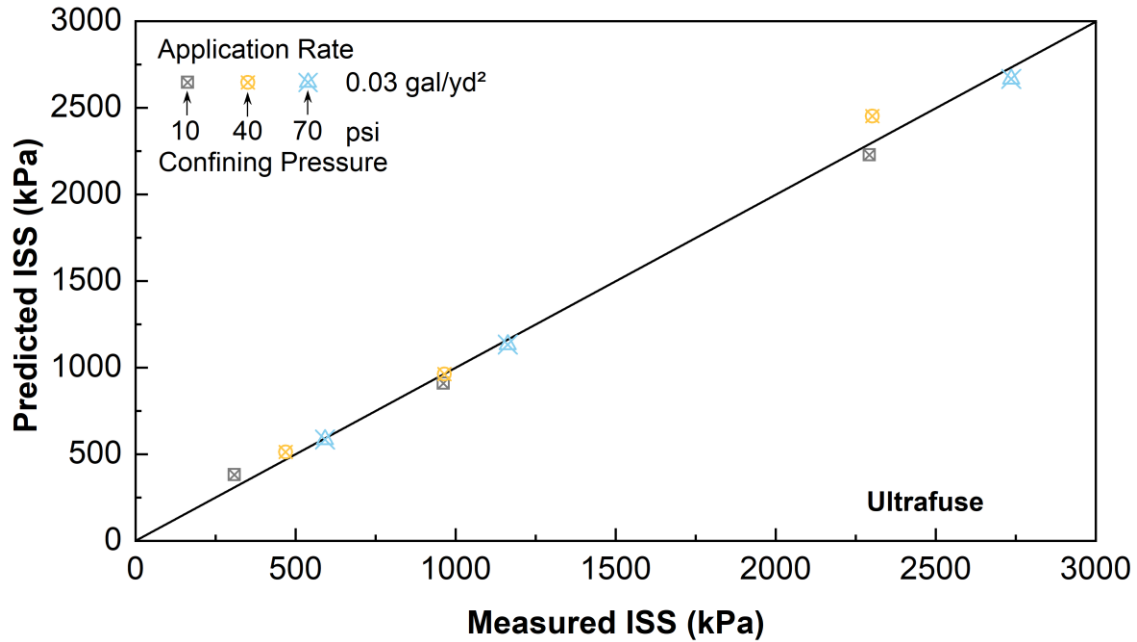
(b)



(c)



(d)



(e)

Figure 6-2 Comparison of interface shear strength values predicted by Equation (30) and actual shear strength data sets for tack coats: (a) CRS-2 (Source 1), (b) CRS-1h, (c) NTCRS-1hM, (d) CRS-2 (Source 2), slab-compacted, and (e) Ultrafuse.

6.2 Development of Predictive Model for Binder Bond Strength

BBS mastercurves for the different tack coats can be constructed based on PATTI tests carried out at 13 temperatures, as shown in Figure 6-1. The reason for carrying out multiple PATTI tests is that the acceptable stress rate range specified in ASTM D4541-17 (ASTM 2017) is limited to within 345 kPa/s to 1,034 kPa/s (50 psi/s to 150 psi/s). Therefore, the reduced stress rate measured at a specific temperature contributes to only a small region in the mastercurve. Furthermore, at lower temperatures, the pull stubs often fail in adhesive mode, which eventually leads to discarding those results. Consequently, considerable time must be spent testing at numerous temperatures to complete each mastercurve.

In order to avoid such extensive effort and time spent testing at 13 different temperatures, a two-point analysis method was developed in this study and presented in Section 5.2.3. This method purports to carry out PATTI tests at two different temperatures, preferably at temperatures above 30°C to avoid adhesive failure. The shift factors obtained from the DSR test results are applied to the two calculated stress rates to measure the reduced stress rates that correspond to the test temperatures. Equations (31) expresses the typical power form predictive equation for BBS. Table

6-3 represents the coefficients measured after fitting the data based on two-point method as described in Section 5.2.3.

$$\sigma_t = a_B \dot{\sigma}_R^{n_B} \quad (31)$$

Table 6-3. Coefficients of Binder Bond Strength Prediction Equation for Different Tack Coats

Tack Coats	BBS results		
	a_B	n_B	R^2
CRS-2 (Source 1)	155.7	0.268	0.88
CRS-2 (Source 2)	287.36	0.1742	0.89
CRS-1h	271.66	0.2676	0.98
NTCRS-1hM	1023.66	0.111	0.93
Ultrafuse	2236	0.1087	0.91

6.3 Identification of Interface Debonding Potential for Tack Coats Based on Numerical Simulation

Field observation of the interface debonding failure indicates that in most cases, the debonding event occurs due to shearing. Therefore, the debonding potential at the interface is quantified by shear ratio (SR), which is defined as a ratio of shear stress (τ_{max}) to shear strength (τ_s). The shear stress is a function of speed and weight of vehicle, temperature, pavement structure, and depth of layer interface. As can be seen in Equation (30), the shear strength is a function of reduced strain rate, which is a combined parameter of temperature and strain rate, and the confining pressure. Therefore, shear strength at the interface can be determined from the laboratory-developed Equation (30) by inputting the temperature at the interface, strain rate at the interface, which can be determined from the pavement response analysis, and the confining pressure, which is a normal stress at the interface and can be determined from the pavement response analysis. That is, by using Equation (30) and the shear stress and strain at the layer interface calculated from the pavement response analysis, the SR can be determined at various locations of pavement interface under various conditions, e.g., vehicle weight and speed, temperature. The location and magnitude of the maximum shear ratio, or MSR, could then be determined using a computed profile of the SR under the tire at the asphalt concrete layer interface. Theoretically, a larger MSR value has the greater potential of debonding. Figure 6-3 presents an example to determine MSR for a pavement interface at a depth of 1.5 in (3.81 cm) under the centerline of one tire (out of a dual tire configuration) along the longitudinal direction. The simulation condition is a dual tire-single axle vehicular load of 80 kN under braking while moving at a speed of 1 mph for an isothermal temperature of 50°C.

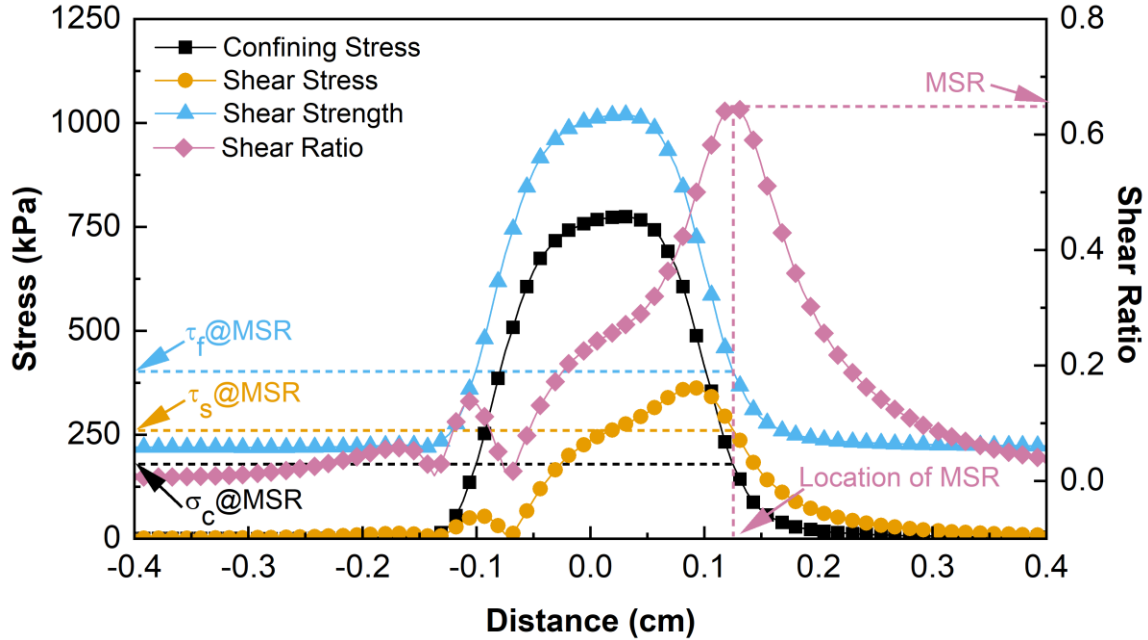


Figure 6-3. Shear ratio, shear strength (CRS-2 (Source1)), and shear and normal stress levels in longitudinal direction under central axis of tire at layer interface.

The interface shear strength (τ_f) for each point along with the layer interface under consideration were computed from the prediction model equation shown in Equation (30). The material coefficients for various tack coats by fitting the Equation (30), reported in Table 6-1 and Table 6-2, enable the prediction of the ISS for an asphalt concrete layer with a specific tack coat material at the layer interface. The ISS prediction model allows the evaluation of ISS at any point on the layer interface for any shear strain rate and temperature combinations as well as at any normal confining stresses. The normal stress (confining) and shear strain rates required for the determination of ISS at any point along the layer interface for a tack coat material were computed from the pavement response analysis carried out using FlexPAVE™. The normal confining stress (σ_{zz}) throughout the layer interface (each data point is the stress at a mesh node present at the interface), as shown in Figure 6-3, was determined for the critical condition (1 mph, 30°C, 1.5 inches) considered for the current study. The maximum shear stress and shear strain at each point of interest were computed using the Equations (32) and (33) respectively.

$$\tau_{\max} = \tau_s = \sqrt{(\tau_{xz})^2 + (\tau_{yz})^2} \quad (32)$$

$$\gamma_{\max} = \gamma_s = \sqrt{(\gamma_{xz})^2 + (\gamma_{yz})^2} \quad (33)$$

where

τ_{xz} = shear stress in the transverse direction under the tire,

- τ_{yz} = shear stress in the longitudinal direction under the tire,
- γ_{xz} = shear strain in the transverse direction under the tire, and
- γ_{yz} = shear strain in the longitudinal direction under the tire.

The shear stress and strain levels in the longitudinal (τ_{yz} and γ_{yz}) and the transverse directions (τ_{xz} and γ_{xz}) were determined from the FlexPAVE™ program. Further, the shear stress and strain were computed as using Equations (32) and (33) respectively. The shear strain (γ_s) history as a function of time was then used to compute the shear strain rates, as presented in Figure 6-4. The difference in the maximum shear strain and the strain at the zeroth time is the strain amplitude (a). The slope of the linear fit over the data set ranging from 0.4 times the strain amplitude to the maximum shear strain gives the shear strain rate ($\dot{\gamma}_s$).

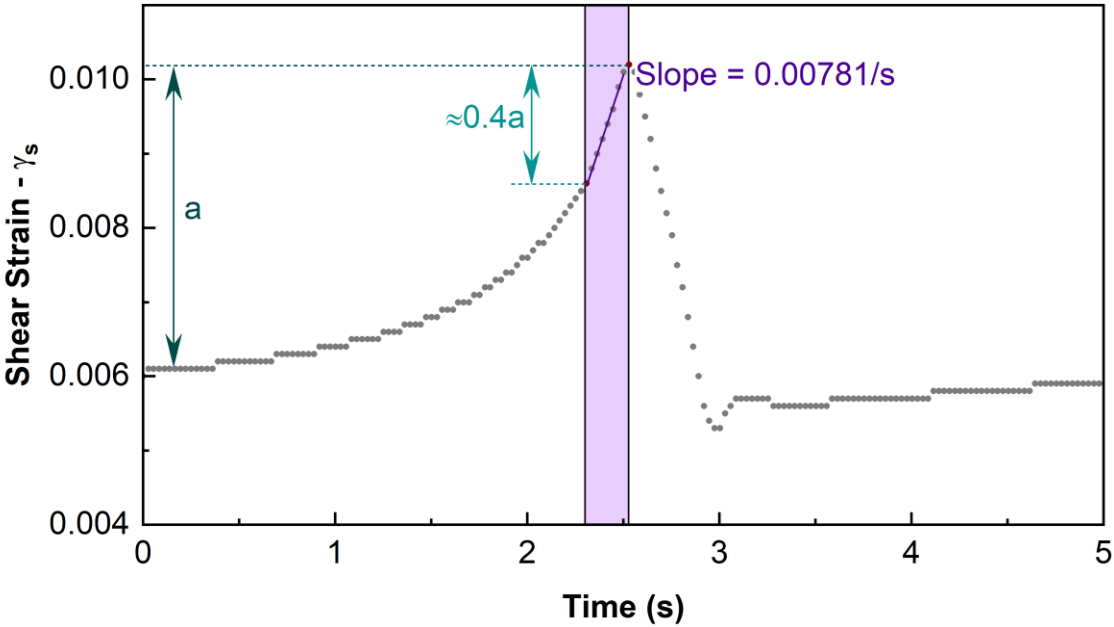


Figure 6-4. Typical interface layer shear strain history.

Once the shear strain rate and confining pressure at the layer interface are known, the shear strength can be computed. The shear stress over the computed shear strength at every mesh nodes gives a potential debonding factor known as Shear Ratio along with the layer interface. The point along the layer interface, which has the maximum shear ratio has the highest potential to debond and is tagged as MSR. Typically, this MSR point is found in front of the center line of the tire along the longitudinal direction. The distance from the edge of the tire to the MSR point typically ranges from 0.1 to 0.14 cm depending upon the simulation condition and tack coat.

Similarly, the shear stress (τ_s) history as a function of time was used to compute the shear stress rates as presented in Figure 6-5. The difference of the maximum shear stress and the stress at the zeroth time is the stress amplitude (a). The slope of the linear fit over the data set ranging from 0.7

times the stress amplitude to the maximum shear stress gives the shear stress rate ($\dot{\tau}_s$). This shear stress rate is used for the prediction of BBS strength at the layer interface. The confining pressure does not have any influence on the predicted BBS strength.

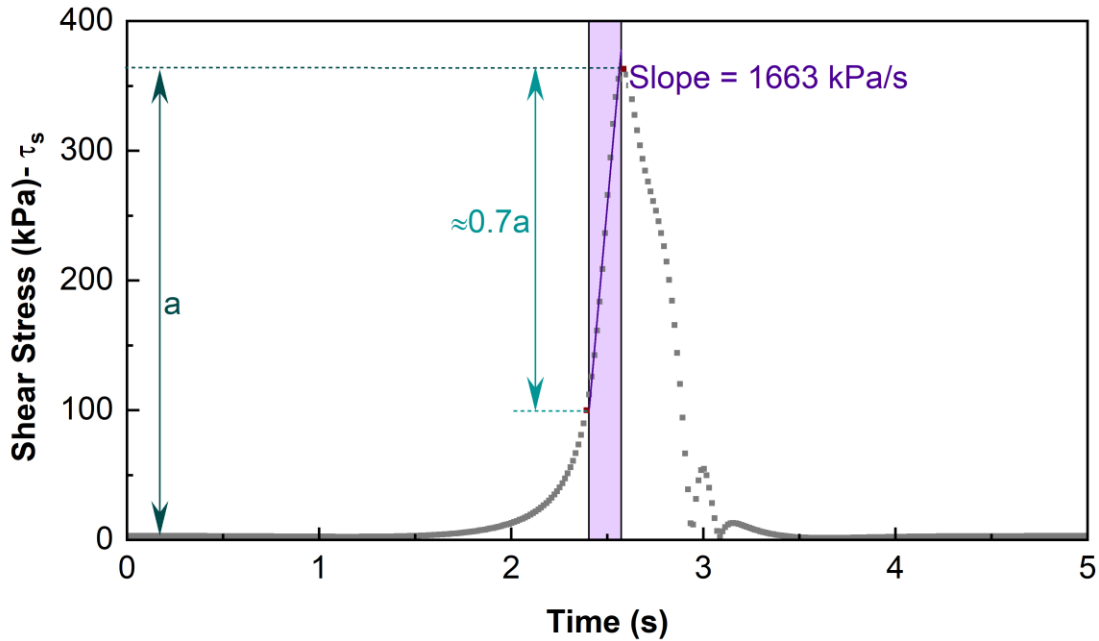


Figure 6-5. Typical interface layer shear stress history.

6.4 Establishing a Universal Relationship between Maximum Shear Ratio and Binder Bonder Strength

In order to establish a universal relation between the ISS and BBS for various tack coats at different pavement depths, the following aspects have to be considered. First, BBS does not represent the effect of confinement on the field. Second, a common link between ISS and BBS through the rate dependence need to be found to develop a universal relation between ISS and BBS. The PATTI test for BBS records only time and stress, and therefore BBS can be represented only as a function of reduced stress rate. However, the ISS predictive equation (Equation (30)) uses the reduced shear strain rate and confining pressure as independent variables. Therefore, the research team choose the pavement response analysis outcome to bridge the ISS and BBS through the field observed shear stress rate and shear strain rate. The pavement response analysis carried out for a specific loading condition generates shear stress, shear strain and confining stress at the layer interface that acts as the input for measuring the ISS and BBS generated at the layer interface.

The reduced stress rates and reduced strain rates for a specific numerical simulation condition is found by multiplying the fitted stress rate and strain rate by the corresponding binder shift factors. The shift factor value depends on the tack coat materials and the temperature selected for the numerical simulation, i.e., 50°C in the current case. The reference temperature selected in this study is 20°C for measuring the binder shift factor coefficients and thereby the ISS and BBS mastercurve construction.

In order to develop a relationship between BBS and ISS, the research team cross-plotted the ISS and BBS results measured at the MSR location for a specific numerical simulation condition that provides unique reduced stress rates and reduced strain rates that act as an input parameter for the predictive equations of BBS and ISS respectively. Figure 6-6 provides the step by step procedure followed to establish the universal relationship between ISS and BBS.

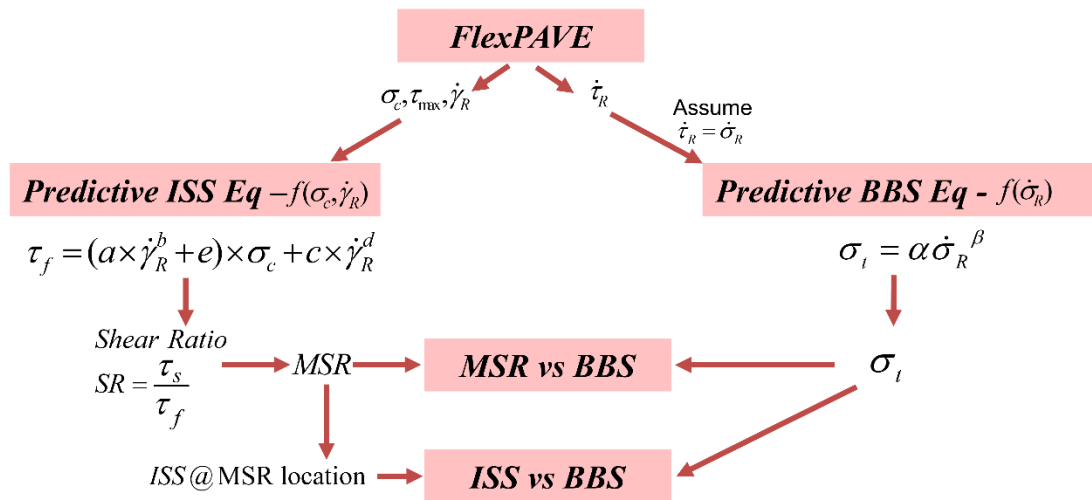
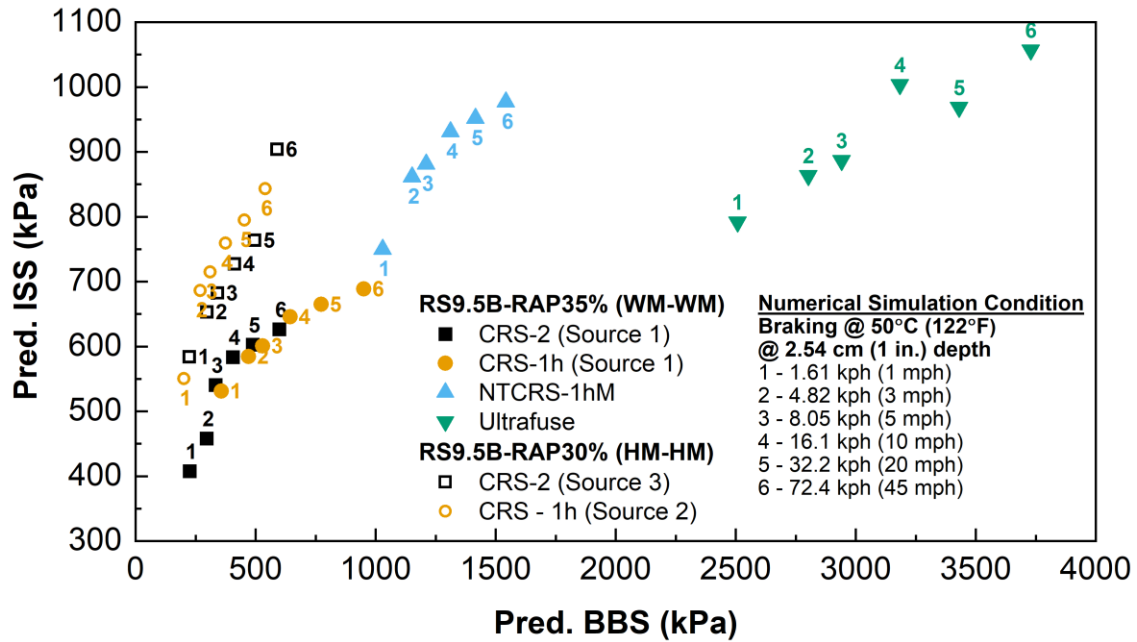


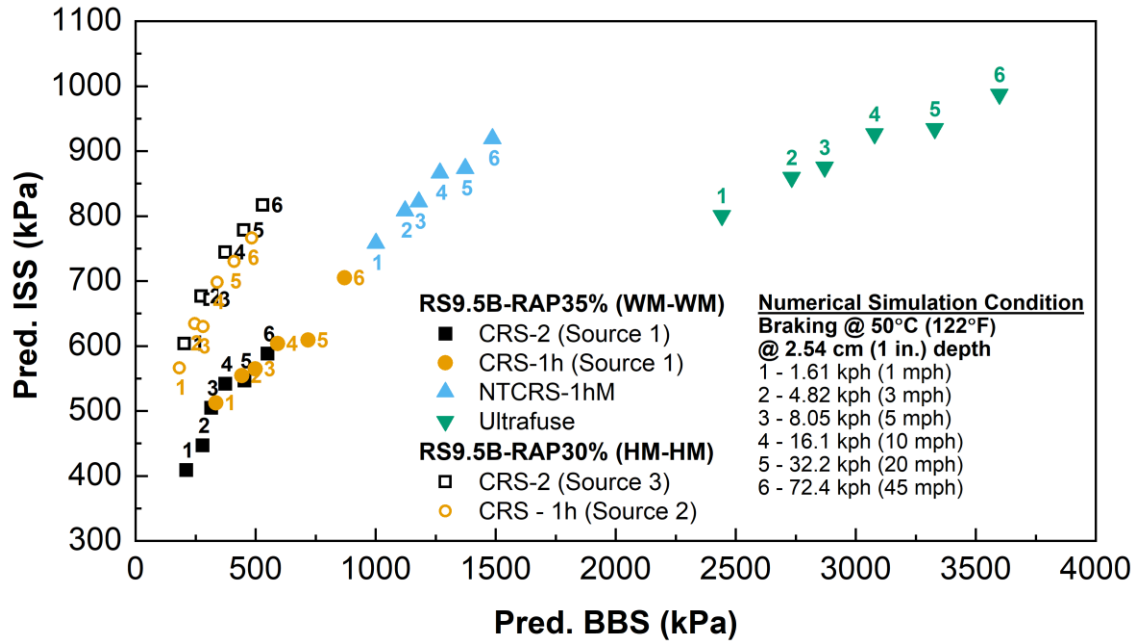
Figure 6-6. Flowchart showing step-by-step procedure to establish universal relationship between interface shear strength (ISS) and binder bond strength (BBS).

Figure 6-7 presents examples of the relationship between the ISS and BBS for all the tack coats placed at various interface depths in a thick pavement section. For any unique combination of the layers that contain each of the AC mixture types (HM-HM and WM-WM in these figures), all the tack coats except Ultrafuse follow a reasonably universal relationship. The overlap of the simulation points for the different loading conditions validates that observation. On the other hand, a polymer-modified tack coat such as Ultrafuse exhibits a high BBS value but fails to reflect that value in terms of the improved effects of the BBS on the ISS. The trend shown in Figure 6-1 reinforces this observation, as the ISS and BBS values in the ranges of the field-observed stress and strain rates have comparable numeric values for all the tack coats except Ultrafuse. In the case of Ultrafuse, even though the BBS observed in *in situ* conditions is high, a similar improvement in ISS was not measured during the tests. Therefore, the ISS value has a cap, and an improvement in BBS will not guarantee a similar improvement in ISS. Also, ISS is not merely a function of the

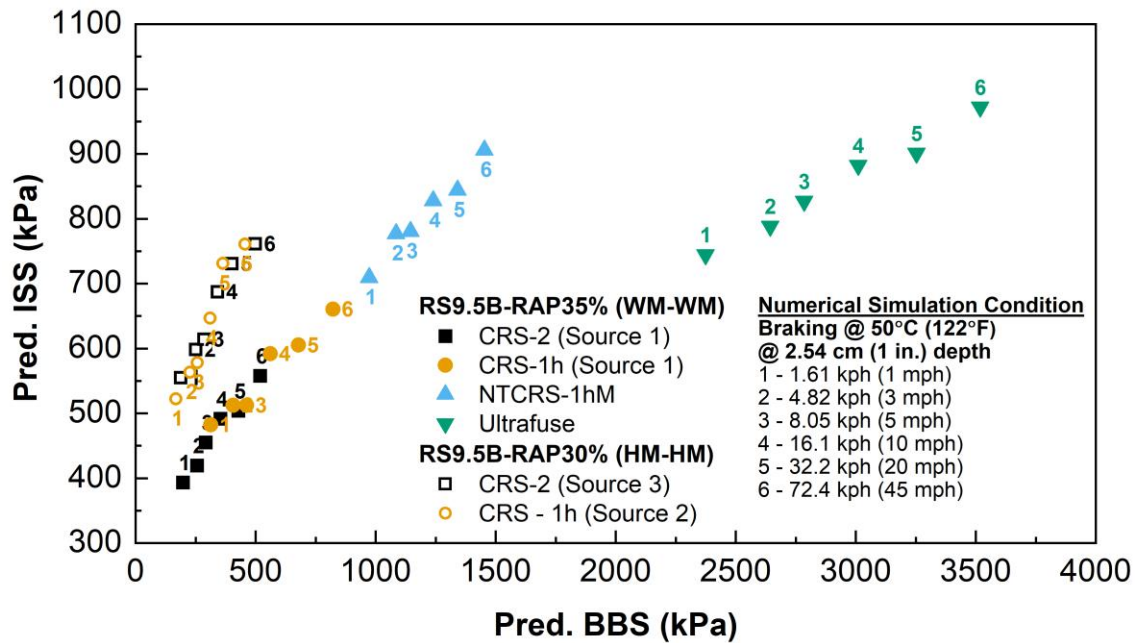
tack coat properties but also is dependent on the AC layers that constitute the whole composite interlayer system. Therefore, the ISS value that is predicted using this study's ISS-BBS universal relationship for a BBS value of 1000 kPa shall be used as the ISS cap. In other words, any tack coat with a BBS value that is higher than 1000 kPa will generate an ISS value that corresponds to the BBS value of 1000 kPa. This criterion also is proposed for measuring debonding potential. In short, an increase in BBS leads to pavements that are likely to perform better under fatigue loading to resist interface damage. This finding needs to be investigated further in future studies.



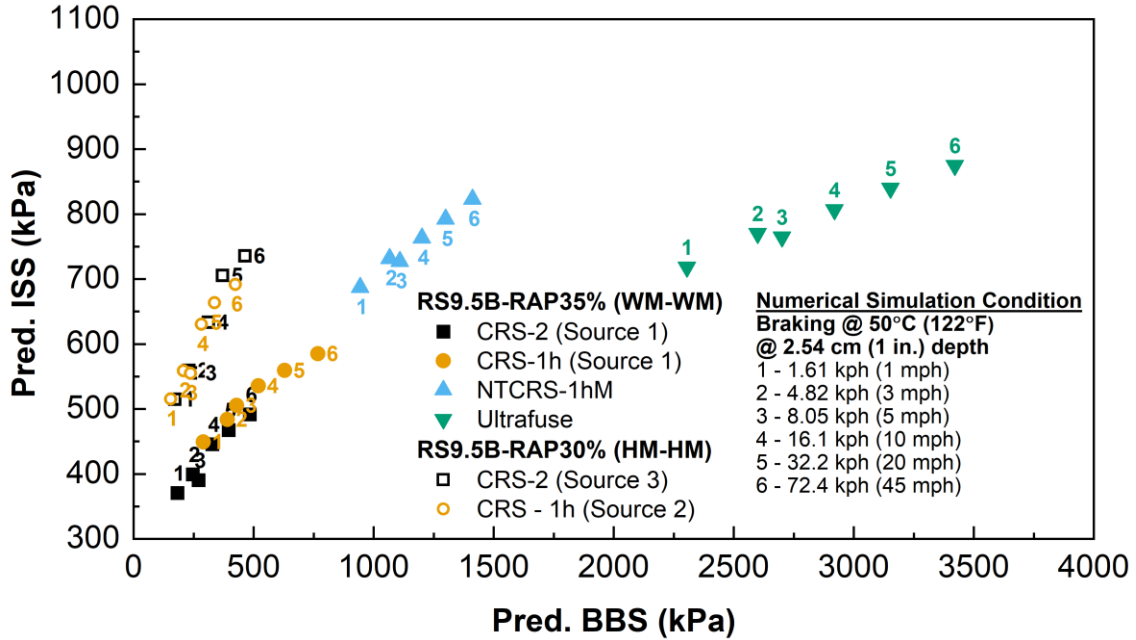
(a)



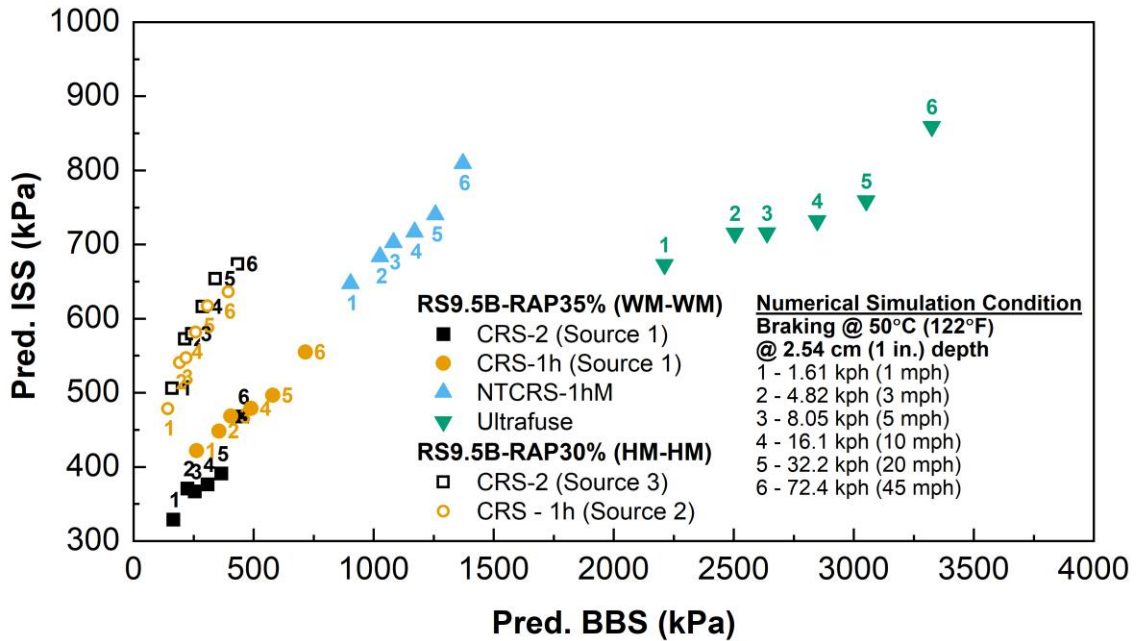
(b)



(c)



(d)



(e)

Figure 6-7. Relationship between ISS and BBS for the tack coats considered in this study at various depths in the pavement section: (a) 1 in., (b) 1.5 in., (c) 2 in., (d) 2.5 in., and (e) 3 in.

6.5 Developing the MSR Failure Envelope

Further to the establishment of universal relation between ISS and BBS, corresponding MSR and BBS for every specific numerical simulation condition were computed for various tack coats and is reported in Figure 6-8. The two mixtures considered for the ISS study, Warm Mix - WM (RS9.5B-RAP35%) and Hot Mix - HM (RS9.5B-RAP30%), with various tack coats follow a similar trend. Figure 6-8 shows the computed MSR and predicted BBS for the layer interface at 1.5 in. and 3 in. during an event of vehicle braking at a driving speed of 45 mph at the pavement temperature of 50°C. Multiple data points in Figure 6-8 for a specific tack coat material at a specific pavement depth represent the MSR and BBS values at different vehicle speeds during the vehicle's deceleration from 45 mph to a standstill. The speeds during deceleration considered for the analysis are 20 mph, 10 mph, 5 mph, 3 mph, and 1 mph. In Figure 6-8, higher MSR corresponds to the 1 mph, and the lowest MSR value corresponds to the 45 mph for a specific tack coat material.

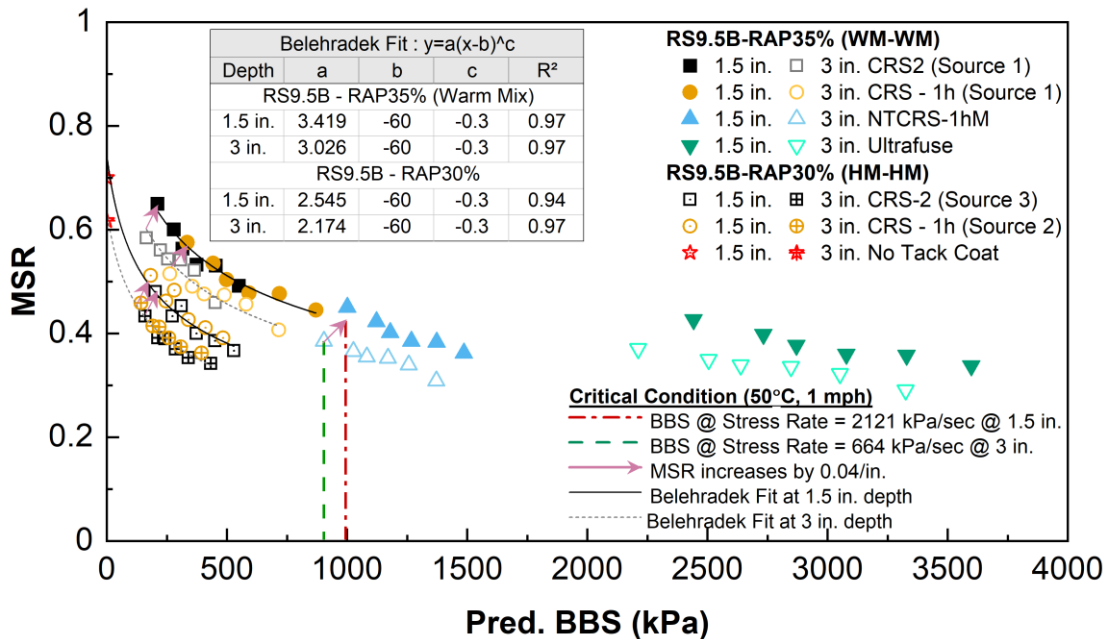


Figure 6-8. MSR failure envelope for different mixtures.

Belehradekit mathematical model was fitted over the available data to create MSR failure envelope as shown in Figure 6-8. The generic form of the Belehradekit mathematical model is shown in Equation (34). However, in the case of Warm Mix, the fitting was carried out over the data set of CRS-2 (Source 1) and CRS-1h only. The data computed for the tack coat, NTCRS-1hM, is left to verify the MSR predictive equation. The Ultrafuse data points were neglected for fitting due to the reason given in Section 6.4 that discusses the ISS-BBS universal relationship. While fitting the data set, the material parameters 'b' and 'c' are fixed to -60 and -0.3

respectively to create a universal relation between different tack coats. Even then, the fitted trendline has an R square value ranging from 0.9 to 0.97. This exercise helps to generalize the MSR predictive equation, and the independent material parameters that influences the MSR are the coefficient 'A' and BBS. It is noticeable that the intercept of each trend line on Figure 6-8 at no tack coat condition (BBS=1) depends on the mixture type. This indicates that MSR is not only the function of the depth and BBS but also the mixture type.

$$y = A(x-b)^c \tag{34}$$

It is also evident that as the depth increase, for the same loading condition, the MSR value decreases. The reduction in shear stress with increase in depth attributes to reduction in the MSR. The effect of depth on MSR values of various tack coats were plotted in Figure 6-9. It was found that the MSR value changes by 0.04 per unit depth change in inch.

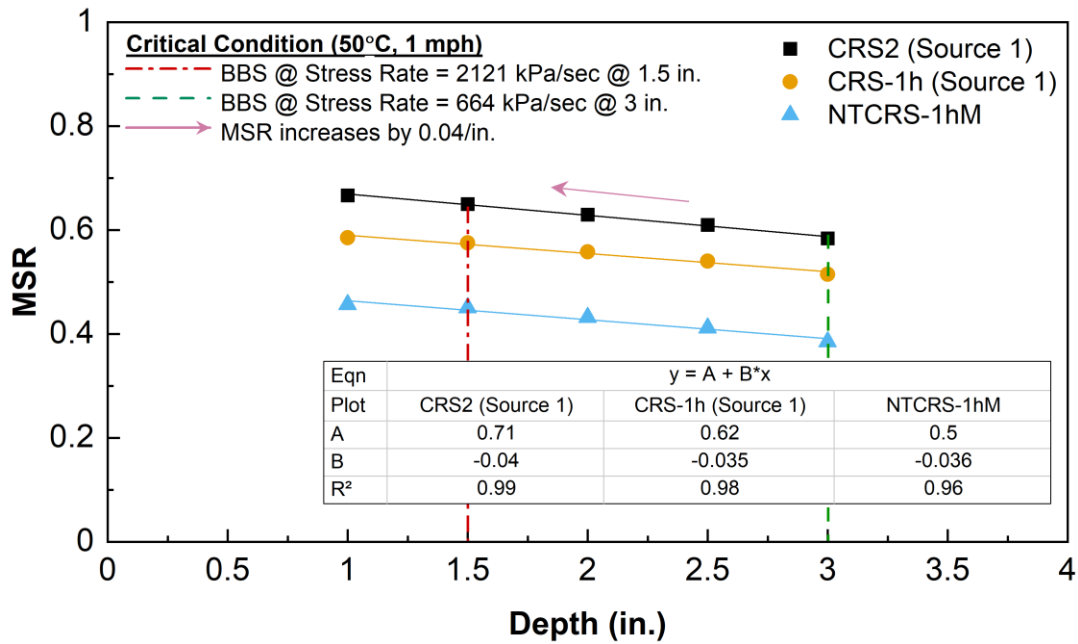


Figure 6-9. Change in MSR with depth.

The BBS measured at the critical condition of 50°C and 1 mph is corresponding to a stress rate at 2121 kPa/s at 1.5 in. while at 3 in. the stress rate is 664 kPa/s. A typical BBS test can be conducted between 620 to 792 kPa/s with at most care. In order to match the stress rate from a typical BBS test and that from the critical condition, an MSR predictive equation at 3 in. depth is used. Then, an additional term that represents the effect of depth on MSR is used to predict the MSR at any depth. The resulting equation, which is shown in Equation (35), is a universal relationship between BBS and MSR, hereafter called the MSR failure envelope.

$$MSR = A(\sigma_{t-crit.} + 60)^{-0.3} + 0.04(3 - d) \quad (35)$$

where

- A = AC mix parameter,
- $\sigma_{t-crit.}$ = BBS in kPa at 50°C and the stress rate of 690 kPa/sec (100 psi/sec), and
- d = depth of interface from the asphalt surface in inches.

6.5.1 Measuring the Mix Parameter A

The material parameter ‘A’ represents the MSR-BBS relationship for the mixture type constituting the pavement layer in question with any tack coat type application. In order to find the effect of tack coat in question on MSR at critical condition, the BBS value of the tack coat has to be measured/predicted at the critical condition. The rigorous experimental method of measuring the material parameter ‘A’ and BBS always invites more effort and time. Thereby, the number of tests is reduced and simplified by making certain assumptions, thereby predicting the required material parameter with fair accuracy in comparison to the rigorous experimental design. The research team developed three levels of measuring the material parameter A and BBS of tack coats where Level 1 represents the most ideal, rigorous and accurate method while Level 3 is a more generic, easy and quick way of measuring the BBS. These approaches are presented in this section.

Level 3: Standard values for various mixtures

The research team has carried out extensive ISS tests on specimens fabricated using various asphalt mixtures as part of the NCDOT projects HWY-2012-02, HWY-2013-04 and HWY 2018-13. The outcomes of all those projects were consolidated, and data collected from the other relevant literature (Danish 2018, Mohammad et al. 2012, Song et al. 2018) that measured the ISS were employed to find the material parameter A as shown in Table 6-4. Depending upon the available data in the literature, either Level 2 or Level 1 is applied appropriately to measure the value A. The proposed value of A depends on the type of asphalt concrete used at the top and bottom of the pavement surface layers. The users can directly choose the A value from the table to predict MSR values for different tack coats. However, it is noteworthy that the values provided are representative and need not be the true representation of the AC mixture considered for the specific project. Moreover, the A values are measured based on laboratory prepared fresh specimens (no damage or ageing), and therefore, the field core specimens and their performance might have some differences. Further study is recommended to establish more reliable A value that predicts the field performance.

Table 6-4. Material Parameter A for Standard Asphalt Mixtures

Asphalt Concrete		A
Top Layer	Bottom Layer	3 in.
OGFC	BM	5.326
OGFC	D	3.996
WM	WM	3.026
BM	BM	3.105
D	BM	2.845
BM	D	2.380
D	D	2.107
HM	HM	2.170

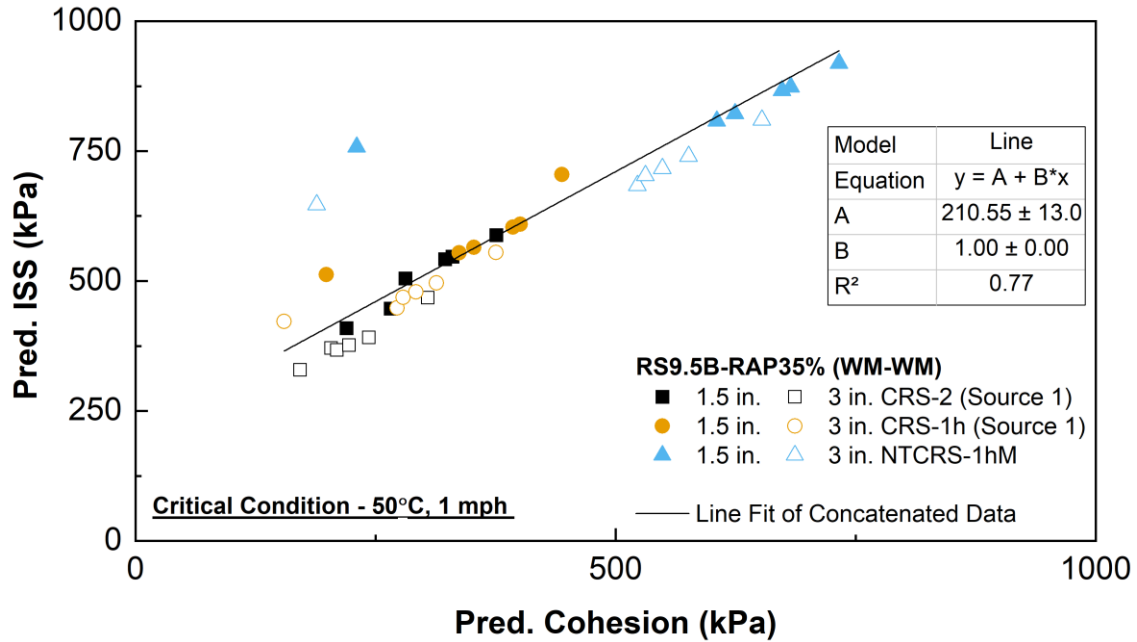
Level 2: Unconfined interface shear strength test

The unconfined interface shear strength test, such as Leutner shear test and Louisiana Interlayer Shear Strength Test (LISST), are easy to carry out and commonly available in comparison to the confined interface shear strength test. However, the effect of confinement on the ISS is undeniably proven and is present in the field. Therefore, the research team proposes a method to predict the ISS at the critical field location with the aid of unconfined interface shear strength (UISS) of specimens. The predictive ISS equation developed using MAST test (Equation (30)) involves two components: one is cohesion, and the other is friction, aka confining pressure. The cohesion component is calculated by removing the term that represents the influence of confining pressure in Equation (30) and is shown in Equation (36). Further, a linear relationship was developed between the cohesion component and ISS at different depths for WM-WM and HM-HM layered pavements at different speeds and 50°C as shown in Figure 6-10. A concatenated fit over the data points at 1.5 in. and 3 in. is used as no significant difference in the ISS value was found between the two depths.

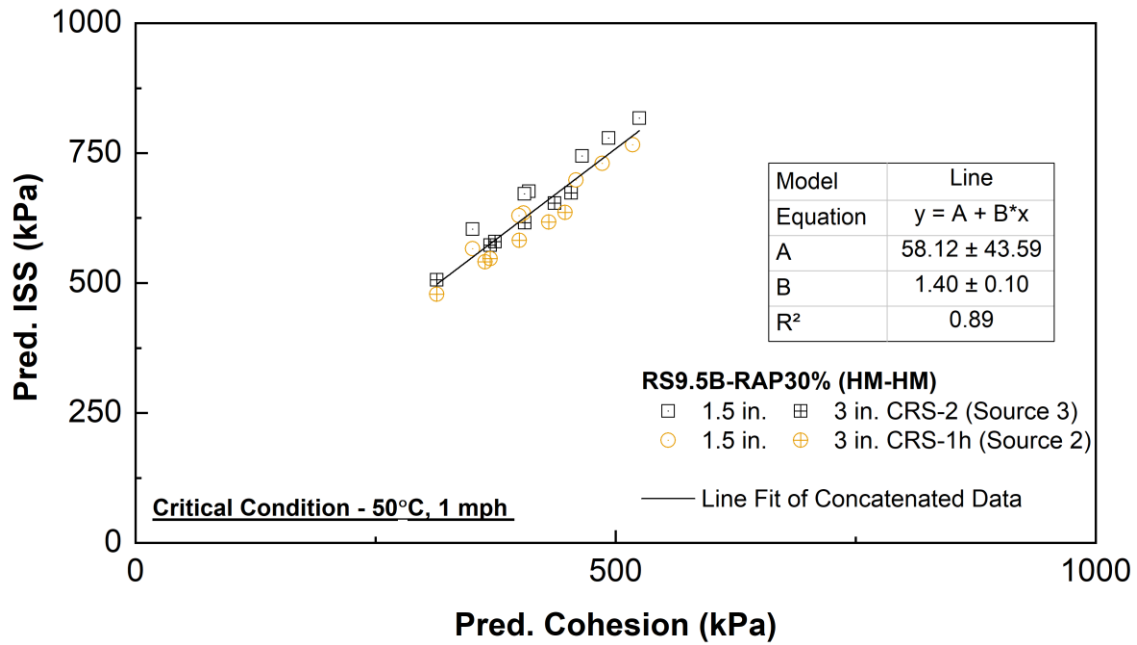
$$\tau_{cohesion} = c_I \times \dot{\gamma}_R^{d_I} \quad (36)$$

where

$\tau_{cohesion}$ = cohesion component of shear strength, kPa.



(a)



(b)

Figure 6-10. Interface shear strength variation with cohesion component at different depths for (a) WM-WM and (b) HM-HM.

In order to predict the ISS at the critical condition, it is recommended to carry out three UISS tests at three different strain rates (50, 5, and 0.5 mm/min) at 50°C. The reduced shear strain rate is measured with the aid of generalized shift factor developed by fitting the measured test results for commonly available mixtures and tack coats in the state of NC as reported in Figure 6-11. If the UISS test is carried out on specimens with No-tack coat condition, then the mixture shift factor value at 50°C computed as 0.000249 should be used for measuring the reduced shear strain rate while for any tack coat applied specimens tested at 50°C, a shift factor value of 0.001705 is recommended to be used. Further, Equation (36) is fitted to the UISS of specimens tested at various reduced strain rates to develop the master curve and evaluate the ‘ c_I ’ and ‘ d_I ’. The UISS for the specimen in question is then predicted from Equation (36) for typical strain rate at the 3 in. depth and is found as 0.0037495/s. Furthermore, the ISS at the critical condition is predicted from UISS using Equation (37) and Equation (38) depending on the mixture under which the test specimen falls into. If the surface layer in the pavement is WM, then use Equation (37) while for HM use Equation (38).

$$\tau_f = \tau_{cohesion} + 210.55 \quad (37)$$

$$\tau_f = 1.4\tau_{cohesion} + 58.12 \quad (38)$$

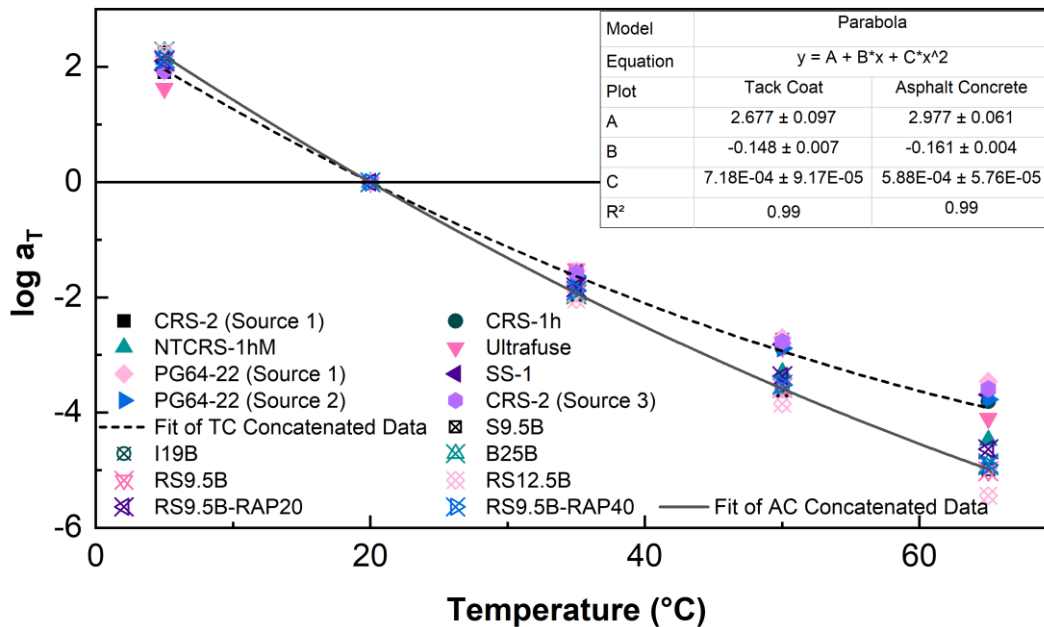


Figure 6-11. Time-temperature shift factor function for different mixtures and tack coats.

Once the ISS at the critical condition is determined, the MSR value is found by taking typical shear stress at 3 in. depth over the shear strength. Figure 6-12 shows the shear stress measured at MSR location for an interface 1.5 in. and 3 in. deep from the surface. As the thickness increases, the

shear stress at the MSR location decreases and vice versa. The average value of shear stress at MSR location at 3 in. is 225 kPa. Therefore, the MSR is calculated as follows

$$MSR = \frac{225}{\tau_f} \quad (39)$$

Now, knowing the MSR, the BBS (σ_i) is assumed as one for no-tack coat specimens, while for a tack coat applied specimens, BBS needs to be calculated as per any level described in Section 6.5.2. Further, parameter *A* is calculated by substituting MSR and BBS on Equation (35) to develop the MSR failure envelope for the specific asphalt mixture layers in question and can be used to predict MSR for any tack coat.

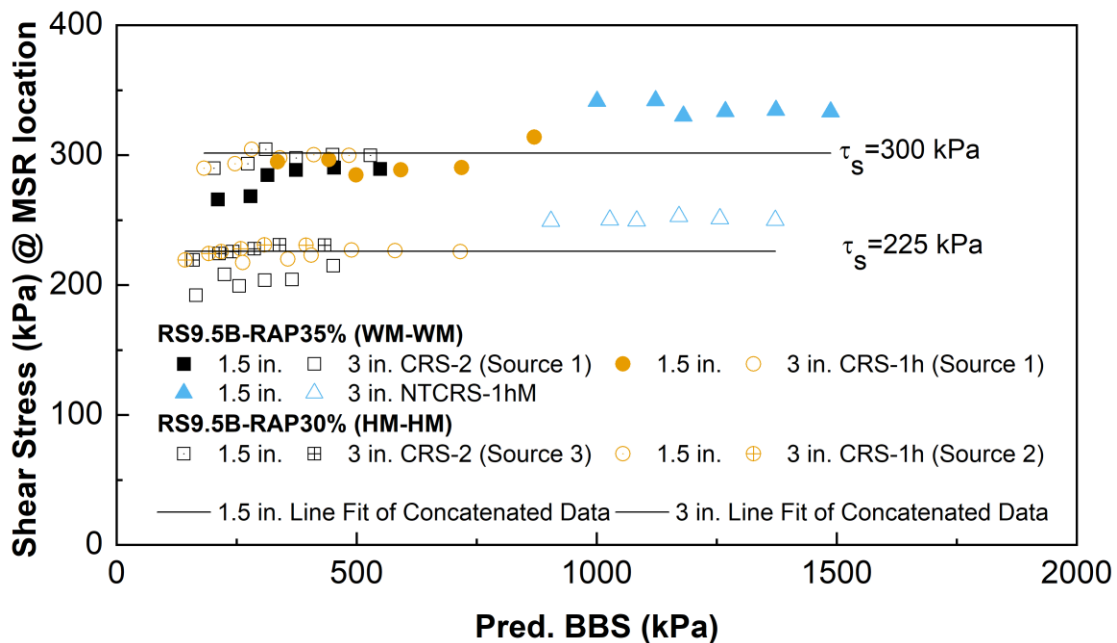


Figure 6-12 Variation of field shear stress at MSR location for different tack coats.

Level 1: Confined interface shear strength test

In Level 1, the confined ISS test at the critical condition is recommended to carry out at three different strain rates (50, 5, and 0.5 mm/min) at 50°C for a unique critical confining pressure. The typical value of confining pressure at 3 in. depth is shown in Figure 6-13. It is ideal to choose a confining pressure ranging from 175 kPa to 210 kPa (25 psi to 30 psi) as critical confining pressure. The reduced shear strain rate is measured with the aid of generalized shift factor developed by fitting the measured test results for commonly available mixtures and tack coats in the state of NC, as reported in Figure 6-11. If the ISS test is carried out on specimens with no-tack

coat condition, then the mixture shift factor value at 50°C computed as 0.000249 should be used for measuring the reduced shear strain rate while for any tack coat applied specimens tested at 50°C, a shift factor value of 0.001705 is recommended to be used. Further, Equation (36) is fitted to the ISS of specimens tested at various reduced strain rates to develop the master curve and to find the values of ‘ c_i ’ and ‘ d_i ’. The ISS for the specimen in question is then predicted for typical strain rate at the 3 in. depth and is found as 0.0037495/s. The predicted ISS already accommodates the effect of confinement; hence the results can be directly used to measure the MSR as shown in Equation (39). Now, knowing the MSR, the BBS (σ_i) is assumed as one for no-tack coat specimens, while for a tack coat applied specimen, BBS need to be calculated as per any of the level described in Section 6.5.2. Further, parameter A is calculated by substituting MSR and BBS on Equation (36) to develop the MSR failure envelope for the specific asphalt mixture layers in question and can be used to predict MSR for any tack coat.

For now, there is not enough data to cross-verify the accuracy of the proposed test levels. However, the theoretical approach helps to formulate the framework for future verification procedure and hence a major objective for later studies.

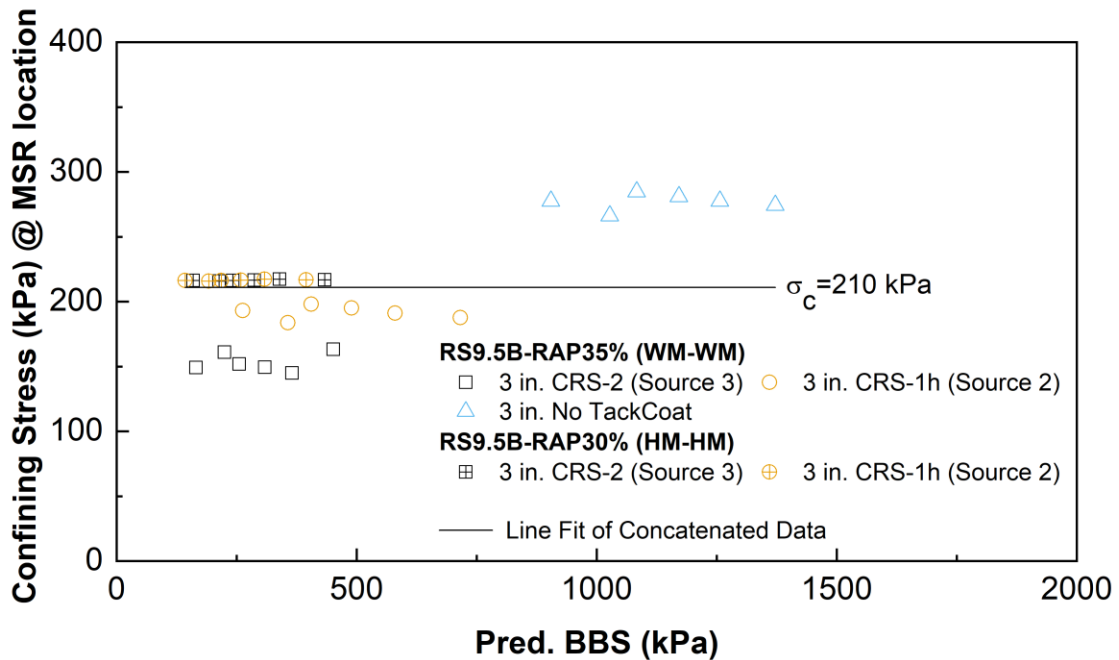


Figure 6-13. Typical variation in confining pressure at MSR location.

6.5.2 Measuring the BBS

BBS is an important property of tack coat materials that is central to the proposed tack coat quality assurance method. Three levels of determining the BBS are presented in this section, with the simplest but least accurate method being Level 3 and the most accurate method being Level 1.

Level 3: Single BBS test

A typical BBS test can be conducted between 620 to 792 kPa/s with at most care. Therefore, if the user carries out the test at 690 kPa/s (average stress rate of four stub tests in a substrate) at 50°C, that test condition represents typical stress rate in the field at 3 in. depth at 50°C. Therefore, the measured BBS can be used directly in Equation (35) to predict the MSR value at any depth.

Level 2: Two Point Method Using Generalized Shift Factor

If the user could not achieve the average stress rate of 690 kPa/s at 50°C, it is recommended to carry out an additional BBS test (four stubs per substrate) at any temperature above 30°C other than 50°C. It is ideal for carrying out at 35°C. Once the BBS and stress rate of the tack coat are measured at both temperatures, use the two-point method described in Chapter 5 to measure the material parameter a_B and n_B of the BBS predictive equation (Equation (27)). In order to do so, the reduced stress rate has to be calculated, which requires the aid of the shift factor function. In order to simplify the effort of the user, it is recommended to use the generalized shift factor, developed by fitting the measured shift factors of various tack coats used for different projects at NCSU laboratories. Figure 6-11 shows the fitting of the shift factor of various tack coats—the generalized shift factor at 50°C is found as 0.001705. Thereby, the material parameter a_B and n_B of the BBS predictive equation for the specific tack coat in question could be found. Subsequently, the BBS is predicted at the critical stress rate of 690 kPa/s. The predicted BBS at 690 kPa/s is substituted in Equation (35) to determine the MSR.

Level 1: Two Point Method Using DSR Shift Factor

Level 1 is the rigorous and most accurate way of carrying out the BBS prediction. It follows all the steps explained in Level 2. The only difference in Level 1 in comparison to Level 2 is the usage of measured shift factor instead of the generalized shift factor. Level 1 requires the user to run the DSR test on a tack coat of interest as per AASHTO T315-12 (AASHTO 2020c) to measure the shift factor coefficients. Even though Level 1 consumes more effort and time of the user, it provides the most reliable BBS prediction compared to other levels.

Figure 6-14 provides the predicted MSR based on the BBS measured using Level 1 and Level 2. The current research did not carry out BBS at 50°C; hence, level 3 is not compared. The predicted MSR values for Level 1 are slightly closer to the line of equality than those for Level 2; however, the data for both levels fall close to the line of equality, which demonstrates the accuracy of the proposed approach.

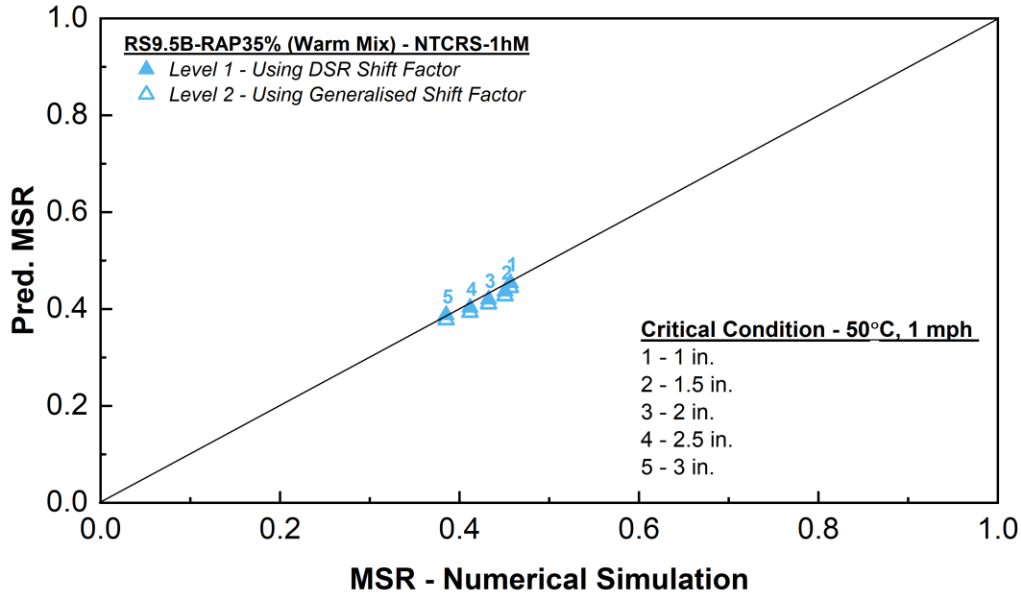


Figure 6-14. Verification of predicted MSR using various levels of BBS measurements.

In summary, predicting the coefficient ‘A’ for different interlayer layer system made out of different mixtures is critical to find the effect of tack coats on the MSR value. Following the different levels to measure the parameter proposed depends on user freedom and requirement. Besides, adopting generalized binder and mixture shift factor coefficients reduces the user’s time and effort to determine the coefficients by carrying out DSR test. Moreover, the MSR failure envelope mimics the critical stress state in the field condition.

6.6 Tack Coat Purchase Criteria

A few assumptions have to be made to propose the generalized tack coat purchase criteria. First, even though the overlay mixture has an effect on the MSR; WM used in this study is considered as a relatively weak material expected in the field. The fitted equation predicts an MSR value of 1.02 for no tack coat pavement with WM as the surface layer at the interface of 1.5 in. This shows that, theoretically, the WM with no tack coat has the potential to fail with the first major truck loading after the construction. Note that there could be mixtures that could perform even worse than WM such as OGFC. The WM used in this study was made as the ideal worst mixture as it is the one mix available with enough experimental data set and has just crossed the theoretical critical MSR condition of one at no-tack coat condition. Second, it is assumed that all the tack coats considered in this study is acceptable in the field. Therefore, the least performing tack coat should be also acceptable. Henceforth, Equation (35) is generalized as shown in Equation (40) for the tack coat selection criteria.

$$MSR = 3.051(\sigma_t + 60)^{-0.3} + 0.04(3 - d) \quad (40)$$

Equation (40) was used to develop the failure envelope for the 3 in. depth as shown in Figure 6-15. The critical MSR value was selected to be 0.7 so that all the tack coats evaluated in this study would pass the criterion. The intersection between the MSR value of 0.7 and the failure envelope shown in Figure 6-15 determines the minimum BBS value for each combination of existing and new layers as shown in the legend. As shown in Figure 6-15, the minimum BBS value of 75 kPa passes all the tack coats for typical mixtures except the OGFC surface layer. When the surface layer is OGFC, the minimum BBS value for the tack coat should be 750 kPa. These selected values represent the most conservative cases expected in the field.

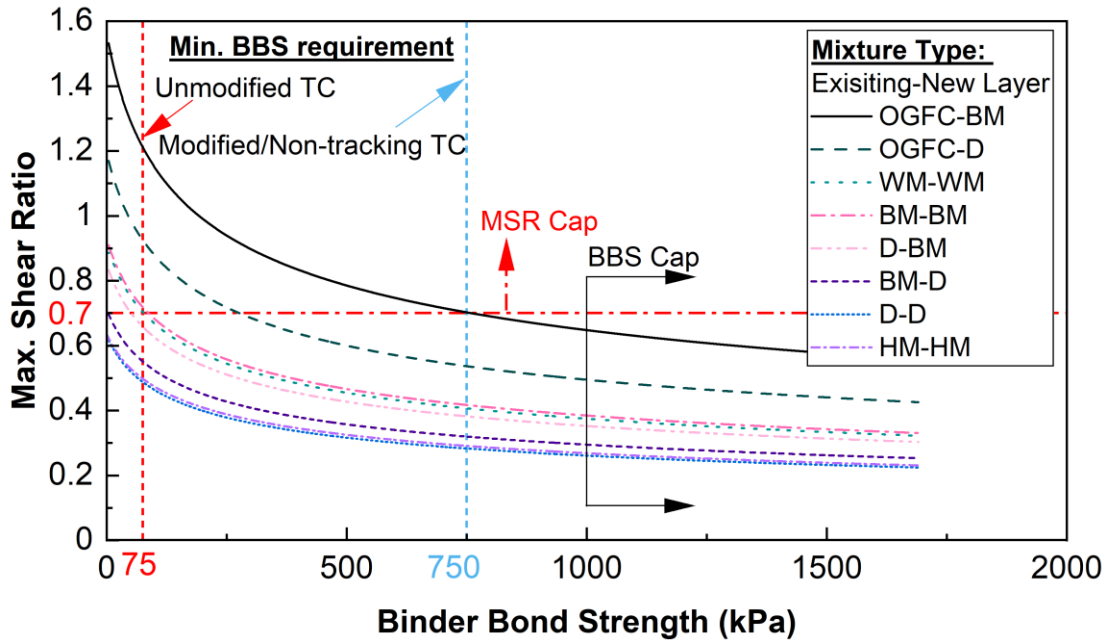


Figure 6-15. Failure envelope for various AC mixture layers.

It is also noteworthy that in certain cases, the MSR value of no-tack coat condition is less than 0.7. Theoretically, any MSR value less than one qualifies to resist debonding. However, the rate of damage that occurs to the interface is unknown. Thereby, it will be difficult to predict the service life of the pavement before debonding occurs. Preliminary fatigue test results on interface bonding show that a tack coat applied at the interface is more resilient than no-tack coat condition. Hence, it is advisable to use a tack coat with a lower strength even if the mixture alone provide sufficient MSR. Note that when the BBS value exceeds about 1000 kPa, only small reduction in the MSR is caused by the large increase in BBS.

6.7 Project-specific Tack Coat Selection Criteria

NCDOT uses PG 58-28, PG 64-22, and non-tracking hot binders with high application rate for OGFC, and usage of emulsion is prohibited due to the flow of emulsion under high application

rate. According to the BBS data shown in Figure 5-29, all the emulsion tack coat materials fail to pass the 750 kPa BBS threshold value, NTCRS-1hM is on the boundary, and Ultrafuse passes the threshold easily. This observation supports the NCDOT's current practice of not using emulsion tack coat materials for OGFC. However, the user/contractor can measure the material parameter A and BBS by following Level 2 and Level 1 to develop a project specific failure envelope. If they can demonstrate that their tack coat meets the minimum MSR requirement of 0.7, the tack coat could be accepted. The recommended values from this study are kept for the most conservative cases, and carrying out the required tests for a specific project will give more freedom for the contractor for the tack coat selection depending upon the mixture in use.

Chapter 7. Best Practices and Usage of Tack Coats in North Carolina

7.1 General

A tack coat is the sprayed application of liquid asphalt binder on an existing asphalt or concrete surface to promote a bond between the old pavement surface and a new asphalt layer. This thin membrane of asphalt binder provides the ‘glue’ between the layers, creating a monolithic structure that performs as a unit as opposed to unbound, independent layers. Poor bonding of a new pavement surface layer is the direct result of inadequate tack coat practices, resulting in slippage and shoving of the pavement, as seen in Figure 7-1 (a). This type of failure is most frequently observed in locations such as intersections where braking or acceleration is common. Other distresses, most notably pavement fatigue cracking, as shown in Figure 7-1 (b), also can be related to a poor tack coat bond.



(a)

(b)

Figure 7-1. Distress due to improper bonding: (a) debonding and (b) fatigue cracking (FHWA 2016).

Numerous interlayer installation techniques can be employed to improve a pavement’s service life. The common interlayer systems used for this purpose are chip seals, slurry seals, and geosynthetic interlayers. Typical chip seal installations do not require a tack coat; however, certain chip seal applications require a flush coat (fog seal and sand cover) on the pavement surface. Similarly, slurry seal or micro-surfacing applications do not require a tack coat unless the pavement surface is extremely dry and raveled or is made of concrete. In the case of geosynthetic pavement interlayers, the asphalt binder must be applied in accordance with the manufacturer's recommended installation procedures. Asphalt binder is preferred over emulsion due to the time required to cure the emulsion; such delay potentially can lead to debonding between the interlayer and asphaltic layers.

7.2 Tack Coat Terminology

Consistent language must be used when discussing tack coat materials. The FHWA (2016) recommends the following definitions regarding the use of emulsions in tack coats.

Anionic: Emulsified asphalt particles can be anionic (negatively charged) and, in theory, should be used with aggregate that carries a positive charge. The absence of the letter ‘C’ in an emulsion type designation denotes anionic emulsified asphalt particles.

Cationic: Emulsified asphalt particles can be cationic (positively charged) and, in theory, should be used with aggregate that carries a negative charge. The type of emulsifying agent that is used in the asphaltic emulsion determines whether the emulsion is cationic or anionic. The principal difference between the two types is that cationic emulsions in general cures faster than anionic emulsions. The letter ‘C’ in the emulsion type designation denotes cationic emulsified asphalt particles.

Undiluted emulsion: An undiluted emulsion consists primarily of a paving grade asphalt binder, water, and an emulsifying agent.

Diluted emulsion: A diluted emulsion has additional water added to it. The most common dilution rate is 1:1 (one part undiluted emulsion to one part additional water).

Residual asphalt: The asphalt that remains after an emulsion has set is the residual asphalt and typically is 57% to 70% of the undiluted emulsion.

Tack coat break: The moment that the water separates from the asphalt and the tack coat changes from brown to black is considered the breaking point of the tack coat.

Tack coat set: When all the water has evaporated, leaving only the residual asphalt, the tack coat has set or is ‘completely broken’.

Not only is consistent terminology important for tack coat applications, but clear directions are needed to ensure that the proper tack coat rate is applied. For example, a specification may read, “Apply the tack coat at a rate of 0.05 gallons per square yard (gsy).” This statement does not provide enough information to make a correct estimation of the tack coat rate because it could be interpreted to mean 0.05 gsy residual asphalt, 0.05 gsy undiluted emulsion, or 0.05 gsy diluted emulsion. Actual residual asphalt values will vary widely according to the interpretation. If the specifier intended 0.05 gsy of residual asphalt, but 0.05 gsy of undiluted emulsion with 60% residual asphalt were applied, then the roadway would have only 0.03 gsy of residual asphalt, which is 40% less than intended. If 0.05 gsy of emulsion diluted 1:1 with water were applied, then the roadway would have 0.015 gsy of residual asphalt, which is 70% less than intended. Henceforth, it is recommended that all application specifications be in terms of residual asphalt.

7.3 Tack Coat Materials

Liquid asphalt binders can be used as tack coat materials and are classified primarily into three types depending on the method used to liquefy the asphalt binder: emulsified asphalt, asphalt binder, and cutback asphalt. Emulsified asphalts are liquefied by emulsifying the asphalt in water using an agent, whereas asphalt binders are liquefied by heating. Cutback asphalts are liquefied by dissolving the asphalt binder using a petroleum solvent such as naphtha, gasoline, kerosene, or diesel oil. The following sections describe each type of asphalt binder tack coat.

7.3.1 Emulsified Asphalt

Emulsified asphalt has three components: asphalt binder, water, and an emulsifying agent. The basic idea behind emulsified asphalt is that water escapes from the emulsion by absorption or evaporation, leaving only the base asphalt binder on the pavement surface. The emulsifying agent disperses the asphalt binder in water to make the binder stable enough for pumping, prolonged storage, and mixing. The emulsifying agent must also allow the emulsion to break down quickly once it comes in contact with the aggregate in a mixer or after spraying on the roadbed. Once the emulsion breaks and cures, the residual asphalt retains all of the adhesive, durability, and water-resistant properties of the base asphalt binder.

Emulsified asphalt is available in different types and grades that are produced by varying the emulsifying agent and base asphalt binder and adding modifiers, etc. The designation of an emulsified asphalt depends on the emulsion's charge, setting time, viscosity, and the presence of any modifiers.

The choice of emulsifying agent decides the emulsion's charge, i.e., anionic (asphalt globules are electro-negatively charged) or cationic (asphalt globules are electro-positively charged) or nonionic (asphalt globules are neutrally charged). The charged asphalt globules within the emulsion keep the globules apart until they come in contact with the opposite charged aggregate surface and become neutralized. The coalescence (joining together) of the asphalt globules separates the asphalt binder and water, which eventually leads to the evaporation of the water, thereby leaving the asphalt binder alone on the pavement surface. These phenomena are referred to as 'breaking' and 'setting'.

Emulsified asphalt is classified further based on how quickly the asphalt will coalesce, i.e., revert to asphalt binder. The relative terms, rapid-setting (RS), medium-setting (MS), and slow-setting (SS), have been adopted to simplify and standardize this classification. The tendency for the asphalt to coalesce is closely related to the mixing of the emulsion. An RS emulsion has little or no ability to mix with an aggregate, an MS emulsion is expected to mix with coarse but not fine aggregate, and an SS emulsion is designed to mix with fine aggregate. These setting terms are applicable during the production of asphalt concrete mixtures in both cold and hot mix plants but can be misleading in terms of the tack coat curing time. The thin emulsion layer can help any type

of emulsion reach terminal mass loss (residual asphalt mass) during the curing process with 10% difference at a given cure time. Therefore, the curing time difference is insignificant irrespective of the setting designation.

High-float emulsions used with cold and hot plant mixes have a specific quality that permits a thicker film coating around the aggregate particles without danger of runoff. A quick-set (QS) type of emulsion has been developed for slurry seals. Its use is rapidly increasing as its unique quick-setting property solves one of the major problems associated with the use of slurry seals. Other additives, such as polymers, sometimes are added to emulsions. Polymers are either preblended with the asphalt binder before emulsification or added as latex. Whenever the term ‘emulsion’ is used in these guidelines, it refers to asphaltic emulsion/emulsified asphalt. Table 7-1 shows the abbreviations that refer to the specific quality of the emulsion designation.

Table 7-1. Abbreviations Used for Typical Emulsion Designations

Modification (1)		Particle Charge (2)		Setting Time (3)		Viscosity (4)	
LM	Latex-modified	C	Cationic	SS	Slow-setting	1	Low viscosity
HF	High-float	-	Anionic	RS	Rapid-setting	2	High viscosity
PM	Polymer-modified	-	Nonionic	QS	Quick-setting	h	Hard grade asphalt

Table 7-2. Nomenclature of Approved Emulsions at NCDOT with Their Corresponding Split-Up Abbreviations (see Table 7-1)

(1)	(2)	(3)	(4)	Nomenclature
		RS	1h	RS-1h
	C	RS	1h	CRS-1h
	C	RS	1	CRS-1
HF		MS	1	HFMS-1
	C	RS	2	CRS-2

7.3.2 Asphalt Cement (Binder)

Asphalt binders constitute the class of black or dark-colored (solid, semisolid, or viscous) cementitious substances, natural or manufactured, which are composed principally of high molecular weight hydrocarbons and of which asphalts, tars, pitches, and asphaltites are typical. The asphalt is liquefied by heating the binder with indirect heat in a storage tank. Asphalt binder, unlike emulsified asphalt, carries no charge and thus is nonionic.

Asphalt binders are sometimes considered as tack coat materials for night work or in cooler weather or when a geosynthetic pavement interlayer is placed. The main advantage of using straight asphalt binder is that no time is required for the material to break, and thus, the hot mix can be placed immediately after spraying. The main disadvantage of using straight binder is that it must be

maintained at higher temperatures than emulsions or cutbacks in order to remain fluid enough to be sprayed through a distributor nozzle. Furthermore, spraying high-temperature asphalt binder in close proximity to workers is a safety concern. Also, the process to heat the binder consumes considerable energy. When the ambient temperature is above 85°F (30°C), asphalt binder will adhere easily to equipment tires, so tracking may be another problem. Note, too, that asphalt binder, when used with tack coat emulsions, would be considered 100% residual asphalt because no added water would be needed for separation and evaporation. Asphalt binder should not be used when the pavement surface is damp or dusty or on a planed surface because the binder will bead and not penetrate the existing surface, thereby preventing a good bond.

Asphalt binders typically are classified based on their performance grade (PG). Generally, using the same grade of asphalt binder that is used in the hot mix asphalt for the tack coat is preferred. Binder PG specifications are based on tests that measure the physical properties of the asphalt binder that relate directly to field performance in accordance with engineering principles. These tests are conducted at temperatures encountered by in-service pavements. Binder specifications adopted by AASHTO are referenced under AASHTO M 320 (AASHTO 2017b).

Performance-graded binders are designated with grades such as PG 64-22. The first number, 64 in this example, is often referred to as the high-temperature grade, which means that the binder would have adequate physical properties to perform satisfactorily at least up to 147°F (64°C) in this case. This temperature would be the pavement's high temperature that corresponds to the climate in which the binder is actually expected to serve satisfactorily. The second number, -22 in this example, is often referred to as the low-temperature grade and implies that the binder would have adequate physical properties to perform satisfactorily to at least -8°F (-22°C) in this case.

An additional consideration in selecting the binder grade to be used is the time of loading (vehicle speed on an open highway, city streets, intersections, etc.), the magnitude of the load (heavy trucks, e.g.), and the level of the material that is within the pavement structure. The binder grade used in standard asphalt mix pavements in North Carolina is PG 64-22. Other grades are required under certain conditions, such as heavy traffic and for recycled mixes.

7.3.3 Cutback Asphalt

Cutback asphalts are not used by the NCDOT because of environmental concerns and therefore are not discussed further in this Manual.

7.4 Selection of Tack Coat Materials

7.4.1 Approved Tack Coat Grades

All tack coat materials shall meet NCDOT Standard Specifications requirements and will be either asphalt binder PG 58-28 or PG 64-22 or asphalt emulsion grade RS-1H, CRS-1H, CRS-1, HFMS-

1, or CRS-2 unless otherwise approved by the asphalt mix design engineer. Section 7.4.2 describes the recommended test method that approved tack coats should undergo. Hard-base emulsions ('h' grades) are recommended to reduce tracking during all seasons; however, data suggest that these emulsions will still tack in summer months or during periods of high pavement temperatures.

Asphalt emulsions shall not be diluted with water. Different grades must not be intermixed in a tanker or distributor because the material could break in the tank and become almost impossible to spray.

Non-tracking asphalt tack coats may be used at the Contractor's discretion based on a new special provision. The Contractor can select from various non-tracking tack coat products on an approved list maintained by the NCDOT's Materials & Tests (M&T) Unit. Refer to:

<https://connect.ncdot.gov/resources/Materials/MaterialsResources/Approved%20Non-Tracking%20Tack%20Coat%20Products%20for%20NC.pdf>

Unless otherwise specified in the Project Special Provisions, the Contractor may select the grade of the tack coat material for the application. Any approved grades may be used, provided a certified delivery ticket accompanies the material in accordance with [Section 1020](#) of the Standard Specifications. The Contractor will advise the Roadway Technician about the actual brand and grade that is being used for the project. The quality assurance (QA) technician will indicate same on the Asphalt Roadway Technician's Daily Report ([M&T Form 605](#)). If there is any concern or question about the quality of the material, samples should be taken and placed in approved containers and submitted to the M&T Unit for testing.

7.4.2 Acceptance of Tack Coat Materials

Performance-graded asphalt binder (PGAB) should be acquired only from sources that are participating in the NCDOT's quality control/quality assurance (QC/QA) program. The PGAB QC/QA program is designed to give Producers or Suppliers more responsibility for controlling the quality of the material they produce and for the NCDOT to utilize the QC information that the Producers or Suppliers provide in the NCDOT's acceptance process. The PGAB QC/QA program requires Producers or Suppliers to perform QC sampling, testing, and record-keeping for the materials they ship for use by the NCDOT. Also, the program requires the NCDOT to perform QA sampling, testing, and record-keeping to confirm the performance of the Producer's QC plan outlined in the QC/QA program.

Asphalt materials used in asphalt pavement construction shall be tested and certified as meeting all applicable specification requirements, as follows.

- Asphalt binder: AASHTO M 320 (AASHTO 2017b) (performance-graded binders) or M 332 (AASHTO 2020e) (multiple stress creep recovery testing)

- Asphalt emulsion: AASHTO M 140 (AASHTO 2020f) (anionic emulsions), AASHTO M 208 (AASHTO 2018a) (cationic emulsions), and AASHTO M 316 (AASHTO 2018b) (polymer-modified cationic emulsions)
- Asphalt cutback: AASHTO M 81 (AASHTO 2004) (rapid-curing), AASHTO M 82 (AASHTO 2017c) (medium-curing), and AASHTO M 316 (AASHTO 2018b) (polymer-modified cationic emulsions)

Note that reduced-tracking/non-tracking materials do not currently have an AASHTO specification.

Certification for acceptance purposes is furnished with each delivered load of material, subject to certain conditions outlined in the specifications. All asphalt transport tankers, rail tankers, and truck tankers must have a sampling valve in accordance with Asphalt Institute Publication MS-18, *Sampling Asphalt Products for Specification Compliance* (Asphalt Institute 1968), and ASTM D140 (ASTM 2016b), or a comparable device that is acceptable to the Engineer. The sampling procedure is described in Section 7.5.3.

[Article 1020](#)-1 outlines the information that is to be shown on load delivery tickets for all asphalt materials. An example statement of certification also must be included on the delivery ticket. The Contractor must furnish a ticket from the supplier that includes a statement of certification of the grade and amount of the asphalt material as well as a statement that is relative to the brand, grade, and quantity or rate of the anti-stripping additive that has been added to the material. In addition, a separate statement of certification from the transporter that the tanker is clean and free of contaminating material is required on the ticket. Each certification shall be signed by an authorized representative of the supplier or transporter. These certifications may be either stamped, written, or printed on the delivery ticket, or may be attached to the delivery ticket. Failure to include or sign the certifications by either the supplier or transporter will be cause to withhold the use of the material until a sample can be taken and tested, except where an alternative testing and invoicing procedure has been pre-approved by the Engineer.

Materials Received Reports (MRRs) are not required to be completed for asphalt binders or emulsions. All asphalt materials will be accepted by certification in accordance with [Article 1020](#)-1 of the Standard Specifications and the following procedures. When a shipment of asphalt binder is received at the asphalt plant, a copy of the bill of lading, attached to the appropriate QC-1 report from that plant, will be furnished to the Pavement Specialist and maintained in the appropriate plant file with the M&T Unit. [Appendix D](#) provides the detailed procedures for maintaining bills of lading for prime and tack coat materials.

M&T Unit representatives will take verification samples from the asphalt terminals, log in and test the samples at the M&T Unit's central facility, and then enter the results into the Asphalt Materials database. If a sample fails, but the failure is considered by the Engineer to be inconsequential, then

terminal personnel will be notified of the test results and allowed to continue shipping, provided the terminal personnel takes corrective action. Samples will continue to be taken at a normal frequency. If a sample fails, and the failure is considered by the Engineer to be consequential, then the terminal personnel will be notified of the results and instructed to discontinue shipments and take corrective action. M&T Unit personnel will resample and retest the material at the terminal. Any materials from this batch in a Contractor's storage tank will be evaluated for acceptability.

In the case of significant material failure, the Engineer will send a failure notification form to all Pavement Specialists. The Pavement Specialists will review the bills of lading in their files to determine if they have received any material from that batch. If so, they will notify the appropriate Resident Engineer(s). They then will review the appropriate QC records for any possible related test deviations. The failure notification form will include an investigation section to be filled out by the Pavement Specialist. This form should include the information regarding test deviations and any actions taken that concern or involve the Resident Engineer(s) and attach the form to the appropriate bill of lading and QC-1 report in the file and send a copy to the Engineer.

Resident Engineers will not receive direct notification of failures from the Engineer because the Engineer is unable to determine who should receive the notifications. By sending these notifications to the Pavement Specialists, a relatively small number of forms can be sent out, and the Pavement Specialists can notify the appropriate Resident Engineers of failures. All actions taken by the Pavement Specialists and Resident Engineers will be noted in the binder database summary by Materials and Tests Asphalt Laboratory personnel.

7.5 Storage and Handling of Emulsions

For general emulsion storage, handling, and sampling guidelines, the Asphalt Institute's MS-19 Basic Emulsion Manual (Asphalt Institute 2008) provides thorough information that has been established through a long history of successful use. The following sections provide an overview of these general emulsion storage, handling, and sampling guidelines drawn from MS-19, except where otherwise noted. Note that specially formulated emulsions may have procedures that differ from the following general procedures.

7.5.1 Storage of Asphalt Emulsions

Storage tanks should be insulated for protection from freezing and for efficient use of heat. A skin of asphalt can form on the surface of emulsions when they are exposed to air. Because tall, vertical tanks expose the least amount of surface area to the air, they are generally thought to be preferable to horizontal tanks. However, horizontal tanks can be kept full to minimize the area exposed to air.

Propellers are turned slowly (approximately 60 rpm) to gently circulate the material. Agitating the emulsion at higher rates may increase the chance that the emulsion will lose its homogenous consistency and separate in the tank. When storing emulsified asphalts:

- Do** store emulsified asphalt the same way as for fluid water, between 50°F (10°C) and 185°F (85°C), depending on the intended use and specific product.
- Do** store at the temperature specified for the particular asphalt emulsion grade and application. Table 7-3 shows the normal storage temperature ranges.
- Do not** permit the asphalt emulsion to be heated above 185°F (85°C). Elevated temperatures will cause the water to evaporate, changing the characteristics of the asphalt emulsion.
- Do not** let the emulsion freeze. Freezing breaks the emulsion and separates the asphalt from the water. The result will be two layers in the tank, neither of which will be suited for the intended use, and the tank will be difficult to empty.
- Do not** allow the temperature of the heating surface to exceed 212°F (100°C) because doing so will cause a premature breakdown of the emulsion on the heating surface.
- Do not** use forced air to agitate the emulsion because it may cause the emulsion to break.

Table 7-3. Storage Temperatures for Asphalt Emulsions (Gierhart and Johnson 2018)

Asphalt Emulsion Grades	Temperature Range	
	Minimum	Maximum
QS-1h, CQS-1h	50°F (10°C)	125°F (50°C)
RS-2, CRS-1, CRS-1h, CRS-2 , HFRS-2, CMS-2, CMS-2h, MS-2, MS-2h, HFMS-2, HFMS-2h, HFMS-1, RS-1h	125°F (50°C)	185°F (85°C)
RS-1, SS-1, SS-1h, CSS-1, CSS-1h, MS-1	50°F (10°C)	140°F (60°C)

7.5.2 Handling of Asphalt Emulsions

Asphalt emulsion handling guidelines tend to be centered around safe handling, protection of equipment, and maintaining the quality characteristics of the emulsion. For worker safety, neither the asphalt emulsion nor the air above it should ever be subjected to an open flame, heat, or strong oxidant. Adequate ventilation within the emulsion handling area is required to avoid overexposure to fumes, vapors, and mists. Copies of the safety information for the specified emulsion(s) should be reviewed and kept readily available. Properly sized pumps should be used when handling asphalt emulsions. Tightly fitted pumps with inadequate clearance can bind and seize. Lines should be cleared and drain plugs opened when the pump is not in service. All temperature, agitation, storage, and handling guidelines must be followed to keep the emulsion from forming two distinct layers in the tank. Tanks with separated emulsion material (asphalt on the bottom with water floating on top) are difficult to clean and restore to their intended function.

In addition to these storage guidelines, several other recommendations are given to preserve the quality characteristics of the emulsion. For example, when filling tanks, different classes, types,

and grades of emulsified asphalt should not be mixed together because of the risk of separation. Even emulsions within the same grade designation can differ chemically and in terms of performance. The emulsion supplier always should be consulted for compatibility information before mixing different emulsions with the same grade. Also, repeated pumping and recirculating should be avoided as the material's viscosity may drop and the air may become entrained, causing the emulsion to become unstable. Pumping from the bottom of the tank will minimize contamination from any skin formation that is present in the tank.

7.5.3 Sampling of Asphalt Emulsions

The purpose of any sampling method is to maintain the representative nature of the sample relative to the larger quantity. AASHTO R 66 (AASHTO 2020g) and ASTM D140 (ASTM 2016b) detail standard practices for sampling asphalt materials. This section describes some of these specifications' requirements regarding the sampling of asphalt emulsions.

The sample is taken from the sampling device on the transport tanker. The type of container used to collect the sample is important in order to maintain the stability of the emulsion. Sample containers must be new and are available from the M&T Laboratory. Glass containers should not be used. Containers for emulsified asphalt samples need to be plastic wide-mouth jars or bottles with screw caps. The top of the container must fit securely. The sample container should not be washed, rinsed out, or wiped off with oily cloths. When obtaining a sample from the sampling valve, approximately 1 gallon (4 liters) of the asphalt material should be drawn and discarded. Figure 7-2 (a) shows a schematic illustration of a typical sampling device and Figure 7-2 (b) shows sampling binder from a tanker.

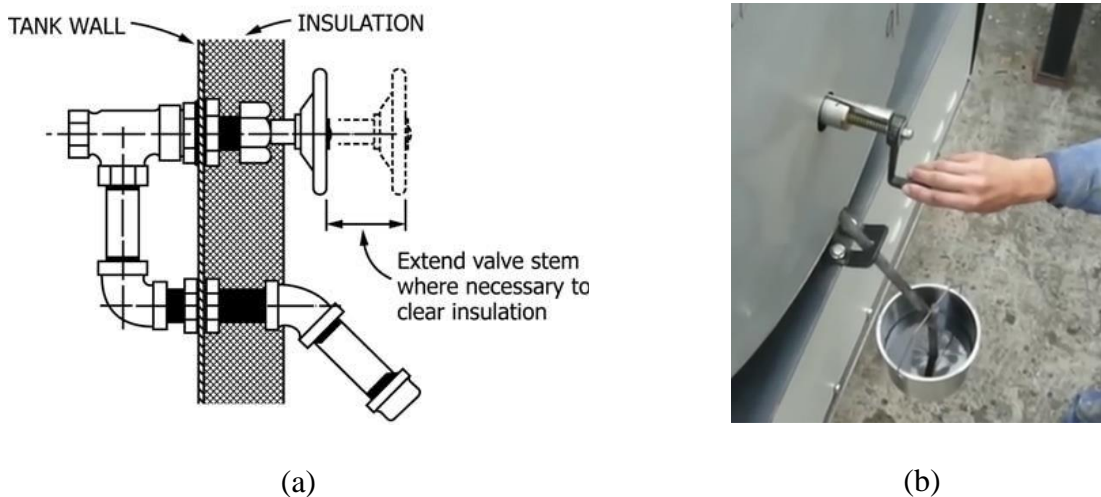


Figure 7-2. Asphalt binder sampling: (a) typical submerged sampling device and (b) sampling asphalt binder from a tanker.

Worker safety is an important consideration when obtaining samples. Gloves should be worn, and long sleeves rolled down and fastened over the wrist while sampling and sealing containers. A face shield also should be worn while sampling. Smoking is prohibited while sampling bituminous materials. Prolonged exposure to fumes, vapors, and mists should be avoided.

A sample should not be transferred from one sample container to another. The filled sample container should be sealed tightly immediately after the sample is taken. The container should not be submerged in a solvent in an attempt to clean the outside of the container, nor should it be wiped with a solvent-saturated cloth. Any residual material on the outside of the container should be wiped with a clean, dry cloth immediately after the container is sealed. During sealing and wiping, the container should be placed on a firm level surface to prevent splashing, dropping, or spilling the sample.

Immediately after filling, sealing, and cleaning the sample containers, each container should be marked for identification with a permanent marker on the container itself, not the lid. All samples should be packaged and shipped or delivered to the laboratory the same day they were taken. The sample containers should not be placed on the dashboard or in direct sunlight in a truck. They also should be secured to keep them from rolling in the transport vehicle. The samples should be tested no more than two weeks from the date of sampling. Specialty emulsions may need to be tested sooner.

7.6 Tack Coat Construction Practices

Tack coat construction practices can be classified into two stages: (1) surface preparation and cleaning and (2) tack coat application. The following sections describe the recommended practices in detail.

7.6.1 Surface Preparation and Cleaning

Surface preparation is vital to provide the best opportunity to achieve good bond strength. The goal of surface preparation is to produce a clean, dry surface. For existing pavements, milling is preferred for its many benefits. First, milling removes the uppermost materials that typically are the most compromised by traffic wear and weathering. Second, milling helps to smooth out any irregularities that may have developed within the pavement. Third, milling improves the bonding of the overlay to the existing pavement. The negative aspects of milling are its cost and the additional cleaning that typically is necessary, as milling can produce excess fine material that may be difficult to eliminate by sweeping or other forms of removal. Milling may also increase the amount of tack coat needed because milling increases the surface area (roughness) of the existing pavement. However, this additional surface area along with an increase in aggregate interlock promotes good bonding characteristics.

Tack coats should be applied only when the surface is dry and when the air temperature is 35°F (2°C) or above, as measured at the location of the paving operation and away from artificial heat. The importance of the cleanliness of the existing asphalt or concrete surface cannot be overly stressed. Any dust, dirt, clay, fuel oil, grass, or other foreign matter on the surface will prevent the tack coat from adhering to the surface, thus causing the overlay not to be bonded properly to the underlying layer and having to be removed. Debris can cause the overlay to slip or ‘shove’ under rolling or traffic. Thorough cleanliness can be achieved only with power brooms and/or by flushing with water and scrubbing. The technician must ensure that all areas are properly cleaned and tacked before the pavement layer is placed. Also, the contractor must remove grass, dirt, and other material from the edge of the existing pavement before the tack coat is placed in order to ensure the bonding of the asphalt overlay. However, the contractor should be cautioned against removing excessive amounts of grass and earth material from the pavement edge such that the material is thrown into roadway ditches or creates hazardous traffic conditions. The contractor also should take necessary precautions to limit tracking and/or the accumulation of tack coat material on either existing or newly constructed pavements. Excessive accumulation of tack may require corrective measures.

On new or reconstructed pavements, or where multiple lifts are a requirement of the construction, surface preparation between lifts is generally minimal. Sweeping may be the only preparation needed. However, if the fresh pavement becomes dirty, the contractor should clean all such locations before the next lift is tacked and paved. Figure 7-3 shows a rotary broom sweeping away milling debris and loading the truck with the debris.



Figure 7-3. Rotary broom eliminating milling debris and loading the truck (courtesy: <https://www.forconstructionpros.com/pavement-maintenance/sweepers/article/11237578/how-to-reduce-costly-delays-in-mill-and-fill-asphalt-road-repair>).

7.6.2 Tack Coat Application

Once the pavement surface has been prepared, the tack coat can be applied. Tack coat applications should be uniform and consistent both transversely and longitudinally, as shown in Figure 7-4. No more tack coat material may be applied than can be covered with base, intermediate, or surface course material during the next day's operation, except where public traffic is being maintained. Where public traffic is being maintained, no more tack coat may be applied than can be covered during the same day's operation. However, the Resident Engineer may limit the application of the tack coat in advance of any paving operation depending on traffic conditions, project location, proximity to business or residential areas, or other reasons. In the event that the tack coat material is not covered during the same day's operation, the Resident Engineer may require the application of suitable granular material or other means to provide safe traffic conditions at no additional cost to the Department. The tack coat must be applied only in the presence of and as directed by the Engineer. No base, intermediate, or surface mixture may be placed until the tack coat has been placed and sufficiently cured. The tack coat shall be applied uniformly by the spray bar on a pressure distributor in the presence of and as directed by the Resident Engineer or his/her

technician. In places where the distributor spray bar cannot reach, the tack coat must be applied using a hand spray attached to the distributor by a hose. When hand spray methods are used, care must be taken to give the surface an adequate and uniform application of the tack coat. All pavement contact surfaces of headers, curbs, gutters, manholes, core sample holes, vertical faces of old pavement, and all exposed transverse and longitudinal edges of each course must be painted or sprayed with tack before any mixture is placed adjacent to such surfaces. Note that each layer of asphalt is required to be tacked. In order to prevent pavement layer slippage, the Engineer shall not waive a tack coat between two layers placed on the same day.



Figure 7-4. Uniform tack application (FHWA 2016).

After the tack coat has been applied, it shall be protected from all traffic until it has cured sufficiently. The tack coat can be considered sufficiently cured when it is tacky to the touch. If emulsified asphalt is used, adequate time should be allowed for the water to evaporate, leaving only the asphalt binder residue. Normally, emulsified asphalt is brownish in color when first sprayed but becomes black and tacky once the water has evaporated. If a PG binder is used for the tack, the plant mix can be placed on the tack coat almost immediately. After the tack coat has cured, it should still be protected as much as possible from traffic. In the event that precipitation falls on the freshly placed tack coat, the Contractor shall place, at the direction of the Resident Engineer or his/her technician, whatever signs, lights, and/or pilot cars that are necessary to protect the traveling public from the slippery tack coat and shall maintain this protection as long as hazardous conditions prevail.



Figure 7-5. Tack coat 'break' (FHWA 2016).

In summary, a proper tack coat application involves the following elements.

- Proper application rate, matched to the pavement surface type and condition
- Proper temperature of the tack coat during application
- Proper application equipment, typically a distributor (except for small areas of handwork)
 - Proper distributor speed
 - Proper distributor bar height
 - Proper distributor bar pressure
 - Proper nozzle type
 - Proper nozzle angle
 - Proper nozzle configuration
- Proper timing to avoid tacking being too far ahead of paving

7.6.3 Tack Coat Application Rates

Table 7-4 presents the target application rates for different pavement surface types; all application specifications are recommended to be in terms of residual asphalt.

Table 7-4. Application Rates for Tack Coats (NCDOT 2018a)

Surface Type	Residual Application Rate gal/yd ² (Var) [L/m ²]	Undiluted Application Rate gal/yd ² (Var) [L/m ²]
New Asphalt	<i>0.024</i> (±0.01) [0.11]	0.04 (±0.01) [0.18]
Oxidized Asphalt or Milled	<i>0.036</i> (±0.01) [0.16]	0.06 (±0.01) [0.27]
Concrete	<i>0.048</i> (±0.01) [0.22]	0.08±0.01) [0.36]

Note: Values in italics represent an example emulsion with 60% residual asphalt binder for comparative purposes only. Plus or minus 0.01 in the rate accounts for any equipment variability only.

The uniformity of the tack coat application and the proper application rate are the keys to successful tack coat performance. A tack coat between new layers of asphalt concrete requires a uniform undiluted target rate of 0.04 gal/yd² (0.18 L/m²) whereas a tack coat on all resurfacing projects requires a minimum of the undiluted target rate of 0.06 gal/yd² (0.27 L/m²) to account for an oxidized asphalt surface. In addition, milled asphalt surfaces need to be properly cleaned and prepared before placing a tack coat at the uniform undiluted target rate of 0.06 gal/yd² (0.27 L/m²).

The proper amount of tack coat for any surface is a matter of judgment that is based on the knowledge that too much asphalt could flush into the mix and cause loss of stability or could sometimes cause the overlay to slip, and that too little tack will not properly bond the surfaces. Regardless of the application rate selected, if the tack coat is not applied uniformly over the surface, then the tack coat will not perform satisfactorily due to the disparity in curing time.

The FHWA/Asphalt Institute Tack Coat Workshop recommended that emulsions used for tack coats should not be diluted. If emulsions are diluted due to indirect circumstances, such as dampness after cleaning or precipitation, then additional curing time should be provided for the breaking and curing of the emulsion.

7.6.4 Tack Coat Temperature during Application

Emulsion and asphalt binder tack are considered equivalent terms from a service viewpoint when applied at the proper rates. The primary advantage of emulsion is that it can be applied at a significantly lower temperature than asphalt binder tack and typically can be applied more uniformly. The lower temperature makes emulsion easier to store and handle and much safer to use than asphalt binder tack. However, regardless of the rate and grade of the tack material used, the material should be heated to the proper temperature so that it is fluid enough to be sprayed instead of coming out in streams from the nozzles. The temperature of the tack coat material at the time of application should be within the ranges shown in Table 7-5.

Table 7-5. Distributor Tank Application Temperature Ranges for Tack Coats

Asphalt Material	Temperature Range
Asphalt Binder, PG 58-28 or PG 64-22	350°F - 400°F (175°C - 205°C)
RS-1h, CRS-1, CRS-1h, HFMS-1, CRS-2	130°F - 160°F (60°C - 72°C)

7.6.5 Tack Coat Distributor

The asphalt distributor, illustrated in Figure 7-6, is one of the most important pieces of equipment on a paving project for prime coat, tack coat, or surface treatment operations. The distributor is designed specifically to apply liquid asphalt material uniformly and in proper quantities onto a roadway surface. The asphalt distributor includes a truck- or trailer-mounted insulated tank that contains a heating system that normally is oil-fired to maintain the asphalt at the proper application temperature. An accurate thermometer must be mounted on the distributor in such a manner that the dial or indicator remains in full view at all times. The distributor shall include a spray bar system that is capable of uniformly applying the material and a hand-held spray attachment for applying asphalt to areas that are inaccessible to the spray bar. The distributor has a power-driven pump that is capable of handling asphalt products ranging from light, cold application liquid to heavy asphalt binders, heated to spraying viscosity. On some distributors, the pressure is regulated by a variable speed pump and on others by a constant speed pump and use of a pressure relief valve.

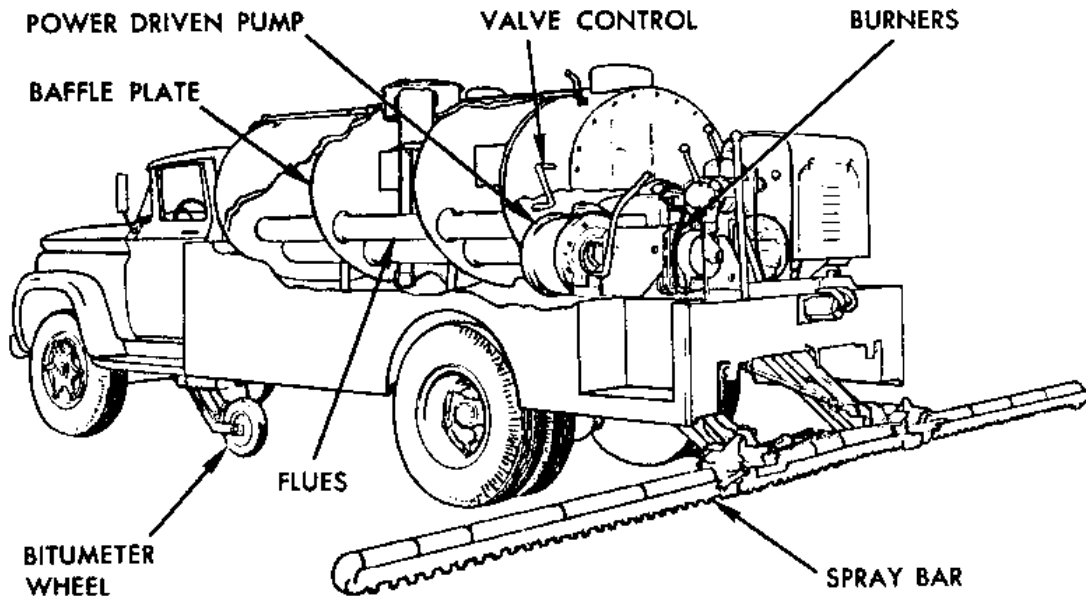


Figure 7-6. Asphalt distributor (NCDOT 2018a).

Although modern distributor trucks have excellent capabilities and typically are computerized to help minimize errors, several reasons that a distributor might produce a tack coat with a non-uniform appearance remain possible. These reasons include a clogged nozzle, incorrect nozzle size, incorrect nozzle orientation (spray direction), insufficient pressure in the spray bar, incorrect spray bar height, improper use of a hand-held spray wand, and improper distributor calibration. These factors are described in the following paragraphs.

Clogged nozzles. When emulsions are sprayed at temperatures higher than ambient, the asphalt binder residue often clogs the distributor nozzles as the binder cools after the distributor work is completed. If the nozzles are not properly cleaned and flushed, some individual nozzles can become clogged, resulting in streaks without any tack on the pavement surface, as shown in Figure 7-7.



Figure 7-7. Examples of streaks: “Zebra Tack” or “Corn Rows.”

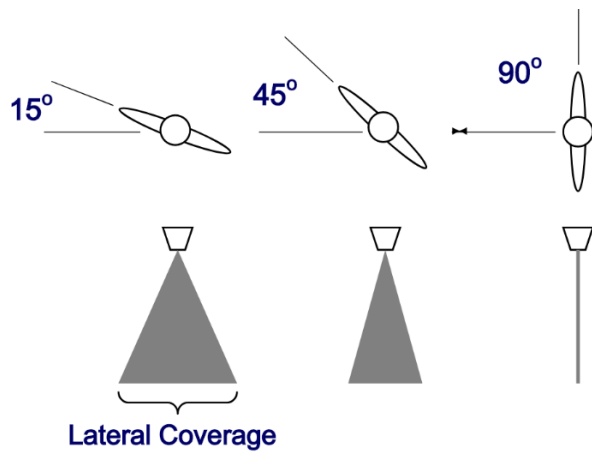
Incorrect nozzle size. Distributors are used to spray liquids of varying viscosities. Thicker liquids, such as emulsions typically used for chips seals, require nozzles with larger openings. Thinner liquids, such as emulsions typically used for tack coats, require nozzles with smaller openings. Also, various distributor manufacturers offer many different opening configurations. Figure 7-8 shows different sizes of openings, all in the ‘coin slot’ configuration. Using a distributor with incorrectly sized nozzles for the given tack coat can result in a non-uniform appearance. In practice, the distributor manufacturer can recommend the nozzle sizes and configurations that best

fit the type of liquid to be sprayed. The cleanliness and uniformity of the nozzles should be verified before use.



Figure 7-8. Examples of different nozzle sizes for different application rates (FHWA 2016).

Incorrect nozzle orientation. Figure 7-9 (a) illustrates the lateral emulsion fan coverage for three nozzle orientations (degrees) and Figure 7-9 (b) shows different directions of the emulsion's fan during field spraying for different nozzle orientations. If the nozzles are oriented perfectly parallel to the spray bar, then the fans of emulsion spray from the different nozzles will intersect and cause splashing, which will result in a non-uniform surface. If the nozzles are angled closer to perpendicular to the spray bar, then the fans of emulsion spray will not overlap at all, but instead will leave uncoated streaks on the pavement. The proper nozzle orientation is 15° to 30° from the spray bar (Asphalt Institute 2008). This orientation will keep the sprayed fans of emulsion from interfering with each other yet will provide sufficient overlap to prevent streaking. Figure 7-10 (a) through (d) show the recommended angle of the emulsion spray from the spray bar from different viewpoints.

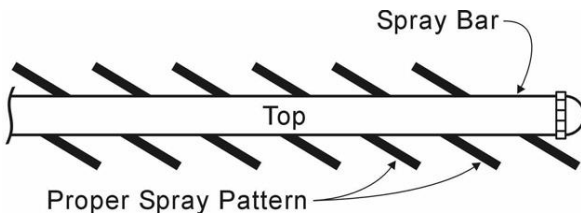


(a)

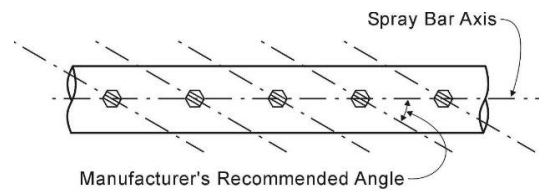


(b)

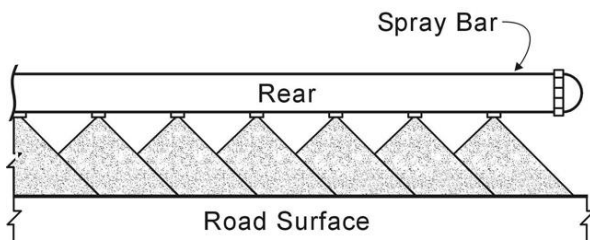
Figure 7-9. Nozzle orientation: (a) fan coverage for different nozzle orientations and (b) field spraying with different nozzle orientations.



(a)



(b)



(c)



(d)

Figure 7-10. Recommended angle of emulsion spray from spray bar: (a) top view of distributor spray bar, (b) nozzles on spray bar set at manufacturer's recommended angle (ground view to spray bar), (c) view of distributor bar from rear of distributor, and (d) typical uniform asphalt distribution (courtesy:

https://roadresource.org/treatment_resources/tack_coat?page=about_process).

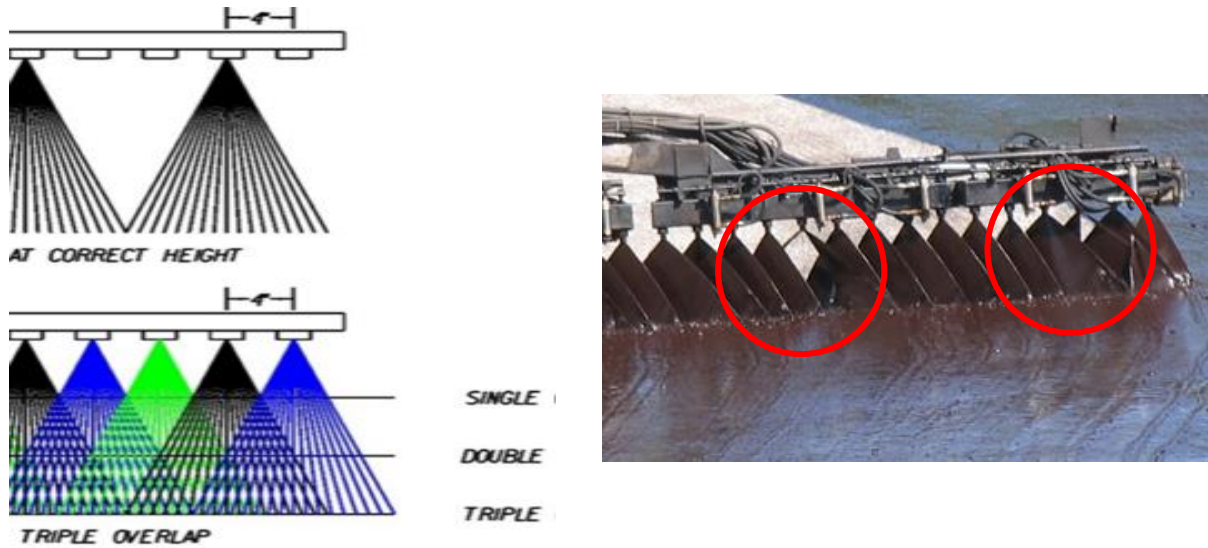
Insufficient pressure in spray bar. The spray bar pressure works in tandem with the properly sized and oriented nozzles to provide a triangular-shaped fan of sprayed tack coat emulsion. If the distributor does not maintain proper pressure in the spray bar, then the emulsion will dribble out of the nozzles, resulting in streaks in a zebra-stripe pattern similar to that shown in Figure 7-11. Although the methods used to maintain pressure may vary, many distributors use gear-type pumps to deliver the asphalt to the spray bar. The correct pressure is that which neither atomizes the asphalt nor distorts the fan of the spray. Low pressure results in streaking from the non-uniform discharge of material from the individual nozzles whereas excessively high pressure will atomize the asphalt and distort the fan of the spray. The manufacturer normally supplies charts and data that give the proper pump speed or pressure required for determining the discharge in gallons per minute for each nozzle size.



Figure 7-11. Non-uniform tack coat: streaks (Mohammad et al. 2012).

Incorrect spray bar height. A spray bar that is too low to the ground may not allow sufficient overlap between the fan-shaped spray patterns, resulting in a streaked appearance. The spray bar height could be raised to a position that would result in single coverage, which would theoretically result in a fully covered surface. However, if problems arise with even one individual nozzle, a bare streak would result. Therefore, single coverage is not recommended. Figure 7-12 (a), taken from the Asphalt Institute's MS-22 Construction Manual (Asphalt Institute 2020), shows the recommended spray bar heights that allow double or triple coverage. The best result is obtained using 4-inch (101.6-mm) nozzle spacing with an exact triple lap of the fans, whereas 6-inch (152.4-mm) nozzle spacing and a spray bar that is set too high allow the emulsion to be subject to wind distortion. In such a case, a double lap pattern should be used. For best results, the height of the

spray bar should not vary more than a half inch (12.7 mm). Some distributors have mechanical controls to maintain a proper spray bar height. The maximum allowed height of the spray bar is 1 foot (304.8 mm). Figure 7-12 (b) shows the proper overlap that is required to mitigate the effect of a clogged nozzle. As the spray bar height is increased, the fan-shaped spray patterns will overlap, greatly increasing the chances of complete coverage, even if a nozzle becomes clogged.



(a)

(b)

Figure 7-12. Spray bar height: (a) fan overlap based on spray bar height (NCDOT 2015) and (b) proper overlap to mitigate effect of clogged nozzle.

Inappropriate use of spray wand on main roadways. A spray wand can be a useful tool for areas that are inaccessible for the distributor spray bar. However, it should never be used in areas where the distributor can drive freely, as shown in Figure 7-13. Even careful applications using a spray wand will inevitably create areas of tack coat that are heavier or lighter than the desired tack coat emulsion application rate.



Figure 7-13. Inappropriate use of spray wand to apply tack coat.

Distributor calibration. Distributor calibration is vital to the application of a proper tack coat. Periodically, a trial tack coat application should be placed over a test area to verify the correct nozzle operation and configuration. At a minimum, distributors should be calibrated annually.

ASTM Method A (ASTM 2014) uses calibration pads that have been weighed and attached to the roadway surface, as shown in Figure 7-14 (a) and (b). The pads should be attached both longitudinally and transversely to the driving direction. The truck with the distributor that is being calibrated drives over the pads while spraying its material. The pads are removed quickly and reweighed. The application rate is then determined by taking the difference between the post spray and pre-spray weights. Any dilution, or water in undiluted emulsion, also must be taken into account to obtain the application rate in terms of the residual material.



(a)



(b)

Figure 7-14. Calibrating distributor in accordance with ASTM D2995 (2014) (FHWA 2016) using calibration pads: (a) distributor truck spraying tack coat onto calibration pads and (b) detail of sprayed calibration pads.

ASTM Method B uses containers that are placed under each nozzle of the spray bar, as pictured in Figure 7-15. The distributor then discharges material into the containers for a set period. The volume of the material in the containers is then calculated. Transverse uniformity of the application can be verified by checking the consistency of the material in each container, and the application rate becomes a function of the truck's ground speed.



Figure 7-16. Calibrating distributor volumetrically (courtesy: http://onlinemanuals.txdot.gov/txdotmanuals/scm/asphalt_distributor.htm#i1007776).

7.6.6 Tack Coat Tracking

One perpetual problem with tack coat applications that rely on distributor trucks is that haul trucks normally drive on the applied tack coat, thus tracking the tack coat material and removing it from the pavement, as shown in Figure 7-17.



Figure 7-17. Tack coat tracking by haul vehicles in work zone (courtesy: https://roadresource.org/treatment_resources/tack_coat?page=about_process).

Substantial tracking can occur as well in areas where the construction zone must allow private vehicles from driveways and side streets, as pictured in Figure 7-18.



Figure 7-18. Tack coat tracking due to allowed traffic.

Tack coat tracking can be mitigated in several ways. In traditional construction, trucks ride on the tack coat to reach the paver and then pull forward over the tack coat as they leave. Delivery truck drivers should be trained to exit and enter active traffic in construction zones safely and be cautioned against driving on freshly applied tack coats as much as possible. If the work zone allows, material transfer vehicles (MTVs) can be used because they can drive in the adjacent lane and convey the material to a hopper on the asphalt paver. This method prevents significant truck traffic over the tack coat. Another way to mitigate tack coat tracking is to use reduced-tracking tack coat materials that typically are manufactured to harden quickly and adhere minimally to tires. When a hot lift of asphalt is subsequently placed over the tack coat, the hardened tack is reactivated by the heat and bonds the new overlay with the existing surface.

Often, the inspector or paving crew superintendent must make a judgment call regarding tracking. If too much tack has been judged to have been removed from the roadway surface, then the distributor must be called back to reapply the tack coat, either over the entire roadway surface or in tracked areas only if these areas are limited to wheel paths, for example. Another scenario related to tracking is the cleanliness of the tack. As aforementioned, no more tack coat material may be applied than can be covered with base, intermediate, or surface course material during the next day's operation, except where public traffic is being maintained. Where public traffic is being maintained, no more tack coat may be applied than can be covered during the same day's operation. This restriction limits the time the tack coat is exposed to dust and debris blown by wind or adjacent traffic. It also limits the amount of tack coat that is exposed to traffic, which can often track dirt or mud onto the tack coat, rendering it ineffective.

7.7 Testing and Acceptance of In-place Tack Coat

7.7.1 Assessment of Tack Coat Coverage

Section 7.6.3 specifies the tack coat application rates for different surfaces. DOT technicians should check the tack coat placement and ensure that the surface is clean, verify uniform coverage across the mat, and inform the Contractor that the tack must be allowed to break before allowing trucks on the tack coat or beginning the paving operation. The DOT technician also should periodically check that the distributor truck's equipment and devices, such as spray nozzles and nozzle angle settings, spray bar height, computerized application rate gauge in the truck, flow-meter gauge to measure gallons, etc., are in proper working order. Note that the volume gauge on the distributor, shown in Figure 7-19 as two different examples, should be used only as a convenience to the operator to know when the tank is getting close to empty, but it should never be used as a basis for payment.



Figure 7-19. Volume gauges on distributor tanks (NCDOT 2012).

The tack coat application rate gauge and temperature gauge, shown in Figure 7-20 (a) and (b), respectively, also should be checked regularly. The tack coat rate must be checked regularly by the DOT technician to determine that the specified amount of tack is being placed. The rate of application may be obtained at intervals by using the total gallons applied divided by the square yards upon which the tack coat is placed. At the end of each operation, a technician must compute the actual rate of the tack coat applied and record this rate on the Asphalt Roadway Technician's Daily Report (M&T Form 605). The rate of application should be calculated separately for each individual application or 'shot'. Also, the technician should check the temperature gauge on the outside of the truck for the proper application temperature of the tack coat.



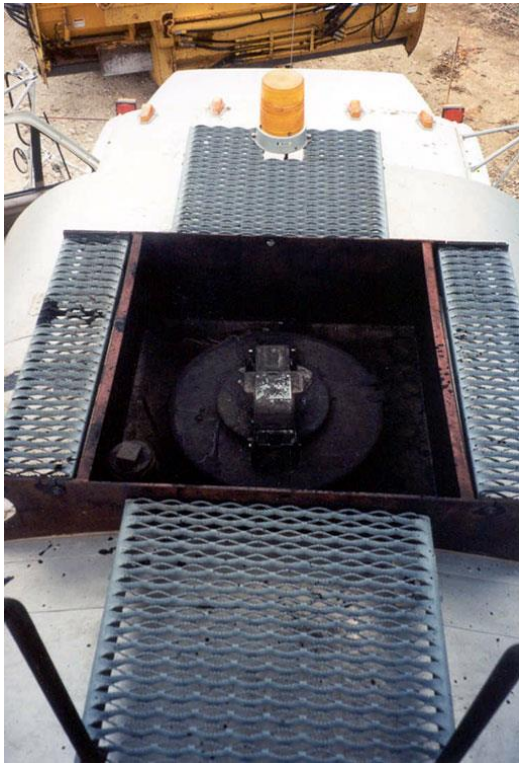
Figure 7-21. Distributor gauges: (a) application rate gauge inside distributor truck and (b) temperature gauge on distributor tank (NCDOT 2012).

The calculations needed to determine the tack coat application rates are straightforward. Most commonly, the tack coat is specified in terms of volume (gallons/square yard). However, it also can be specified in terms of mass (pounds/square yard). The following steps are taken when using the volume method.

- Step 1. Determine the distance traveled.
- Step 2. Calculate the area sprayed = distance traveled \times width sprayed and convert from sq. ft. to sq. yd. if needed.
- Step 3. Calculate the gallons of material applied = beginning volume – ending volume. The volumes may be determined by using a dipstick calibrated to the truck's tank or onboard meters.
- Step 4. Correct for temperature back to 60°F by applying the correction factor.
- Step 5. Account for any dilution. (Note that the NCDOT does not allow dilution.)
- Step 6. Calculate the residual asphalt by accounting for the water in the undiluted emulsion.
- Step 7. Calculate the residual emulsion application rate, which is the gallons of residual emulsion applied divided by the area of application.

Strapping the distributor is important for pay purposes and also for determining the average asphalt application rate for each shot, which allows for immediate information to be obtained to make adjustments from one shot to the next. The following procedure may be used to strap the distributor. Immediately before and after the asphalt shot, the operator should stop the distributor truck on a level spot such that the tank is as level as possible. Some distributors have a level attached to the tank; if not, then a 3- to 4-foot carpenter's level may be used. The strap stick should be clean so that the level of asphalt can be read easily. The manhole cover at the top of the tank, shown in Figure 7-22 (a), should be opened, and the strap stick inserted into the tank and held as

nearly vertical as possible. The strap stick, shown in Figure 7-23 (b), should be lowered into the asphalt until it touches the bottom of the tank. The strap stick then should be removed from the tank. The number of gallons is read at the top of the line that is covered by asphalt. On some distributor models, the strap stick itself is not graduated and must be held against a graduated scale mounted on the side of the tank in order to be read.



(a)



(b)

Figure 7-24. Strapping the distributor: (a) manhole cover on top of distributor tank and (b) strap stick used to measure quantity of asphalt in distributor tank (courtesy: http://onlinemanuals.txdot.gov/txdotmanuals/scm/asphalt_distributor.htm#i1007629).

An example of a tack coat rate calculation is as follows.

CRS-1 was applied over a 12-ft wide pavement from Station 1 (12+00 ft) to Station 2 (45+00 ft) at a directed rate of 0.06 gals/yd². The tank distributor's strap stick reading at Station 1 was 123 gallons and at Station 2 was 398 gallons. The temperature gauge read 150°F. CRS-2 shows residue by evaporation to be 65% as per the catalog. What is the actual tack coat rate of application in gallons per yard?

$$\text{Undiluted Rate of application} = \frac{\text{No of Gallons Applied}}{\text{No of Square Yards Tacked}} = \frac{\text{Gallons}}{\text{Square Yards}}$$

Part 1: No. of Gallons Applied

Total Gallons of Tack Used = Beginning Distributor Reading (Station 1) - Ending Distributor Reading (Station 2)

Total Gallons of Tack Used = 123 - 398 = 275 gallons measured

$$V_{60} = V_t \times CF$$

where V_{60} = volume at 60°F (15.6°C), V_t = volume at given temperature, and CF = corrected factor (see [Appendix Table D.3](#)).

Corrected Total Gallons of Tack Used, $V_{60} = 275 \text{ gallons} \times 0.97750$ (Appendix Table) = 268.8 gallon used

Part 2: No of Square Yards Tacked

Length = Ending Station - Beginning Station = (45+00) - (12+00) = 3300 LF

Rectangular Area of tack applied = Length covered by distributor \times Width of Pavement

$$\text{Rectangular Area of tack applied} = \frac{3000 \text{ ft.} \times 12 \text{ ft.}}{9 \text{ ft}^2 / \text{yd}^2} = 4000 \text{ yd}^2$$

Part 3: Undiluted Rate of Application

$$\text{Undiluted Rate of application} = \frac{\text{Corrected Gallons Applied}}{\text{No of Square Yards Tacked}} = \frac{268.8}{4000} = 0.067 \text{ gal} / \text{yd}^2$$

Say 0.07 gal/yd² (Note: Significant decimal for tack coat rate is 0.01.)

Part 4: Tack Coat Residual Rate

Tack Coat Residual Application Rate = Undiluted Application Rate \times % residual

Tack Coat Residual Application Rate = $0.067 \times 0.65 = 0.043 \text{ gal/yd}^2$

Say 0.04 gal/yd² (Significant decimal for tack coat rate is 0.01.)

7.7.2 Assessment of Tack Coat Binder Bond Strength

The step-by-step procedure for measuring the BBS is described in Section 3.3. If the BBS value measured at 50°C is above 75 kPa, then the tack coat can be accepted for purchase. However, for a non-tracking tack coat, the cut-off must be kept at 750 kPa. Assessment of the tack coat performance depends on the type of asphalt concrete mixture along with the tack coat that is applied. The evaluation of a tack coat during specific project conditions is described in Section 6.7.

7.8 Method of Payment

No direct payment is made for the work described in this Section 7. Payment at the contract unit prices for the various mix items covered by Sections 610, 650 and 654 will be full compensation for all work covered by this section.

Chapter 8. Conclusions and Recommendations

Despite the importance of tack coat application on the bond strength of the asphalt interface and the long-term behavior of the pavement structure, no standard quality control method is currently available to ensure the proper application of tack coats. The current research approach and the test results help to propose a standard quality control protocol for tack coats. The following conclusions have been drawn based on the experimental work and computational analysis conducted in this research.

8.1 Experimental Work

8.1.1 Interface Shear Strength

- The verification of the time-temperature superposition principle on interface shear strength and binder bond strength was successfully carried out. The t-T shift factors determined from the dynamic modulus tests of the AC mixture can be used successfully to develop ISS mastercurves. In contrast, the t-T shift factors determined from the dynamic shear rheometer (DSR) of tack coat emulsion can be used successfully to develop BBS mastercurve.
- The predictive model equation for ISS developed by Cho (2016) is fitted to obtain the coefficients of the five different tack coat material. Further, the model should be able to contribute to a mechanistic design that can prevent shear bond failure between the asphalt layers by comparing the shear stress calculated from the pavement analysis program for a critical condition to the shear strength determined from the prediction model developed in this study.
- The ISS strength reduces with an increase in test temperature and vice versa at a specific strain rate. This response is applicable irrespective of the tack coat type considered for the testing.
- The increment in strain rate increases the ISS strength at a specific temperature and vice versa. This applies to all the tested MAST specimens, independent of the tack coat type.
- The three different confining pressures are applied to find the effect of confinement on ISS. The results clearly indicate that the ISS is proportional to applied confinement pressure. The aggregate interlocking is improved results in increased frictional resistance to the applied shear stresses. Therefore, the increase in shear strength with an increase in confinement.
- Three different tack coat application rates (0.01, 0.03, and 0.05 gal/yd²) were studied. MAST specimens were fabricated with three application rates for the five different tack coats. The outcome does not show any influence on the ISS. The statistical analysis on the effect of application rate on the ISS also supports these findings. However, it is noteworthy that the ISS test is a quick monotonic shear test which acts as a quality control test. Hence, the real effect and performance of the application rate cannot be completely captured with

this test. A cyclic shear fatigue test is considered as a more reliable test to understand the effect of application rate as the loading mode is realistic to the field conditions.

- Tack coat type does not have an effect on the ISS. Statistical analysis of all the outcomes at different testing conditions also converges to the same opinion. However, the strain at failure and the strain at plateau stress for non-tracking emulsions (NTCRS-1hM and Ultrafuse) are significantly larger than the unmodified tack coats (CRS-2, CRS-1h) especially at temperatures greater than 35°C. This clearly indicates that focusing merely on the shear strength may cause a discrepancy in the field performance. The energy dissipated during an ISS test could be a better indicator of the debonding potential. However, for the current study, the test is not allowed to reach till the stress plateaus as the displacement recorded are far more substantial than the typical strains observed for unmodified tack coat specimens. Therefore, it is unfair to conclude that the performance of non-tracking or modified emulsion is equivalent to the unmodified emulsion-based of shear strength. Cyclic shear fatigue should be a promising test to capture the performance differences of tack coat types.
- Milled and Unmilled are the two surface conditions considered in this study. The grooved surface of the laboratory specimens was created using a mechanical rotary milling machine that mimics the field milled surface and matches with the field milled Mean Profile Depth (MPT). The results show that the ungrooved surface shear strength is comparable with the grooved surface specimens. Besides, the grooved surface often worsens the strength than ungrooved surfaces. The milled surface in the field is highly uneven and rough, even though the visual impression looks like well-defined grooved surface texture. The smoother groove surface created by the drill bit against the rougher milled surface in the field can be attributed to weak bonding. In addition, the testing is carried out with the groove path in line with the testing direction. As a result, the grooves facilitate the easy slippage through rather than resisting the shear displacement. Hence, testing with specimens extracted from the field and comparing it with the fabricated laboratory specimens is the apt way to reach a final verdict.

8.1.2 Binder Bond Strength

- The prediction model equation for BBS was also developed, which is a function of reduced tensile stress rate. A new two-point method was proposed to predict the mastercurve of BBS with the aid of two tests at two different temperatures. Mastercurve construction typically requires 13 different conditioning temperatures per tack coat, which consumes enormous amounts of time and effort. The proposed two-point method reduced the mastercurve construction time to within eight hours of testing, with a degree of accuracy that is comparable to the predictive model that uses the all-point method.
- The ranking of the mastercurves constructed using the dynamic shear modulus values of each tack coat type follows the same ranking pattern as for the predicted BBS

mastercurves, thereby verifying that the prediction model can estimate the BBS in adhesive failure regions.

- Three residual application rates of 0.045 L/m² (0.01 gal/yd²), 0.14 L/m² (0.03 gal/yd²), and 0.23 L/m² (0.05 gal/yd²) were used at a single temperature, i.e., 44°C for NTCRS-1hM and 22°C for CRS-2 and CRS-1h, to identify the effects of application rate on BBS. Even though no definite trend emerged among the different tack coat application rates for the different tack coats, the optimum residual application rate for the tested emulsions was below 0.14 L/m² (0.03 gal/yd²). Agencies, including the NCDOT, should specify the tack coat application rate as the residual application rate instead of the emulsion application rate in order to gain more consistent BBS test outcomes, thereby avoiding the residue variation within different emulsions that can affect the performance of the pavement system.

8.2 Numerical Simulation

- In this research, an MSR that is close to 1.0 implies a high potential for interface debonding between the asphalt concrete layers due to the repeated braking conditions. All the tack coats considered for the current study generate sufficient shear strength to resist the shear stress in the field based on numerical simulation. Hence, the potential for interface debonding is minimal.
- The MSR value is typically observed along the center of the longitudinal axis of the tire at 10 cm to 14 cm in front. The location depends upon the depth of the interface and tack coat interface considered for the analysis for a specific pavement structure and loading conditions. In this study, it is a thin pavement with a dual tire of 80 kN under braking condition at a speed of 5 mph.

8.3 The Minimum Required Binder Bond Strength (BBS)

- A tack coat quality control methodology is proposed to ensure the appropriate bonding quality of tack coat emulsions as well as to provide acceptable field performance. This methodology uses the PATTI test to evaluate the BBS of the tack coat material tested at a temperature of 50°C.
- The minimum BBS for acceptance for tack coat application should be above 75 kPa. However, for non-tracking tack coat the cut-off is kept at 750 kPa.
- The advanced assessment of the tack coat performance depends on the type of AC mixture along with the tack coat is applied is also proposed.

8.4 Recommendations for Further Research

The following topics are recommended to be investigated in future research:

- Effect of mixture type on ISS

- Relationship between unconfined ISS and confined ISS to establish a simplified test protocol
- Effect of fatigue on ISS with and without a tack coat and at different tack coat application rates
- Effect of milled surface that properly represents the field condition

REFERENCES

- AASHTO. (2004). *Standard Specification for Cutback Asphalt (Rapid-Curing Type)*. Standard, AASHTO M81, American Association of State and Highway Transportation Officials, Washington DC, USA.
- AASHTO. (2017a). *Bulk Specific Gravity (G_{mb}) and Density of Compacted Hot Mix Asphalt (HMA) Using Automatic Vacuum Sealing Method*. Standard, AASHTO T331, American Association of State and Highway Transportation Officials, Washington DC, USA.
- AASHTO. (2017b). *Standard Specification for Performance-Graded Asphalt Binder*. Standard, AASHTO M320, American Association of State and Highway Transportation Officials, Washington DC, USA.
- AASHTO. (2017c). *Standard Specification for Cutback Asphalt (Medium-Curing Type)*. Standard, AASHTO M82, American Association of State and Highway Transportation Officials, Washington DC, USA.
- AASHTO. (2018a). *Standard Specification for Cationic Emulsified Asphalt*. Standard, AASHTO M208, American Association of State and Highway Transportation Officials, Washington DC, USA.
- AASHTO. (2018b). *Standard Specification for Polymer-Modified Emulsified Asphalt*. Standard, AASHTO M316, American Association of State and Highway Transportation Officials, Washington DC, USA.
- AASHTO. (2019). *Provisional Standard Method of Test for Determining the Dynamic Modulus for Asphalt Mixtures Using Small Specimens in the Asphalt Mixture Performance Tester (AMPT)*. Standard, AASHTO TP132, American Association of State and Highway Transportation Officials, Washington DC, USA.
- AASHTO. (2020a). *Standard Method of Test for Theoretical Maximum Specific Gravity (G_{mm}) and Density of Asphalt Mixtures*. Standard, AASHTO T209, American Association of State and Highway Transportation Officials, Washington DC, USA.
- AASHTO. (2020b). *Standard Practice for Recovering Residue from Emulsified Asphalt Using Low-Temperature Evaporative Techniques*. Standard, AASHTO R78, American Association of State and Highway Transportation Officials, Washington DC, USA.
- AASHTO. (2020c). *Standard Method of Test for Determining the Rheological Properties of Asphalt Binder Using a Dynamic Shear Rheometer (DSR)*. Standard, AASHTO T 315, American Association of State and Highway Transportation Officials, Washington DC, USA.
- AASHTO. (2020d). *Standard Method of Test for Determining Asphalt Binder Bond Strength by Means of the Asphalt Bond Strength (ABS) Test*. Standard, AASHTO T 361, American Association of State and Highway Transportation Officials, Washington DC, USA.

AASHTO. (2020e). *Standard Specification for Performance-Graded Asphalt Binder Using Multiple Stress Creep Recovery (MSCR) Test*. Standard, AASHTO M332, American Association of State and Highway Transportation Officials, Washington DC, USA.

AASHTO. (2020f). *Standard Specification for Emulsified Asphalt*. Standard, AASHTO M140, American Association of State and Highway Transportation Officials, Washington DC, USA.

AASHTO. (2020g). *Standard Practice for Sampling Asphalt Materials*. Standard, AASHTO R66-16, American Association of State and Highway Transportation Officials, Washington DC, USA.

Al-Qadi, I. L., Carpenter, S. H., Leng, Z., Ozer, H., and Trepanier, J. (2008). *Tack coat optimization for HMA overlays: Laboratory testing*. Technical Report, FHWA-ICT-08-023, Illinois Center for Transportation, Rantoul, IL, USA.

Amelian, S., and Kim, Y.-R. (2018). “Performance Assessment of Interlayers with Different Tack Coats by Considering Loading Types and Failure Modes.” *Transportation Research Record: Journal of the Transportation Research Board*, SAGE Publications Inc, 2672(28), 1–9.

Asphalt Institute. (1968). *MS-18 Sampling asphalt products for specifications compliance*. The Asphalt Institute, College Park, MD, USA.

Asphalt Institute. (2007). *MS-4 The Asphalt Handbook*. The Asphalt Institute, College Park, MD, USA.

Asphalt Institute. (2008). *MS-19 Basic Asphalt Emulsion Manual*. The Asphalt Institute, College Park, MD, USA.

Asphalt Institute. (2020). *MS-22 Construction of Quality Asphalt Pavements*. The Asphalt Institute, College Park, MD, USA.

ASTM. (1960). *Specification for Heavy Petroleum Spirits (Heavy Mineral Spirits)*. Standard, ASTM D965-59, American Standards for Testing Materials International, West Conshohocken, PA, USA.

ASTM. (2014). *Standard Practice for Estimating Application Rate and Residual Application Rate of Bituminous Distributors*. Standard, ASTM D2995, American Standards for Testing Materials International, West Conshohocken, PA, USA.

ASTM. (2016a). *Standard Test Method for Determining Density of Emulsified Asphalt*. Standard, ASTM D6937, American Standards for Testing Materials International, West Conshohocken, PA, USA.

ASTM. (2016b). *Standard Practice for Sampling Asphalt Materials*. Standard, ASTM D140 / D140M, American Standards for Testing Materials International, West Conshohocken, PA, USA.

ASTM. (2017). *Standard Test Method for Pull-Off Strength of Coatings Using Portable Adhesion Testers*. Standard, ASTM D4541, American Standards for Testing Materials International, West Conshohocken, PA, USA.

ASTM. (2018). *Standard Terminology Relating to Materials for Roads and Pavements*. Standard, ASTM D8-18a, American Standards for Testing Materials International, West Conshohocken, PA, USA.

ASTM. (2019). *Standard Specification for Steel, Sheet, Carbon, Structural, and High-Strength, Low-Alloy, Hot-Rolled and Cold-Rolled, General Requirements for*. Standard, ASTM A568 / A568M-19a, American Standards for Testing Materials International, West Conshohocken, PA, USA.

Bae, A., Mohammad, L. N., Elseifi, M. A., Button, J., and Patel, N. (2010). “Effects of temperature on interface shear strength of emulsified tack coats and its relationship to rheological properties.” *Transportation research record*, SAGE Publications Inc, 2180(1), 102–109.

Bahia, H. U., Sufian, A., Swiertz, D., Mohammad, L. N., Akentuna, M., and Bitumix Solutions, L. L. C. (2019). *Investigation of Tack Coat Materials Tracking Performance*. Technical Report, 0092-17-06, Wisconsin Department of Transportation. Research and Library Unit, Madison, WI, USA, 71.

Braham, A. F. (2008). “Fracture characteristics of asphalt concrete in Mode I, Mode II, and Mixed-mode.” Ph.D Dissertation, University of Illinois at Urbana-Champaign, Urbana-Champaign, IL, USA.

Buchanan, M. S., and Woods, M. E. (2004). *Field Tack Coat Evaluator (ATAcker™)*. Technical Report, FHWA/MS-DOT-RD-04-168, Mississippi Transportation Research Center, Starkville, MS, USA, 124.

Caltrans. (2009). *Tack Coat Guidelines*. California Department of Transportation, Sacramento, CA, USA.

Canestrari, F., and Santagata, E. (2005). “Temperature effects on the shear behaviour of tack coat emulsions used in flexible pavements.” *International Journal of Pavement Engineering*, Taylor & Francis, 6(1), 39–46.

Chaignon, F., and Roffe, J. (2002). “Characterization Test on Bond Coats: Worldwide Study, Impact, Tests, Recommendations.” *3rd International Conference on Bituminous Mixtures and Pavements*, Thessaloniki, Greece, 603–14.

Chehab, G. R., Kim, Y. R., Schapery, R., Witzak, M. W., and Bonaquist, R. (2002). “Time-temperature superposition principle for asphalt concrete with growing damage in tension state.” *Technical Sessions 71*, Association of Asphalt Paving Technologists, Lino Lakes, MN, 559–593.

Chehab, G. R., O’Quinn, E., and Kim, Y. R. (2000). “Specimen Geometry Study for Direct Tension Test Based on Mechanical Tests and Air Void Variation in Asphalt Concrete Specimens

Compacted by Superpave Gyrotory Compactor.” *Transportation Research Record*, SAGE Publications Inc, 1723(1), 125–132.

Chen, J.-S., and Huang, C.-C. (2010). “Effect of surface characteristics on bonding properties of bituminous tack coat.” *Transportation Research Record*, SAGE Publications Inc, 2180(1), 142–149.

Cho, S. H. (2016). “Evaluation of interfacial stress distribution and bond strength between asphalt pavement layers.” Ph.D Dissertation, North Carolina State University, Raleigh, NC, USA.

Christensen, D. W., and Anderson, D. A. (1992). “Interpretation of dynamic mechanical test data for paving grade asphalt cements (with discussion).” *Journal of the Association of Asphalt Paving Technologists*, Association of Asphalt Paving Technologists (AAPT), 61, 67–116.

Coleri, E., Villarreal, R., Kumar, V., Wruck, B., Sreedhar, S., and Lewis, S. (2020). *Implementation of ODOT Tack Coat Technologies and Procedures to Improve Long-Term Pavement Performance*. Technical Report, SPR 818, Oregon State University, Corvallis, OR, USA, 230.

Crispino, M., Festa, B., Giannattasio, P., and Nicolosi, V. (1997). “Evaluation of the interaction between the asphalt concrete layers by a new dynamic test.” *Eighth International Conference on Asphalt Pavements*, International Society for Asphalt Pavements, Seattle, WA, USA, 741–754.

Cross, S. A., and Shrestha, P. P. (2005). *Guidelines for Prime and Tack Coats*. Technical Report, FHWA-CFL/TD-05-002, Oklahoma State University, Stillwater, OK, USA, 111.

D’Andrea, A., Tozzo, C., Boschetto, A., and Bottini, L. (2013). “Interface Roughness Parameters and Shear Strength.” *Modern Applied Science*, Canadian Center of Science and Education, 7(10), 10.

Danish, B. (2018). “Investigation of Bonding between Open Graded Friction Courses and Underlying Asphalt Pavement Layers.” Ph.D Dissertation, Clemson University, Clemson, SC, USA.

Das, R., Mohammad, L. N., Elseifi, M., Cao, W., and Cooper, S. B. (2017). “Effects of Tack Coat Application on Interface Bond Strength and Short-Term Pavement Performance.” *Transportation Research Record: Journal of the Transportation Research Board*, SAGE Publications Inc, 2633(1), 1–8.

De Beer, M., Fisher, C., and Kannemeyer, L. (2004). “Towards the application of stress-in-motion (SIM) results in pavement design and infrastructure protection.” *8th International Symposium on Heavy Vehicle Weights and Dimensions*, Document Transformation Technologies, Johannesburg, South Africa.

Donovan, E. P., Al-Qadi, I. L., and Loulizi, A. (2000). “Optimization of Tack Coat Application Rate for Geocomposite Membrane on Bridge Decks.” *Transportation Research Record*, SAGE Publications Inc, 1740(1), 143–150.

FHWA. (2016). *Tack Coat Best Practices*. Technical Bulletin, FHWA-HIF-16-017, Federal Highway Administration, Washington DC, USA, 17.

Flexible Pavements of Ohio. (2012). *Proper Tack Coat Application*. Technical Bulletin, Flexible Pavements of Ohio, Dublin, OH, USA, 6.

Ghabchi, R., Zaman, M. M., and Rani, S. (2018). *Development of Guidelines for Selection and Evaluation of Tack Coats in Oklahoma*. Technical Report, FHWA-OK-18-02, University of Oklahoma, Norman, OK, USA, 118.

Gierhart, D., and Johnson, D. R. (2018). *Tack Coat Specifications, Materials, and Construction Practices*. NCHRP Project 20-5, Synthesis, 516, The National Academies Press, Washington, D.C., USA.

Hachiya, Y., Umeno, S., and Sato, K. (1997). "Effect of tack coat on bonding characteristics at interface between asphalt concrete layers." *Doboku Gakkai Ronbunshu*, Japan Society of Civil Engineers, 1997(571), 199–209.

Hu, X., Lei, Y., Wang, H., Jiang, P., Yang, X., and You, Z. (2017). "Effect of tack coat dosage and temperature on the interface shear properties of asphalt layers bonded with emulsified asphalt binders." *Construction and Building Materials*, Elsevier, 141, 86–93.

Karshenas, A. (2015). "Tack Coat Bond Strength Evaluation Methods and Mechanistic Design of the Interface for Multilayer Asphalt Pavement." Ph.D Dissertation, North Carolina State University, NC, USA.

Kim, H., Arraigada, M., Raab, C., and Partl, M. N. (2011). "Numerical and experimental analysis for the interlayer behavior of double-layered asphalt pavement specimens." *Journal of materials in civil Engineering*, American Society of Civil Engineers, 23(1), 12–20.

Kim, Y. R., and Adams, J. (2011). *Development of a new chip seal mix design method*. Technical Report, FHWA/NC/2008-04, North Carolina State University, NC, USA, 112.

Kim, Y.R., Tayebali, A. A., Guddati, M. N., Karshenas, A., and Cho, S. (2015). *Surface Layer Bond Stresses and Strength*. Technical Report, FHWA/NC/2013-04, North Carolina State University, NC, USA, 286.

Kruntcheva, M. R., Collop, A. C., and Thom, N. H. (2006). "Properties of Asphalt Concrete Layer Interfaces." *Journal of Materials in Civil Engineering*, American Society of Civil Engineers, 18(3), 467–471.

Lavin, P. (2003). *Asphalt Pavements: A Practical Guide to Design, Production and Maintenance for Engineers and Architects*. Spoon Press, Taylor & Francis, NY, USA.

- Leng, Z., Al-Qadi, I. L., Ozer, H., and Carpenter, S. (2008). “Tack coat application rate optimization and environmental effect on HMA Overlay-PCC pavement bonding.” *International ISAP Symposium on Asphalt Pavements and Environment*, Zurich, Switzerland, 18–20.
- Medani, T. O. (2006). “Design principles of surfacings on orthotropic steel bridge decks.” Doctoral Thesis, Delft University of Technology (TU Delft), Delft, Netherlands.
- Mohammad, L. N., Elseifi, M. A., Bae, A., and Patel, N. (2012). *Optimization of Tack Coat for HMA Placement*. NCHRP 9-40, Technical Report, 712, The National Academies Press, Washington, D.C., USA, 146.
- Mohammad, L. N., Elseifi, M. A., Das, R., Cao, W., National Cooperative Highway Research Program, Transportation Research Board, and National Academies of Sciences, Engineering, and Medicine. (2018). *Validation of the Louisiana Interlayer Shear Strength Test for Tack Coat*. Transportation Research Board, Washington, D.C.
- Mohammad, L. N., Raqib, M., and Huang, B. (2002). “Influence of Asphalt Tack Coat Materials on Interface Shear Strength.” *Transportation Research Record: Journal of the Transportation Research Board*, SAGE Publications Inc, 1789(1), 56–65.
- NCDOT. (2012). *Tack Coat Best Practices*. Field Guide, North Carolina Department of Transportation, NC, USA, 20.
- NCDOT. (2015). *Chip Seal Best Practices Manual*. Manual, SEPI Engineering & Construction, Inc, NC, USA, 58.
- NCDOT. (2018a). *Asphalt Quality Management System*. Guide, North Carolina Department of Transportation, NC, USA, 364.
- NCDOT. (2018b). *Standard Specifications for Road and Structures*. Standard, North Carolina Department of Transportation, NC, USA, 829.
- Park, H. J. (2013). “Investigation of Primary Causes of Load-Related Cracking in Asphalt Concrete Pavements in North Carolina.” Ph.D Dissertation, North Carolina State University, Raleigh, NC, USA.
- Park, S. W., Richard Kim, Y., and Schapery, R. A. (1996). “A viscoelastic continuum damage model and its application to uniaxial behavior of asphalt concrete.” *Mechanics of Materials*, Elsevier, 24(4), 241–255.
- Paul, H. R., and Scherocman, J. A. (1998). “Friction testing of tack coat surfaces.” *Transportation Research Record*, SAGE Publications Inc, 1616(1), 6–12.
- Romanoschi, S. A., and Metcalf, J. B. (2001). “Characterization of asphalt concrete layer interfaces.” *Transportation Research Record*, SAGE Publications Inc, 1778(1), 132–139.

Safavizadeh, S. A., and Kim, Y. R. (2017). "DIC Technique to Investigate Crack Propagation in Grid-Reinforced Asphalt Specimens." *Journal of Materials in Civil Engineering*, American Society of Civil Engineers, 29(6), 04017011.

Schapery, R. A. (1962). *A simple collocation method for fitting viscoelastic models to experimental data*. GALCIT, Technical Report, SM 61-23A, California Institute of Technology, Pasadena, CA, USA, 15.

Seo, Y., Kim, Y., Witczak, M. W., and Bonaquist, R. (2002). "Application of Digital Image Correlation Method to Mechanical Testing of Asphalt-Aggregate Mixtures." *Transportation Research Record*, SAGE Publications Inc, 1789(1), 162–172.

Sholar, G. A., Page, G. C., Musselman, J. A., Upshaw, P. B., and Moseley, H. L. (2004). "Preliminary investigation of a test method to evaluate bond strength of bituminous tack coats (with discussion)." *Journal of the Association of Asphalt Paving Technologists*, Association of Asphalt Paving Technologists (AAPT), 73, 771–806.

Song, W., Shu, X., Huang, B., and Woods, M. (2015). "Factors affecting shear strength between open-graded friction course and underlying layer." *Construction and Building Materials*, Elsevier, 101, 527–535.

Song, W., Shu, X., Huang, B., and Woods, M. (2018). "Effects of Asphalt Mixture Type on Asphalt Pavement Interlayer Shear Properties." *Journal of Transportation Engineering, Part B: Pavements*, American Society of Civil Engineers, 144(2), 04018021.

Sudarsanan, N., Karpurapu, R., and Amrithalingam, V. (2018). "An investigation on the interface bond strength of geosynthetic-reinforced asphalt concrete using Leutner shear test." *Construction and Building Materials*, Elsevier, 186, 423–437.

Tashman, L., Nam, K., and Papagiannakis, A. T. (2006). *Evaluation of the influence of tack coat construction factors on the bond strength between pavement layers*. Technical Report, WA-RD 645.1, Washington State Department of Transportation Olympia, Pullman, WA, USA, 91.

Tayebali, A. A., Rahman, M. S., Kulkarni, M. B., and Xu, Q. (2004). *A mechanistic approach to evaluate contribution of prime and tack coat in composite asphalt pavements*. Technical Report, FHWA/NC/2004-05, North Carolina State University, Raleigh, NC, USA, 300.

Tran, N. H., Willis, R., and Julian, G. (2012). *Refinement of the Bond Strength Procedure and Investigation of a Specification*. Technical Report, 12–04, National Center for Asphalt Technology, Auburn, AL, USA, 88.

Transit N. Z., RCA, and Roding NZ. (2005). *Chipsealing in New Zealand*. Transit New Zealand, Road Controlling Authorities, Roding New Zealand., Wellington, New Zealand.

Uzan, J., Livneh, M., and Eshed, Y. (1978). "Investigation of adhesion properties between asphaltic-concrete layers." *Association of Asphalt Paving Technologists Proc*, Lake Buena Vista, FL, USA, 495–521.

Vaitkus, A., Žilionienė, D., Paulauskaitė, S., Tuminienė, F., and Žiliūtė, L. (2011). “Research and assessment of asphalt layers bonding.” *Baltic Journal of Road & Bridge Engineering*, VGTU Press, 6(3).

Wang, J., Xiao, F., Chen, Z., Li, X., and Amirkhanian, S. (2017). “Application of tack coat in pavement engineering.” *Construction and Building Materials*, Elsevier, 152, 856–871.

West, R. C., Zhang, J., and Moore, J. (2005). *Evaluation of bond strength between pavement layers*. NCAT Report 05-08, Auburn University. National Center for Asphalt Technology, Auburn, AL, USA, 63.

Wheat, M. (2007). “Evaluation of bond strength at asphalt interfaces.” MS Thesis, Kansas State University, KS, USA.

Zofka, A., Maliszewski, M., Bernier, A., Josen, R., Vaitkus, A., and Kleizienė, R. (2015). “Advanced shear tester for evaluation of asphalt concrete under constant normal stiffness conditions.” *Road Materials and Pavement Design*, Taylor & Francis, 16(sup1), 187–210.

Appendix A. Literature Review

A.1. Factors that Affect Interface Bond Strength

A tack coat is an application of bituminous material onto an existing, relatively non-absorptive surface to provide a thorough bond between the old and new surfaces. Some of the most important factors that affect the performance of tack coats are the materials used, the application rate, surface texture, temperature, normal pressure, curing time, surface conditions and cleanliness, and whether the surface is wet or dry. This literature review describes current tack coat practices and research. As shown in the following section, researchers have not reached consensus regarding the effects of the various factors. The lack of a definitive answer to debonding problems may be attributable partly to the different test methods used by the different researchers, which makes it difficult to compare test results. The factors that affect interlayer bond strength are described briefly in the following subsections.

A.1.1 Type of Tack Coat Materials

The National Cooperative Highway Research Program (NCHRP) Project 9-40 (Mohammad et al. 2012) included a comprehensive survey of tack coat practices worldwide. According to the results of the survey, the most commonly used tack coats for new, existing, and milled hot mix asphalt surfaces are CSS-1h (32%-34%), SS-1 (30%-32%), SS-1h (29%-32%), and CSS-1 (21%-27%) asphalt emulsions. PG 64-22 is reported as the most often used asphalt cement at an average of 11%, and RC-70 as the most commonly used cutback (or liquid) asphalt at 5% to 7 percent.

Research indicates that the use of a high-quality tack coat is important to developing high shear bond strength at the interface of pavement layers. However, due to the various methodologies employed in the different research studies, different results are given for similar materials, and the performance rankings may change from researcher to researcher. In general, tack coat materials that produce high shear bond strength tend to be performance-graded binders that are used as tack coats or modified tack coat materials, such as those containing polymer or rubber. However, other commonly used tack coats are not necessarily inadequate or deficient (Buchanan and Woods 2004, Hachiya et al. 1997, Mohammad et al. 2012, Tayebali et al. 2004, West et al. 2005).

A.1.1 Application Rate

Although results vary throughout the literature, recommendations for residual tack coat rates that range from 0.02 gal/yd² to 0.09 gal/yd² are fairly common. In general, lower application rates are recommended for new or subsequent layers, intermediate application rates are recommended for normal surface conditions on relatively smooth existing pavements, and higher application rates are recommended for old, oxidized, cracked, pocked, or milled asphalt pavements and Portland concrete cement pavements (Asphalt Institute 2007, Caltrans 2009, Flexible Pavements of Ohio 2012, Kruntcheva et al. 2006, Lavin 2003, Mohammad et al. 2002, 2012, Sholar et al. 2004,

Tashman et al. 2006). In general, researchers have found that the use of tack coat materials improves the bond strength between pavement layers, although some researchers suggest that in some situations tack coats may not be needed at all (Kruncheva et al. 2006, Sholar et al. 2004, Tashman et al. 2006).

Table A1 presents a summary of tack coat specifications from three different state highway agencies. These agency specifications contain either a maximum recommended application rate or an application rate range for tack coats. Table A2 also shows that limitations with regard to temperature, surface, dilution, and application coverage are considered in some of the specifications. A few agencies specify that asphalt emulsions should be diluted with water for uniform coverage and several agencies recommend, via their specifications, applying tack coat to all vertical surfaces, including longitudinal and transverse joints, curbs and gutters, and other structures. Moreover, most agencies require that the surface should be clean and dry during the tack coat application process (Cross and Shrestha 2005). Table A2 provides specific application rates according to different tack coat materials and surface types (Cross and Shrestha 2005).

Table A1. Summary of Agency Tack Coat Specifications (Cross and Shrestha 2005)

Agency	Application Rates (L/m ²)	Temperature Limitations	Require Dry Surface	Tack Vertical Surfaces	Require Dilution	Limits on Application
Arizona	Target rate of 0.3-0.5 (0.06-0.12 gal/yd ²)	NF ^a	Yes	NF ^a	NS ^b	Same Day Coverage
California	See Table 2.2	Asphalt & Base mix >10°C (50°F) Base mix >5°C (40°F)	Yes	Yes	NS ^b	Same Day Coverage
Oklahoma	<0.45 (0.10 gal/yd ²)	Surface or Ambient > 5°C (40°F)	Yes	Yes	40% Water	Same Shift Coverage

^aNF: Not found in specification. ^bNS: Not specified.

Table A2. Recommended Tack Coat Application Rates (Cross and Shrestha 2005)

Asphalt Concrete Overlay (Except Open-Graded) (liters per square meter)			
Type of Surface to be Tack-Coated	Slow-Setting Asphaltic Emulsion	Rapid-Setting Asphaltic Emulsion	Paving Asphalt
Dense, Tight Surface (e.g., between lifts)	0.20 - 0.35	0.10 - 0.20	0.05 - 0.10
Open Textured or Dry, Aged Surface (e.g., milled surface)	0.35 - 0.90	0.20-0.40	0.10 - 0.25
Open-Graded Asphalt Concrete Overlay (liters per square meter)			
Type of Surface to be Tack-Coated	Slow-Setting Asphaltic Emulsion	Rapid-Setting Asphaltic Emulsion	Paving Asphalt
Dense, Tight Surface (e.g., between lifts)	0.25 - 0.50	0.10 - 0.25	0.05 - 0.15
Open Textured or Dry, Aged Surface (e.g., milled surface)	0.50 - 1.10	0.25 - 0.55	0.15 - 0.30

A.1.2 Existing Surface Conditions

The surface conditions (or overall roughness) of the pavement also play an important role in the development of the bond strength between pavement layers. This roughness may be expressed as the texture of the underlying layer or as large-scale roughness caused by cold milling the pavement prior to the placement of new pavement layers. In general, a rougher texture produces greater shear bond strength (D’Andrea et al. 2013, Tashman et al. 2006).

A.1.3 Temperature

Various researchers have found that the bond strength of tack coat materials decreases significantly with an increase in temperature (Crispino et al. 1997, Flexible Pavements of Ohio 2012, Kim et al. 2011, NCDOT 2018b, Romanoschi and Metcalf 2001, Uzan et al. 1978, West et al. 2005).

A.1.4 Normal Confining Pressure

Various studies have shown that an increase in normal pressure (also known as confining stress) increases the shear bond strength. This phenomenon can be attributed to the fact that, as normal pressure increases, more stone-to-stone contact occurs across the interface. Subsequently, greater pressure is needed to overcome this enhanced frictional resistance. Research also has found that the magnitude of the effect of normal pressure is dependent on the temperature and tack coat rate, with

higher temperatures and lower tack coat rates leading to a greater change in shear resistance due to the change in normal pressure (Canestrari and Santagata 2005, Mohammad et al. 2012, West et al. 2005).

A.1.5 Other Factors

Dust

Although results vary from researcher to researcher, it is generally accepted that a clean, dust-free surface is preferable to dusty or dirty conditions and provides greater bond strength than an unclean dusty surface (Caltrans 2009, Flexible Pavements of Ohio 2012).

Curing

The literature lacks complete agreement on how long a tack coat should remain uncovered before placing the subsequent asphalt layer. Many highway agencies specify minimum curing times and some also specify maximum curing times (Chaignon and Roffe 2002, Hachiya et al. 1997, Paul and Scherocman 1998). However, some construction practices and specifications allow for the placement of the emulsion directly in front of the paver, meaning that the emulsion is covered prior to breaking (Lavin 2003). Trapped moisture is the greatest concern with this method, whereas a uniform surface due to reduced tracking and pickup is its chief advantage.

Wet or Dry Surface

Although results vary, it is generally accepted that having a dry surface prior to tack coat placement is preferable to a damp or wet surface in order to ensure sufficient shear bond strength (Flexible Pavements of Ohio 2012, Mohammad et al. 2012, Sholar et al. 2004).

A.2. Debonding Performance Evaluation Methods

Given the aforementioned factors that affect interlayer bond strength, the methods used to evaluate the shear bond strength between layers are important because ensuring that any given combination of factors actually will provide adequate shear bond strength is a difficult task. One common way to evaluate the shear bond strength of pavements is to perform laboratory tests. These tests include, e.g., the Florida Department of Transportation (FDOT) Shear Test, the Virginia Shear Fatigue Test, the Direct Shear Apparatus Test developed at the Illinois Center for Transportation, the Louisiana Interlayer Shear Strength Tester test, the Tack Coat Shear Test, the Four-Point Shear Test, the Kansas State University Bond Strength Test, the Ancona Shear Testing Research and Analysis (ASTRA) Test, and the Leutner Shear Test, to name a few (Al-Qadi et al. 2008, Bae et al. 2010, Braham 2008, Chen and Huang 2010, Donovan et al. 2000, Leng et al. 2008, Medani 2006, Romanoschi and Metcalf 2001, Tashman et al. 2006, Vaitkus et al. 2011, Wheat 2007).

The Washington Center for Asphalt Technology (WCAT) conducted a research study titled ‘Evaluation of the Influence of Tack Coat Construction Factors on the Bond Strength between Pavement Layers’ (Tashman et al. 2006). In this study, WCAT researchers used three different test devices to evaluate different strength properties related to debonding. The WCAT research team considered and investigated several factors that affect bond strength at the interface of pavement layers and found that the condition of milled surfaces is a significant factor for bond strength. The WCAT researchers used the FDOT shear test, torque bond test, and University of Texas at El Paso (UTEP) pull-off test to investigate tack coats. Figure A1 and Table A3 presents details about each test. The figure and table show that these three test methods have different mechanisms and purposes.



(a) FDOT shear test device



(b) Torque bond test device



(d) UTEP pull-off test device

Figure A1. Test devices used in Washington Center for Asphalt Technology research.

Table A3. Test Methods: Washington Center for Asphalt Technology Study

	FDOT Shear Test	Torque Bond Test	UTEP Pull-Off Test
Load Type	Direct Shear	Torsion	Tension
Loading Rate	2 inches/min.	Wrench sweep 90° within 30 ± 15 sec.	N/A
Specimen Diameter	5.91 inches	5.91 inches	5 inches
Conditions Prior to Testing	77°F ± 1.8°F for a minimum of 2 hours	68°F ± 3.6°F for 4-16 hours	40-pound load for 10 minutes

A.3. Substantial Literature Review

An additional comprehensive literature review was conducted with a focus on a few important aspects such as effects of tack coat material type, application rate, and surface condition so that several literatures which concentrate on the aspects mentioned above, were chosen. The reason why these factors and literatures were chosen is they are still controversial issue or factors. Many of literatures even have different or conflicting conclusions.

A.3.1 Wisconsin DOT Research

Wisconsin Department of Transportation (WisDOT) research team implemented a research named “Investigation of Tack Coat Materials Tracking Performance” to evaluate the performance of asphalt tack coat (Bahia et al. 2019). Especially, in this research, interlayer shear strength tests were conducted with Louisianan Interlayer Shear Strength Tester (LISST) to assess the bond performance of tack coat with asphalt mixture specifically, shear bonding performance property.

Figure A2 shows the levels of the factors for laboratory testing. The Mean Texture Depth (MTD) was used as a quantification of surface condition in mm and measured by a modified Sand Patch test (ASTM 1960). The surface texture was categorized to two levels and the actual images are shown in Figure A2.

Factor	Level	Description of Levels
Emulsion Type	4	CSS-1, CSS-1hL, CQS-1h, Trackless (NTQS-1hh)
Residual Application Rate (gal/yd ²)	2	0.02 gal/yd ² 0.05 gal/yd ²
Existing Surface Texture*	2	Low – Dense graded, fine mix (Mean Texture Depth, (MTD** = 0.17 mm) High – Stone Mastic Asphalt (SMA) type mix (MTD = 0.96 mm)
Test Temperature	2	25°C 46°C
Confining Pressure	1	7 psi
Replicate Samples	3	Three specimens tested per factor combination.

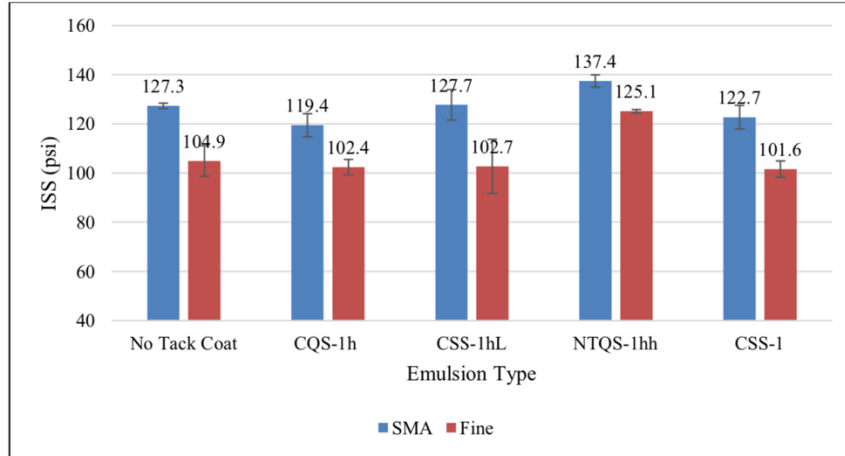
*As quantified using modified Sand Patch Method

** Average Pavement Macrotexture Depth

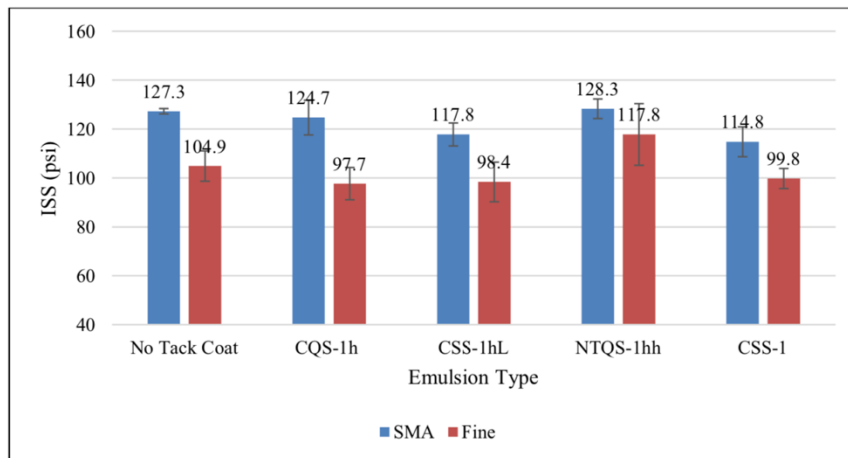
Figure A2. List of factors and level descriptions for laboratory shear testing study (Bahia et al. 2019).



Figure A3. High texture (left) and low texture (right) mixtures (Bahia et al. 2019).



(a)



(b)

Figure A4. Effect of surface texture and application rate at various tack coats: (a) 0.02 gal/yd², (b) 0.05 gal/yd² (Bahia et al. 2019).

The shear strength test results with lab fabricated specimens shows that it is a function of surface texture and tack coat material. First, the effect of texture is pronounced so, high texture leads better ISS. Second, there is no clear trend or effect of tack coat material type but NTQS-1hh (Trackless) has the best performance. Last but not the least, the application rate is not found to significantly affect shear strength performance but lower rates (0.02 gal/yd²) present slightly high ISS results than higher rates (0.05 gal/yd²) except CQS-1h tack coat. Moreover, the majority of tack coat indicate worse ISS performance than no tack coat circumstance except NTQS-1hh. Figure A4 describes the effect of texture, material type, and application rate. The surface textures condition is the most significant factor and the emulsion type (material type) is insignificant without trackless

tack, shown in Figure A5. The research team mentioned that it is a challenge to decide optimal application rate and tack type by using ISS result from lab.

Main Factor	F Ratio	p-value	R ² _{ADJ}
Surface Texture	103.5	<0.0001	0.79
Emulsion Type	59.3	<0.0001	
Application Rate	7.6	0.0085	
Replicate	6.8	0.0123	

(a)

Main Factor	F Ratio	p-value	R ² _{ADJ}
Surface Texture	114.11	<0.0001	0.78
Replicate	6.28	0.0177	
Application Rate	4.05	0.0530	
Emulsion Type	0.59	0.4468	

(b)

Figure A5. ANOVA for ISS main factors: (a) trackless included and (b) without trackless (Bahia et al. 2019).

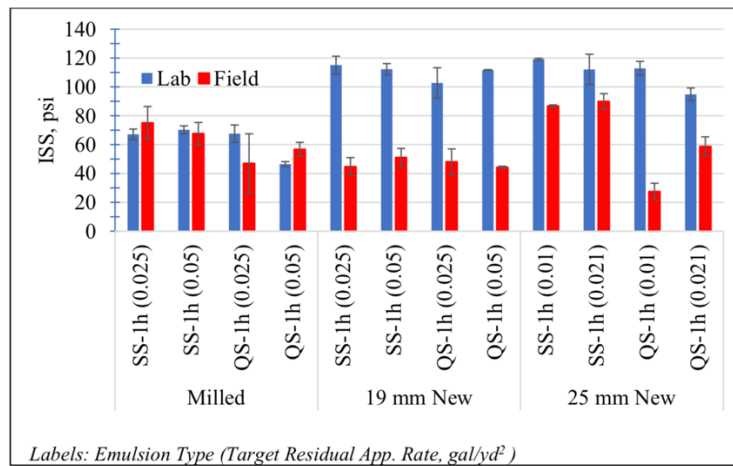


Figure A6. Comparison of lab and field ISS for field validation study (Bahia et al. 2019).

In order to validate relationship between lab and field ISS, field cores were taken from various project and new and same materials such as tack coats and mixture were also collected from the field for laboratory fabricated specimen to remove material effect and test results are shown in Figure A6. The field ISS is significantly lower than the lab ISS and the research team explains possible reasons that there were some uncertainties of field condition such as inconsistency of the application rate meaning the application rate which presented above was target application rate

instead of actual rate especially, 25 mm New field data show a fluctuation of ISS because of inconsistency of application rate. Besides, range of application rate is relatively narrower (0.01 ~ 0.021 gal/yd²). Dusty or dirty surface also made negative effect to ISS results. The ISS of lab milled condition is similar with field milled condition while the ISS results of lab new condition are better than field ones. There is comment from the research team that some damages exist in the milled bottom layer and the direction of milling was not specified. Eventually, the team reached a conclusion that a clear relationship of ISS result between field and laboratory is not found.

A.3.2 NCHRP Report 712

This research is the result of NCHRP Project 9-40, “Optimization of Tack Coat for HMA Placement” (Mohammad et al. 2012). The research team developed testing device referred Louisiana Interlayer Shear Strength Tester (LISST). The main purposes of this research were to obtain optimum methods for application, device type, application rate, tack coat materials.

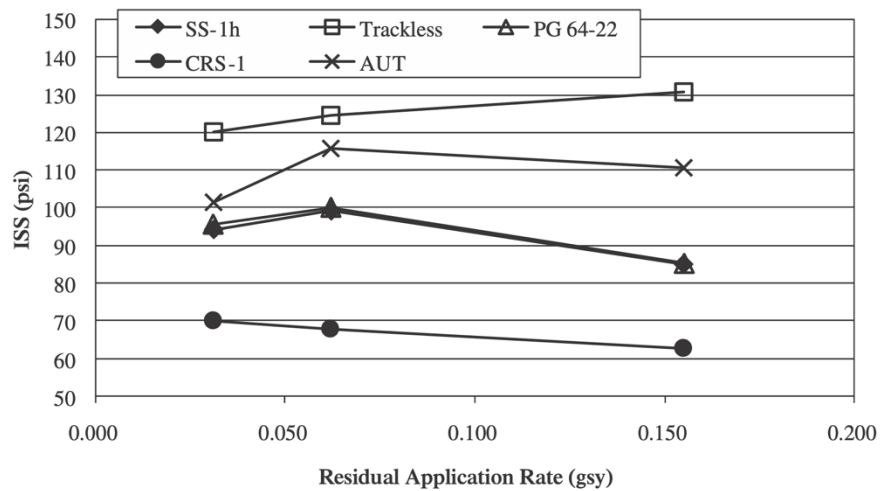


Figure A7. Effects of residual application rate on ISS for lab-compacted samples (Mohammad et al. 2012).

In Figure A7, ISS tests with lab fabricated samples are plotted to see the effect of application rate. Only trackless tack coat obtains better ISS performance when the application rate increase but CRS-1 shows opposite trend from trackless and the other tack coats have optimum rates at 0.061 gal/yd².

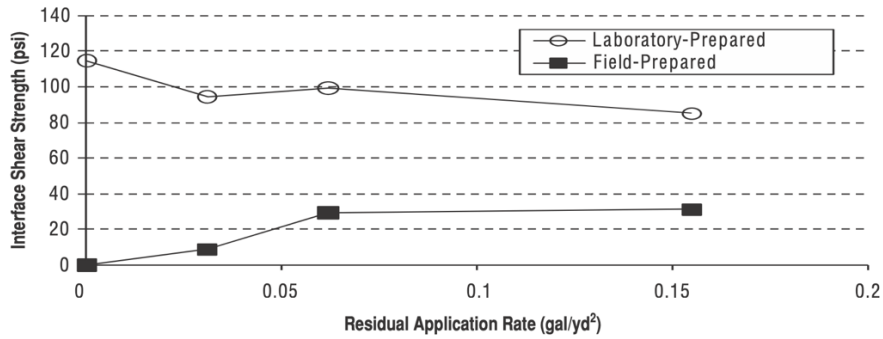


Figure A8. Effects of sample preparation methods on ISS (Mohammad et al. 2012).

The trends of ISS from lab and field are different shown in Figure A8. The research team mention that different compaction method and lack of uniformity of application rate in the field lead the gap of ISS results between lab and field.

Figure A9 presents the effect of texture by comparing ISS according to different mixtures such as open-graded friction course (OGFC), sand, and SMA mixtures. The research team expects that ISS performance with sand mixture get worse while application rate higher because tack coat performs as lubricant on smooth surface. For OGFC, when the air void is filled with tack coat, ISS gets higher. SMA mixture shows that it has optimum application rate for ISS performance.

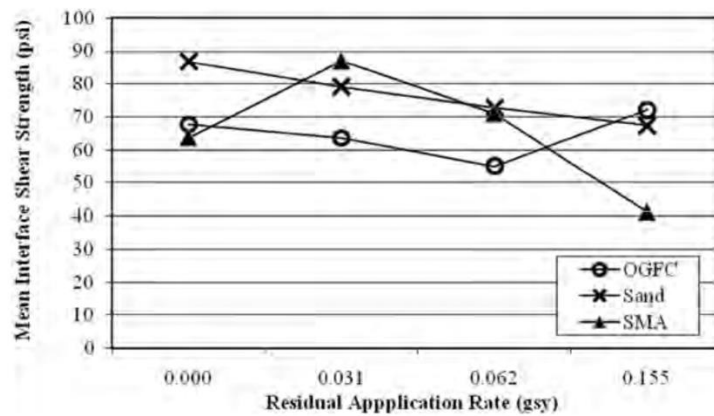


Figure A9. Mean interface shear bond strengths for the OGFC, sand, and SMA mixtures (Mohammad et al. 2012).

A.3.3 FHWA-OK-18-02 Project

In this research, Louisiana Interlayer Shear Strength Tester (LISST) is used to measure shear bond performance. The objectives of research are to evaluate effects of tack coat type, application rate, surface type and temperature. Five different tack coats, three different application rates, four different surface conditions and three different temperatures are used for the objectives (Ghabchi et al. 2018).

Figure A10 presents the effect of tack coat type and application rate, simultaneously. The trackless tack coats (NTHAP and NTQS-1HH) have better ISS performance than the other emulsion type of tack coats. Even the emulsion types of tack coats have lower ISS results than no tack condition. For application rate effect wise, the trackless tack coats show higher ISS results when the application rate increases but the other tack coats get worse performance when the application rate is getting higher.

Figure A11 shows effect of surface condition with various tack coat materials. The trackless tack coats have relatively high ISS results in all surface conditions and the differences of ISS values by surface conditions are insignificant. The emulsion tack coats have especially, the low ISS results with PCC surface and the gap of ISS values between PCC and the other surface conditions are significant. The ISS results on milled HMA cores from field condition from all emulsion tack coats are slightly better than the other surface conditions.

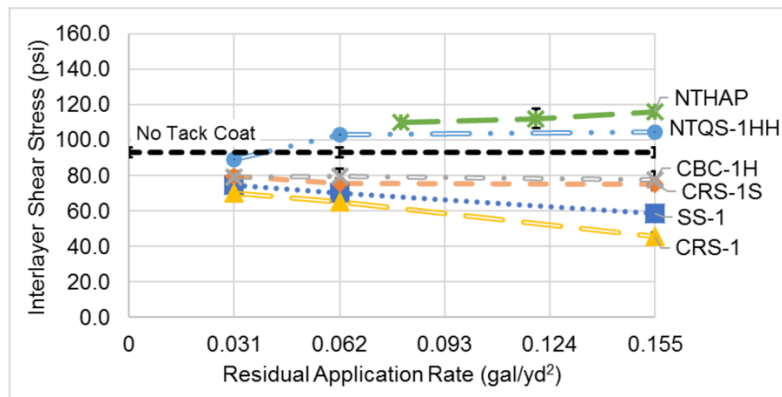


Figure A10. Effect of residual application rate on ISS: unaged HMA layer (Ghabchi et al. 2018).

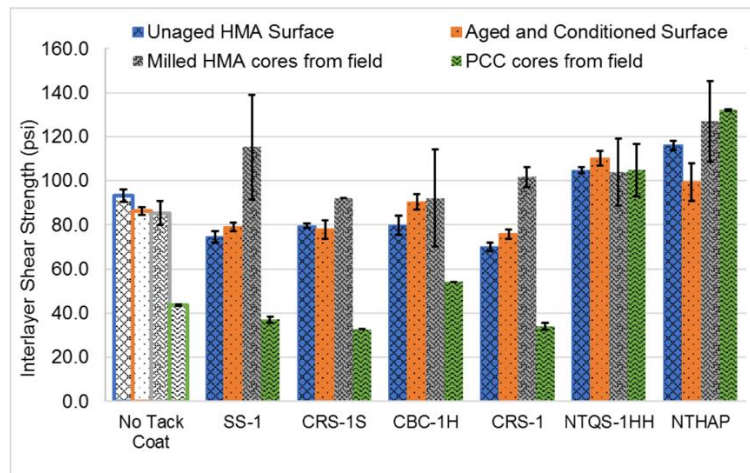


Figure A11. ISS values for different surface types and optimum residual application rates of tack coats (Ghabchi et al. 2018).

A.3.4 Research from Louisiana (Das et al. 2017)

This research named “Effects of Tack Coat Application on Interface Bond Strength and Short-term Pavement Performance” has purposes which are to evaluate the effects of surface type, tack coat material type, and residual application rate for ISS performance as well. In order to obtain these goals, 14 test sections in three different field projects were investigated. Louisiana Interlayer Shear Strength Tester (LISST) is utilized as testing device and Mean Texture Depth (MTD) is used as parameter to measure the surface property. Figure A12 indicates the surface conditions from each project with MTD and Figure A13 shows the effect of surface condition by plotting ISS values. In Figure A12, high MTD conditions lead high ISS performances except PCC surface condition and the average ISS result on PCC surfaces is the lowest among all surface conditions.

Project	Surface Type	Surface Mean Texture Depth (mm)
Missouri	Milled HMA	2.2
	Existing HMA	0.8
	New HMA	1.0
	PCC	1.1
Louisiana	Milled HMA	2.9
Florida	Existing HMA	0.9

Figure A12. Surface mean texture depths in field projects (Das et al. 2017).

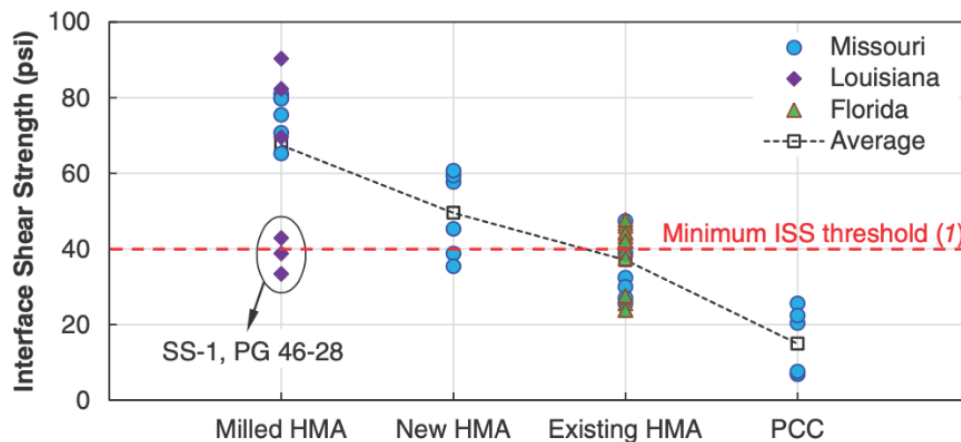


Figure A13. Effects of pavement surface type on ISS in all projects (Das et al. 2017).

Figure A14 shows the effect of tack coat type and non-tracking tack coat material has better ISS result than the other materials regardless of surface condition except existing HMA condition in Florida. Figure A15 presents the effect of application rate and in this research, the higher

application rate (0.04 gal/yd²) better but this conclusion can be skeptical because the number of data points are only four.

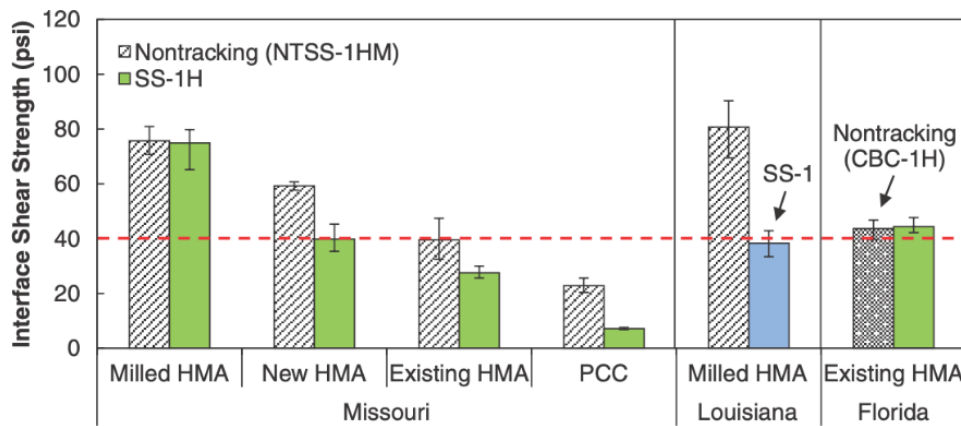


Figure A14. Effect of tack coat material type on ISS in all projects (Das et al. 2017).

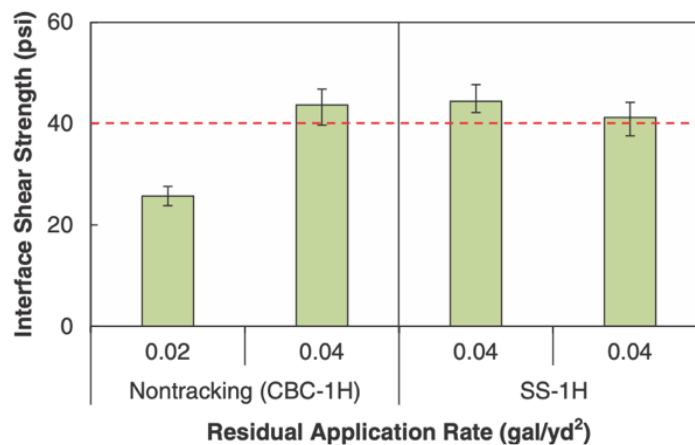


Figure A15. Effect of residual application rate on ISS on existing HMA pavement surface in the Florida project (Das et al. 2017).

A.3.5 Research from Illinois (Leng et al. 2008)

This research named “Interface Bonding Between Hot-Mix Asphalt and Various Portland Cement Concrete Surfaces” presents the effects of surface condition by selecting different mixture, application rate, and tack coat type. Figure A16 shows all the effects mentioned above. SM-9.5 mixture surface serves better ISS than IM-19.0 and 0.05 gal/yd² is considered as the optimum application rate, and finally, SS-1hP has better ISS performance than RC-70. Figure A17 describes three different PCC surface condition and expecting tining direction by indicating the traffic direction. Figure A18 explains the effect of PCC surface texture. The direction of tining in this PCC surface leads no effect for the ISS. Even the smooth surface has better performance than all tined surface at 0.05 gal/yd² application rate condition.

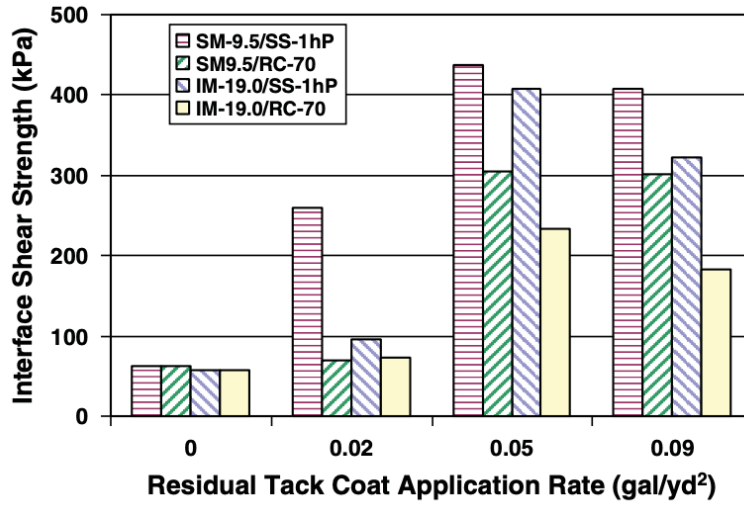


Figure A16. Effects of HMA, tack coat, and tack coat application rate (Leng et al. 2008).

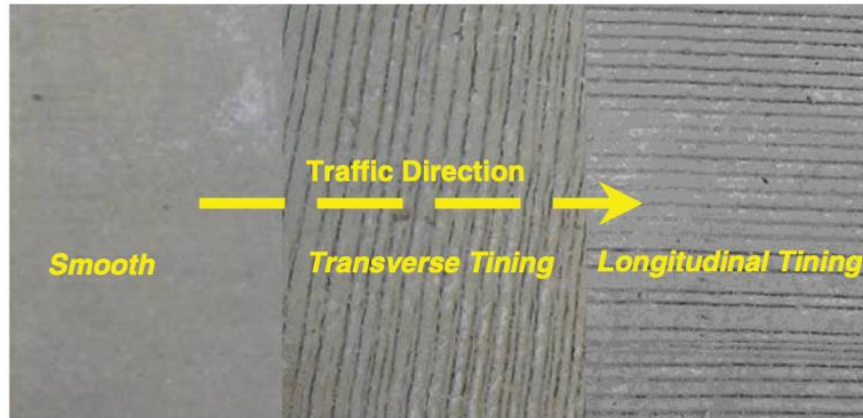


Figure A17. PCC surface texture (Leng et al. 2008).

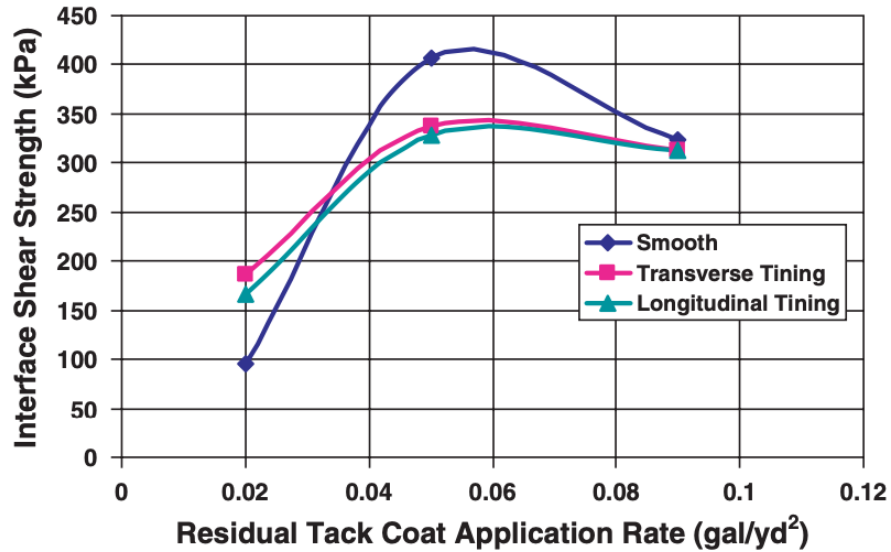


Figure A18. Effect of PCC surface texture (Leng et al. 2008).

A.3.6 Research from China (Hu et al. 2017)

This research named “Effect of Tack Coat Dosage and Temperature on the Interface Shear Properties of Asphalt Layers Bonded with Emulsified Asphalt Binders” explains the effects of application rate and temperature and shows relationship of these two factors. In Figure A19, for tack coat material, PC-3 has better ISS performance when the application rate gets lower at 50 °C temperature condition but this trend has gone at 25°C while HV have same trends at different temperatures.

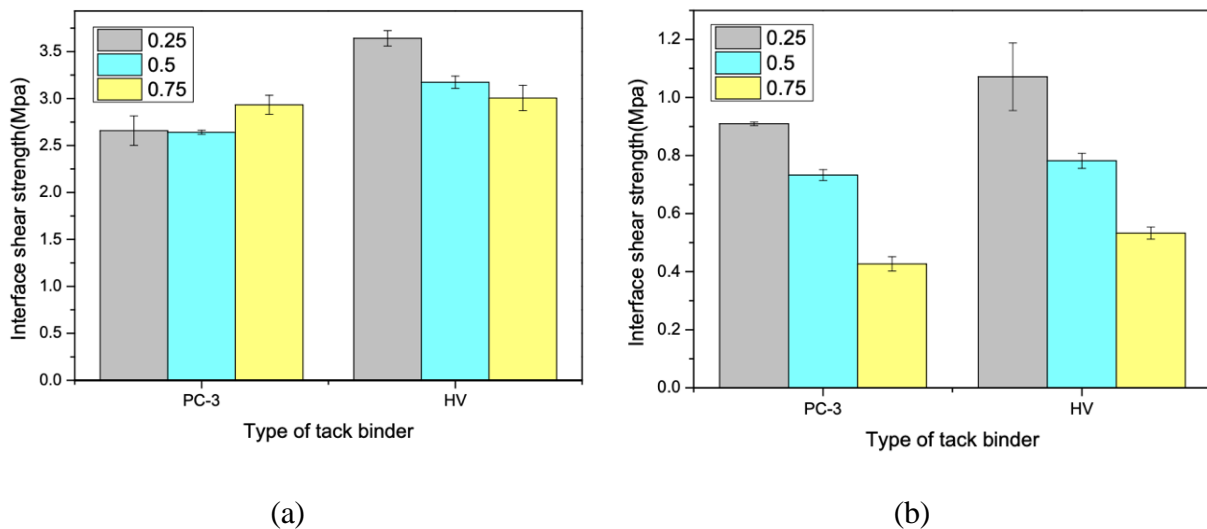


Figure A19. The ISS by different material and application rates at different temperatures: (a) 25 °C and (b) 50°C (Hu et al. 2017).

A.3.7 Research from Tennessee (Song et al. 2015)

This research named “Factors Affecting Shear Strength between Open-graded Friction Course and Underlying Layer” also claims the effects of application rate and temperature and explains relationship of these two factors at various surface conditions. The surface texture was assessed with sand patch method and significance present with texture depth like D, TLD and SMA have 0.2, 0.5 and 1.1 mm, respectively. In Figure A20 higher texture leads higher shear strength except 0 °C temperature condition. The effects of application rate and surface texture get less significant at low temperature (0 °C). The research team mentioned that at low temperature, asphalt is stiff so that application rate and surface texture affect to the shear strength less.

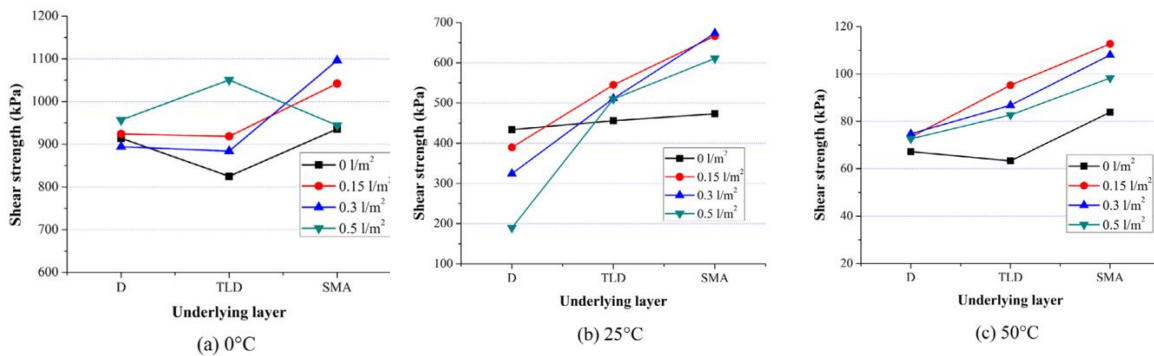


Figure A20. Effect of underlying layer on shear strength at different temperatures (Song et al. 2015).

A.3.8 Research from Oregon (Coleri et al. 2020)

Oregon Department of Transportation (ODOT) research team implemented a research named “Implementation of ODOT Tack Coat Technologies and Procedures to Improve Long-Term Pavement Performance” to develop a quality control (QC) and a tool to monitor the long-term tack coat performance. So, the effect of existing tack coat types used in Oregon, pavement surface, and the effect of application rate were investigated and evaluated. The engineered tacks which are modified and trackless tacks from company 1 (CO1) and company 3 (CO3) have higher ISS than the other, shown in Figure A21 but significant difference is not shown through the statistical analysis.

Figure A22 presents the effect of surface condition and the quantification of surface condition is MTD. The graph for the relationship between ISS and MTD indicates no significant correlation.

In order to find the effect of application rate, two different rates (0.05 and 0.09 gal/yd²) were chosen and the better performance were found in the higher rate for unmilled overlay surfaces. However, in some milled surface cases, higher application rates lead worse ISS results shown in Figure A23. There is a comment that additional research is needed to evaluate optimum application rates for each tack.

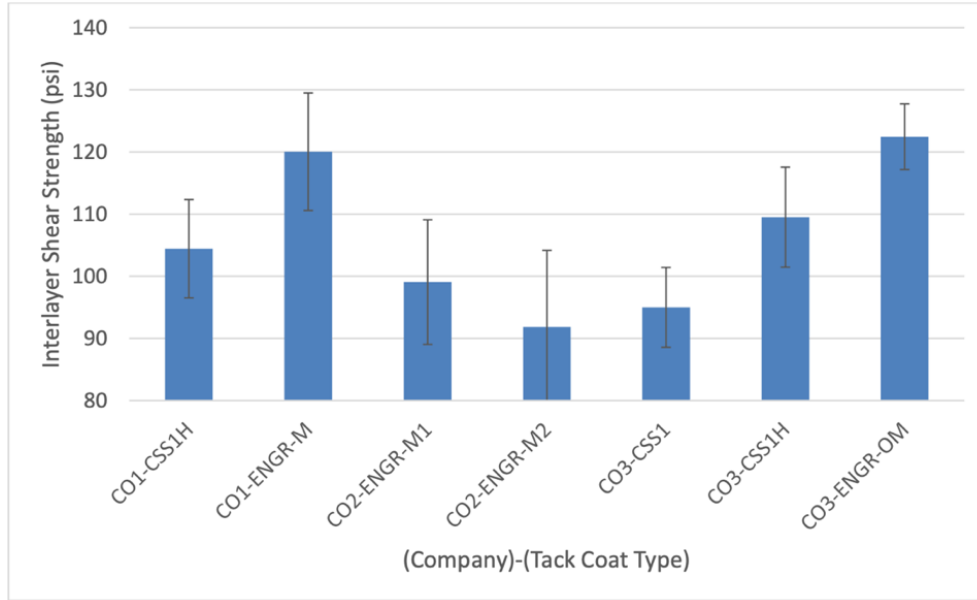


Figure A21. Average ISS results for all tack coats (Coleri et al. 2020).

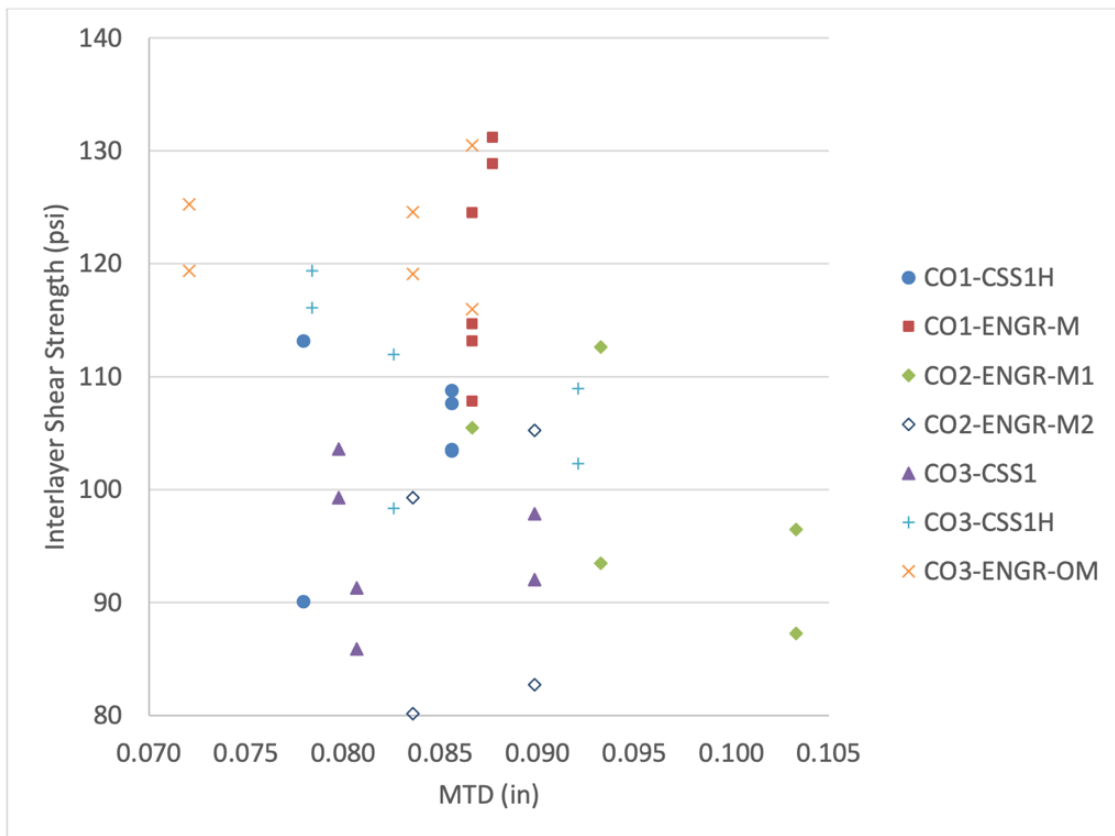


Figure A22. ISS versus MTD for each tack (Coleri et al. 2020).

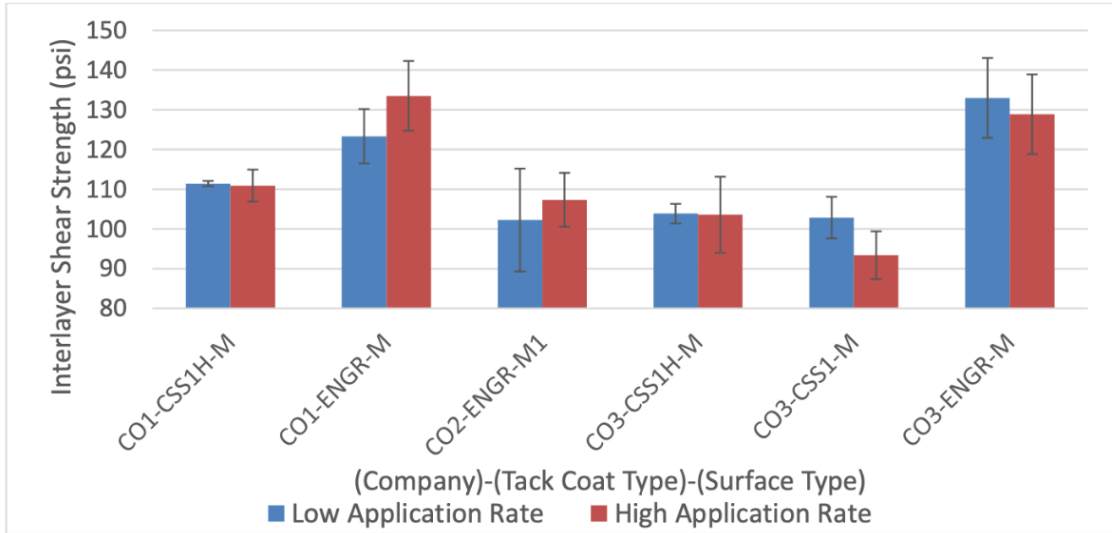


Figure A23. Milled surface tack response (Coleri et al. 2020).

The ISS performance results between the lab and field fabricated samples shown in Figure A24 were not dissimilar. Field conditions can be observed though the lab ISS tests with specimens produced by using roller compactor.

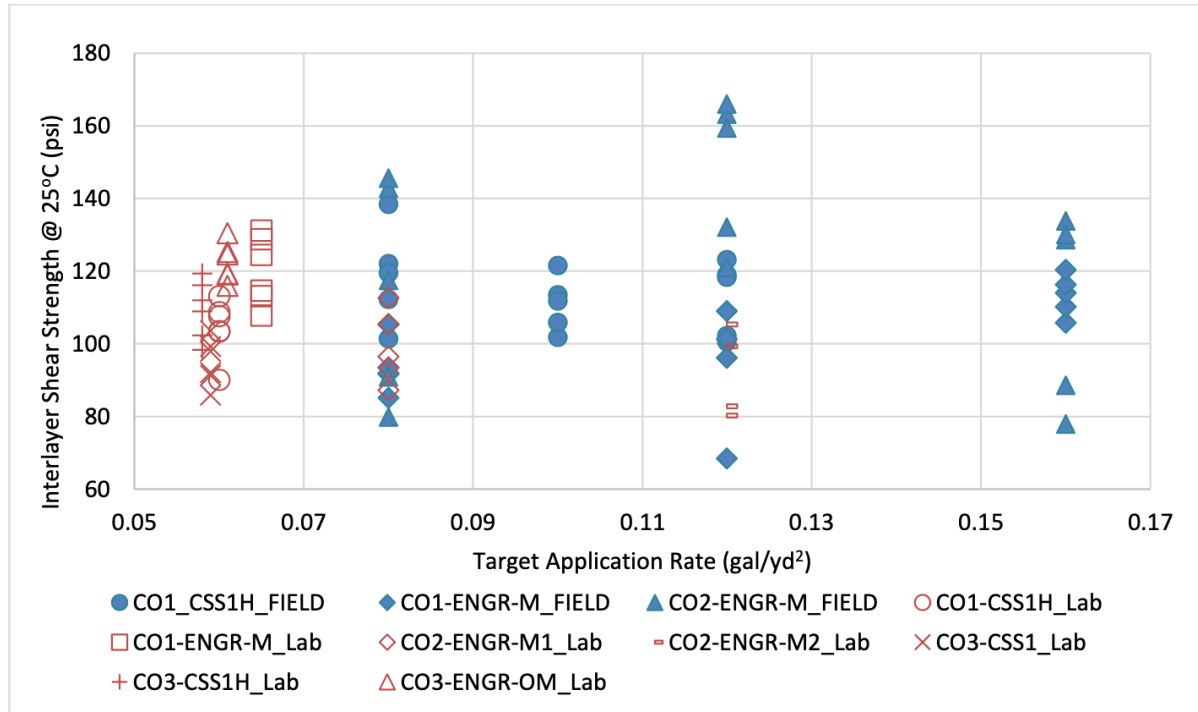


Figure A24. ISS versus application rate for field and lab samples (Coleri et al. 2020).

A.4. Critical Summary

In this substantial literature review, the effects of tack coat material type, application rate, and surface condition were primary concerns or topics. The effect of tack coat material type is insignificant but the trackless tack coat materials show better performance than the emulsion type materials. The NTQS-1hh (Trackless) is the only tack which exhibits higher ISS than no tack condition at the same application rate (0.05 gal/yd²) condition. ANOVA results also indicate that effect of tack coat is insignificant when the trackless coat is excluded from the analysis (Bahia et al. 2019). The Trackless tack shows the best ISS performance among all tacks (Mohammad et al. 2012). The trackless tacks (NTHAP and NTQS-1HH) exhibit better ISS performance than the other emulsion types. Even the emulsion types have lower ISS values than the no tack condition (Ghabchi et al. 2018). A research by Coleri et al. (2020) notes that the engineered (modified and trackless) tacks show better performance in some cases but the difference is insignificant via statistical analysis.

The application rate is still controversial factor and effect of this factor is insignificant. The optimum application rate is various by the factors such as surface or texture, temperature and material type. Nonetheless, the trackless tack has mostly better performance at higher application rate. The lower rate (0.02 gal/yd²) corresponds to slightly higher ISS values than the higher rate (0.05 gal/yd²). The F Ratio and p-value from ANOVA also indicate the insignificance of the application effect (Bahia et al. 2019) on ISS results. Only the trackless tack shows higher ISS when the application rate increase, and CRS-1 shows the opposite trend. The others have same optimum rate which they show the best ISS. The ISS of the sand mixture worsen while the application rate was increase because the tack acts as a lubricant. At the same time, for the OGFC mix, when the air voids are filled with tack, the ISS becomes greater (Mohammad et al. 2012). In the FHWA-OK-18-02 project, the trackless tacks show higher ISS with the higher application rate, but the performance of the other emulsion type tacks is worsen when the application rate increases (Ghabchi et al. 2018). The higher application rate (0.04 gal/yd²) corresponds to greater ISS with the trackless tack (CBC-1H) (Das et al. 2017). The project conducted by Leng et al. (2008) presents that 0.05 gal/yd² is considered as optimum application rate with four different tacks. The study by Song et al. (2015) concludes that the effect of application rate and surface texture become less significant at the low temperature such as 0°C. A study by Coleri et al. (2020) found that it is difficult to specify optimum application rate because optimum rate is changed by surface condition.

The surface condition affects to shear strength significantly compared to the other factors such as tack coat material type and application rate. Rough surfaces or high textures mostly support better ISS performance, but the significance or trend of the effect of the surface or texture cannot be guaranteed because these significance or trends is different by certain conditions or factors especially, field condition. In the WisDOT research, the ISS results present the shear strength is a

function of texture and tack type and ANOVA also shows texture is the most significant factor but the comparison of the milled and new surface conditions (19 mm and 25 mm) with lab-fabricated specimens shows that high texture surface worse ISS and the damage by the milling process was chosen as a possible reason (Bahia et al. 2019). In NCHRP Report 712, the ISS of the sand mixture would worsen while the application rate was increased because the tack coat acts as a lubricant on the smooth surface. On the contrary, for the OGFC mix, when the air voids are filled with tack coat material, the ISS becomes greater. Otherwise, the SMA mixture results indicate that it has optimum application rate for ISS performance. The effect of surface is depended on application rate (Mohammad et al. 2012). The emulsion type tacks have low ISS with the PCC surface, and the difference in ISS values between the PCC and other surface conditions is significant but only trackless tacks show good ISS performance with PCC surface. The ISS test results for the milled HMA cores extracted from the field for all emulsion tack coat types are slightly better than for the other smooth surface conditions (Ghabchi et al. 2018). High MTD values correlate to good ISS performance (Das et al. 2017). At the lowest application rate (0.02 gal/yd²), the effect of surface by tining direction in PCC surface exists for ISS, and at the 0.05 gal/yd² of the application rate, there is no advantage by the surface effect on the ISS. Even the smooth surface exhibits better performance than all the tined surfaces conditions at that condition. In the highest application rate condition (0.09 gal/yd²), all the ISS values from different surface conditions become same and the effect of surface disappears. The effect of surface on PCC is various by application rate (Leng et al. 2008). There is no significant correlation between ISS and MTD (Coleri et al. 2020).

Finally, there is an uncertainty of relationship between lab and field shear bond performance properties and this is controversial issue as well as the application rate effect. The WisDOT research team explained that possible reasons for this assumption include uncertainties surrounding the field conditions, such as inconsistency in the application rate and also commented that some damage was present in the milled bottom layer; the direction of milling was not specified. A dusty or dirty surface also may have negatively affected the ISS test results (Bahia et al. 2019). The NCHRP research team noted that different compaction methods and lack of uniformity of application rate in the field led to the discrepancy between the lab and field ISS test results (Mohammad et al. 2012). Coleri et al. (2020) suggests that the ISS test results with lab fabricated specimens by roller compactor can be utilized to observe field conditions because the ISS test results for lab versus field samples are not dissimilar.

A.4.1 Binder Bond Strength

The overall performance of a multilayered flexible pavement structure depends on its ability to act as a monolithic structure to withstand traffic and environmental loading. A poor bond between the layers can result in slippage, delamination, shoving, fatigue cracking, and eventually to the formation of potholes. Figure A25 shows the differences in load distribution among pavement systems that are fully bonded, partially bonded, and not bonded between the asphaltic layers. In the case of no-bond conditions, each layer experiences tension-compressive stress individually,

thereby facilitating debonding and cracking, whereas a fully bonded asphalt pavement experiences the same stress state at the top and bottom of the intact asphaltic layers with less strain magnitude due to enhanced structural stiffness. However, real pavements may experience partially bonded conditions where the induced strain within the section can be anywhere between the fully-bonded and no-bond conditions, depending upon the bond strength.

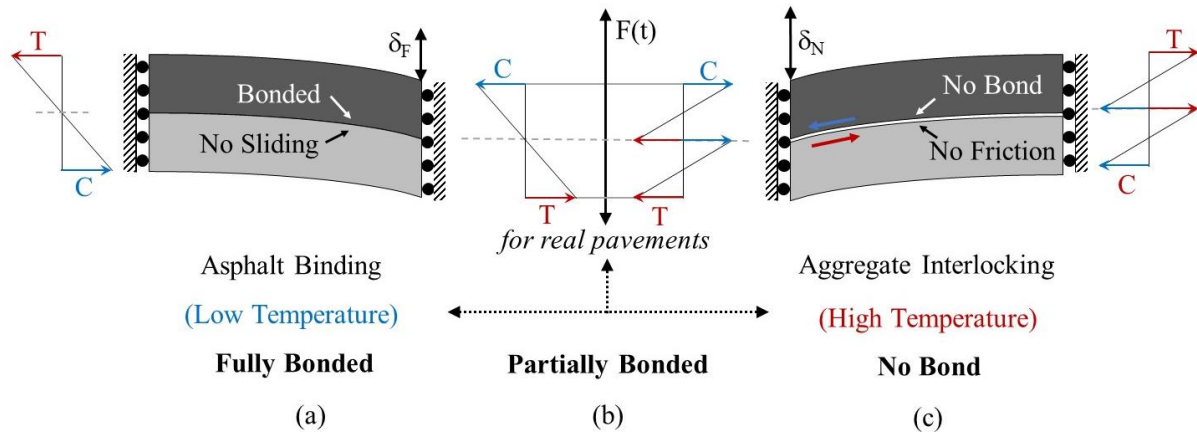


Figure A25. Behavior of pavement layers during bending under different bond conditions: (a) fully bonded, (b) partially bonded, and (c) no bond (Kim et al. 2011).

The application of a tack coat between the asphaltic layers is an effective way to enhance bonding. The American Society for Testing and Materials (ASTM) defines a tack coat as “an application of bituminous material to an existing relatively non-absorptive surface to provide a thorough bond between old and new surfacing” (ASTM 2018). Although asphalt tack coat material makes up only a small percentage of any paving project (Asphalt Institute 2007), the lack of a proper tack coat can cause debonding issues, which in turn invites extensive maintenance work before the end of the pavement’s design life. The major distresses associated with the lack of a good bond are slippage and shoving of the pavement, fatigue cracking, potholes, and delamination. These distresses impose an extra financial burden on the project; hence, the importance of tack coats cannot be ignored. This fact has motivated many researchers to conduct significant investigations into the characteristics of tack coats and its influence on pavement performance over the past two decades.

A.4.2 Factors That Affect Bond Strength

A tack coat is a complex material and multiple variables affect its performance. A review of past research, standards, and technical papers shows that five main factors affect interlayer bond strength: application rate, tack coat material, temperature, curing time, and existing surface conditions.

Application Rate

The amount of tack coat that is applied onto a pavement surface is a critical factor that helps to decide the interlayer bond strength. Researchers have found that the use of a tack coat improves the bond strength between pavement layers in comparison to a no-tack coat condition (Chen and Huang 2010, Mohammad et al. 2012, Tran et al. 2012). However, many research groups have reported contrasting outcomes regarding bond strength with a change in the tack coat application rate. Too little or an excessive tack coat can result in debonding or slippage (Amelian and Kim 2018, Buchanan and Woods 2004, Chen and Huang 2010, Cross and Shrestha 2005, Mohammad et al. 2012, Tashman et al. 2006, Tayebali et al. 2004, West et al. 2005). Surface type is another major influential factor that affects the tack coat application rate. In general, lower application rates are recommended for new or subsequent layers, and higher application rates are recommended for old, oxidized, cracked, pocked, or milled asphalt pavements. Table A4 shows the different application rates specified by various agencies and organizations across the United States based on their experience and research.

Table A4. Recommended Application Rates Used by Various Industries

Source	Unit	Surface Type			
		New Asphalt Mixture	Existing/Old Asphalt Mixture	Milled Asphalt Mixture	Portland Cement Concrete
Mohammad et al. (2012) (Residual Rate)	L/m ²	0.16	0.25	0.25	0.2
	gal/yd ²	0.035	0.055	0.055	0.045
Asphalt Institute (2007) (Residual Rate)	L/m ²	0.09-0.20	0.18-0.32	0.18-0.36	0.14-0.23
	gal/yd ²	0.02-0.045	0.04-0.07	0.04-0.08	0.03-0.05
FHWA (2016) (Residual Rate)	L/m ²	0.09-0.23	0.18-0.32	0.18-0.36	0.14-0.23
	gal/yd ²	0.02-0.05	0.04-0.07	0.04-0.08	0.03-0.05
NCDOT QMS Manual (2018)	L/m ²	0.14-0.23	0.23-0.32	0.23-0.32	0.32-0.41
	gal/yd ²	0.03-0.05	0.05-0.07	0.05-0.07	0.07-0.09
Caltrans (2009)	L/m ²	0.23*	0.32*	0.32*	0.50*
	gal/yd ²	0.05*	0.07*	0.07*	0.11*
Flexible Pavements of Ohio (2012) (Residual Rate)	L/m ²	0.14-0.18	0.23-0.27	0.23-0.27	0.18-0.23
	gal/yd ²	0.03-0.04	0.05-0.06	0.05-0.06	0.04-0.05

*minimum requirement

Tack Coat Materials

The most common tack coat materials found in the literature are emulsions, performance grade (PG) binders, and occasionally, cutbacks. The National Cooperative Highway Research Program

(NCHRP), under Project 9-40, conducted a worldwide survey on tack coat materials and found that the most commonly used tack coats for new, existing, and milled hot mix asphalt surfaces are CSS-1h, SS-1, SS-1h, and CSS-1 asphalt emulsions. PG 64-22 was reported as the most often used asphalt cement, while RC-70 as the most commonly used cutback asphalt (Mohammad et al. 2012). Although there is global agreement on the most commonly used tack coat materials, the ranking of tack coat materials varies depending on the methodology employed for the performance evaluation. Wang et al. (2017) reviewed numerous studies in the literature to find that trackless tack coats outperform commonly used conventional cationic and anionic emulsions as well as hot asphalt binders. On the other hand, shear bond tests of field core specimens that used five different tack coats types (CSS-1h, CRS-2P, CFS-1, PG 64-22, and a trackless tack coat) at the interface under monotonic and cyclic loading showed that CFS-1, a modified CSS-1, ranked first under both loading conditions (Amelian and Kim 2018).

Temperature

Temperature is one of the most significant factors that affects tack coat performance. A vast majority of research shows that, with an increase in temperature, the bond strength or stiffness of the tack coat material decreases (Chen and Huang 2010, Cho 2016, Karshenas 2015, Kim et al. 2011, Leng et al. 2008, Romanoschi and Metcalf 2001, Sholar et al. 2004, Sudarsanan et al. 2018, West et al. 2005). Chen and Huang (2010) investigated the effect of temperature on bond strength and concluded that the peak shear stress at elevated temperatures is related to interlayer surface characteristics, such as interlock and friction, whereas at lower temperatures the dependency is more on tack coat characteristics. Rheological properties of tack coat materials suggest that the shear bond characteristics are dependent not only on the temperature but also on the rate or frequency of loading and normal confinement pressure at which the tests are carried out. Hence, instead of a fixed test temperature and loading rate, testing at multiple test conditions is recommended to capture the true behavior of the interface (Kim et al. 2011).

Curing

Coalescence (join together) of the asphalt globules in emulsions separates asphalt binder and water, eventually leads to the vaporization of water, thereby leaving the asphalt binder alone on the pavement surface. These phenomena are referred to as “breaking” and “setting.” Breaking is evidenced by the change in color of the emulsion from brown to black. The recommended curing times by different researchers also vary, as shown in Table A5.

Table A5. Different Recommended Curing Times

Source	Recommended Curing Time
Hachiya and Sato (1997)	1 to 24 hours
Roffe and Chaignon (2002)	20 minutes to several hours
Mohammad et al. (2002)	1 hour
Bahia et al. (2019)	30 to 60 minutes

The applied thin layer emulsions during the curing process help any type of emulsion (RS, MS, and SS) to reach the terminal mass loss (residual asphalt mass) with a 10% difference at a given curing time. Thereby, the curing time difference is insignificant irrespective of the setting designation (Bahia et al. 2019).

Existing Surface Conditions

The existing surface condition of the pavement is another crucial factor that not only helps determine the tack coat application rate but also plays an important role in the development of the bond strength between pavement layers. Such surface conditions include roughness and the presence of dust and moisture. Roughness may be described as the texture of the underlying layer. Large-scale roughness is caused by cold-milling the pavement prior to the placement of new pavement layers. In general, a rougher texture produces greater bond strength, which is a maxim that holds true not only when comparing milled surfaces to new surfaces (Al-Qadi et al. 2008, Leng et al. 2008, Mohammad et al. 2012, Tran et al. 2012), but also when comparing coarse mixtures to fine mixtures (Sholar et al. 2004). Researchers have observed a direct relationship between surface roughness and bond strength, but an inverse relationship between tack coat effectiveness and roughness (Sholar et al. 2004, Tashman et al. 2006, West et al. 2005). A generally accepted construction practice is that a clean, dust-free surface is preferable prior to tack coat application over dusty or dirty conditions, as a clean surface provides greater bond strength than an unclean, dusty surface (Caltrans 2009, Flexible Pavements of Ohio 2012). Besides, the presence of moisture on the pavement surface greatly reduces the bond strength both in the lab and in the field (Al-Qadi et al. 2008, Sholar et al. 2004).

In summary, many factors, such as application rate, type of emulsion, temperature, curing time, and existing pavement surface conditions, affect the tack coat’s performance. Asphalt binder bond strength (BBS), measured by the Pneumatic Adhesion Tensile Testing Instrument (PATTI), is gaining popularity for a routine tack coat quality control measure due to its simplicity, low cost, and efficiency. Karshenas (2015) found a strong relationship between BBS of tack coats and the shear strength of sandwiched asphalt concrete specimens with tack coat in the middle. In order to determine the shear strength of asphalt overlay interface as a function of temperature and loading rate (i.e., vehicle speed) using Karshenas’s relationship, it is desirable to have the BBS as a

function of temperature and loading rate. In addition, establishing BBS mastercurves will help to predict the shear strength of tack coats under different loading conditions for different pavement sections from a few temperature-loading rate combinations. Hence, the one of the focus of this study is to prove that the time-temperature superposition principle is applicable to BBS of various tack coat materials.

Appendix B. Numerical Simulation

B.1. Analysis of Stress Distribution at Interface

Figure B1 shows the shear stress transition as a function of pavement depth at different temperatures. The conditions chosen in Figure B1– i.e., thin pavement, 106.8 kN (24 kips), 88 km/hour (55 mph), rolling resistance coefficient of 0.55 for the braking condition, and various temperature conditions – were assumed the critical pavement depth by previous researchers (Cho 2016) for the FlexPAVE™ simulations in terms of shear stress levels. The analysis results that were used to evaluate the critical depth show that the shear stress increases from the surface to the depth of 5.08 cm (2.0 in.) or 3.81 cm (1.5 in.) which is typical thickness of surface layer of asphalt pavements, except at 60°C. Then, the shear stress starts to decrease and, after a depth of around 10.16 cm (4.0 in.), it gradually decreases. This evaluation indicates that the depth of 5.08 cm (2.0 in.) below the surface course is the critical depth for shear stress.

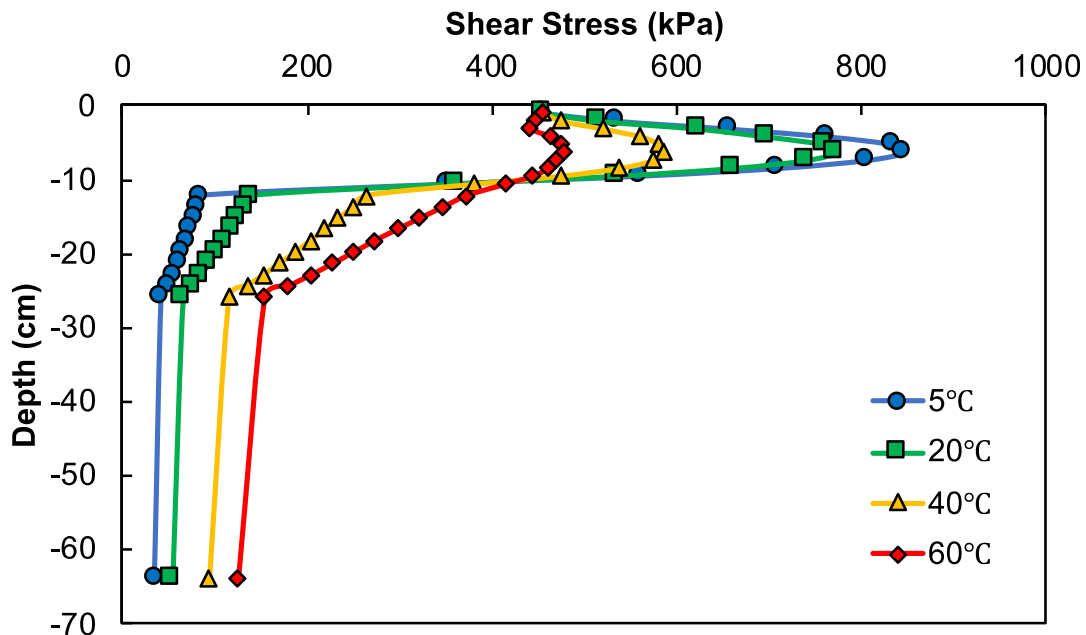
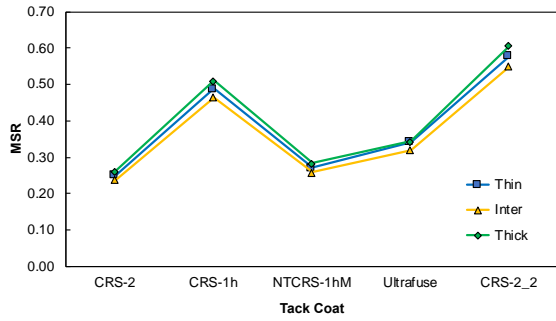
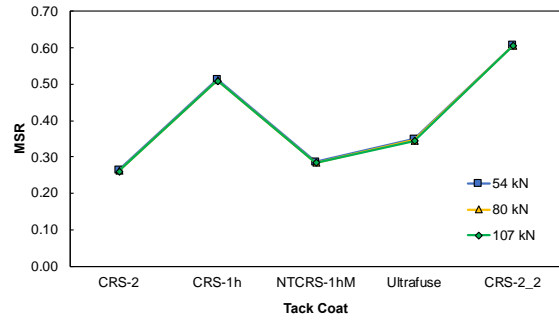


Figure B1. Shear stress distribution throughout pavement depth at various temperatures (thin pavement, 106.8 kN, 88 km/h, 0.55 braking condition).

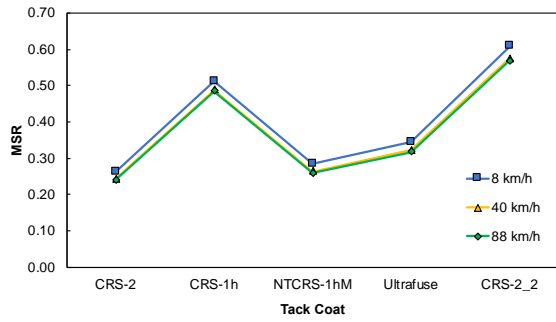
Moreover, in order to examine the effects of various factors such as temperature, speed, load level, structural type, and rolling resistance, coefficients were evaluated in terms of the MSR for each tack coat material shown in Figure B2 and Table B1. To evaluate the effect of each factor, each factor was fixed except the factor considered. However, at the high temperature, the effect of the axle load was not significant, so additional analysis was implemented at the low temperature (5°C), as shown in Figure B3



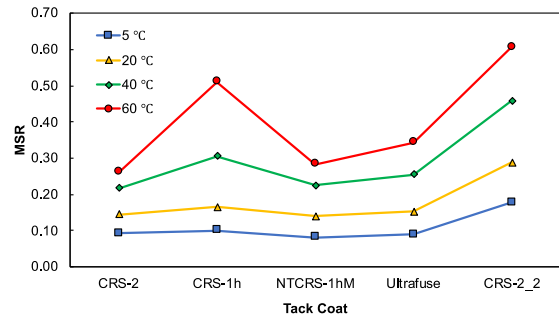
(a)



(b)



(c)



(d)

Figure B2. Critical conditions according to several factors.

Table B1. Maximum Shear Ratios According to Different Conditions

Factor	Structure	Axle Load (kN)	Speed (km/h)	Temp. (°C)	CRS-2	CRS-1h	NTCR S-1hM	Ultra fuse	CRS-2_2
Structure	Thin	107	8	60	0.25	0.49	0.27	0.34	0.58
	Intermediate	107	8	60	0.24	0.46	0.26	0.32	0.55
	Thick	107	8	60	0.26	0.51	0.28	0.34	0.61
Axle Load	Thick	54	8	60	0.26	0.51	0.29	0.35	0.61
	Thick	80	8	60	0.26	0.51	0.29	0.35	0.61
	Thick	107	8	60	0.26	0.51	0.28	0.34	0.61
Speed	Thick	107	8	60	0.26	0.51	0.28	0.34	0.61
	Thick	107	40	60	0.24	0.49	0.26	0.32	0.57
	Thick	107	88	60	0.24	0.48	0.26	0.32	0.57
Temperature	Thick	107	8	5	0.09	0.10	0.08	0.09	0.18
	Thick	107	8	20	0.15	0.17	0.14	0.15	0.29
	Thick	107	8	40	0.22	0.31	0.23	0.26	0.46
	Thick	107	8	60	0.26	0.51	0.28	0.34	0.61

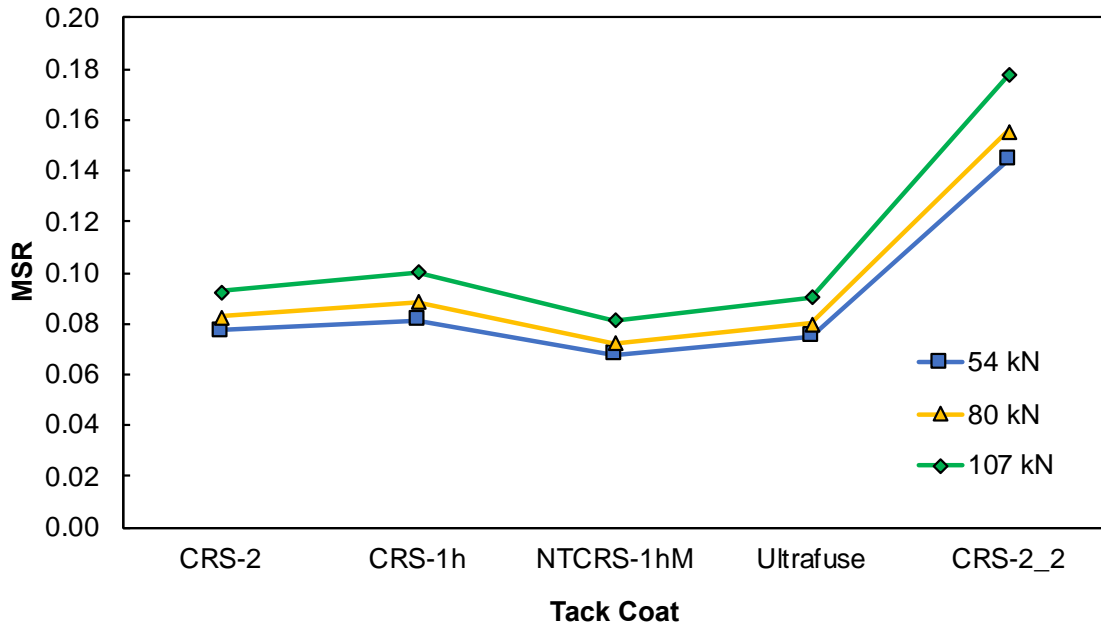


Figure B3. Effect of axle load on maximum shear ratio.

The critical conditions were determined based on simulations of the pavement responses. The MSR value was used as a parameter and consists of the shear stress of the pavement response as the numerator and the shear strength derived from tests as the denominator. So, a higher MSR means that the conditions at that moment are more susceptible to traffic loading. In this analysis, a thick pavement structure, 107-kN axle load, 8 km/h speed, and 60°C temperature were the critical conditions for every tack coat material.

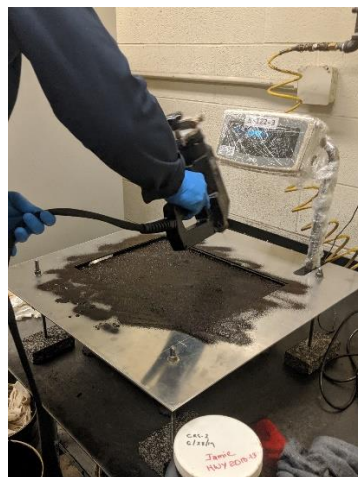
Appendix C. Test Methodology

C.1. Roller Compactor for ISS Test Specimens

For the current study, a James Cox & Sons CRT-RC2S roller compactor was used to make a double-layered slab with the thickness of 50 mm (1.97 in.) for each layer. The compaction procedure was carried out in two stages. The first stage consisted of the bottom layer fabrication, and the second stage consisted of the hot asphalt tack coat application with the top layer compacted above the bottom layer. Following the compaction process, six Modified Advanced Shear Tester (MAST) specimens were cored from the slab. Figure C1 shows each stage in detail.



(a)



(b)



(c)

Figure C1. (a) Fabricated bottom layer interface shear strength test specimen, (b) using hot spray gun to apply tack coat, and (c) core pattern on slab.

C.2. Milling Procedure

An end mill drilling technique was adopted for the current study to mimic a real field milling pattern by matching the mean profile depth (MPD) of the grooved specimen with the MPD of the milled surface. The MAST specimens that were fabricated using this technique did not show improvement in ISS, which is contrary to the field response. In order to confirm this finding, the NCSU research team sought a mini-milling machine that could resemble the field milling pattern. Figure C2 (a) shows the inlay grooving machine that the research team found for this purpose, the Graco GrindLazer Pro with a ‘tooth-pick’ drum. Graco personnel demonstrated the capabilities of the machine by milling the asphalt pavement at an NCSU parking lot. Figure C2 (b) shows that the milling pattern produced by the milling drum is regular, which is due to the high RPM (1500 – 3000 RPM) of the drum. Therefore, the research team concluded that this machine might be able to create specimens that eventually provide the same response as that of pavements with groove patterns made from end mills.



(a)



(b)

Figure C2. (a) Graco GridLazer Pro with tooth-pick drum and (b) milling pattern produced by the mini-milling machine.

Appendix D. Best Practices and Usage of Tack Coats in North Carolina

D.1. Section 1020

Asphalt materials are accepted at the source of the shipment subject to the conditions herein.

All asphalt transport tankers, including rail and truck tankers, shall have a sampling valve in accordance with Asphalt Institute Publication MS-18, AASHTO R66, ASTM D140 or a comparable device acceptable to the Engineer.

Each transport tanker delivering asphalt materials to the project or rail siding shall keep a running log showing the date, destination and type and grade of material hauled on each trip. Print, stamp, or write in ink information appearing in the log and have available for examination upon request.

Furnish with each shipment 2 copies of a delivery ticket. Ensure both copies accompany the shipment and are delivered to the Engineer or his representative at the destination. The delivery ticket shall contain the following information:

- A.** Name of Producer/Supplier and location
- B.** A statement that the material has been tested and meets AASHTO specifications or is being provided by an approved supplier under Approved Supplier Certification (ASC)
- C.** The grade of the material
- D.** If applicable, the rotational viscosity in Pascal-Seconds (Pa-S) at 135°C and 165°C
- E.** If applicable, the recommended laboratory mixing and compaction temperature (°C for the PGAB)
- F.** Delivery ticket number
- G.** Date and time loaded (mrrn/dd /yyyy AM:PM)
- H.** Date and time shipped (mrrn/dd /yyyy AM:PM)
- I.** State project or purchase order number
- J.** NCDOT assigned batch number
- K.** Destination
- L.** Name of consignee
- M.** Trailer or car number
- N.** Producer's or Supplier' s storage tank and batch number
- O.** Quantity loaded in tons or gallons (kg/L) at 60°F
- P.** Specific Gravity or lbs/gal (kg/L) at 60°F
- Q.** Loading temperature
- R.** Net gallon at 60°F
- S.** If applicable, the brand, grade and percentage or quantity of anti-strip additive
- T.** See below for the required certification format

When anti-strip additive is introduced into the asphalt binder, ensure the delivery ticket notes the brand, grade and percentage or quantity at which the additive was introduced. The Contractor's asphalt materials supplier shall furnish to the Materials and Tests Unit a typical viscosity-

temperature chart at the beginning of each calendar year and a new chart whenever a change in production results in a shift of 5°F or more.

Furnish a statement of certification from the supplier and a separate statement of certification from the transporter. Sign each certification by an authorized representative of the supplier or transporter. Stamp, write or print these certifications on the delivery ticket, or attach to the delivery ticket.

Unless otherwise approved by the Engineer, the following form shall be used in the supplier's certification:

This is to certify that this shipment of _____gallons/liters or tons/metric tons of _____grade asphalt including _____gallon s/liters of _____anti-strip meet all requirements of NC Department of Transportation Specifications.

Signed _____

Authorized Representative of Supplier

When no anti-strip additive is included with the load, the supplier shall indicate zero (0) in the gallons field and "NA" in the anti-strip field on the above certification.

Unless otherwise approved by the Engineer, the following form shall be used in the transporter's certification:

This is to certify that this transport tank was clean and free from contaminating materials when loaded. The material transported on the previous load in this tanker was _____

Signed _____

Authorized Representative of Transporter

Failure to sign the certifications by either the supplier or transporter will be cause to withhold use of the material until a sample can be taken and tested, except where an alternative testing and invoicing procedure has been pre-approved by the Engineer.

The Engineer reserves the right to sample and test any shipment regardless of whether or not the above conditions have been met and to reject any material not meeting the Specifications.

D.2. M&T Form 605

M&T FORM 605

NORTH CAROLINA DEPARTMENT OF TRANSPORTATION

Revised 01-2016

ASPHALT ROADWAY INSPECTOR'S DAILY REPORT

Contract/PO/WBS No.:		County:		Div.:		Report No.	
Date:		Weather:		Temp. High:		Low:	
Type of Construction:				Route No.		Miles:	
Map Project No.:		Map No.:		Map Length:			
Contractor (Prime):				Paving Contractor:			
Contractor Producing Asphalt Mix:				Plant Site:			
SPREADING/ROLLING EQUIPMENT				ROADWAY OPERATIONS			
No.	Make	Type	Weight	No. Loads Received:		Total Hours:	
				Time First Rec'd	Time Last Rec'd	Delay Time	Hrs. Operation
TACK COAT							
Source		Batch No.		Grade		Gallons	Temp.
MATERIAL PLACED TODAY							
Mix Type							
JMF No.							
Map No.	Mat Location						
Base Type (ABC, New Mix, Exist Pav't)							
Begin Station							
End Station							
Linear Feet							
Width							
Square Yards							
Today's Tons							
Rate of Spread (lbs. per sq. yd.)							
Tack Coat Rate (gals. per sq. yd.)							
Air Temp. (°F)	Surface Temp. (°F)						
Time Placed							
Mix Temperature (°F)							
Type of Density Control							
# QC Density Tests							
# QA / # Verification Density Tests							
Paving Application Type (check one)							
Full Width Paving							
Widening - 4 ft. or greater							
Uniform Paved Shldr - 4 ft. or greater							
Widening - Less than 4 ft.							
Intersections (separate operation)							
Driveways / Irregular Areas							
Patching / Wedging / Leveling							
Remarks:							
*Print Rdwy Tech's. Name:				RD1-		Res. Eng.	
*Rdwy Tech Signature:							

*By providing this data under my signature and/or HiCAMS certification number, I attest to the accuracy and validity of the data contained on this form and certify that no deliberate misrepresentation of the test results in any manner has occurred.

D.3. Asphalt Delivery Tickets for Emulsified Asphalt

When a shipment of asphalt emulsion that is to be used as either prime or tack coat is received at an asphalt plant or on a project, a copy of the bill of lading will be furnished to the appropriate Resident Engineer and retained in their project records. When receiving asphalt emulsion, follow these guidelines:

1. Verify source of tack coat on Bill of Lading (BOL) as coming from terminal on approved NCDOT list.
2. Verify that BOL contains NCDOT assigned batch numbers. (First two numbers are the Approved Asphalt Terminal (AT) number).
3. Obtain a copy of the BOL for every shipment and include it with the materials received report (MRR) for each project. Note that in most cases, one BOL may represent several distributor truck loads, since many Contractors have tankers shipped to central locations and fill distributor trucks from the tanker.
4. BOLs may be obtained from the Contractor's project personnel on site or may be sent from plant personnel managing the tack shipment directly to the Resident Engineer's office. Arrangements for obtaining the BOL should be discussed prior to beginning work.
5. Confirm that all approved suppliers have an asphalt terminal (AT) number.
6. Confirm that BOL has supplier and transporters certifications recorded.
7. Create a record of net gallons delivered to the project.
8. Confirm that approved grade of material is recorded on BOL.
9. If BOL is lacking any required information, then decline that tack on the project until BOL is corrected.
10. For more detailed information refer to M&T Unit's "Asphalt Emulsion Receiving Guide" at the following website:

<https://connect.ncdot.gov/resources/Materials/MaterialsResources/Asphalt%20Emulsion%20Receiving%20Guide.pdf>

D.4. Temperature-Volume Corrections for Emulsified Asphalt

LEGEND: t = Observed Temperature in Degrees Celsius (Fahrenheit)
M = Multiplier for Correcting Volumes to the Basis of 15.6°C (60°F)

*Multiplier (M) for °C is a close approximation.

°C ^t	°F	M*	°C ^t	°F	M*	°C ^t	°F	M*
10.0	50	1.00250	35.0	95	0.99125	60.0	140	0.98000
10.6	51	1.00225	35.6	96	0.99100	60.6	141	0.97975
11.1	52	1.00200	36.1	97	0.99075	61.1	142	0.97950
11.7	53	1.00175	36.7	98	0.99050	61.7	143	0.97925
12.2	54	1.00150	37.2	99	0.99025	62.2	144	0.97900
12.8	55	1.00125	37.8	100	0.99000	62.8	145	0.97875
13.3	56	1.00100	38.3	101	0.98975	63.3	146	0.97850
13.9	57	1.00075	38.9	102	0.98950	63.9	147	0.97825
14.4	58	1.00050	39.4	103	0.98925	64.4	148	0.97800
15.0	59	1.00025	40.0	104	0.98900	65.0	149	0.97775
15.6	60	1.00000	40.6	105	0.98875	65.6	150	0.97750
16.1	61	0.99975	41.1	106	0.98850	66.1	151	0.97725
16.7	62	0.99950	41.7	107	0.98825	66.7	152	0.97700
17.2	63	0.99925	42.2	108	0.98800	67.2	153	0.97675
17.8	64	0.99900	42.8	109	0.98775	67.8	154	0.97650
18.3	65	0.99875	43.3	110	0.98750	68.3	155	0.97625
18.9	66	0.99850	43.9	111	0.98725	68.9	156	0.97600
19.4	67	0.99825	44.4	112	0.98700	69.4	157	0.97575
20.0	68	0.99800	45.0	113	0.98675	70.0	158	0.97550
20.6	69	0.99775	45.6	114	0.98650	70.6	159	0.97525
21.1	70	0.99750	46.1	115	0.98625	71.1	160	0.97500
21.7	71	0.99725	46.7	116	0.98600	71.7	161	0.97475
22.2	72	0.99700	47.2	117	0.98575	72.2	162	0.97450
22.8	73	0.99675	47.8	118	0.98550	72.8	163	0.97425
23.3	74	0.99650	48.3	119	0.98525	73.3	164	0.97400
23.9	75	0.99625	48.9	120	0.98500	73.9	165	0.97375
24.4	76	0.99600	49.4	121	0.98475	74.4	166	0.97350
25.0	77	0.99575	50.0	122	0.98450	75.0	167	0.97325
25.6	78	0.99550	50.6	123	0.98425	75.6	168	0.97300
26.1	79	0.99525	51.1	124	0.98400	76.1	169	0.97275
26.7	80	0.99500	51.7	125	0.98375	76.7	170	0.97250
27.2	81	0.99475	52.2	126	0.98350	77.2	171	0.97225
27.8	82	0.99450	52.8	127	0.98325	77.8	172	0.97200
28.3	83	0.99425	53.3	128	0.98300	78.3	173	0.97175
28.9	84	0.99400	53.9	129	0.98275	78.9	174	0.97150
29.4	85	0.99375	54.4	130	0.98250	79.4	175	0.97125
30.0	86	0.99350	55.0	131	0.98225	80.0	176	0.97100
30.6	87	0.99325	55.6	132	0.98200	80.6	177	0.97075
31.1	88	0.99300	56.1	133	0.98175	81.1	178	0.97050
31.7	89	0.99275	56.7	134	0.98150	81.7	179	0.97025
32.2	90	0.99250	57.2	135	0.98125	82.2	180	0.97000
32.8	91	0.99225	57.8	136	0.98100	82.8	181	0.96975
33.3	92	0.99200	58.3	137	0.98075	83.3	182	0.96950
33.9	93	0.99175	58.9	138	0.98050	83.9	183	0.96925
34.4	94	0.99150	59.4	139	0.98025	84.4	184	0.96900
						85.0	185	0.96875